

Jan Petter Morten

Coherent and Correlated Spin Transport in Nanoscale Superconductors

Thesis for the degree of philosophiae doctor

Trondheim, March 2008

Norwegian University of
Science and Technology
Faculty of Natural Sciences and Technology
Department of Physics



NTNU

Norwegian University of
Science and Technology

NTNU
Norwegian University of Science and Technology

Thesis for the degree of philosophiae doctor

Faculty of Natural Sciences and Technology
Department of Physics

©Jan Petter Morten

ISBN 978-82-471-7409-8 (printed ver.)
ISBN 978-82-471-7412-8 (electronic ver.)
ISSN 1503-8181

Theses at NTNU, 2008:72

Printed by Tapir Uttrykk

Abstract

Motivated by the desire for better understanding of nanoelectronic systems, we theoretically study the conductance and noise characteristics of current flow between superconductors, ferromagnets, and normal-metals. Such nanostructures can reveal information about superconductor proximity effects, spin-relaxation processes, and spintronic effects with potential applications for different areas of mesoscopic physics. We employ the quasiclassical theory of superconductivity in the Keldysh formalism, and calculate the nonequilibrium transport of spin and charge using various approaches like the circuit theory of quantum transport and full counting statistics. For two of the studied structures, we have been able to compare our theory to experimental data and obtain good agreement.

Transport and relaxation of spin polarized current in superconductors is governed by energy-dependent transport coefficients and spin-flip rates which are determined by quantum interference effects. We calculate the resulting temperature-dependent spin flow in ferromagnet-superconductor devices. Experimental data for spin accumulation and spin relaxation in a superconducting nanowire is in agreement with the theory, and allows for a spin-flip spectroscopy that determines the dominant mechanism for spin-flip relaxation in the studied samples. A ferromagnet precessing under resonance conditions can give rise to pure spin current injection into superconductors. We find that the absorbed spin current is measurable as a temperature dependent Gilbert damping, which we calculate and compare to experimental data.

Crossed Andreev reflection denotes superconducting pairing of electrons flowing from different normal-metal or ferromagnet terminals into a superconductor. We calculate the nonlocal currents resulting from this process in competition with direct electron transport between the normal-metal terminals. We take dephasing into account, and study the nonlocal current when the types of contact in the system varies from e.g. ballistic conductors or tunnel barriers. In the tunneling case, we calculate the magnetization-dependent full counting statistics, which determines all noise properties including the cross-correlations that can resolve the contributions due to crossed Andreev reflection and direct electron transport. We evaluate the magnetization-dependent two-particle probability that the constituents of spin-entangled pairs from crossed Andreev reflection flow into different ferromagnetic contacts. This probability implies violation of a Bell inequality, and determines the performance of a superconductor-ferromagnet entangler.

Preface

This thesis is submitted as part of the requirement for the degree *Philosophiae Doctor*, and concludes my studies at the Department of Physics, the Norwegian University of Science and Technology (NTNU). My thesis work was carried out between August 2003 and January 2008, and has included teaching equivalent to one academic year. I have also completed courses amounting to one full semester of study. Professor Arne Brataas has been the supervisor of this work, which was financed by the NTNU Strategic area Materials.

Throughout my studies, I have collaborated closely with Professor Wolfgang Belzig at the University of Konstanz, Germany. During the last three years of the study, I have enjoyed working together with Daniel Huertas-Hernando at the department. Moreover, I have highly appreciated collaborations with Gerrit Bauer, Yaroslav Tserkovnyak, Ninos Poli and Vladislav Korenivski.

In the first part of the thesis, we will provide a short introduction to the research field and discuss the relevance and motivation to study the systems we have considered. Moreover, we will briefly account for the theoretical tools that have been utilized in this research, and summarize some of the research results. The main part of the research results are presented in the second part of the thesis, where the papers produced during the thesis work are appended.

In addition to the papers in the second part of this thesis, I have presented my research and discussed it with other scientists at conferences and workshops. In particular, the conferences “Electronic and Spin Transport in Superconductor/Ferromagnet Nanostructures” (2005) in Leiden, The Netherlands, and “Spin physics of superconducting heterostructures” (2006) in Bad Honnef, Germany, were very rewarding. Additionally, I have attended the 2004 Les Houches summer school “Nanophysics: Coherence and Transport” in France, and the 2005 “Spring School on Mesoscopic Physics” in Kilpisjärvi, Finland. From November 2006 to January 2007, I enjoyed a very productive and interesting stay at the Centre for Advanced Study in Oslo.

List of papers

Paper [1]

Jan Petter Morten, Arne Brataas, and Wolfgang Belzig,
Spin transport in diffusive superconductors,
Phys. Rev. B **70**, 212508 (2004) [arXiv:cond-mat/0401580]

Paper [2]

Jan Petter Morten, Arne Brataas, and Wolfgang Belzig,
Spin transport and magnetoresistance in ferromagnet/superconductor/ferromagnet spin valves,
Phys. Rev. B **72**, 014510 (2005) [arXiv:cond-mat/0501566]

Paper [3]

Ninos Poli, Jan Petter Morten, Mattias Urech, Arne Brataas, David B. Haviland,
and Vladislav Korenivski,
Spin injection and relaxation in a mesoscopic superconductor,
Phys. Rev. Lett. (2008) [arXiv:0707.2879]

Paper [4]

Jan Petter Morten, Arne Brataas, Gerrit Bauer, Wolfgang Belzig,
and Yaroslav Tserkovnyak,
Proximity effect-assisted absorption of spin currents in superconductors,
Preprint (2007) [arXiv:0712.2814]

Paper [5]

Jan Petter Morten, Arne Brataas, and Wolfgang Belzig,
Circuit theory of crossed Andreev reflection,
Phys. Rev. B **74**, 214510 (2006) [arXiv:cond-mat/0606561]

Paper [6]

Jan Petter Morten, Arne Brataas, and Wolfgang Belzig,
Circuit theory for crossed Andreev reflection and nonlocal conductance,
Appl. Phys. A **89**, 609 (2007) [arXiv:0709.4020]

Paper [7]

Jan Petter Morten,
Quantum physics and the boundaries of space and time,
In *Complexity*, edited by W. Østreng, Centre for Advanced Study, Oslo, (2008)

Paper [8]

Jan Petter Morten, Daniel Huertas-Hernando, Wolfgang Belzig, and Arne Brataas,
Elementary Charge Transfer Processes in a Superconductor-Ferromagnet Entangler,
Europhys. Lett. **81**, 40002 (2008) [[arXiv:cond-mat/0612197](#)]

Paper [9]

Jan Petter Morten, Daniel Huertas-Hernando, Wolfgang Belzig, and Arne Brataas,
Full counting statistics of crossed Andreev reflection,
Preprint (2008)

My contribution to the papers

In the papers where I am listed as the first author (all except [3]), I have contributed substantially to all parts of the paper. I performed the majority of the calculations and produced the graphs and figures, and was a significant contributor to all parts of the text. In paper [3], where I am the second author, I developed the theoretical model and performed the fitting analysis in close collaboration with Arne Brataas. The theoretical modeling part of this paper was mainly written by me, in collaboration with Arne Brataas and the other authors. The experimental studies were performed by the experimentalists at the Royal Institute of Technology in Stockholm, who are the main contributors to the text.

Table of Contents

1	Introduction	1
1.1	Superconductivity in nanoelectronic circuits	2
1.2	Magnetoelectronics	4
1.3	Superconductor ferromagnet nanoelectronic circuits	4
1.4	Outline	5
2	Theory toolbox	7
2.1	Quasiclassical theory of superconductivity	7
2.2	Circuit theory	11
2.3	Full counting statistics	14
3	Spin injection into superconductors	17
3.1	Quantum kinetic equations	17
3.2	Spin polarized current injection	28
3.3	Magnetization dynamics in F S heterostructures	32
3.4	Conclusion	35
4	Crossed Andreev reflection	37
4.1	Circuit theory model	38
4.2	Results	42
4.3	Conclusion	47
5	Quantum mechanics and nonlocality	49
6	Supercurrent beamsplitter statistics	51

6.1	Single-node tunnel barrier circuits	52
6.2	S F entangler	54
6.3	FCS of crossed Andreev reflection and electron transfer	57
6.4	Conclusion	58
7	Outlook	59
8	Acknowledgements	61
A	Notation	63
	Bibliography	63

List of Figures

2.1	Example circuit theory diagram	12
3.1	Order parameter of gapless superconductor	26
3.2	Spectral properties of gapless superconductor	27
3.3	Conversion of currents in F S F spin valve	29
3.4	Spin current in F S F spin valve	30
3.5	Magnetoresistance in F S F spin valve	31
3.6	Temperature dependent spin-flip length	32
3.7	F S R enhanced Gilbert damping, no spin-flip	34
3.8	F S enhanced Gilbert damping	35
4.1	Crossed Andreev generic circuit	39
4.2	Conductances: Connectors of tunnel type	44
4.3	Conductances: Dependence on S connector type	46
6.1	S F entangler	53

1 Introduction

Quantum mechanics emerged in the early 20th century, and is the theory that describes Nature on the microscopic scale. It was at first a controversial and much disputed theory, since it did not comply with such concepts as determinism and locality [10]. These ideas are important properties of classical mechanics, which was established before quantum mechanics and explains phenomena on the macroscopic scale. However, the predictions of quantum mechanics agreed well with the accumulating experimental observations, and today this theory constitutes the basis of our understanding of the microscopic world and even cosmological events like star formation and the Big Bang. Moreover, quantum theory is the foundation of modern technologies like computers, nuclear power, and medical imaging.

In the past, experimental studies of quantum phenomena were limited to atomic and molecular properties like, e.g., the light emission spectra of the elements. Recent technological developments have now made it possible to artificially fabricate structures of high quality and small size so that quantum properties become apparent. In electronic circuits, components less than the mesoscopic scale of the order 100 nm in size are probing the domain where inter-atomic interactions and quantum mechanical properties can determine quantities like the conductance or a voltage drop. Nanoelectronics is the research field aiming to take advantage of quantum properties in such electronic devices, and represents the “marriage” of quantum physics with the engineering science of electronics. Examples of nanoelectronic technologies are giant magnetoresistance read heads in hard drives, and superconducting quantum interferometers that can accurately measure minute magnetic fields.

Research in nanoelectronics is an interesting game to play on two levels. First, it holds the potential to probe novel quantum mechanical effects like e.g. entanglement in electrical circuits within a controlled environment. Second, nanoelectronics could lead to novel technologies operating radically different from traditional electronics.

In this thesis we have studied non-equilibrium spin transport in hybrid structures of superconductors, normal-metals, and ferromagnets. The interplay between spin transport and superconductivity is interesting due to the competing ferromagnetic and superconducting orders. In a superconductor, Cooper pairing between a spin up and a spin down electron leads to condensation of electrons in a boson-like state. On the other hand, in ferromagnets the electronic spins tend to align along the same direction so that there is an excess of one spin species. The temperature-, voltage-, and magnetic field dependence of superconductor-ferromagnet hybrid structures therefore reveal information about quantum phenomena resulting from the competing spin-dependent effects.

In this chapter we will introduce some of the systems and concepts that are considered in this thesis, and discuss some relevant applications. Finally, an outline of the following content is given.

1.1 Superconductivity in nanoelectronic circuits

Below a critical temperature T_c , elements and alloys like Al, Nb, Nb_3Al , and NbN become superconducting and exhibit features such as dissipationless current flow and Meissner effect [11,12,13,14]. A microscopic theory of these properties was developed by J. Bardeen, L. N. Cooper and J. R. Schrieffer [15]. This work, now known as the BCS theory, was awarded the 1972 Nobel prize in physics.

In the BCS theory, electrons are coupled in pairs via phonon interaction. The paired electrons behave like a bosonic condensate, and the quantum mechanical state function of the electrons becomes a macroscopic property of the superconductor over a length scale known as the superconducting coherence length, ξ . In this thesis we will consider diffusive superconductors for which $\xi = \sqrt{\hbar D/\Delta}$ where D is the diffusion coefficient and Δ the superconducting order parameter. In the BCS ground state, the order parameter sets the energy scale to break up Cooper pairs from the condensate. This property can be studied by transport measurements at a superconductor|normal-metal (S|N) interface. For a tunnel barrier interface, the superconducting energy gap manifests itself in that the current across the interface vanishes when the applied bias voltage is smaller than Δ/e [16]. For the experimental demonstration of this effect, former student at NTNU, Ivar Giæver, was awarded the 1973 Nobel prize in physics.

The tunneling current at a S|N interface is modified in comparison to the case discussed above when the the normal-metal part of the heterostructure is so small that its size is comparable to the phase coherence length, l_ϕ . This length is the typical distance electrons can travel before they lose quantum mechanical phase coherence, and is limited by temperature and interactions. Nanoelectronic structures can be fabricated such that l_ϕ exceeds the sample size L , and in this case quantum phase coherent effects become important. In the case of S|N tunneling, the phase coherence of superconducting electrons can modify the

properties of N close to the interface by the *superconducting proximity effect* [17]. In the presence of proximity effect, electron transport across the tunnel barrier interface can take place at energy below Δ by Andreev reflection [18], where an electron incident on the superconductor is retro-reflected as a hole with opposite spin and one Cooper pair is created in S. Conversely, when the current flows into N, a Cooper pair from the superconductor is transferred into N as an electron and hole pair with opposite spins.

When L is smaller than the phase coherence length, $L \lesssim l_\phi$, proximity effect can lead to some remarkable phenomena in S|N heterostructures. One example is the so-called reflectionless tunneling [19,20,21] in diffusive systems. This is a quantum interference effect where the interplay between elastic impurity scatterings and Andreev reflections leads to an effective resistance of the S|N interface of the order of the normal state resistance by coherently redirecting outgoing trajectories of normally reflected particles at the N side back to the interface. As a result, an electron will be normally reflected many times until it is finally Andreev reflected at the interface and the conductance becomes the same as in the normal state.

In the *inverse proximity effect* the properties of superconductors in hybrid structures are modified by contacted non-superconducting materials. Such effects are important over length scales of the order ξ from the interface to non-superconducting materials. Deep inside the superconductor, the BCS state is recovered. The inverse proximity effect is the basis of proposed superconducting spin switches, where the critical temperature of a superconductor sandwiched between two ferromagnets is determined by the magnetization configuration [22]. Close to T_c , a change from antiparallel to parallel magnetizations can drive the superconductor into the normal state. This results in a large resistance difference for current flow through the superconductor.

The superconducting state is characterized by a macroscopic quantum wavefunction that determines the phase of the superconducting electrons. When two superconductors are brought in electrical contact, a phase difference between them can lead e.g. to supercurrent flow without the application of a voltage. For the discovery of this effect, B. D. Josephson was awarded the 1973 Nobel prize in physics [23]. The *Josephson effect* is now the building block of several superconductor technologies. In superconducting quantum interference devices (SQUIDs), the phase sensitivity of Josephson junctions are utilized in high resolution magnetic field detectors. Magnetoencephalography is an important example of the application of this technology, where SQUIDs are used to study the magnetic fields induced by activity in the human brain [24]. A more exotic application of Josephson junctions is the realization of quantum bits (qubits) for quantum information processing [25, 26]. As an example of the ongoing efforts in this field, the recently published Ref. [27] reports on the communication of two distant superconducting qubits.

1.2 Magnetoelectronics

Magnetoelectronic circuits make use of the quantum spin of electrons in addition to their charge. An important example is spin valves, where two ferromagnetic layers are separated by a thin normal-metal (F|N|F). In such devices, the resistance can increase by up to 200% when the configuration of the magnetizations of the two ferromagnetic layers changes from parallel to antiparallel. This phenomenon is known as *giant magnetoresistance* (GMR) [28, 29] in magnetic multilayers, and earned the discoverers A. Fert and P. Grünberg the 2007 Nobel prize in physics. GMR is the basis of the dominating technology used for read heads in hard disk drives.

The GMR effect can be understood as the result of spin-dependent scattering rates and density of states in the ferromagnets. When a current is passed through a ferromagnet, the resistivity will be smaller for electrons with their spin aligned along the magnetization direction of the ferromagnet than for electrons with their spin antiparallel to the magnetization. As a result, a current passed through a ferromagnet becomes spin polarized. On the other hand, the resistance of the spin polarized current flowing through the second F layer of a spin valve depends on the angle between the spin polarization and the magnetization. This gives the magnetization configuration-dependent resistance in the spin valve.

Magnetization dynamics in nanoscale ferromagnets is the subject of intensive investigation (see Ref. [30] and references within). When the magnetization of a ferromagnet is driven in precessional motion, electronic spins will be emitted by the ferromagnet into the surroundings. This effect is referred to as *spin pumping*, and is a way to induce spin current flow in nanoelectronic devices. Conversely, a spin current flowing into a ferromagnet can excite magnetization dynamics [31]. The possibility to manipulate magnetizations by this so-called *spin transfer torque* can provide write functionality in future magnetic random-access memory devices.

1.3 Superconductor|ferromagnet nanoelectronic circuits

As we have seen, nanoscale superconductor and ferromagnet devices display a variety of interesting effects, and provides new functionality in modern technology. In combination, the interplay of superconductivity and magnetism can be used to study the coherent transport and relaxation of spins, with potential applications for different areas of mesoscopic physics.

Ferromagnetic elements in nanoelectronic circuits can be used to create and control spin accumulations in non-magnetic materials. In this thesis, we have considered ferromagnet spin injection into superconductors. When the size of the superconductor is comparable to the superconducting coherence length, there are interesting effects following from the

interplay between superconducting order and the injected spin accumulation. For example, when substituting the spacer in the spin valve discussed above with a superconducting material (producing a F|S|F structure), a strong size- and temperature-dependence of the magnetization-dependent resistance can be observed. The spin polarized current flowing into the superconductor is inhibited by superconducting pairing which is only possible for the opposite-spin ordered electrons. This means that the length scale for penetration of the spin current into S is limited by the superconducting coherence length which for elemental superconductors like Al is $\xi \approx 125$ nm. Spin flow and relaxation in superconductors is studied for various structures in Chapter 3.

When a Cooper pair from a superconductor flows into a non-superconducting material, the quasiparticle pair thus transferred will be in a special quantum state. This state is characterized by phase coherence between the two quasiparticles and quantum entangled degrees of freedom. These properties have some very interesting potential applications if the quasiparticles can be individually manipulated. The process in which the electrons are transferred into two separate leads is known as *crossed or nonlocal Andreev reflection* and has received considerable interest since it is an inherent mesoscopic phenomenon and also because of the relevance for quantum information experiments. In Chapter 4 we discuss some aspects and models of crossed Andreev reflection. In Chapter 6 we consider the statistics of crossed Andreev reflection and related processes, and show how noise properties can reveal the quantum entanglement of Andreev reflected electrons.

Mesoscopic superconductor|ferromagnet structures display very rich physics, and many interesting effects that have not been mentioned above are currently under intensive investigation. One example is that the proximity effect can induce triplet superconducting correlations in the F parts of a system (see Refs. [32, 33, 34, 35] and references therein). This effect has been experimentally demonstrated, and can be utilized to produce superconducting π -junctions with possible application to qubits in quantum information science.

1.4 Outline

In Chapter 2 we introduce the formalisms and theoretical tools that are utilized. Then we discuss the motivations for each of the systems studied and summarize the research results in chapters according to the topic: In Chapter 3 we discuss transport equations for spin flow in superconductors, which is the focus of papers [1, 2, 3, 4]. Chapter 4 discusses crossed Andreev reflection, and summarizes the results obtained in papers [5] and [6] using the circuit theory of mesoscopic transport. In Chapter 5 we discuss some general aspects of quantum entanglement which is the focus of the popular-scientific paper [7]. Entanglement is an important concept in Chapter 6 where the full counting statistics results for the beamsplitters studied in papers [8] and [9] are summarized. Finally, I provide some personal thoughts on the outlook of my research and give my acknowledgements.

2 Theory toolbox

In this Chapter, we will describe the theoretical tools that are utilized for the calculations and introduce the notation used in this thesis. A full account of these techniques are beyond the scope of this text, but adequate reference is given to review articles.

We will first discuss the Usadel equation for Green functions in the Keldysh formalism, which allows us to determine the nonequilibrium transport properties of superconducting nanostructures. This formalism was extended and cast into the language of a finite-element circuit theory by Yu. V. Nazarov, and Section 2.2 gives a brief account of this technique. Subsequently, the circuit theory has been extended to allow calculations of full counting statistics. This is discussed in Section 2.3.

2.1 Quasiclassical theory of superconductivity

The quasiclassical theory of superconductivity was developed between 1950 and 1980 and has recently, due to advances in experimental physics, attained a lot of interest. This has resulted in several excellent reviews, see [36, 37, 38, 39, 40] and references therein. In this section, we will briefly reproduce the main results.

2.1.1 Eilenberger and Usadel equations

The Gor'kov equations [41] are a set of generalized Dyson equations for superconductors. These equations determine e.g. the retarded Green function¹

$$\hat{G}^R(\mathbf{r}_1, t_1; \mathbf{r}_2, t_2) = -i\Theta(t_1 - t_2)\bar{1}\hat{\tau}_3\langle[\psi(\mathbf{r}_1, t_1), \psi^\dagger(\mathbf{r}_2, t_2)]_-\rangle, \quad (2.1)$$

¹The (anti)commutator of A and B is denoted $[A, B]_{(+)-}$.

which is a matrix in $\text{spin} \otimes \text{Nambu}$ space (see Appendix A) and we have introduced the unit matrix in spin space $\hat{1}$, the Pauli matrix in particle-hole space $\hat{\tau}_n$, and the pseudo-spinor $\hat{\psi}^\dagger = (\psi_\uparrow^\dagger, \psi_\downarrow^\dagger, \psi_\uparrow, \psi_\downarrow)$ where ψ_σ is the field annihilation operator for spin σ . The angular brackets $\langle \dots \rangle$ denote quantum statistical averaging. The Gor'kov equations incorporate the BCS model and can in principle be used to describe most transport properties of nonequilibrium superconductors.

To solve the Gor'kov equations for a real system can be a formidable task, and the solutions often contain redundant information. A simplified equation was derived by Eilenberger [42] by applying what is known as the quasiclassical approximation. This approximation is valid when the characteristic length scales in the problem are large compared to interatomic distances, so that rapid oscillations of the Green function on the scale of the Fermi wavelength can be averaged out. It is then assumed that Green functions and self-energies depend weakly on the magnitude of the momentum, and are determined by their values on the Fermi surface. In this case, it is possible to perform an average over the kinetic energy to eliminate the dependence on the magnitude of the momentum, but keeping the dependence on the direction in the equation obtained by subtracting the Gor'kov equation with its conjugate. This approximation scheme can be incorporated conveniently after a Wigner transformation of the Gor'kov equations, which is basically a Fourier transform of the difference coordinates $\mathbf{r}_1 - \mathbf{r}_2$ and $t_1 - t_2$. The quasiclassical Green functions in the $\text{spin} \otimes \text{Nambu}$ matrix space can be written $\hat{G}(\mathbf{r}, t, \mathbf{p}_F, E)$ where $\mathbf{r} = (\mathbf{r}_1 + \mathbf{r}_2)/2$ and $t = (t_1 + t_2)/2$ are the center-of-mass position and time, \mathbf{p}_F is the momentum on the Fermi surface, and E the quasiparticle energy. The Wigner transformation also reduces the convolutions in the Gor'kov equation into Taylor series in derivatives with respect to center-of-mass coordinates and momentum. We will consider problems where short range oscillations can be neglected [43, 44], so it is possible to terminate these series after linear order in derivatives with respect to \mathbf{r} . This is known as the gradient approximation. The Eilenberger equation for the retarded Green function, derived under the above approximations, can in the stationary state be written

$$\left[(E + i0)\hat{\tau}_3 + i\frac{\mathbf{p}_F}{m} \cdot \hat{\boldsymbol{\partial}} - e\phi\hat{1} - \hat{\Delta} - \hat{\Sigma}, \hat{G}^R \right]_- = 0. \quad (2.2)$$

Here $\hat{\boldsymbol{\partial}} = \nabla\hat{1} - ie\mathbf{A}\hat{\tau}_3$ is the gauge invariant derivative, ϕ is the electromagnetic scalar potential, $\hat{\Delta} = \text{offdiag}(\Delta, -\Delta, \Delta^*, -\Delta^*)$ contains the superconducting order parameter and $\hat{\Sigma}$ is the quasiclassical self-energy in which we will include effects from elastic impurity scattering and spin-flip scattering. Mean-field theory for the BCS Hamiltonian determines the superconducting gap by a self-consistency relation in terms of the anomalous propagator contained in the off-diagonal matrix block of \hat{G}^R (see Eq. (2.5)). The anomalous propagator describes nonvanishing electron-hole correlations of the type $\langle \psi_\uparrow \psi_\downarrow \rangle$ that are the hallmark of superconductivity. For vanishing Δ , Eq. (2.2) reduces to the Boltzmann transport equation. An additional constraint on quasiclassical Green functions is the normalization condition

$$\hat{G}^R \hat{G}^R = \hat{1}. \quad (2.3)$$

The limit of strong elastic impurity scattering² (the dirty limit) is often the most experimentally relevant. In the Born approximation, the quasiclassical elastic impurity scattering self-energy becomes $\hat{\Sigma}_{\text{imp}} = \langle \hat{G}^{\text{R}} \rangle_{\Omega} / 2\tau$ where $\langle \dots \rangle_{\Omega}$ denotes angular averaging and τ is the elastic impurity scattering time [40]. To obtain the dirty limit, we expand the quasiclassical Green functions in spherical harmonics to first order, i.e. $\hat{G}^{\text{R}}(\mathbf{r}, \mathbf{p}_{\text{F}}, E) = \hat{G}^{\text{R}}(\mathbf{r}, p_{\text{F}}, E) + \mathbf{p}_{\text{F}} \cdot \hat{\mathbf{G}}^{\text{R}}(\mathbf{r}, \mathbf{p}_{\text{F}}, E)$. The equation that determines the dominating isotropic contribution (s -wave) $\hat{G}^{\text{R}}(\mathbf{r}, p_{\text{F}}, E)$ following from Eq. (2.2) becomes

$$D \left[\hat{\boldsymbol{\partial}}, \hat{G}^{\text{R}} \left[\hat{\boldsymbol{\partial}}, \hat{G}^{\text{R}} \right]_{-} \right]_{-} + \left[(E + i0)\hat{\tau}_3 - e\phi\hat{1} - \hat{\Delta} - \hat{\Sigma}, \hat{G}^{\text{R}} \right]_{-} = 0, \quad (2.4)$$

where $\hat{\Sigma}$ now denotes the remaining contributions to the self energy like e.g. spin flip scattering. This equation is known as the Usadel equation [45], which has been successfully applied to describe superconducting proximity effects and is the starting point for most of the calculations in this thesis. We now supply the self-consistency relation that determines the superconducting order parameter,³

$$\Delta(\mathbf{r}) = \frac{N_0\lambda}{2} \int_0^{E_{\text{D}}} dE \tanh\left(\frac{E}{2k_{\text{B}}T}\right) \text{Re} \left(\hat{G}^{\text{R}}(\mathbf{r}, p_{\text{F}}, E) \right)_{1,4}. \quad (2.5)$$

Here N_0 is the density of states at the Fermi level, λ is the effective electron-electron interaction parameter, T is the temperature and the integration is cut off at the Debye energy E_{D} . The quantities λ and E_{D} are determined by the microscopic mechanism that results in the effective electron-electron attraction in the BCS model. Inside a normal metal, the interaction parameter λ vanishes, but the anomalous propagator contained in \hat{G}^{R} can be nonzero because of boundary conditions to superconducting parts of the system. This gives rise to proximity effect.

Interfaces between different parts of a nanostructure can be atomically sharp and the sudden changes in the Green functions are thus not captured by the quasiclassical theory described above, which is only valid when properties of the system vary on length scales much larger than the Fermi wavelength. However, boundary conditions for the quasiclassical Green functions can be derived from scattering theory [46, 47], and allows practical calculations for heterostructures containing constrictions, interfaces and boundaries between different materials. For the Green functions in the dirty limit discussed above, the boundary conditions for a tunneling interface in the yz -plane between two regions 1 and 2 are

$$\sigma_1 \hat{G}_1 \frac{\partial \hat{G}_1}{\partial x} = \sigma_2 \frac{\partial \check{G}_2}{\partial x} = \frac{g}{2\mathcal{A}} [\check{G}_1, \check{G}_2]_{-}, \quad (2.6)$$

²We are considering the semiclassical regime where the mean free path l is much larger than the Fermi wavelength λ_{F} , but smaller than other relevant length-scales in the problem. Thus Anderson localization effects are disregarded

³The notation $(A)_{m,n}$ denotes the matrix element in the m -th row and n -th column of A .

where σ is the conductivity of the materials, g is the tunnel conductance and \mathcal{A} the cross section area.

The equilibrium properties of proximity superconducting systems can be determined by the equations discussed in this Section, and has been successfully applied to model experimental data. As an example, the normalized density of states is obtained from the retarded Green function

$$N(\mathbf{r}, E) = \text{Re} \left(\hat{G}^{\text{R}}(\mathbf{r}, p_{\text{F}}, E) \right)_{1,1}. \quad (2.7)$$

This relation can be used, e.g., to determine proximity induced suppression of the density of states in normal metals.⁴ Another important application is the evaluation of the critical temperature and field for superconducting heterostructures, where the properties of the superconductor are influenced by the environment in the so-called inverse proximity effect.

2.1.2 Keldysh Green functions

The construction of the equilibrium many-body Green functions introduced above involves the procedure of adiabatically turning interactions on from a noninteracting ground state at $t = -\infty$. Then, at times (t_1, t_2) the Heisenberg field operator averages in the Green functions are evaluated before the interactions are turned off adiabatically, recovering the noninteracting ground state at $t = \infty$ [48, 49]. This scheme allows calculation of linear response transport properties by the use of the Kubo formula. A critical assumption is that the states obtained by adiabatically switching interactions on and off are unique up to some phase factor. Out of equilibrium, this can break down as the quantum system can evolve into an unpredictable state that depends on the switching procedure as interactions are turned on and off, and in particular the final state can be different from the initial state.

In the Keldysh diagrammatic technique, the quantum system first evolves in the forward direction in time, and then the effect of turning on interactions is “unwound” by evolving the system in the backwards time direction [50]. The gain is that one avoids references to the state at $t = \infty$ so that quantum averages are calculated only with reference to the initial state at $t = -\infty$. The structure of the resulting theory is more complicated since field operators residing on both forward and backward branches of the Keldysh time evolution contour must be defined, leading to a doubling of the degrees of freedom.

Taking advantage of the internal symmetries of the theory, one can define nonequilibrium Green functions in Keldysh matrix space (denoted by $\tilde{}$ accents) where the elements are

⁴See <http://www-drecom.cea.fr/drecom/spec/Pres/Quantro/Qsite/archives/...preprints/AFM-STMPproximity.pdf> for some impressive applications of the theory to S|N|S systems.

linear combinations of averages from different parts of the Keldysh contour,

$$\check{G} = \begin{pmatrix} \hat{G}^R & \hat{G}^K \\ 0 & \hat{G}^A \end{pmatrix}; \quad \check{G}\check{G} = 1. \quad (2.8)$$

In this matrix space, superscripts denote Retarded, Keldysh, and Advanced Green functions. A diagrammatic theory can be formulated for the \check{G} matrix Green functions that has the same structure as the equilibrium diagrammatic technique. Thus we obtain Usadel equations for \check{G} that allow calculation of nonequilibrium transport effects. Moreover, the quasiclassical normalization condition of the Green function applies also in the Keldysh space, as indicated in (2.8). Generally, the Green functions \check{G}^R and \check{G}^A contain information about dispersion relations (spectral properties) in the system like e.g. the energy-dependent density of states, whereas the Keldysh Green function \check{G}^K describes the occupation of states in the system i.e. distribution functions. This facilitates a reduction of the problem into quantum kinetic equations as will be discussed in Chapter 3. An important advantage of this approach is that the resulting equations have the structure of continuity equations for the physical currents of e.g. charge and spin which allow straightforward interpretations.

2.2 Circuit theory

An important achievement in the study of nanostructures is the *circuit theory of mesoscopic transport*. This circuit theory can be formulated in much the same way as the circuit theory of conventional electronics, and incorporates not only the flow of charge, energy and spin in the system, but also describes quantum coherence effects.

By discretizing the Usadel equation for the matrix Green functions in Keldysh space, and deriving a very general boundary condition [see (2.9)], Nazarov was able to formulate a circuit theory that reduces the solution of a nonequilibrium transport problem into an exercise of applying a set of generalized “Kirchhoff’s rules” [51, 52] for a finite-element representation of the nanostructure under consideration. The theory has been extended to treat F|N [53] and S|F (see Sec. 2.2.3) heterostructures, and is reviewed in Ref. [54].

2.2.1 Finite element description

The first step in the circuit theory approach is to define the circuit in terms of reservoirs (voltage or current sources), connectors (contacts, interfaces), and nodes (islands or discrete lattice points of wires). The reservoirs are described by thermal equilibrium Green functions that depend on temperature (T) and voltage (V). A normal-metal terminal has quasiclassical Green function $\check{G}_N = \hat{\tau}_3 + (\hat{\tau}_3 h_L + h_T)(\hat{\tau}_1 + i\hat{\tau}_2)$, where we have introduced the charge- and energy-distribution functions that can be written

$h_T = 1 - f_{\text{FD}}(E) - f_{\text{FD}}(-E)$ and $h_L = -f_{\text{FD}}(E) + f_{\text{FD}}(-E)$ in terms of the Fermi-Dirac distribution function $f_{\text{FD}}([E - eV]/k_B T)$. The Green function of a conventional superconductor reservoir is given by $\hat{G}_S^{\text{R(A)}} = ([E \pm i0]\hat{\tau}_3 + \Delta i\hat{\tau}_2)/\Omega$, where $\Omega = \sqrt{(E \pm i0)^2 - \Delta^2}$, and $\hat{G}_S^{\text{K}} = \hat{G}_S^{\text{R}}\hat{h}_S - \hat{h}_S\hat{G}_S^{\text{A}}$ where $\hat{h}_S = \hat{\tau}_3 h_L + h_T$. Connectors will be described by their scattering transmission and reflection amplitudes, which gives the matrix current flow. The conservation of matrix current in the nodes will determine the node Green functions. This will be discussed in the next sections.

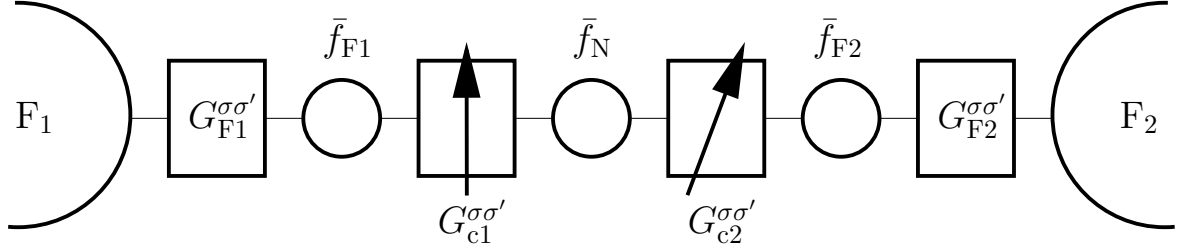


Figure 2.1: Circuit theory diagram for the angular magnetoresistance effect in a ferromagnetic heterostructure. Adapted from Ref. [55].

A complicated nanostructures is thus represented by a simple circuit theory diagram. As an example of such a system, we show in Figure 2.1 the equivalent circuit of a ferromagnetic spin valve [55] that exhibits the behaviour discussed in Chapter 1. Here, ferromagnetic reservoirs F_1 and F_2 are connected to the nanostructure by contacts (boxes) that are described by spin-dependent conductance parameters $G^{\sigma\sigma'}$ determined by the transmission eigenvalues. Associated with the nodes (circles) that represent the ferromagnetic layers and the normal-metal spacer are 2×2 distribution function matrices in spin space \bar{f} that parametrize the Green functions.

2.2.2 Matrix currents

Once the nanostructure under consideration has been defined in terms of its equivalent circuit, a set of generalized Kirchhoff's rules for each node will determine the unknown Green functions of the nodes. The conserved quantity for the quantum transport theory that we consider, are matrix currents \check{I} that depend on the properties of the connectors and the Green functions of the adjacent nodes or reservoirs. This current describes not only the particle flow, obtained from $\int dE \text{Tr} \check{\tau}_1 \hat{\tau}_3 \check{I}$, but also the flow of energy, spin, and coherence. The matrix current in a S|N heterostructure through a connector described by the set of transmission eigenvalues $\{T_k^{(n)}\}$ between a node with Green function \check{G}_c and another element with Green function \check{G}_n is [52]

$$\check{I}_n = -\frac{2e^2}{\pi\hbar} \sum_k T_k^{(n)} \frac{[\check{G}_n, \check{G}_c]_-}{4 + T_k^{(n)} ([\check{G}_n, \check{G}_c]_+ - 2)}. \quad (2.9)$$

A powerful feature of the circuit theory technique is that the general expression for the matrix current (2.9) can be used to model many different types of contacts. For e.g. tunnel junctions all transmission eigenvalues are small $T_k^{(n)} \ll 1$, and for a diffusive connector the transmission probability distribution has peaks at low and high probability, with few transport channels at intermediate transmission probability (bimodal distribution). [56].

The generalized Kirchhoff's rules state that conservation of matrix current at each energy should be imposed at each node,

$$\sum_n \check{I}_n + \check{I}_{\text{leakage}} = 0, \quad (2.10)$$

where the sum runs over all connectors to the node and we have included the possibility of a ‘‘coherence leakage’’ current which can generally be written $\check{I}_{\text{leakage}} = -ie^2 N_0 \mathcal{V}_c [\check{G}_c, \check{H}_c]_- / \hbar$ where N_0 is the density of states at the Fermi level, \mathcal{V}_c is the volume of the node, and \check{H}_c is the quasiclassical Hamiltonian that describes interactions inside the node. The leakage current can describe a variety of effects like dephasing of Andreev reflected electron-hole pairs due to mismatching wavevectors or spin-dependent reflection at interfaces, superconducting pairing, or spin-flip scattering.

The matrix current conservation equations for the circuit will determine the unknown Green functions of the nodes. When these have been obtained, we can extract the physical transport properties of the system from the matrix currents and Green functions.

2.2.3 Spin-active interfaces

Due to the noncommutativity of Green functions that describe superconducting correlations with the scattering matrix [57] describing a spin-active connector, the algebraic structure of the matrix current in S|F systems [58, 59, 60, 61] is much more complicated than the result for S|N interfaces (2.9). However, in the limit of a weakly polarizing tunnel barrier, a tractable expression was found in Ref. [62]. The spin-active connector is described by spin dependent transmission and reflection amplitudes $t_{k,\sigma}^n$ and $r_{k,\sigma}^n$ for particles incident on the interface n from the cavity side in channel k with spin σ . The matrix current \check{I}_n is

$$\check{I}_n = \left[\frac{g_n}{2} \check{G}_n + \frac{g_{\text{MR}n}}{4} [\mathbf{m}_n \cdot \bar{\boldsymbol{\tau}} \hat{\boldsymbol{\tau}}_3, \check{G}_n]_+ + i \frac{g_{\phi n}}{2} \mathbf{m}_n \cdot \bar{\boldsymbol{\tau}} \hat{\boldsymbol{\tau}}_3, \check{G}_c \right]_-. \quad (2.11)$$

Here, $g_n = g_Q \sum_{k,\sigma} |t_{k,\sigma}^n|^2$ is the tunnel conductance and $g_Q = e^2/h$ the conductance quantum. The unit vector \mathbf{m}_n points in the direction of the magnetization of the spin polarizing contact, $g_{\text{MR}n} = g_Q \sum_k (|t_{k,\uparrow}^n|^2 - |t_{k,\downarrow}^n|^2)$ is the conductance spin polarization, and $g_{\phi n} = 2g_Q \sum_k \text{Im} \{r_{k,\uparrow}^n r_{k,\downarrow}^{n*}\}$ induces spin-dependent phase shifts upon reflection at the interface.

2.3 Full counting statistics

The terminology *full counting statistics* (FCS) was adopted by Levitov and Lesovik in the context of mesoscopic electron transport, and refers to a “counting” of individual electrons into a certain lead in the system. A famous result due to Levitov and Lesovik is the probability distribution to transfer N charges between electronic reservoirs through a quantum channel of transmission probability T_k and applied bias voltage $eV \gg k_B T$ (shot noise limit) [63],

$$P_k(N; t_0) = \binom{N_{\text{at}}}{N} T_k^N (1 - T_k)^{N_{\text{at}} - N}. \quad (2.12)$$

Here, t_0 is the time interval for the electron counting and $N_{\text{at}} = 2t_0 eV/h$. For integer values of N_{at} this result can be interpreted as follows: Electrons attempt to traverse the channel N_{at} times, and for each attempt the probability for transmission is T_k and the probability to be reflected is $(1 - T_k)$. The probability distribution (2.12) is binomial, and the mean current becomes $I = eN_{\text{at}}T_k$. Going to the limit of small T_k and large N_{at} , the binomial distribution may be approximated by a Poisson distribution. In this limit, there is no temporal correlation between two subsequent electron transfers, and from (2.12) we obtain the Schottky formula for incoherent transport, $C_2 = 2eI$, for the current noise power defined as

$$C_2 = \frac{2e^2}{t_0} \langle (N - \langle N \rangle)^2 \rangle = \int_{-\infty}^{\infty} dt' \langle [\delta I(t'), \delta I(0)]_+ \rangle. \quad (2.13)$$

The Schottky result shows that a noise measurement gives access to the charge e of the discrete carriers responsible for the current. In the case of general T_k , the current noise following from (2.12) is $C_2 = 2eI(1 - T_k)$, i.e. a current noise measurement also provides information about the transmission probability of the quantum channel. This simple example illustrates how studies of noise and FCS can be used to understand the microscopic details of the electron transport, and that the noise properties of quantum transport reveals information about the transport which is not accessible from average current measurements.

Full counting statistics [63, 64] is a useful tool to compute currents and noise in a multi-terminal structure [65], and also provides the higher statistical moments that may become experimentally accessible in these systems [66]. Additionally, one can obtain information about the elementary charge transport processes by studying the probability distributions, as seen in the example of transport in a quantum channel above. An extension of the circuit theory discussed in Section 2.2 which facilitates calculation of FCS is reviewed in Refs. [67, 54]. Below, we will reproduce some of the main results that are used in Chapter 6.

The *cumulant generating function* (CGF) $\mathcal{S}(\{\chi_n\})$ of a multiterminal probability distribu-

tion is directly accessible by the Green function method, and is defined by the relations

$$e^{-\mathcal{S}(\{\chi_n\})} = \sum_{N_n} P(\{N_n\}; t_0) e^{-i \sum_n \chi_n N_n}$$

$$P(\{N_n\}; t_0) = \frac{1}{(2\pi)^M} \int_{-\pi}^{\pi} d^M \chi e^{-\mathcal{S}(\{\chi_n\}) + i \sum_n N_n \chi_n}. \quad (2.14)$$

Here, $M = \max(n)$ is the number of terminals, and $P(\{N_n\}; t_0)$ is the probability to transfer N_n electrons into terminal N_n in time t_0 . The CGF depends on the set of counting fields $\{\chi_n\}$ that are fictitious quantum fields coupled to the current operator at interfaces where we would like to count the particle flow. These can be embedded in the Green function at each terminal by the transformation

$$\check{G}_n \rightarrow e^{i\chi_n \tilde{\tau}_K/2} \check{G}_n e^{-i\chi_n \tilde{\tau}_K/2} \quad (2.15)$$

where $\tilde{\tau}_K = \hat{\tau}_3 \tilde{\tau}_1$. The CGF will be determined by the following relation [65]

$$\frac{ie}{t_0} \frac{\partial \mathcal{S}(\{\chi_n\})}{\partial \chi_n} = \int dE I_n(\{\chi_n\}), \quad (2.16)$$

where $I_n(\{\chi_n\})$ is the particle (counting) current through connector n in presence of the counting fields.

The cumulants of the transport probability distribution are obtained by successively differentiating the CGF with respect to the counting fields, and subsequently setting all $\chi_n = 0$. Specifically, we obtain the mean current into terminal n from

$$I_n = -\frac{ie}{t_0} \left. \frac{\partial \mathcal{S}(\{\chi\})}{\partial \chi_n} \right|_{\{\chi=0\}}. \quad (2.17)$$

The current noise power defined in (2.13) is given by

$$C_{m,n} = 2 \frac{e^2}{t_0} \left. \frac{\partial^2 \mathcal{S}(\{\chi\})}{\partial \chi_m \partial \chi_n} \right|_{\{\chi=0\}}, \quad (2.18)$$

where in the multiterminal structure, the autocorrelation noise at terminal n is given by $C_{n,n}$. When $m \neq n$, (2.18) gives the noise cross-correlations.

The higher order moments of the CGF $\partial^k \mathcal{S} / \partial \chi^k |_{\{\chi=0\}}$ give additional information about the probability distribution. For example, the $k = 3$ and $k = 4$ moments describe the skewness and sharpness of the probability distribution, respectively.

3 Spin injection into superconductors

Spin injection and manipulation in normal metals was recently demonstrated [68, 69] and has the prospect of providing new functionality in electronic devices. Fundamental insight into the transport processes relevant for such systems can be obtained by considering spin injection into superconductors. The energy-dependent spin-flip processes and superconducting proximity physics modifies the spin transport properties and provides information that would not be accessible in the normal state.

In papers [1, 2, 3] and [4] we have studied transport of spin polarized current in superconductors. Paper [2] was in part motivated by experimental studies on superconducting spin valves [70]. The formalism that was developed in papers [1] and [2] was successfully applied to model experimental data for spin injection into superconductors obtained by experimentalists at the Royal Institute of Technology in Stockholm, Sweden, and the results of this collaboration is reported in [3]. Paper [4] was motivated by a recent experimental study of magnetization dynamics in F|S bilayers [71], which was modeled by our theory of energy-dependent spin pumping into superconductors [4].

In Section 3.1, we will outline the formalism and numerical technique developed in papers [1, 2, 3, 4], and describe some properties of the systems that have been studied. Finally, the results in papers [1, 2, 3] and [4] are summarized in Sections 3.2 and 3.3, respectively.

3.1 Quantum kinetic equations

From the field theory of superconductors introduced in Chapter 2, we derive the Usadel equation for Green functions in spin \otimes Nambu \otimes Keldysh space. This equation describes the flow not only of charge and energy, but also the spin polarized flow. The algebraic structure of the 8×8 matrix equations makes practical calculations difficult, and in this section we will obtain a reduced description in terms of quantum kinetic equations. We will include

spin-flip effects, and these interactions are discussed in Section 3.1.1. We will use the same notation as Ref. [72].

3.1.1 Spin-flip scattering

The “dirty limit” was introduced in Section 2.1.1. Assuming a dominant contribution to the self-energy from elastic impurity scattering and employing the Born approximation, we obtained the Usadel equation for the isotropic part of the quasiclassical Green function $\check{G}(\mathbf{r}, E)$. Another type of impurity interaction is spin-flip scattering, in which the spin of a conduction electron is randomized. This interaction is significant in studies of spin transport, and causes spin polarization decay of a spin current injected into a nonmagnetic material.

We have considered two different types of spin-flip scattering and the interplay with superconducting correlations, spin-flip by interaction with magnetic impurities and spin-orbit interaction with nonmagnetic impurities. Due to quantum interference effects, the energy-dependent spin-flip scattering rate and the effect on the spectral properties of the superconductor associated with these interactions differ below T_c . This fact can be understood from the symmetry of the spin-flip Hamiltonians under time-reversal [73]. Cooper pairs consist of opposite spin electron and hole quasiparticles which are related by time-reversal, and therefore the Cooper pairs have time-reversal symmetry. A spin-flip Hamiltonian that respects this symmetry is not pair-breaking. Moreover, the spin-flip relaxation rate of quasiparticles in the superconducting state will be modified by quantum interference effects. When the spin-flip Hamiltonian has time-reversal symmetry, the so-called type I BCS coherence factor modifies the spin-flip rate in the superconducting state [13, 74]. When the spin-flip Hamiltonian breaks time-reversal symmetry, we instead obtain a type II BCS coherence factor. An important difference between the type I and type II coherence factors is the energy-dependence at energy close to Δ . The type I BCS coherence factor does not modify the spin-flip rate significantly at $E > \Delta$, whereas the type II BCS coherence factor diverges as $E \rightarrow \Delta$. This has important consequences which we have studied in papers [2, 3] and [4].

Magnetic impurities

In the ferromagnet|superconductor heterostructures that we aim to describe, we expect that magnetic impurity atoms will be introduced to the superconductor in the fabrication process. These impurities result in localized magnetic moments inside the superconductor, which can interact with the spin of conduction electrons. The Hamiltonian that describes

this interaction is

$$H_m = \sum_{\sigma\sigma'} \int d\mathbf{r} \psi_{\sigma}^{\dagger}(\mathbf{r}) (\bar{\boldsymbol{\tau}} \cdot \mathbf{S}(\mathbf{r}))_{\sigma\sigma'} V_m(\mathbf{r}) \psi_{\sigma'}(\mathbf{r}), \quad (3.1)$$

where \mathbf{S} is the impurity spin operator and V_m the magnetic impurity interaction potential. Spin operators are odd under time-reversal, $\mathcal{T}\bar{\boldsymbol{\tau}}_n\mathcal{T}^{-1} = -\bar{\boldsymbol{\tau}}_n$, where \mathcal{T} is the time-reversal symmetry operator. Therefore, H_m is odd under time-reversal and we expect the type II BCS coherence factor.

The BCS state renormalization of the spin-flip rate following from H_m can be found by introducing the Bogoliubov transformation of the field operators ψ_{σ} , and using the Fermi golden rule [11, 13]. The spin-flip transition rate then becomes

$$\alpha_s = \frac{2\pi}{\hbar} |T_m|^2 N_0^2 \int_{\Delta}^{\infty} dE \frac{E^2 + \Delta^2}{E^2 - \Delta^2} (f_{\uparrow}(E) - f_{\downarrow}(E)), \quad (3.2)$$

where $|T_m|^2$ is the energy independent part of the matrix element for the interaction. The integrand in (3.2) diverges at $E = \Delta$, so that the spin-flip rate for quasiparticles injected into the superconductor at $E \gtrsim \Delta$ is much larger than in the normal state.

The contribution from H_m to the quasiclassical self-energy in (2.4) is found employing the Born approximation as in the case of elastic impurity scattering. Assuming that the spin configuration of the impurities is random, the leading contribution becomes

$$\check{\Sigma}_m(\mathbf{r}, E) = -\frac{i}{8\tau_m} \hat{\boldsymbol{\alpha}} \check{G}(\mathbf{r}, E) \hat{\boldsymbol{\alpha}}, \quad (3.3)$$

where $\hat{\boldsymbol{\alpha}}$ is a vector of 4×4 matrices in spin \otimes Nambu space $\hat{\boldsymbol{\alpha}} = \text{diag}(\bar{\boldsymbol{\tau}}, \bar{\boldsymbol{\tau}}^T)$, and the spin-flip relaxation time is $\tau_m^{-1} = 8\pi n_m N_0 S(S+1) |v_m|^2 / 3$. This relaxation time depends on the magnetic impurity concentration n_m , the Fourier transformed spin-flip impurity potential v_m and the impurity spin quantum number S . For the elemental superconductors we have studied, this timescale is usually $\tau_m \sim 100$ ps [3] which is consistent with magnetic impurity concentrations of the order 0.01 % of the atoms [75].

Spin-orbit coupling

The relativistic interaction of the spin with the electrical potential of nonmagnetic impurities through spin-orbit coupling can induce spin-flip scattering. The spin-orbit interaction Hamiltonian is

$$H_{\text{so}} = \frac{\gamma}{2} \sum_{\sigma'\sigma} \int d\mathbf{r} \psi_{\sigma'}^{\dagger} \{ (\bar{\boldsymbol{\tau}} \times \nabla V_{\text{imp}})_{\sigma'\sigma} \cdot \mathbf{p} \} \psi_{\sigma} + \text{H.c.}, \quad (3.4)$$

where γ is the interaction strength, V_{imp} the nonmagnetic impurity scattering potential, \mathbf{p} the momentum operator and H.c. denotes the Hermitian conjugate operator. The

momentum operator is odd under time reversal, $\mathcal{T}\mathbf{p}\mathcal{T}^{-1} = -\mathbf{p}$. The operator in (3.4) is therefore time-reversal symmetric,

$$\mathcal{T}\bar{\boldsymbol{\tau}} \cdot (\nabla V_{\text{imp}} \times \mathbf{p}) \mathcal{T}^{-1} = \bar{\boldsymbol{\tau}} \cdot (\nabla V_{\text{imp}} \times \mathbf{p}). \quad (3.5)$$

This shows that H_{so} is time-reversal symmetric, and thus the coherence factor for this interaction is type I. Therefore, we do not expect H_{so} to give pair-breaking perturbations in the superconducting state.

Using the Bogoliubov transformation and the Fermi golden rule as above, the net spin-flip transition rate becomes

$$\alpha_s = \frac{2\pi}{\hbar} |T_{\text{so}}|^2 N_0^2 \int_{\Delta}^{\infty} (f_{\uparrow}(E) - f_{\downarrow}(E)) dE, \quad (3.6)$$

where $|T_{\text{so}}|^2$ is the energy independent part of the matrix element. In contrast to the case of magnetic impurity spin-flip scattering (3.2), there is no divergence in the integral for energies close to the gap. Therefore, the spin-flip scattering rate by spin-orbit coupling is different in the superconducting state than the spin-flip rate by interaction with magnetic impurities, even if the normal-state transition rates are equal.

In the Born approximation, the spin-flip contribution from the spin-orbit interaction H_{so} to the quasiclassical self-energy becomes

$$\check{\Sigma}_{\text{so}}(\mathbf{r}, E) = -\frac{i}{8\tau_{\text{so}}} \hat{\boldsymbol{\alpha}} \hat{\tau}_3 \check{G}(\mathbf{r}, E) \hat{\tau}_3 \hat{\boldsymbol{\alpha}}, \quad (3.7)$$

where we have defined the spin-orbit scattering time $\tau_{\text{so}}^{-1} = 8\gamma^2 p_{\text{F}}^4 / 9\tau$. Here, τ is the elastic scattering time. The different Nambu-space matrix structure of $\check{\Sigma}_{\text{so}}$ and $\check{\Sigma}_{\text{m}}$ takes into account the difference in time-reversal properties and its effect on superconductivity.

3.1.2 Transport theory

We will now introduce a parametrization of the Green function that allows us to reduce the complexity of the matrix equations. The parametrization takes into account the internal symmetries of the theory and the normalization condition. We then obtain simplified scalar equations from the Usadel equation.

Parametrization of \hat{G}^{R}

One possible representation of the retarded Green function that respects the normalization condition (2.3) is [38]

$$\hat{G}^{\text{R}} = \begin{pmatrix} \bar{1} \cosh(\theta) & i\bar{\tau}_2 \sinh(\theta) e^{i\chi} \\ i\bar{\tau}_2 \sinh(\theta) e^{-i\chi} & -\bar{1} \cosh(\theta) \end{pmatrix}, \quad (3.8)$$

where we have introduced the complex functions $\theta(\mathbf{r}, E)$ and $\chi(\mathbf{r}, E)$. The symmetries of the superconducting retarded Green function implies that $\theta^*(\mathbf{r}, -E) = -\theta(\mathbf{r}, E)$ and $\chi^*(\mathbf{r}, -E) = \chi(\mathbf{r}, E)$. For systems with non-collinear magnetizations, off-diagonal structure in the diagonal blocks of \hat{G}^R would have to be taken into account. Moreover, the ansatz (3.8) has the symmetry of singlet superconductivity and does not describe triplet superconducting correlations. From (3.8) the corresponding parametrization of the advanced Green function is found using the symmetry $\hat{G}^A = -(\hat{\tau}_3 \hat{G}^R \hat{\tau}_3)^\dagger$.

Two independent equations that determine θ and χ are obtained from the retarded part of the Usadel equation. The first relation is

$$\hbar D \nabla^2 \theta + 2iE \sinh(\theta) - 2i|\Delta| \cosh(\theta) - \hbar \left(\frac{D}{2} (\nabla \chi - 2e\mathbf{A})^2 + \frac{3}{4\tau_m} \right) \sinh(2\theta) = 0, \quad (3.9a)$$

and defining the spectral supercurrent density $\mathbf{j}_E = D(\nabla \chi - 2e\mathbf{A}) \sinh^2(\theta)$,

$$\nabla \cdot \mathbf{j}_E = 0. \quad (3.9b)$$

These equations should be solved together with the self-consistency relation (3.14) to be discussed below. The solution for θ and χ determine all spectral properties like e.g. the local superconducting order parameter $\Delta(\mathbf{r})$, and the density of states. For vanishing superconducting correlations, these equations give $\theta = 0$ which is the solution for a normal-metal reservoir. The spin-flip term proportional to τ_m^{-1} describes the pair-breaking effect of magnetic impurities [76].

Let us now consider boundary conditions for the differential equations (3.9) at interfaces to normal-metal or superconducting reservoirs. At interfaces with good, metallic contact between the adjacent materials, the interface resistance can in some cases be disregarded. At such boundaries, the functions θ and χ are continuous. At the interface to a superconducting reservoir, the boundary conditions then become

$$\theta = \text{Arctanh} \left(\frac{\Delta_0}{E} \right); \quad \chi = \varphi_0, \quad (3.10)$$

where Δ_0 is the energy gap and φ_0 the phase of the superconducting reservoir. At the interface to normal reservoir, we have that $\theta = 0$ and χ can be arbitrary. When the interface resistance is significant, equations following from (2.9) determine boundary conditions for θ and χ .

Parametrization of \hat{G}^K

A representation of the Keldysh block in the Green function \check{G} that satisfies the normalization (2.8) is

$$\hat{G}^K = \hat{G}^R \hat{h} - \hat{h} \hat{G}^A, \quad (3.11)$$

where \hat{h} will be a diagonal matrix determined by the distribution functions in the system. We represent this matrix by the following decomposition,

$$\hat{h} = h_L + \bar{\tau}_3 h_{LS} + \hat{\tau}_3 h_T + \bar{\tau}_3 \hat{\tau}_3 h_{TS}. \quad (3.12)$$

The notation L,T refers to ‘‘longitudinal’’ and ‘‘transverse’’ changes of Δ in the complex plane and stems from Ref. [77]. However, we will refer to the h_L and h_T components as energy- and charge-distribution functions for electrons and holes. The spin-resolved distribution functions h_{LS} and h_{TS} describe spin-energy and spin-charge distributions respectively. To illustrate these features, we express the distribution functions in terms of the conventional, spin resolved electron distribution functions $f_\sigma(E)$,

$$\begin{aligned} h_L &= - [f_\uparrow(E) + f_\downarrow(E) - f_\uparrow(-E) - f_\downarrow(-E)] / 2, \\ h_T &= 1 - [f_\uparrow(E) + f_\downarrow(E) + f_\uparrow(-E) + f_\downarrow(-E)] / 2, \\ h_{LS} &= - [f_\uparrow(E) - f_\downarrow(E) - f_\uparrow(-E) + f_\downarrow(-E)] / 2, \\ h_{TS} &= - [f_\uparrow(E) - f_\downarrow(E) + f_\uparrow(-E) - f_\downarrow(-E)] / 2. \end{aligned} \quad (3.13)$$

The L-components are odd as function of energy, and the T-components are even. In equilibrium, only the L-component is nonzero, $h_L^{(0)} = \tanh(E/2k_B T)$.

Self-consistency relation

The self-consistency relation, given in (2.5) for the equilibrium case, will be modified under nonequilibrium conditions [78, 79]. This is described by the Keldysh Green function, which depends on the nonequilibrium distributions introduced above. It is convenient to choose a gauge where the superconducting order parameter is a real number. This is possible when there is only one superconducting reservoir in the system, such that Josephson effects can be disregarded, and more generally through a gauge transformation of the electromagnetic potentials and field operators. In such a gauge, supercurrents and the chemical potential of Cooper pairs are described by contributions in the vector potential \mathbf{A} and the electromagnetic potential ϕ [36]. When Δ is real, inspection of the self-consistency relation reveals that we can choose $\chi = 0$ in (3.8) and the resulting self-consistency relation becomes

$$\Delta(\mathbf{r}) = \frac{1}{2} \text{sgn}(\Delta_0) N_0 \lambda \int_0^{E_D} dE h_L(\mathbf{r}, E) \text{Re} \sinh[\theta(\mathbf{r}, E)], \quad (3.14)$$

where the factor $\text{sgn}(\Delta_0)$ is determined by boundary conditions at superconducting reservoirs. A purely imaginary contribution to (3.14) has been neglected as a consequence of charge conservation. This condition follows from the continuity equation for the charge, which must be supplemented by corrections beyond the quasiclassical approximation far from equilibrium [36].

Kinetic equations

Generalizing the definition of the quantum mechanical current operator, we construct a matrix current in terms of the isotropic Green functions, $\hat{\mathbf{j}} = D\check{G}[\hat{\boldsymbol{\theta}}, \check{G}]_-$. The current flow of interest is obtained from this matrix by multiplying with a suitable matrix and taking the trace. We obtain the spectral current components associated with the h distributions (3.13) from the Keldysh matrix block of $\hat{\mathbf{j}}$ (upper right block, see (2.8)), e.g. $\mathbf{j}_T = \text{Tr} \hat{\tau}_3 \hat{\mathbf{j}}^K/4$ and $\mathbf{j}_{TS} = \text{Tr} \hat{\tau}_3 \hat{\tau}_3 \hat{\mathbf{j}}^K/4$. In terms of the distributions and parametrization functions θ and χ that determine the Green function, the currents become

$$\mathbf{j}_L = -D_L \nabla h_L + \text{Im} \mathbf{j}_E h_T, \quad (3.15a)$$

$$\mathbf{j}_T = -D_T \nabla h_T + \text{Im} \mathbf{j}_E h_L, \quad (3.15b)$$

$$\mathbf{j}_{LS} = -D_T \nabla h_{LS} + \text{Im} \mathbf{j}_E h_{TS}, \quad (3.15c)$$

$$\mathbf{j}_{TS} = -D_L \nabla h_{TS} + \text{Im} \mathbf{j}_E h_{LS}. \quad (3.15d)$$

Here, we have defined generalized diffusion coefficients that depend on position and energy,

$$D_L = D [(\text{Re} \cosh(\theta))^2 - (\text{Re} \sinh(\theta))^2], \quad (3.16a)$$

$$D_T = D [(\text{Re} \cosh(\theta))^2 + (\text{Im} \sinh(\theta))^2]. \quad (3.16b)$$

The terms in (3.15) proportional to gradients in the distributions describe current carried by quasiparticles, and the terms proportional to \mathbf{j}_E describe the supercurrent contributions. From the current components defined above, we can obtain the total charge (spin-charge) current from $\mathbf{I}_{\text{charge}(\text{spin})}(\mathbf{r}) = -eAN_0 \int_{-\infty}^{\infty} dE \mathbf{j}_{T(TS)}/2$. The energy (spin-energy) current is obtained from $\mathbf{I}_{\text{energy}(\text{spin})}(\mathbf{r}) = -eAN_0 \int_{-\infty}^{\infty} dE E \mathbf{j}_{L(LS)}/2$.

The Keldysh matrix block of the Usadel equation gives four coupled transport equations that determine the distribution functions (3.13). These equations describe the diffusive transport of charge, energy and spin, and can be presented like continuity equations,

$$\nabla \cdot \mathbf{j}_L = 0, \quad (3.17a)$$

$$\nabla \cdot \mathbf{j}_T = -2|\Delta| \alpha_{TT} h_T, \quad (3.17b)$$

$$\nabla \cdot \mathbf{j}_{LS} = - \left(2|\Delta| \alpha_{TT} + \frac{\alpha_{LSLS}^m}{\tau_m} + \frac{\alpha_{LSLS}^{\text{so}}}{\tau_{\text{so}}} \right) h_{LS}, \quad (3.17c)$$

$$\nabla \cdot \mathbf{j}_{TS} = - \left(\frac{\alpha_{TSTS}^m}{\tau_m} + \frac{\alpha_{TSTS}^{\text{so}}}{\tau_{\text{so}}} \right) h_{TS}. \quad (3.17d)$$

where we have defined renormalization factors in terms of $\theta(\mathbf{r}, E)$,

$$\alpha_{TT} = \text{Im} \sinh(\theta), \quad (3.18a)$$

$$\alpha_{LSLS}^m = [\text{Re} \cosh(\theta)]^2 - [\text{Im} \sinh(\theta)]^2, \quad (3.18b)$$

$$\alpha_{TSTS}^m = [\text{Re} \cosh(\theta)]^2 + [\text{Re} \sinh(\theta)]^2, \quad (3.18c)$$

$$\alpha_{LSLS}^{\text{so}} = [\text{Re} \cosh(\theta)]^2 + [\text{Im} \sinh(\theta)]^2, \quad (3.18d)$$

$$\alpha_{TSTS}^{\text{so}} = [\text{Re} \cosh(\theta)]^2 - [\text{Re} \sinh(\theta)]^2. \quad (3.18e)$$

The equation for the \mathbf{j}_L component (3.17a) describes the conservation of energy at each energy E for the elastic transport we are considering. The terms in (3.17b) and (3.17c) proportional to Δ describe the effect of superconducting pairing that converts quasiparticle current into supercurrent. Charge conservation in (3.17b) far from equilibrium is ensured by additional terms beyond the quasiclassical approximation that are not included here, see the discussion in Ref. [36]. Spin-flip scattering leads to the “sink-terms” in (3.17c) and (3.17d). Note that spin-flip scattering due to magnetic impurities and spin-orbit coupling are renormalized by different factors α^m and α^{so} in the superconducting state, in correspondence with the results of Section 3.1.1.

Linear response

When deviation from equilibrium is small, e.g. when the applied bias in the system is smaller than relevant energy scales like Δ , we can linearize the equations above. The equations following from the retarded part of the Usadel equation (3.9) then decouple from the kinetic equations (3.17) since the perturbations on the system from current flow are small. Moreover, the deviation from equilibrium in the energy distribution function $h_L - h_L^{(0)}$ is of second order so that the self-consistency relation (3.14) reduces to the equilibrium result (2.5). The resulting equations describe the first order nonequilibrium contributions to the distribution functions, and spectral properties are determined by their equilibrium values.

3.1.3 Numerical solution of the Usadel equation

A numerical code to solve the Usadel equations self-consistently has been developed for the spin and charge flow studies in papers [2] and [4]. The code benefits from several routines in the NAG C library.¹ The self-consistency relation is taken into account by an iterative procedure that can be summarized with the following algorithm [38],

1. Start with a given $\Delta(\mathbf{r})$ and obtain $\theta(\mathbf{r})$, $\chi(\mathbf{r})$ from equilibrium theory (3.10)
2. With $\theta(\mathbf{r})$, $\chi(\mathbf{r})$ as ansatz to differential equations solver, solve the retarded part of the Usadel equation (3.9) to obtain new solution $\theta'(\mathbf{r})$, $\chi'(\mathbf{r})$
3. Calculate spectral properties in kinetic equations (3.16) and (3.18) from new solution $\theta'(\mathbf{r})$, $\chi'(\mathbf{r})$
4. Solve the kinetic equations (3.17) and obtain distribution functions (3.13)
5. Calculate new $\Delta'(\mathbf{r})$ using (3.14)

¹<http://www.nag.co.uk/numeric/CL/CLdescription.asp>

6. If new (primed) solutions differ from ansatz, iterate from step 2 using $\theta'(\mathbf{r})$, $\chi'(\mathbf{r})$ and $\Delta'(\mathbf{r})$ as input

In linear response, the spectral properties are independent of the nonequilibrium contribution to the distribution functions as discussed above. This simplifies the iteration procedure since step 4 can be performed independently after self-consistency has been achieved. The nonequilibrium distribution functions are in this case calculated using the self-consistent equilibrium solutions for $\theta(\mathbf{r})$, $\chi(\mathbf{r})$ and $\Delta(\mathbf{r})$.

3.1.4 Gapless superconductivity

The superconducting order parameter and energy gap are two different concepts [80]. The energy gap can be observed e.g. in the vanishing low-energy density of states in large, bulk superconductors. However, in mesoscopic superconductors containing magnetic impurities or suffering from the inverse proximity effect, there is a finite density of states even at very low temperature. Still, the superconducting order parameter sets the energy scale for basic features of superconductivity like, e.g., Meissner effect and vanishing electrical resistance. Such systems are referred to as gapless superconductors. In a gapless superconductor, electrons in quasiparticle states coexist with superconducting condensate at low energy due to pair-breaking perturbations.

The superconducting systems considered in this chapter are gapless either due to the inverse proximity effect, presence of magnetic impurities, or both. Some features of a gapless Al superconductor sandwiched between a strong ferromagnet (F) at $x = 0$ and a normal metal reservoir (R) at $x = L = 1.7 \mu\text{m}$ is shown in Figure 3.1. The main panel shows the superconducting order parameter given by (2.5) normalized to the bulk, zero-temperature superconducting gap Δ_0 . The boundary conditions used in the calculation are as follows. At the F|S interface the superconducting order parameter is completely suppressed. This boundary condition was used in paper [4], and is due to the large exchange energy in F and the pair-breaking effect of spin-dependent interface scattering. At the S|R interface, partial suppression of $\Delta(x)$ follows from the boundary condition (2.6). We see that the order parameter recovers to values close to Δ_0 deep inside S over a length scale given by ξ . The inset shows the energy- and position-dependent density of states given by (2.7) which is finite even at very low energy. The superconducting order parameter shown in the main panel sets the energy scale for the peak in the density of states.

Renormalization factors for the spin-dependent transport properties in the superconducting state was introduced in Section 3.1 in terms of the effective spin-charge current diffusion coefficient D_L , and the renormalization factors α^{m} and α^{so} for spin-flip scattering by magnetic impurities and spin-orbit coupling. The energy-dependence of these quantities in a gapped BCS state was discussed in Section 3.1.1, and is studied in paper [1]. Here, we will consider the spatial evolution and energy-dependence of these transport properties in the

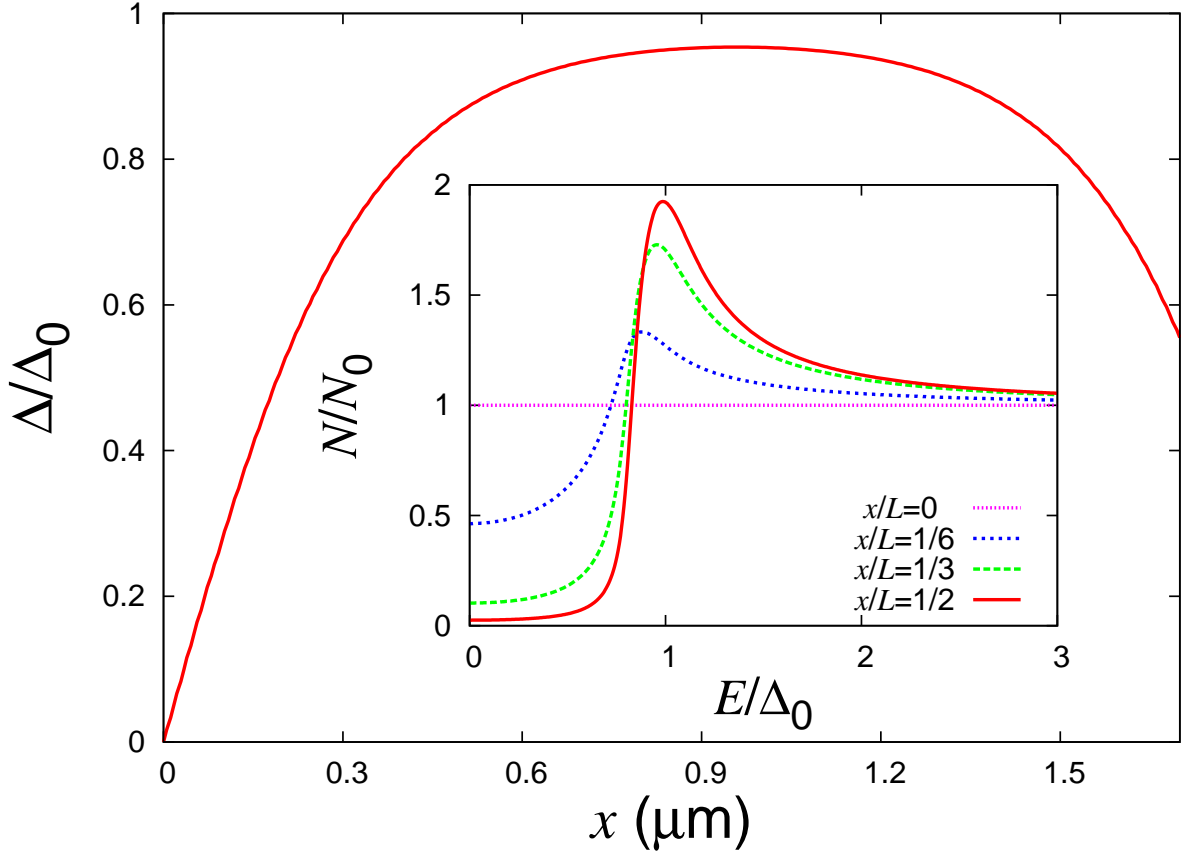


Figure 3.1: Main panel: Spatially dependent superconducting order parameter in a F|S|R trilayer. The S layer is Al with bulk critical temperature $T_c = 1.26$ K and superconducting gap at $T = 0$, $\Delta_0 = 192 \mu\text{eV}$. The length of S is $L = 1.7 \mu\text{m}$. Inset: Density of states in S at different positions x/L .

gapless superconductor discussed above where spin transport below Δ is possible.

Comparison of the renormalization factors $\alpha_{\text{TSTS}}^{\text{m}}$ and $\alpha_{\text{TSTS}}^{\text{so}}$ in Figure 3.2 a) and b) shows that for quasiparticles with energy close to Δ , the spin-flip rate differs dramatically when spin-flip is induced by magnetic impurities or spin-orbit coupling. This will be discussed in more detail in Section 3.3. By comparing panels b) and d) with regard to the diffusion coefficients in the expressions for the spin-charge current (3.15d) and the usual charge current (3.15b), we see that a superconductor is a low carrier system for spin but not for charge. Some consequences of this will be discussed in Section 3.2.

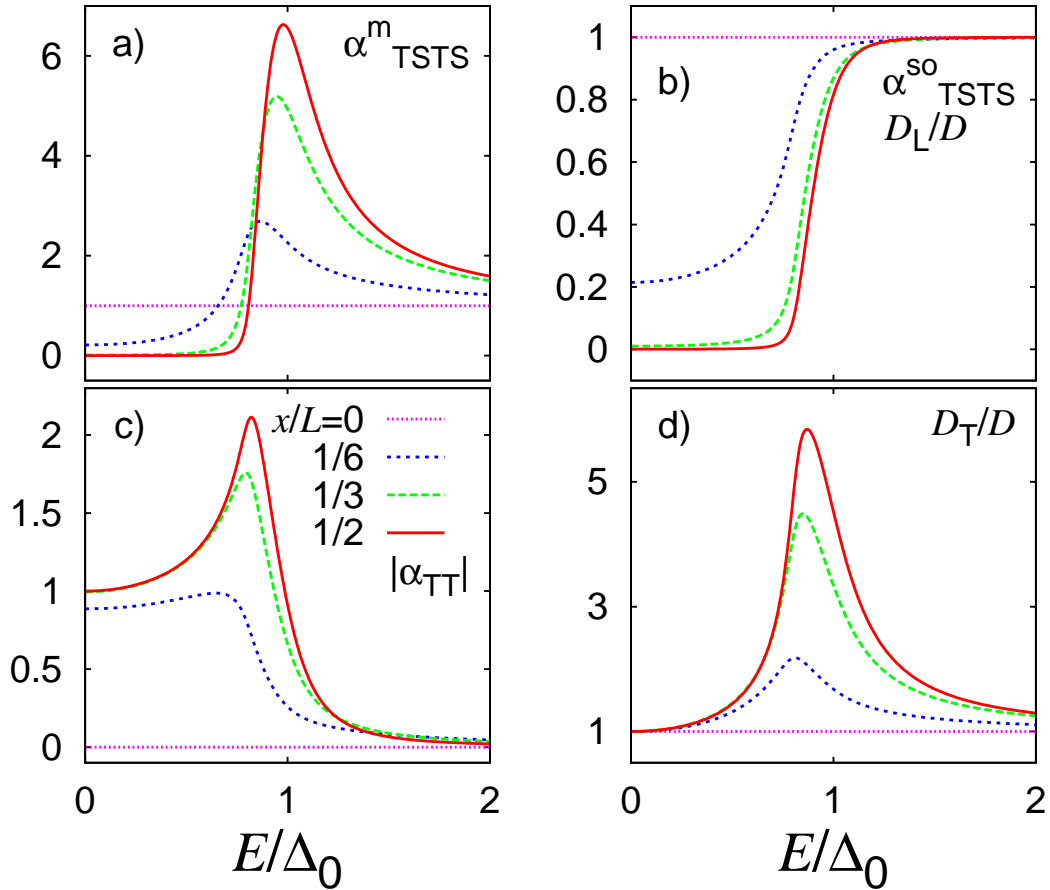


Figure 3.2: Energy- and position-dependent renormalization factors for the transport properties of the superconducting system considered in Fig. 3.1. Note that the ordinate scale differs in all plots. Key in c) shows position in S and applies to all panels. a) Renormalization factor for spin-flip scattering by magnetic impurities, see (3.18c). b) Renormalization factor for spin-flip scattering induced by spin-orbit coupling, see (3.18e). This factor coincides with the renormalization for the spin-charge current diffusion coefficient, see (3.16a). c) Superconducting pairing strength, see (3.17b). d) Renormalization of the charge current diffusion coefficient, see (3.16b).

3.2 Spin polarized current injection

The theory of spin transport in superconductors introduced in Section 3.1 was reported in papers [1] and [2]. Using suitable subsets of this formalism, we have shown in papers [1, 2] and [3] how superconducting correlations determine the transport in systems where spin currents are injected into superconductors. In this section we will summarize some of these results.

3.2.1 Gapped BCS superconductor

In paper [1] we considered the spectral properties and renormalization factors of a gapped BCS superconductor. To demonstrate the effect of the energy-dependent renormalization of spin-flip scattering from magnetic impurities (3.18c), we proposed a device where a bias-controlled spin-accumulation generated by two ferromagnets with opposite polarization could flow into a superconductor. Effects from the spin-flip renormalization is measurable by a magnetization-dependent voltage detection scheme. The measured spin signal shows a temperature- and bias-dependent spin-accumulation along a superconducting nanowire following from the energy-dependent renormalization.

3.2.2 F|S|F spin valves

In paper [2] we used the spin-transport formalism in the linear response to study the magnetoresistance of F|S|F spin valves. We calculated the spectral properties self-consistently using realistic material parameters. Our results agree qualitatively with experimental results in Ref. [70], but in the experiment the materials considered were Py and Nb as opposed to Co and Al in our model. The Py|Nb interface resistance probably contributes substantially to the magnetoresistance, and since boundary conditions for such spin-active interfaces are generally not known, modeling of the experimental system is complicated.

When a bias is applied on the F|S|F structure, spin-polarized quasiparticles are injected into the superconducting layer. Due to the superconducting pairing potential, the charge-current component (\mathbf{j}_T) will be converted into supercurrent inside S. This conversion of currents is governed by the renormalization factor α_{TT} which is shown in Figure 3.2 panel c). Upon exiting S, the supercurrent is converted back into quasiparticle current. This conversion process is shown in Figure 3.3. In this Figure we have also indicated the level of the spatially constant quasiparticle charge current in the normal state. The total resistance of the structure in the superconducting state is lower due to the dissipationless flow of the supercurrent.

Due to the ferromagnet spin-dependent conductivity, the current flowing through the F

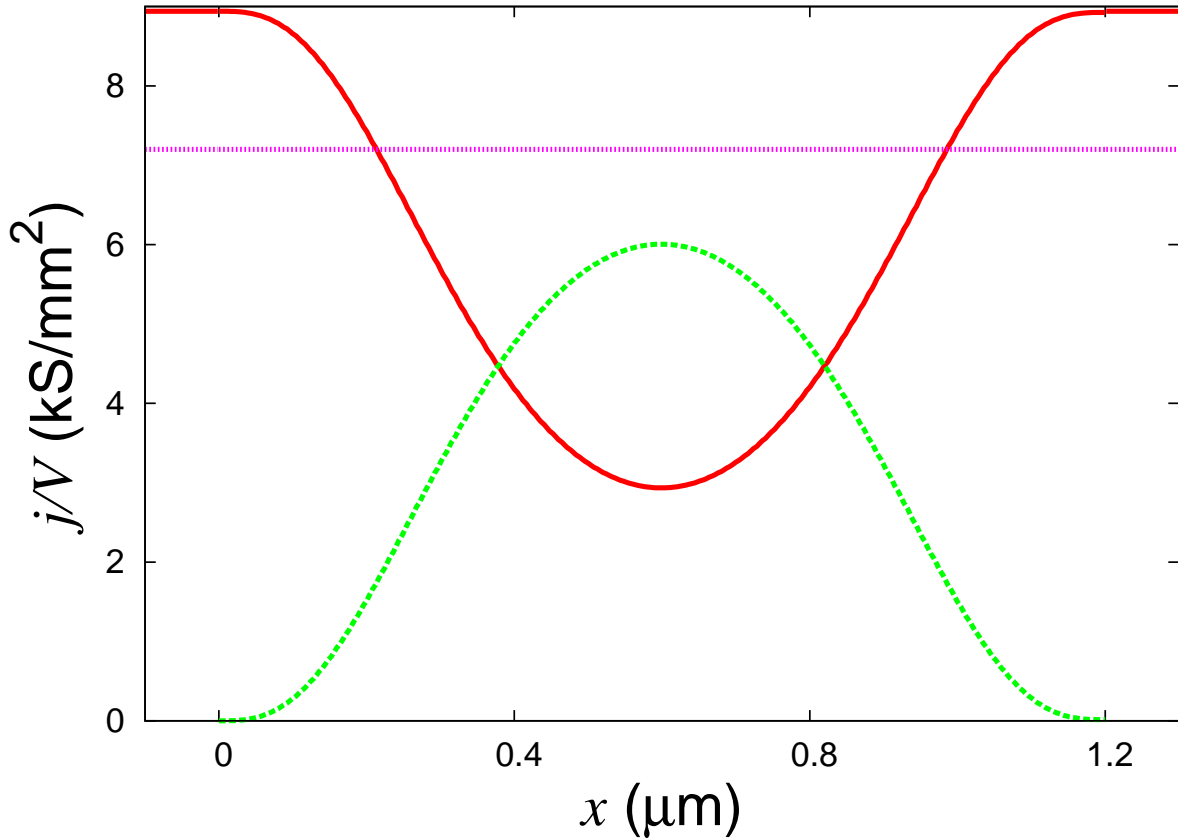


Figure 3.3: Spatial dependence of charge current in a biased and symmetric F|S|F spin valve. S is located in the interval $(0, 1.2)$ μm . Solid line (red) shows the quasiparticle current which is converted into supercurrent in S shown by dashed (green) line. Dotted line (purple) shows the current in the normal state. Adapted from [2].

parts of the spin valve will be spin-polarized. Spin-current can not be converted into supercurrent in the singlet superconductor, but will decay due to spin-flip scattering governed by (3.17d). In Figure 3.4 we show the spatial dependence of the spin current in the F|S|F structure both in the normal and superconducting state. The trilayer is symmetric and the magnetizations are in parallel alignment. The magnitude of spin current flowing in S in the superconducting state is reduced since the system becomes a low carrier system for spin current. This effect is described by the diffusion coefficient for spin current D_L which is shown in Figure 3.2 panel b).

The magnetoresistance, defined as the difference of the total resistance when the F parts of the trilayer have antiparallel (R^{AP}) and parallel magnetizations (R^{P}), is a measure of the spin-dependent transport properties of the spin valve. In Figure 3.5 we show the temperature dependence of $R^{\text{AP}} - R^{\text{P}}$ for two systems where the length of S is either 900 or 1200 nm. In each case we show calculations when spin-flip is induced by magnetic impurities or spin-orbit coupling. Generally, we see that the magnetoresistance decreases

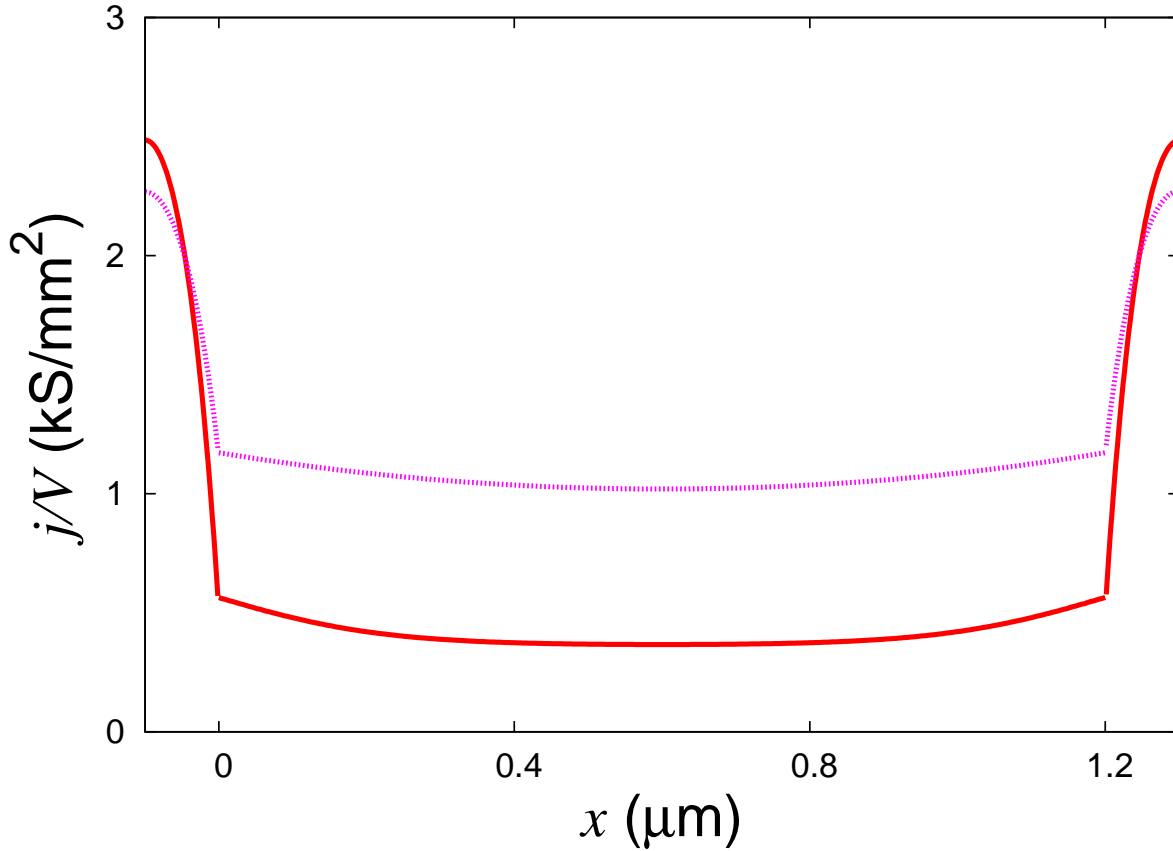


Figure 3.4: Spatial dependence of spin current in biased F|S|F spin valve with magnetizations in parallel alignment. S is located in the interval $(0, 1.2) \mu\text{m}$. Solid line (red) shows the quasiparticle spin current in the superconducting state, and dotted line (purple) in the normal state. Adapted from [2].

with increasing length of the superconductor and decreasing temperature. This behaviour is due to the resilience of the superconductor for spin transport. Moreover, we see that the critical temperature of the superconductor depends on the spin-flip scattering mechanism. This is due to the pair-breaking effect of the magnetic impurities discussed in Section 3.1.1.

3.2.3 Spin-flip spectroscopy

The different renormalization of the spin-flip rates induced by magnetic impurities and spin-orbit scattering facilitates a novel spin-flip spectroscopy. In paper [3] we used the spin transport theory of Section 3.1 to model experimental data for spin-current injection from Co into an Al superconducting nanowire by tunnel junctions. The superconducting state is assumed to be weakly modified by the contacts and small concentrations of magnetic

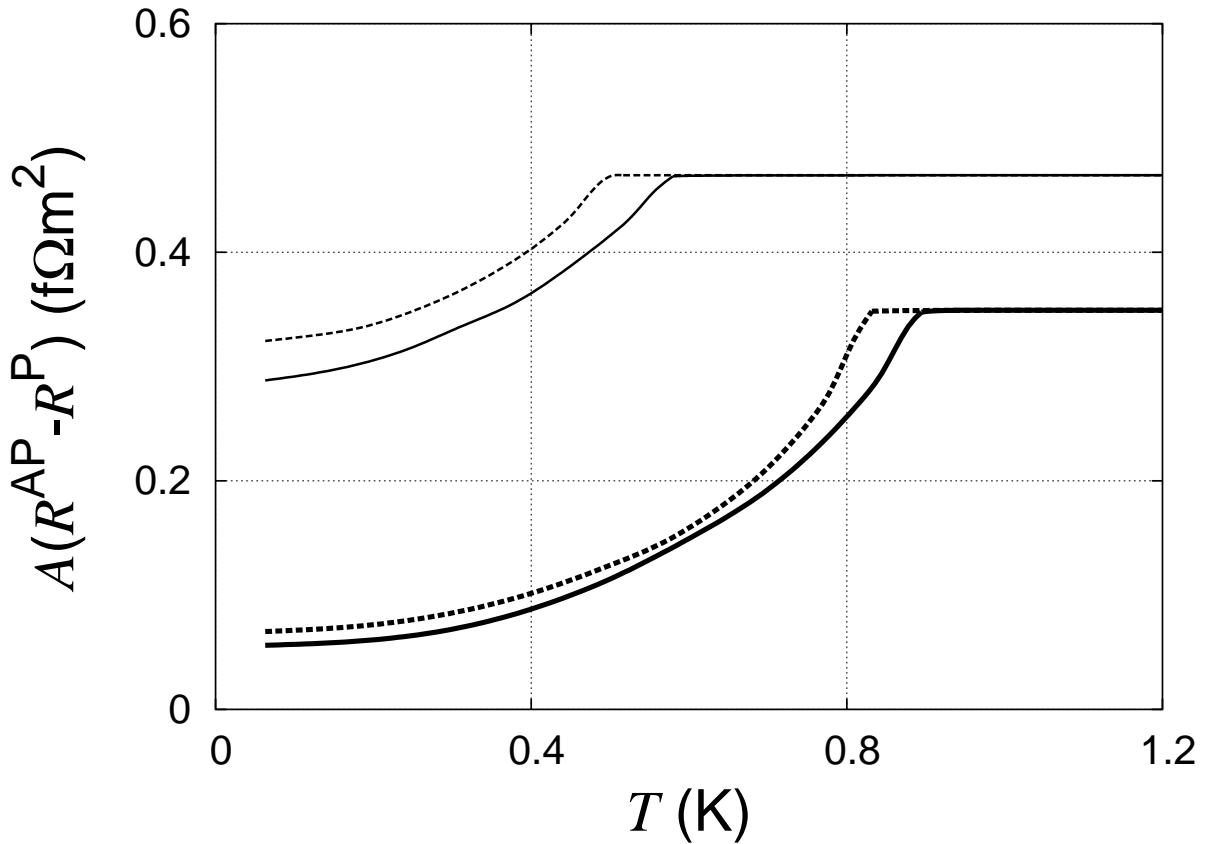


Figure 3.5: Temperature dependence of the magnetoresistance for spin-orbit (solid lines) and magnetic impurity (dashed lines) induced spin flip. The top set of curves is a system with Al length 900 nm, and the lower curves with Al length 1200 nm. Adapted from [2].

impurities. In this case, the spectral properties can be approximated by the gapped BCS equilibrium solutions studied in paper [1]. The microscopic mechanisms that gives rise to spin-flip scattering can be distinguished in the superconducting state as seen from the BCS renormalization factors $\alpha_{\text{TSTS}}^{\text{m}} = (E^2 + \Delta^2)/(E^2 - \Delta^2)$ and $\alpha_{\text{TSTS}}^{\text{so}} = 1$ that differ strongly at the gap edge $E \gtrsim \Delta$ where quasiparticle injection takes place. We use the parameter $\beta = (\tau_{\text{so}} - \tau_{\text{m}})/(\tau_{\text{so}} + \tau_{\text{m}})$ to quantify the difference of spin-flip due to magnetic impurities and spin-orbit coupling. In paper [3] the effective spin-flip length is extracted from measurements of the spatial decay of the spin-accumulation in the nanowire at several temperatures. Using β as a fitting parameter, we obtain good agreement with the measurements, see Figure 3.6. The numerical analysis of the energy-dependent transport shows that $\tau_{\text{m}}^{-1} = 3\tau_{\text{so}}^{-1}$, thus spin-flip scattering by magnetic impurities is three times more efficient in the normal state than spin-flip scattering induced by spin-orbit coupling in the system.

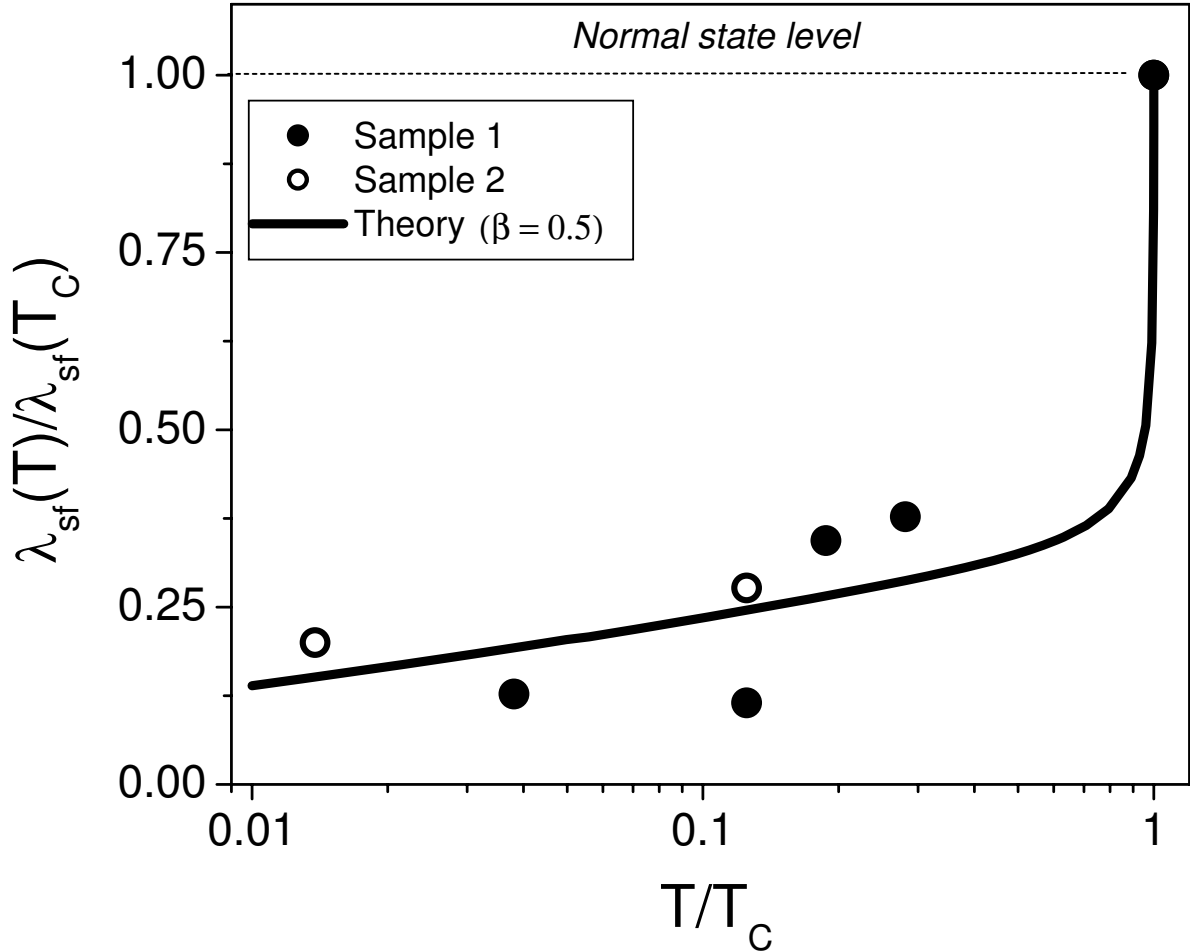


Figure 3.6: Temperature dependence of the effective spin-flip length λ_{sf} for two samples 20-25 nm in thickness. $T_c \approx 1.6$ K and $\lambda_{\text{sf}}(4 \text{ K}) \approx 1 \mu\text{m}$. Adapted from [3].

3.3 Magnetization dynamics in F|S heterostructures

In the systems studied in Section 3.2, a spin-polarized current was generated by passing a charge current through a bulk ferromagnet. This current will in addition to the spin-polarized part described by the TS-component, be accompanied by a charge current described by the T current component. In the experiments reported in Ref. [71], a pure spin current was injected into a superconductor by the magnetization dynamics of ferromagnet-superconductor heterostructures under ferromagnetic resonance (FMR) conditions. The ferromagnet acts as a “spin pump” [30], and the magnitude of the spin current leaving F is measured as an enhanced broadening of the FMR spectrum. Thus the magnitude of spin current absorbed in the superconductor in contact with the ferromagnet can be directly measured.

Magnetization dynamics experiments facilitates studies of spin relaxation and pure spin current flow through superconductors. In paper [4] we developed a theory of energy-dependent spin pumping and calculated the resulting spin flow and relaxation in F|S heterostructures. We also show that under typical experimental conditions, the FMR spectral broadening is directly related to phenomenological Gilbert damping of the magnetization dynamics. This allowed us to numerically study the enhanced Gilbert damping by spin current absorption and transport in superconductors of F|S bilayers and ferromagnet|superconductor|spin-reservoir (F|S|R) trilayer proximity heterostructures. We obtained quantitative agreement with experimental data from Ref. [71], and studied the magnetization dynamics as a function of the nature and strength of spin-flip scattering, temperature and system size.

The quasiparticle energy of the spin-current carriers emitted by the ferromagnet in FMR experiments is typically lower than the bulk superconducting gap. This means that the low-energy behaviour of the spectral quantities in the spin-charge diffusion equation (3.17d) determine the spin flow in the superconducting part of the system. To illustrate the effect of the reduced spin current conductivity of superconductors described by D_L , let us consider the magnetization dynamics in a F|S|R trilayer in the simplified situation where spin-flip in S can be disregarded. The spin-reservoir is a material with efficient spin-flip scattering so that any spin current reaching this layer is dissipated immediately. Thus magnetization damping due to enhanced Gilbert damping will be determined by the magnitude of the spin flow out of F that reaches R. We further simplify the description by assuming that the spin current pumped out of F is stationary. The diffusion equation (3.17d) can be solved analytically in this case and shows that the spin flow through S into R is limited by the series resistance of the spin-mixing resistance of the F|S interface r^\perp , the spin transport resistance of S described by the resistivity $\rho_L = 1/hN_0D_L$, and the conventional resistance of the S|R interface r ,

$$R_{\text{eff}}^\perp(E) = \frac{r^\perp}{N(0, E)} + \int_0^L dx' \frac{\rho_L(x', E)}{\mathcal{A}} + \frac{r}{N(L, E)}. \quad (3.19)$$

Here R_{eff}^\perp is the effective spin transport resistance in units of e^2/h , and L is the width of the superconducting layer. The resistance at the interfaces also depends on the energy-dependent density of states of S at the contact points $x = 0$ and $x = L$. The Gilbert damping is explicitly given

$$G = G_0 + \frac{(g_L\mu_B)^2}{2\pi\hbar} \frac{1}{d} \int dE \frac{-df_{\text{FD}}(E)/dE}{AR_{\text{eff}}^\perp(E)}, \quad (3.20)$$

where g_L is the g -factor, μ_B is the Bohr magneton, f_{FD} is the Fermi-Dirac distribution function and G_0 the intrinsic Gilbert damping. As we have seen in Figure 3.2 b), the diffusion coefficient D_L is very small for energy less than Δ . Thus we expect a monotonous decrease of the enhanced Gilbert damping with decreasing temperature as $\Delta(x, T)$ grows. The spin transport resistivity and thus R_{eff}^\perp then become large inside S. Numerical calculations for

the temperature dependence of the enhanced Gilbert damping $G - G_0$ confirms this picture as seen in Figure 3.7. The Figure also shows some effects from the inverse proximity effect. For short L , the inverse proximity effect suppresses superconductivity more efficiently than for the longer S. This gives the increasing T_c with increasing L .

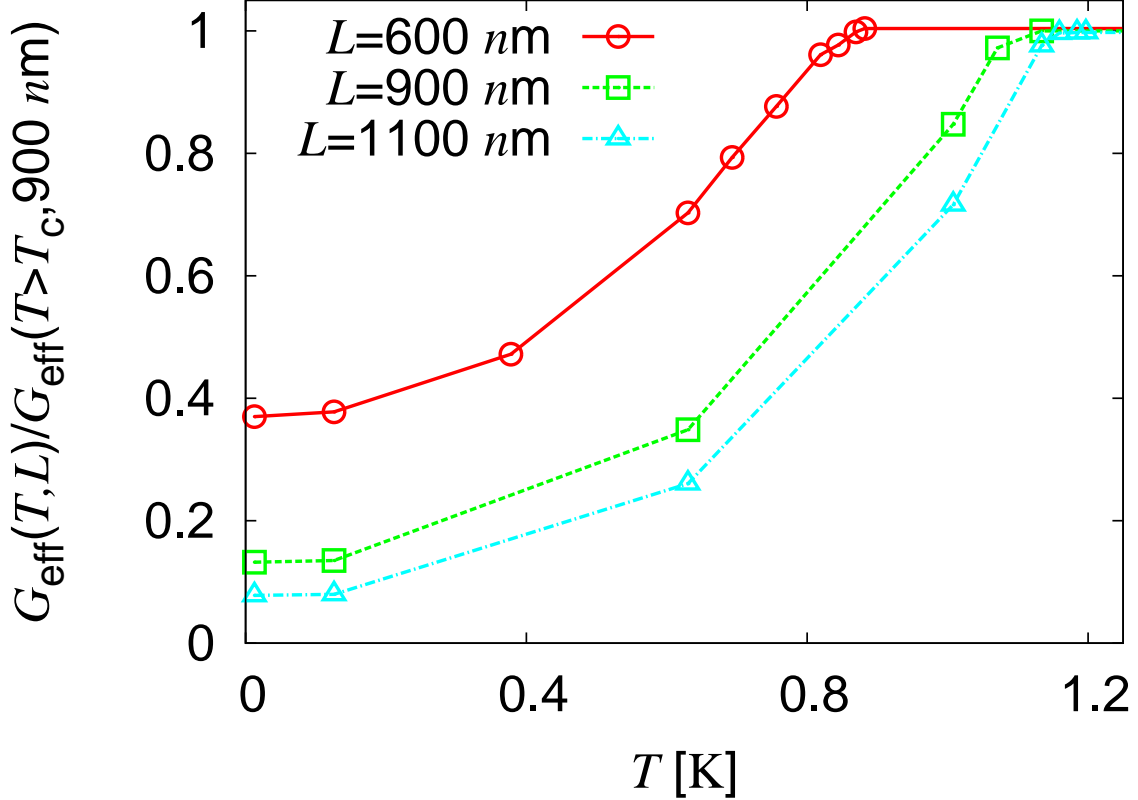


Figure 3.7: Temperature dependence of the enhanced Gilbert damping in F|S|R trilayers given by (3.20) for different S thickness L . Lines are guides to the eye. The superconductor is Al, and the parameters of the calculation are the bulk critical temperature $T_{c0} = 1.26$ K, $D = 160$ cm²s⁻¹. Spin flip in S is disregarded.

In an F|S bilayer, the spin-current dissipation in S by spin-flip determines the damping of the magnetization dynamics by spin current transport out of F. As a consequence of the different renormalization of the spin-flip scattering rates shown in Figure 3.2 a) and b), we expect different temperature dependence of the enhanced Gilbert damping close to T_c where the energy of the pumped quasiparticles, which is set by the temperature, is close to Δ . Numerical calculations of the enhanced Gilbert damping are shown in Figure 3.8. We see that the Gilbert damping at $T \lesssim T_c$ can exceed the Gilbert damping in the normal state as a consequence of the large renormalization factor α_{TSTS}^m at energies $E \gtrsim \Delta$, see Figure 3.2 a).

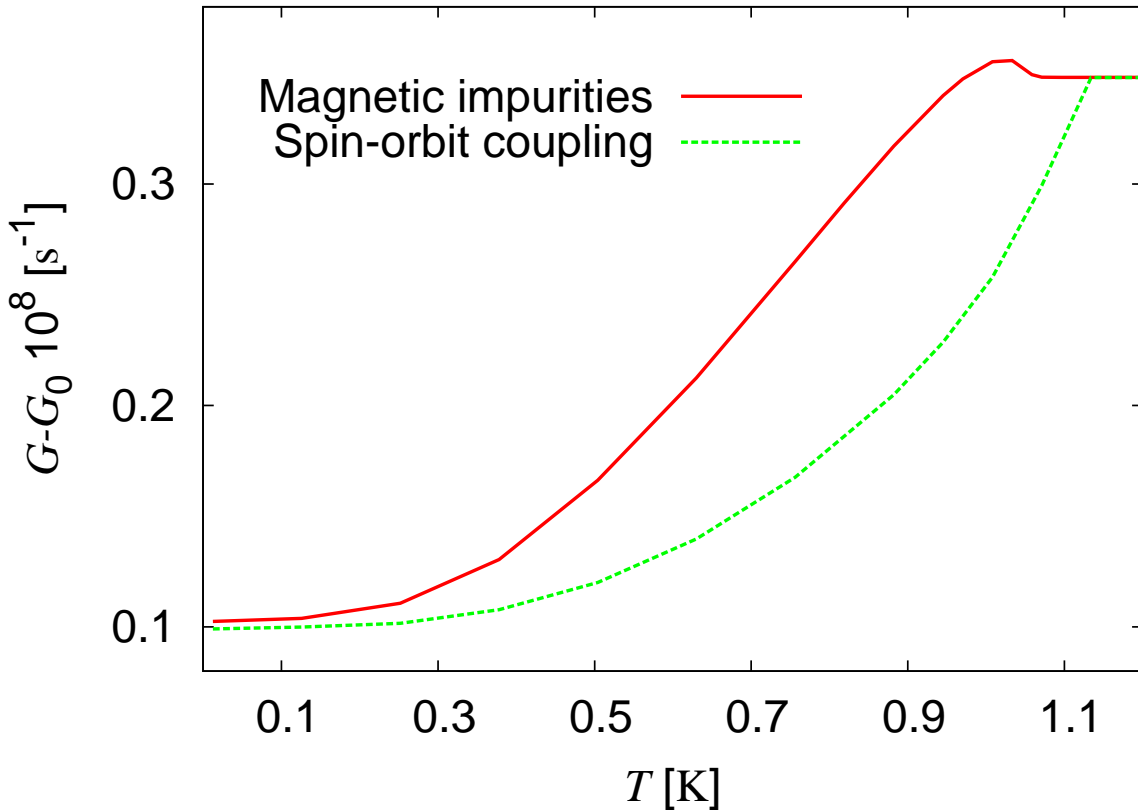


Figure 3.8: Temperature dependence of the enhanced Gilbert damping in a F|S bilayer where solid line (red) shows a system where spin-flip scattering is induced by magnetic impurities, and dotted line (green) shows a system with spin-orbit coupling induced spin-flip. The thickness of S is $L = 900$ nm and the spin-flip length in the normal state is $l_{\text{sf}} = 1.1$ μm . Other material parameters for S correspond to those listed in the caption of Figure 3.7. Adapted from paper [4].

3.4 Conclusion

In conclusion, we have studied spin injection into superconductors and seen that the energy-dependent transport properties of superconductors facilitates studies of spin-flip mechanisms. The results agree with experimental data in [3] and [71].

We have also found that superconducting layers in in FMR driven spin pumping experiments can reveal information about the spin transport properties of the heterostructures that is not available in the normal state. Therefore, such systems may become useful to understand physics beyond the proximity superconductivity studied here.

4 Crossed Andreev reflection

Andreev reflection was introduced in Section 1.1. This is the process where two quasiparticles at subgap energy are transferred across an interface between a non-superconducting material and a superconductor (S), thus creating or removing a Cooper pair in S. Cooper pairs are in quantum coherent states on the spatial scale ξ , which can exceed the resolution of state-of-the-art nanofabrication techniques. Thus it was suggested that the two quasiparticles that combine as a Cooper pair can flow from different normal metal (N) or ferromagnet (F) electrodes contacted with shorter separation than ξ to the superconductor [81,82]. This process is known as nonlocal or crossed Andreev (CA) reflection. It is an inherently mesoscopic phenomenon, with the prospect of creating entangled electrons (see Chapter 6).

Electron transfer (ET) between the two non-superconducting electrodes competes with crossed Andreev reflection, and is a parasitic process for purposes of quantum information experiments. An important challenge is therefore to understand and control the relative rates of these two processes in a given nanostructure. Theoretically, it was calculated by second order perturbation theory in the tunneling probability that the rates for CA and ET are equal when the electrodes are normal-metals [83]. Subsequently, it was shown that ET dominates to the next order of perturbation theory for normal-metal electrodes [84]. Recently, several theoretical papers have studied the competition between CA and ET, see references within papers [6] and [9].

Use of ferromagnetic leads is a way to control the relative rates of CA and ET, and was also considered in Ref. [83]. In CA, the spin of the transferred quasiparticles must be opposite to create a Cooper pair in singlet superconductors. Thus we expect the rate of CA to be favoured by an antiparallel alignment of the magnetization directions of the two ferromagnetic electrodes. In ET on the other hand, a single particle with a definite spin is transferred across both S|F interfaces and we expect this process to be favoured in a parallel alignment.

The experimental studies of crossed Andreev reflection in S|N systems reported in Refs. [85, 86, 87] have not enabled a clear conclusion for the relative strengths of CA and ET. In Ref. [85] a bias dependent nonlocal conductance was observed in metallic multilayers. For bias voltages corresponding to energies below the Thouless energy associated with the distance between the two normal terminals, a nonlocal signal with sign corresponding to ET was measured. The sign of the nonlocal signal in Ref. [85] changed for bias voltage exceeding the Thouless energy, and this was interpreted as a consequence of dominating crossed Andreev reflection. A dominating contribution from ET was measured in Ref. [86] where Au probes were contacted to a wire of superconducting Al by transparent interfaces. For ferromagnetic electrodes, the experimental data of Refs. [88, 89] have been modeled using the theory of Ref. [83], and agrees with the qualitative picture of the magnetization-configuration dependence discussed above.

In papers [5] and [6] we have studied crossed Andreev reflection in S|N systems using the circuit theory described in Section 2.2. We take into account the proximity effect and dephasing, and study the dependence on the type of contact which in our model can range from i.e. ballistic conductor to tunnel barrier.

In Section 4.1 we describe our circuit theory model and how the conductances associated with the various charge transfer processes can be determined. Some of the main results contained in papers [5] and [6] are presented in Section 4.2.

4.1 Circuit theory model

According to the “rules” of circuit theory [52], the first step is to define a discrete circuit representation for the system we would like to study. We will first give a short description of the systems we have in mind, and present a generic circuit capable of describing a range of different experimental realizations. We then go on by applying the generalized Kirchhoff’s rules and determine the nonlocal conductance due to CA and ET.

4.1.1 Equivalent circuit

The experimental studies of CA discussed above were performed on Al|Nb|Al multilayers with by tunnel barriers [85], and on systems where Fe or Au nanowires were contacted to an Al bar [88, 86]. In the future, experimental results for crossed Andreev reflection in gated semiconductor systems coupled to superconductors are expected.

We have studied the generic circuit theory model shown in Figure 4.1. The circuit theory representation consists of two normal-metal terminals (N_n) and one superconducting terminal (S) that are connected to a node (c). The terminals are assumed to be equilibrium

reservoirs, and we assume that isotropization in c results from scattering by impurities or chaotic interface scattering. Furthermore, we assume that charging effects can be disregarded. The coupling to “ground” in the figure represents a “coherence leakage current” which will be discussed below.

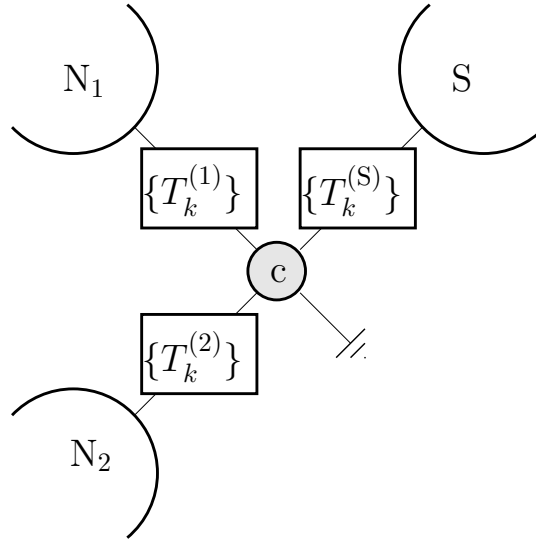


Figure 4.1: Equivalent circuit for the studies of crossed Andreev reflection and electron transfer in superconductor|normal-metal hybrid structures. Adapted from paper [6].

The boundary condition for the quasiclassical Green functions (2.9) that describes the connectors between the node and the terminals in terms of transmission probabilities $T_k^{(n)}$ is very general and allows us to model a wide range of experimental systems. We will now discuss the correspondence between the circuit theory model and the experimental systems mentioned above. In the systems where normal metal wires are connected to a mesoscopic superconductor, the terminals of the circuit correspond to regions away from the contact. Transparent contacts between the normal-metal electrodes and the superconductor is described by transmission probabilities close to unity for the open channels, and for tunnel barriers the probabilities are close to zero for all channels. The node describes a small region of the superconductor adjacent to the normal-metal electrodes where we must take into account inverse proximity effects and nonequilibrium distribution functions. The diffusive transport between the node and the bulk superconducting reservoir (terminal S) is described by a bimodal distribution of transmission probabilities [56] in the boundary condition (2.9). In a superconductor-semiconductor heterostructure, S could be coupled to a ballistic cavity with point contacts to the leads N_1 and N_2 . The node describes the nonequilibrium state of the cavity, and the point contacts are modeled by $T_k^{(n)} = 1$ for the open channels k and zero otherwise. The transparency and number of conducting modes of the contact to the superconductor can be determined experimentally.

4.1.2 Generalized Kirchhoff's law

The matrix current conservation (2.10) determines the Green function of the node in terms of the known, equilibrium Green functions of the reservoirs which are given in terms of electrochemical potential, temperature and the superconducting gap Δ_0 . The leakage current in (2.10) will describe dephasing on the node and superconducting pairing. In the circuit diagram shown in Figure 4.1, it is represented by the coupling to “ground”. The leakage current is determined by the Hamiltonian on the node which is $\check{H}_c = E\hat{\tau}_3 + i\hat{\tau}_2\Delta_c$ with Δ_c the superconducting order parameter in the node, see Section 2.2.2.¹

We have found the parametrization of the Green function used in Section 3.1 useful since it allows us to get analytical results for the transport properties.² The retarded and advanced parts of the node Green function $\hat{G}_c^{\text{R(A)}}$ is thus given by a complex function $\theta(E)$ (we use $\chi = 0$) determined by equations following from (2.10). For $E \ll \Delta_0$, this equation becomes

$$\begin{aligned} & \left(i\frac{e^2}{\hbar}N_0\mathcal{V}_cE - \frac{e^2}{\pi\hbar} \sum_{k,n} \frac{T_k^{(n)}}{2 + T_k^{(n)}(\cosh(\theta) - 1)} \right) \sinh(\theta) \\ -i & \left(\frac{e^2}{\hbar}N_0\mathcal{V}_c\Delta_c + \frac{e^2}{\pi\hbar} \sum_k \frac{T_k^{(S)}}{2 - T_k^{(S)}(i\sinh(\theta) + 1)} \right) \cosh(\theta) \\ & - \frac{3}{4} \frac{e^2}{\hbar}N_0\mathcal{V}_c \frac{\hbar}{\tau_m} \sinh(\theta) \cosh(\theta) = 0. \end{aligned} \quad (4.1)$$

This equation follows from the retarded matrix block of the Kirchhoff equation and has similar structure as the retarded Usadel equation (3.9). We have included the effect of spin-flip scattering in the last line for illustration, this effect will not be studied here. Comparison with the known results for the retarded Usadel equation (3.9) from e.g. Ref. [36] allows us to determine the physical effect on the spectral properties of the different contacts. The normal-metal terminals give quasiparticles a finite life-time, similar to inelastic scatterings, and the superconducting terminal induces superconducting correlations. The effect of pairing on the node induced by Δ_c will be taken into account as renormalization of the coupling to the superconductor, thus we omit the term proportional to Δ_c in the following. For tunnel barriers $T_k^{(n)} \ll 1$, the equation can be expanded and solved analytically. Also, at high energy $E \rightarrow \infty$ we see that the only acceptable solution is $\theta = 0$ which corresponds to an incoherent normal-metal state. In the general case however, (4.1) must be solved numerically at each energy.

The Keldysh matrix block of the Kirchhoff equation gives linear equations in the distribution functions that describe the conservation of charge and energy at each energy. The

¹In the case of S|N transport considered here, we may project the $\text{spin} \otimes \text{Nambu}$ matrix structure of the Green functions defined in Section 2.1.2 onto the basis spanned by $(\psi_\uparrow, \psi_\downarrow^\dagger)$.

²In paper [5] we have used a variation of the parametrization discussed in Chapter 3 which is obtained by the transformation $\theta \rightarrow i\theta$ and $\chi \rightarrow \chi - \pi/2$.

equations for the spin currents also include sinks given by spin-flip similar to (3.17).³ The node Keldysh Green function is parametrized $\hat{G}_c^K = \hat{G}_c^R \hat{h} - \hat{h} \hat{G}_c^A$ where $\hat{h} = h_{L,c} + \hat{\tau}_3 h_{T,c}$. The equations that determine $h_{T,c}$ and $h_{L,c}$ in the node become

$$\sum_n G_{L,n} (h_{L,c} - h_{L,n}) + G_{L,S} (h_{L,c} - h_{L,s}) = 0, \quad (4.2a)$$

$$\sum_n G_{T,n} (h_{T,c} - h_{T,n}) + G_{T,S} (h_{T,c} - 0) = 0, \quad (4.2b)$$

where $h_{T(L),n}$ are the distribution functions in the reservoirs and we have defined effective, energy-dependent conductances $G_{T(L)}$ that are determined by $\theta(E)$ and $T_k^{(n)}$. These expressions are generally quite complicated, but when $E \ll \Delta_0$ they can be written ($n = 1, 2$)

$$G_{L,n} = 2 \frac{e^2}{\pi \hbar} \sum_k T_k^{(n)} \frac{(2 - T_k^{(n)}) \text{Re} \cosh(\theta) + T_k^{(n)} D_{L,c}}{\left| 2 + T_k^{(n)} (\cosh(\theta) - 1) \right|^2}. \quad (4.3a)$$

$$G_{T,n} = 2 \frac{e^2}{\pi \hbar} \sum_k T_k^{(n)} \frac{(2 - T_k^{(n)}) \text{Re} \cosh(\theta) + T_k^{(n)} D_{T,c}}{\left| 2 + T_k^{(n)} (\cosh(\theta) - 1) \right|^2}, \quad (4.3b)$$

$$G_{T,S} = 2 \frac{e^2}{\pi \hbar} \sum_k T_k^{(S)} \frac{-(2 - T_k^{(S)}) \text{Im} \sinh(\theta) + T_k^{(S)} D_{T,c}}{\left| 2 - T_k^{(S)} (i \sinh(\theta) + 1) \right|^2}, \quad (4.3c)$$

where $D_{T,c} = [\text{Re} \cosh(\theta)]^2 + [\text{Im} \sinh(\theta)]^2$ and $D_{L,c} = [\text{Re} \cosh(\theta)]^2 - [\text{Re} \sinh(\theta)]^2$. The conductance $G_{T,S}$ describes Andreev reflection at the interface to the superconducting terminal, which is the only accessible transport channel into S at subgap energy. Since no net energy is transferred in an Andreev reflection, the conductance $G_{L,S}$ vanishes when $E < \Delta_0$.

4.1.3 Currents and conductances

When the properties of the node have been determined by solving the Kirchhoff equations of the type (4.1) and (4.2), all currents and transport properties of the system can in principle be accessed. We would like to resolve the conductance associated with each of the charge transfer processes in the system, and to that end we study the energy-dependent current between N_1 and c. The possible processes are ET and CA as well as direct Andreev (DA) reflection where two quasiparticles from N_1 is transferred into S. Also, at energy above Δ_0 we must take into account quasiparticle transfer (QP) into S. Semiclassical probability

³Since we will not consider spin-polarized transport in this chapter, we omit the equations for the TS and LS modes here.

arguments then show that the current can be written

$$I_1(E) = \frac{G_{\text{ET}}(E)}{e} [f_2(E) - f_1(E)] + \frac{G_{\text{CA}}(E)}{e} [1 - f_1(E) - f_2(-E)] \\ + \frac{G_{\text{QP}}(E)}{e} [f_S(E) - f_1(E)] + 2 \frac{G_{\text{DA}}(E)}{e} [1 - f_1(E) - f_1(-E)]. \quad (4.4)$$

Here, the functions $f_n(\pm E)$ denote the Fermi-Dirac distribution functions in the terminals ($n = 1, 2, S$) at energy $\pm E$, and we have defined energy dependent conductances $G(E)$ for the transport processes discussed above. The total charge current is given by $I_{\text{charge},1} = \int dE I_1(E)$. From (4.4) we find that the nonlocal differential conductance which relates to the competition between ET and CA discussed above is

$$\frac{\partial I_{\text{charge},1}}{\partial V_2} = - \int dE [G_{\text{ET}}(E) - G_{\text{CA}}(E)] \frac{\partial f(E - eV_2)}{\partial E}. \quad (4.5)$$

This result shows how the sign of an induced voltage in N_1 by a current flowing from N_2 into S is determined by competing contributions from crossed Andreev reflections and electron transfer.

The currents following from the circuit theory calculations can be compared to (4.4) in order to determine the conductances associated with the various charge transfer processes,

$$G_{\text{QP}}(E) = \frac{G_{L,1}G_{L,S}}{G_{L,1} + G_{L,2} + G_{L,S}}, \quad (4.6a)$$

$$G_{\text{DA}}(E) = \frac{1}{4} \left(\frac{G_{T,1}(G_{T,2} + G_{T,S})}{G_{T,1} + G_{T,2} + G_{T,S}} - \frac{G_{L,1}(G_{L,2} + G_{L,S})}{G_{L,1} + G_{L,2} + G_{L,S}} \right), \quad (4.6b)$$

$$G_{\text{CA}}^{\text{ET}}(E) = \frac{1}{2} \left(\frac{G_{L,1}G_{L,2}}{G_{L,1} + G_{L,2} + G_{L,S}} \pm \frac{G_{T,1}G_{T,2}}{G_{T,1} + G_{T,2} + G_{T,S}} \right). \quad (4.6c)$$

These expressions immediately demonstrate that the nonlocal conductance $G_{\text{nl}} = G_{\text{ET}} - G_{\text{CA}}$ is positive and dominated by ET in our model, regardless of the contact parameters. We interpret this result as the consequence of a symmetry between the CA and ET processes. Both processes involve the transfer of quasiparticles through the contacts to the normal metals and the network between them, but CA also involves Andreev reflection at the interface to the superconducting terminal. Thus the resistance limiting CA can at minimum be as small as the resistance for ET unless other physical processes affect these quantities.

4.2 Results

The solution of the retarded part of the Kirchhoff equation determines the conductances through the expressions (4.6) and the explicit dependence of the quantities $G_{T(L)}$ on θ

(4.3). In this section we will discuss results for different types of interfaces. However, to make contact with previous results in other papers, let us first consider tunnel interfaces with conductance g_n for $n = 1, 2, S$ and zero energy. The retarded equation can then be solved analytically and we obtain

$$G_{\text{ET}} = \frac{g_1 g_2}{2} \frac{2g^2 + g_S^2}{[g^2 + g_S^2]^{3/2}}, \quad G_{\text{CA}} = \frac{g_1 g_2}{2} \frac{g_S^2}{[g^2 + g_S^2]^{3/2}}. \quad (4.7)$$

The nonlocal conductance $G_{\text{nl}} = G_{\text{ET}} - G_{\text{CA}}$ is dominated by ET and is of order $\mathcal{O}(g_n^4)$ with $n = 1, 2$. This is in agreement with the vanishing nonlocal conductance obtained in second order perturbation theory in Ref. [83], and the dominating contribution from ET in higher order tunneling [84]. When $g_S/g \gg 1$ the nonlocal conductance vanishes due to equal probability for ET and CA.

Let us now consider subgap transport $E \ll \Delta_0$, but take into account the energy-dependence induced by dephasing in the node. In the limit of large energy in (4.1), the spectral properties following from $\theta = 0$ describe incoherent transport in c. In the case of tunnel barrier interfaces, the subgap transport into S vanishes and the only transport channel in the network is double-barrier tunneling between N_1 and N_2 described by

$$1/G_{\text{ET}} = 1/g_1 + 1/g_2. \quad (4.8)$$

The Thouless energy is the relevant energy scale for the proximity effect in S|N systems since it sets the scale for dephasing of electron-hole correlations. Let us illustrate this by considering the diffusion of electrons and holes in the proximity coupled system. An Andreev reflected electron-hole quasiparticle pair is initially in a quantum coherent state. However, a phase difference develops due to their small difference in wavevector. The wavevector of the electron (hole) is $k = k_F \sqrt{1 + (-)E/E_F}$ where k_F and E_F are the Fermi wavevector and energy respectively. The phase difference that evolves between the electron and the hole in the system is $\Delta\phi \sim 2E\tau_D/\hbar \approx \max(eV, k_B T)/E_{\text{Th}}$ where the dwell time in the disordered system is τ_D and we have defined the effective Thouless energy as $E_{\text{Th}} = \hbar/(2\tau_D)$. This dephasing is represented by the leakage current above. We now see that when the characteristic energy of the quasiparticles $\max(eV, k_B T)$ exceeds the Thouless energy, phase coherence is lost in the system since $\Delta\phi$ is large and indefinite. This corresponds to $\theta = 0$ considered above with transport given by (4.8). When the quasiparticle energy is smaller than E_{Th} on the other hand, $\Delta\phi \ll 1$ and phase coherence induced by Andreev reflections persists. This gives the proximity effect regime governed in the tunneling case by the conductances (4.7).

In a diffusive normal metal coupled to a superconductor through connectors with negligible resistance, the Thouless energy can be defined as $E_{\text{Th}} = \hbar D/(2L^2)$ where L is a characteristic size for the transport. This result is captured by the Usadel equation and is recovered in the circuit theory by discretizing the diffusive system as a network of nodes. The inter-node matrix currents are given by tunnel-like expressions parametrized by a resistance ρd where ρ is the resistivity and d the lattice size in the discretized network. In the

single-node model we are considering here, the dwell time in the effective Thouless energy is determined by the resistances between the node and the reservoirs that limit the escape rate from the node. Below, we will consider systems where $g_S \gg g_1, g_2$, and in this case the effective Thouless energy becomes $E_{\text{Th}} \approx \hbar g_S / (2e^2 \nu_0 V_c)$

The conductances for the various charge transfer processes are obtained numerically by solving (4.1) with given connector parameters, and using the expressions for the conductances (4.6). In Figure 4.2 we show the energy-dependence of the conductances when all connectors are of tunnel type. In the limiting cases of vanishing and high energy with respect to E_{Th} , the nonlocal conductance agrees with the analytical results (4.7) and (4.8). In the intermediate regime, we see that the conductances for processes involving Andreev reflection are peaked at $E = E_{\text{Th}}$. This is a result of the interplay between the density of states in the node and the Andreev reflection rate $G_{\text{T,S}}$. The nonlocal conductance is a positive, and monotonously increasing function of the energy.

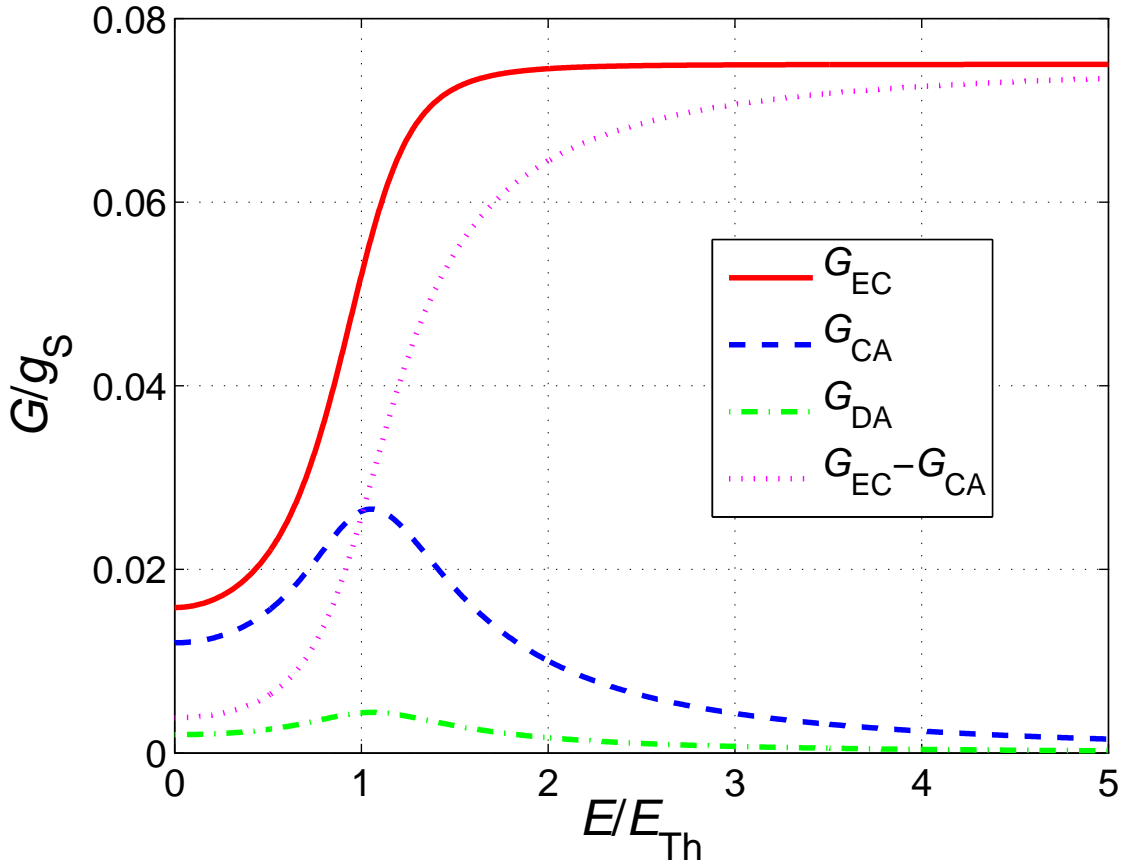
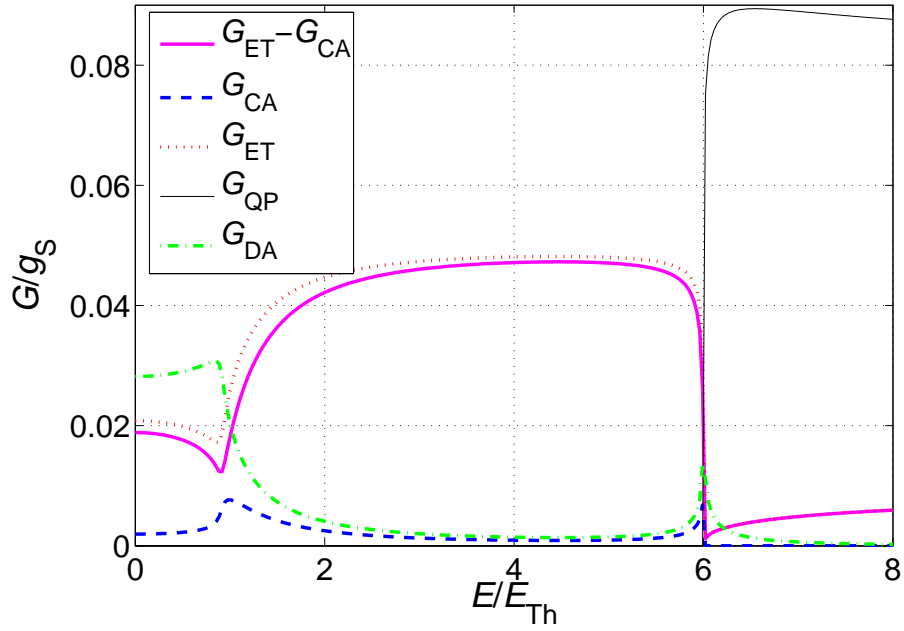
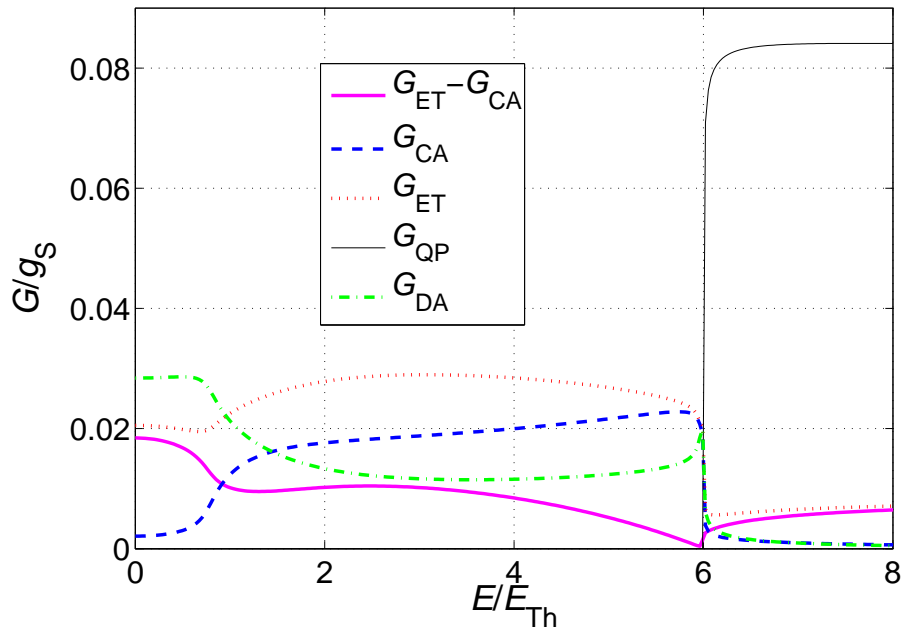


Figure 4.2: Conductances for the various charge transfer processes when all connectors are of tunnel type. The input parameters for the calculation is the conductances $g_1/g_S = g_2/g_S = 0.1$. Adapted from paper [5].

To demonstrate the dependence on the contact type, we present numerically calculated conductances for the case when the normal terminals are connected by point contacts, and the superconducting terminal either by a tunnel barrier (Figure 4.3(a)) or a connector with intermediate transparency $T_k^{(S)} = 0.5$ for the open channels (Figure 4.3(b)). We have extended the model to account for energy comparable to the superconducting gap in S, Δ_0 . From Figure 4.3 we see that the nonlocal conductance is qualitatively different in the two cases. In the tunneling case, the largest value for G_{nl} is at low energy, whereas in the case of intermediate transparency the largest nonlocal conductance is at energy between E_{Th} and Δ_0 . If we consider the conductance for the individual processes, we see that the contribution from CA is much larger in the case of intermediate transparency.



(a) Tunnel connector to S.



(b) Intermediate transparency connector to S.

Figure 4.3: Conductances for the various charge transfer processes. The connectors to N_n are point contacts and the connector to S is (a) a tunnel barrier, or (b) an interface of intermediate transparency. The conductivities are defined as $g_n = e^2 \sum_k T_k^{(n)} / (\pi \hbar)$ and we have chosen $g_n / g_S = 0.1$ for $n = 1, 2$. The superconducting gap of the S terminal is at $\Delta_0 = 6E_{Th}$. Adapted from paper [6].

4.3 Conclusion

In the model we have investigated above, we have seen that the conductance due to ET dominates the nonlocal transport. While this general property seems to agree with the experiments in Ref. [86], this does not comply with the results of Ref. [85] and specifically the behaviour at the Thouless energy is not reproduced in our model. The latter experimental data are still not completely understood, and it has been suggested that effects due to interactions could be important [90].

In the context of the present calculations, it would be interesting to compare the predictions to systematic, experimental investigations of the dependence on the type of contacts in the system and the energy-dependence. Superconductor-semiconductor systems are promising systems to pursue these questions since contact properties can be experimentally manipulated by gate voltages.

5 Quantum mechanics and nonlocality

The seminal 1935 paper “Can Quantum-Mechanical Description of Physical Reality Be Considered Complete?” by A. Einstein, B. Podolsky, and N. Rosen (EPR) proposed a thought experiment that reveals how quantum mechanics implicates nonlocality and non-classical correlations. In this paper, nonlocality refers to the possibility that two events involving particles in so-called *quantum entangled states* can influence each other *instantaneously* even with arbitrarily large spatial separation of the particles.

Paper [7] is intended for readers who do not necessarily have a physics background, and is published in the *Interdisciplinary Communications* book series of the Centre for Advanced Study in Oslo. In this text, we first describe the thought experiment proposed by EPR and provide some historical background. Then we discuss the formulation of a mathematical inequality by J. S. Bell [91] that determines the conditions under which the outcomes of EPR experiments can no longer be accounted for by a theory adhering to locality. Finally, we review some of the work that has established that the Bell inequality is experimentally violated. This demonstrates nonlocality, and comparison of the measurements and the predictions following from quantum mechanics are in good agreement.

Bell’s inequality and entanglement is studied in paper [8], and is at the heart of quantum information theory. In Chapter 6, we will summarize our results for the current noise cross-correlations in multiterminal superconductor|ferromagnet beamsplitters which lead to correlations that violate a Bell inequality. To demonstrate nonlocality, the measurements would have to be performed with terminal spatial separation such that no information can be transferred between them during the timescale set by the temporal resolution of the measurement. The necessary length scale for this condition can not be met in a condensed matter, electronic system. However, given a quantum mechanical description of reality, violation of a Bell inequality is a demonstration of entanglement in the studied system. The interest in entanglement in condensed matter physics is due to the fact that a computer utilizing quantum entanglement can perform certain computational tasks faster than classically possible.

6 Supercurrent beamsplitter statistics

In Chapter 4 we studied nonlocal transport in systems where current flows between superconducting reservoirs and normal-metals by Andreev reflection. To this end we calculated the conductances that determine mean currents in the network. Studies of current fluctuations and noise properties in mesoscopic structures has become an important experimental and theoretical method to understand the correlations and microscopic structure of the transport processes. In this chapter we will consider the noise properties of Andreev reflection in multiterminal structures by calculating the *full counting statistics* (FCS). FCS is of direct experimental interest since recent advances have enabled experimentalists to measure the higher order moments of the noise, which is contained in the FCS [66]. More important for the present discussion however, is the fact that the probability distribution following from FCS can yield information about the elementary charge transfer processes in the system (see Section 2.3). In the context of crossed Andreev (CA) reflection, we will see that FCS also reveals entanglement of Andreev reflected electrons and holes. Some aspects of entanglement and its experimental consequences were introduced in Chapter 5. Studies of entanglement in F|S systems have attained considerable interest lately, and experimental results will probably follow in near future.

It was noted in the introduction to Chapter 4 that ferromagnetic electrodes in antiparallel alignment is a way to enhance crossed Andreev reflection in singlet superconductor|ferromagnet heterostructures. A simplified explanation of this effect is the following: The supercurrent flowing into the node in the circuit shown in Figure 6.1 gives rise to Andreev reflected electron-hole quasiparticle pairs with opposite spin. Thus the transfer of each spin into different leads with opposite magnetizations is enhanced since the conductance is larger when the magnetization is parallel to the spin. This effect can be utilized to produce currents of entangled electrons in separated leads by enhancing the CA process, and constitutes one of the motivations to study CA. The transport into the separated leads in CA is correlated, because of the coherence induced by the Andreev reflection process. Thus we expect CA processes to lead to correlated current fluctuations in the two leads

involved, i.e. the cross-correlation noise $C_{m,n}$ (with $m \neq n$) is positive (see Section 2.3 for a definition). This result was predicted using scattering theory [92,93], and received some attention since cross-correlations for fermion transport is usually *negative* because of the Pauli exclusion principle (for an interesting discussion of this point, see Ref. [94]). It is now understood that positive cross-correlations in fermion transport can occur in various systems due to interactions [95, and references therein].

In paper [8] we have studied the performance of a superconductor|ferromagnet *entangler*, which is a circuit designed to produce currents of entangled electrons in different leads. The understanding of such systems is important for the developing field of solid-state quantum information technology. We show how the FCS provides information about the microscopic processes in the proposed circuit, and discuss the experimentally accessible transport properties. In paper [9] we study the FCS of crossed Andreev reflection in competition with electron transport.

In Section 6.1 we will outline how the *cumulant generating functions* (CGFs) that are considered in this chapter are calculated. Some of the main results in papers [8] and [9] are then summarized in Sections 6.2 and 6.3 respectively.

6.1 Single-node tunnel barrier circuits

The circuit theory and its extension for calculations of FCS was briefly introduced in Chapter 2. The circuits we will study in this chapter consist of a single node (c) connected by tunnel barriers to one superconducting terminal (S) and several normal-metal or ferromagnet terminals (F_n), see Figure 6.1.

The matrix current conservation (2.10) for these systems can be written

$$[\check{M}, \check{G}_c]_- = 0. \quad (6.1)$$

This relation defines the matrix \check{M} which is independent of the Green function of the node \check{G}_c . An analytic solution of (6.1) can be found taking into account the normalization of the Green function (2.3) [96],

$$\check{G}_c = \frac{\check{M}}{\sqrt{\check{M}^2}}. \quad (6.2)$$

The matrix square root is defined in the standard way by diagonalizing \check{M} , $\sqrt{\check{M}^2} = \check{X}\sqrt{\check{D}^2}\check{X}^{-1}$ where \check{X} is the matrix composed of the column eigenvectors of \check{M} and \check{D} the diagonal eigenvalue matrix. The square root of \check{D}^2 is defined by taking the square root of each diagonal element.

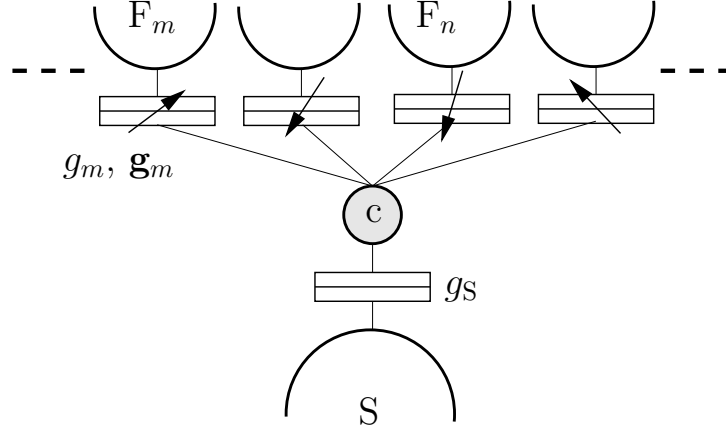


Figure 6.1: Circuit theory representation of a generic S|F entangler. Entangled electrons from the singlet superconductor S enter the cavity c through a tunnel barrier with conductance g_s and escape through ferromagnetic tunnel barriers with conductance g_n and spin polarization g_{MRn}/g_n into drains F_n . Arrows indicate magnetization directions \mathbf{m}_n , and we have introduced the notation $\mathbf{g}_n = \mathbf{m}_n g_{MRn}$. Adapted from paper [8].

The equation that determines the CGF of the multiterminal structure (2.16) can be integrated using the solution for the Green function (6.2) by noticing that

$$I_n(\{\chi_n\}) = \frac{1}{8e} \text{Tr} \check{\tau}_K \check{I}_n = \frac{1}{4ie} \partial_{\chi_n} \text{Tr} \sqrt{\check{M}^2}. \quad (6.3)$$

Diagonalizing the matrix \check{M} , we arrive at the very useful formula

$$\mathcal{S} = -\frac{t_0}{4e^2} \int dE \sum_k \sqrt{\lambda_k^2}, \quad (6.4)$$

where the set $\{\lambda_k\}$ are the eigenvalues of \check{M} . This result is valid also in the presence of spin-active tunnel contacts described by (2.11). The normalization condition $\mathcal{S}(\{\chi_n = 0\}) = 0$ should be imposed to ensure normalization of the probability distribution $P(\{N_n\}; t_0)$ (2.14).

We will consider the limit of negligible temperature. In this case, the Green functions of the reservoirs are described by energy-independent matrices defined in the intervals $|E| > |eV_n|$ and $|E| \leq |eV_n|$ where V_n is the bias voltage applied on terminal n . The Green function of a normal terminal is $\hat{\tau}_3 \check{\tau}_3 + (\check{\tau}_1 + i\check{\tau}_2)$ in the former energy interval and $\hat{\tau}_3 \check{\tau}_3 + \text{sgn}(E) \hat{\tau}_3 (\check{\tau}_1 + i\check{\tau}_2)$ in the latter. When $|eV| \ll \Delta_0$, where Δ_0 is the gap of superconducting terminal (S), the Green function of a singlet superconducting reservoir becomes $\hat{\tau}_1$ in the matrix representation used in papers [8] and [9]. The Green function of the reservoirs and the connector parameters (2.11) determine \check{M} . Finally, the CGF is given by (6.4).

6.2 S|F entangler

Solid-state entanglers have been studied by several authors [97,98,99,100,101] (for a review, see [102]) and it has been established that entanglement can be experimentally detected by constructing a Bell inequality from the measured cross correlations. Here, we will consider the FCS of a superconductor|ferromagnet entangler, and show that the obtained CGF provides direct access to the probabilities of elementary charge transfer processes in terms of normal-state conductance parameters. We will then show how these probabilities demonstrate entanglement by violation of a Bell inequality. Moreover, the positive cross-correlation resulting from CA gives direct access to the two-particle probability that Andreev reflected electron-hole pairs flow to different drains, in the limit of large asymmetry between the conductance of the source and drain terminals.

In the circuit shown in Figure 6.1, a superconducting reservoir (S) at ground is connected by a tunnel barrier with conductance g_S to a node (c). The node is also connected to several drain leads (F_n) at equal voltage V by ferromagnetic tunneling barriers described by their conductance g_n and conductance spin polarization $\mathbf{m}_n g_{MRn} = \mathbf{g}_n$ (see Section 2.2.3).

6.2.1 Probability distributions

As a general property of CGFs with functional dependence on the counting fields given by

$$\mathcal{S} = \mathcal{S} \left(\sum_{m,n} p_{m,n} e^{-i\chi_m - i\chi_n} \right), \quad (6.5)$$

we have found that the probability distribution factorizes into two parts,

$$P(\{N_n\}) \equiv \int \frac{d^M \chi}{(2\pi)^M} e^{-\mathcal{S}(\{\chi_n\}) + i \sum_n \chi_n N_n} \quad (6.6a)$$

$$= P_S \left(\sum_n N_n \right) P \left(\{N_n\} \middle| \sum_n N_n \right) \quad (6.6b)$$

for $\sum_n N_n$ even and positive. We have defined M as the total number of terminals in the circuit. The interpretation of (6.6b) is that the charge transfer is given by two independent processes: The first factor $P_S(2N)$ is the probability that $N = \sum_n N_n/2$ pairs of particles are transferred onto the node from the source terminal S. The second factor $P(\{N_n\}|2N)$ in (6.6b) is the conditional probability that N_n out of the $2N$ electrons are subsequently transferred into terminal F_n . The factorization (6.6) holds regardless of the specific expression for $p_{m,n}$.

The factorization above will facilitate the interpretation of the FCS for the entangler in

Figure 6.1. Using the equations described in Section 6.1, we calculate the CGF

$$\mathcal{S} = -\frac{t_0 V}{\sqrt{2}e} \sqrt{g_\Sigma^2 + \sqrt{(g_S^2 - g^2 + \mathbf{g}^2)^2 + 4g_S^2(g^2 - \mathbf{g}^2)} \sum_{m,n} p_{m,n} e^{2i\chi_S - i\chi_m - i\chi_n}}, \quad (6.7)$$

where we have defined $g_\Sigma^2 = g_S^2 + g^2 + \mathbf{g}^2$, $g = \sum_n g_n$, $\mathbf{g} = \sum_n \mathbf{g}_n$, and the two-particle probability

$$p_{m,n} = \frac{g_m g_n - \mathbf{g}_m \mathbf{g}_n}{g^2 - \mathbf{g}^2}. \quad (6.8)$$

The interpretation of $p_{m,n}$ as the probability to detect the electrons from one Cooper pair transferred out of S into terminals m and n follows from (6.6b) when we consider the CGFs for the factors $P_S(2N)$ and $P(\{N_n\}|2N)$.

The Cooper pair transfer probability distribution $P_S(2N) = \int d\chi_S / (2\pi) \exp(-\mathcal{S}_S(\chi_S) + iN_S \chi_S)$ in (6.6b) has a CGF given by

$$\mathcal{S}_S = -\frac{t_0 V}{\sqrt{2}e} \sqrt{g_\Sigma^2 + \sqrt{(g_S^2 - g^2 + \mathbf{g}^2)^2 + 4g_S^2(g^2 - \mathbf{g}^2)} e^{2i\chi_S}}. \quad (6.9)$$

The π -periodicity of this function on χ_S ensures that an even number of charges $2N$ are transferred. The charges are then distributed among the F_n terminals according to a multinomial distribution $P(\{N_n\}|2N) = \int d^{M-1}\chi / (2\pi)^{M-1} \exp(-\mathcal{S}_N(\{\chi_n\}) + i\sum_n \chi_n N_n)$ with a CGF

$$\mathcal{S}_N(\{\chi_n\}) = N \ln \left(\sum_{m,n} p_{m,n} e^{-i\chi_m - i\chi_n} \right). \quad (6.10)$$

The functional dependence of the multinomial probability distribution $P(\{N_n\}|2N)$ on $p_{m,n}$ shows that (6.8) gives the probability that the quasiparticles of an Andreev quasiparticle pair are transferred into terminals F_m and F_n . The factorization of (6.7) in (6.6) can be shown directly from the definition of the probability distribution in terms of the CGFs (2.14) and the expressions for \mathcal{S}_S and \mathcal{S}_N .

6.2.2 Bell inequality violation

The entangled nature of the electrons flowing from the superconductor can be demonstrated by utilizing the ferromagnetic drains of the circuit in Figure 6.1 as detectors for spin [103]. Classically, there is a maximum for the correlation of the properties of two spatially separated and individual particles. The Bell-Clauser-Horne-Shimony-Holt (CHSH) inequality [104] determines the conditions under which the correlation between measurements on two separated particles cannot be explained by a classical and local theory (local realism).

Let us consider that there are four drains F_n ($n = 1..4$). Let pairs of drains F_1, F_2 (Left) and F_3, F_4 (Right) have pairwise equally large and antiparallel magnetizations, i.e. $\mathbf{g}_1 = -\mathbf{g}_2 = \mathbf{g}_L$ and $\mathbf{g}_3 = -\mathbf{g}_4 = \mathbf{g}_R$. We assume $g_1 = g_2$ and $g_3 = g_4$. The left and right pairs of drains form spin detectors with respect to magnetizations $\mathbf{m}_{L,R}$: Spins up in left detector are measured by the current in F_1 etc. Experiments should be performed with each spin detector in two different magnetization direction $\mathbf{m}_{L,R}$ and $\mathbf{m}'_{L,R}$.

The BCHSH inequality for the spin-entanglement setup in Figure 6.1 can be expressed in the two-particle probability that a spin σ is measured in the left detector and a spin σ' is measured in the right detector, $P_{\sigma,\sigma'}$. We discard events where both particles of a Cooper pair flow to the same detector by normalizing the probabilities to go to different detectors. The probability to measure e.g. spin up in the left and right detectors now becomes $P_{++} = p_{1,3}/(p_{1,3} + p_{1,4} + p_{2,3} + p_{2,4})$ where $p_{m,n}$ is the probability to measure simultaneously an electron into F_m and F_n given in (6.8). The Bell parameter is defined

$$\mathcal{E} = |E(\mathbf{m}_L, \mathbf{m}_R) + E(\mathbf{m}'_L, \mathbf{m}_R) + E(\mathbf{m}_L, \mathbf{m}'_R) - E(\mathbf{m}'_L, \mathbf{m}'_R)| \quad (6.11)$$

where the correlators are $E(\mathbf{m}, \mathbf{m}') = P_{++} + P_{--} - P_{+-} - P_{-+}$. Substituting the expressions for the probabilities $P_{\sigma,\sigma'}$ we obtain $E = -\mathbf{g}_L \mathbf{g}_R / g_L g_R$. Thus $\mathcal{E} = \mathcal{E}_0 g_{MRL} g_{MRR} / g_L g_R$ where $\mathcal{E}_0 = |\mathbf{m}_L \mathbf{m}_R + \mathbf{m}'_L \mathbf{m}_R + \mathbf{m}_L \mathbf{m}'_R - \mathbf{m}'_L \mathbf{m}'_R|$ is the expression for fully efficient spin detection. The largest possible value of \mathcal{E} in a local theory is 2. Since the maximum of \mathcal{E}_0 is $2\sqrt{2}$ in the optimum orientation of the magnetizations, violation of the BCHSH inequality $\mathcal{E} \leq 2$ can occur provided $g_{MRL,R}/g_{L,R} \geq 2^{-1/4}$. This condition on the efficiency of the detectors can be satisfied with half-metallic ferromagnets or magnetically engineered magnetic tunnel junctions [105].

Our counting statistics (6.7) describes how the two-particle probabilities are directly accessible in an experimental system. When the magnitude of the conductances of source and drains terminals are asymmetrically distributed ($g_S \gg g$ or $g \gg g_S$), the cross-correlations are a direct measure of the probabilities that electrons from a Cooper pair flow are transferred into different drains m and n ,

$$C_{mn} \xrightarrow{g_n g_S / (g^2 + g_S^2) \rightarrow 0} 2eI p_{m,n}. \quad (6.12)$$

Here, I is the net current flowing out of S. Although nonlocality cannot be demonstrated in a mesoscopic solid state device, our result for the cross-correlation above and the Bell parameter determines the experimental conditions to construct an entanglement witness. The result (6.12) also shows how the electron-hole pairs flowing into the ferromagnets give positive cross correlations in a fermion system. A negative contribution due to the Pauli principle is suppressed in the system with asymmetric conductances between source and drain, since the incoming beam of particles is noisy such that temporal correlations between different charge transfer events vanish.

6.3 FCS of crossed Andreev reflection and electron transfer

In Chapter 4 we considered the nonlocal conductance resulting from the competition between crossed Andreev reflection and electron transfer (ET) in circuits with one superconducting terminal and two normal-metal terminals N_1 and N_2 . In paper [9] we have calculated the full counting statistics for these processes, also considering spin polarizing interfaces (ferromagnetic terminals).

In the limit of strong conductance asymmetry between the superconducting and the ferromagnet terminals ($g_S \gg g$ or $g_{1(2)} \gg g_S, g_{2(1)}$), the CGF for the interesting energy range where both CA and ET processes occur ($eV_1 < E < eV_2$) can be expanded and interpretation of the statistics is straightforward,

$$\mathcal{S}_b = -\frac{t_0(V_2 - V_1)}{2eg_\Sigma^3} \left\{ [g_\Sigma^2 + (g - g_{MR})^2] (g_1g_2 + g_{MR1}g_{MR2})e^{ix_1 - ix_2} + g_S^2 \sum_n (g_n g_2 - g_{MRn} g_{MR2})e^{2ix_S - ix_n - ix_2} \right\}. \quad (6.13)$$

Here, we have considered collinear magnetization directions and the sign of g_{MRn} describes magnetization directions up (positive) or down (negative) along the z quantization axis. This CGF describes independent charge transfer by CA and ET according to Poissonian statistics. The conductances for ET and CA following from (6.13) are

$$G_{ET} = (g_1g_2 + g_{MR1}g_{MR2}) \frac{[g_\Sigma^2 + (g - g_{MR})^2]}{2g_\Sigma^3}, \quad (6.14a)$$

$$G_{CA} = (g_1g_2 - g_{MR1}g_{MR2}) \frac{g_S^2}{2g_\Sigma^3}. \quad (6.14b)$$

The magnetization dependence demonstrates that ET is favoured in a parallel configuration of the magnetizations ($g_{MR1}g_{MR2} > 0$) as the same spin in this case tunnels through both interfaces. On the other hand, CA is favoured by antiparallel magnetizations ($g_{MR1}g_{MR2} < 0$) since the opposite spins of a singlet tunnel through different interfaces.

The cross-correlation following from (6.13) is given by competing contributions from the CA and ET processes. This is natural since CA events lead to correlated currents of same sign in the two drain terminals, whereas ET events lead to correlated current flow of opposite sign in the drains,

$$C_{1,2} = 2e(V_2 + V_1)G_{CA} - 2e(V_2 - V_1)G_{ET}. \quad (6.15)$$

The sign of cross correlations are determined by two experimentally controllable parameters: The bias voltages in the prefactors and the relative magnetization directions through G_{CA} and G_{ET} . Thus the noise properties of the three-terminal circuit is a favourable candidate to experimentally demonstrate crossed Andreev reflection.

6.4 Conclusion

In conclusion, we have found the full counting statistics in systems where entangled quasi-particle pairs are created by Andreev reflection at a superconducting terminal. The statistics of the current flow into ferromagnet drains reveal the entangled nature of the Andreev reflected pairs. Theoretically, such properties have been considered by many authors [102, and references within] and experimental results are anticipated in the community.

The formalism to calculate the full counting statistics that we have used above is a powerful tool to investigate quantum information properties in solid state systems. With appropriate modifications and extensions, it may become useful in the study of more complicated systems in the future.

7 Outlook

At the end of the PhD study, one possesses the tools and knowledge needed to take on a bunch of relevant problems in the research field one has been working. In a way, your research carrier is just beginning! But different challenges and new opportunities await.

A number of ideas have crystallized during the work on this thesis, which I have not been able to pursue. Some of these project ideas are natural extensions of what we have considered so far, and some discussions have spawned ideas in completely different directions. Other projects have not been completed yet.

A complete theory of circuit theory boundary conditions for spin-active interfaces in superconducting systems is still lacking. During this study I spent months of effort together with Daniel Huertas-Hernando to obtain a better understanding of this problem. However, we have so far not reached this goal, but I hope our efforts can still bear fruits with the help of Severin Sadjina.

Experimental work on systems where concepts from quantum information theory is tested in a solid state environments will probably drive this research field forward in the near future. Paper [8] in this PhD explores an aspect in this area. Continued work in such directions would be very interesting.

8 Acknowledgements

*Ofte synes klok
den inkje vert spurd,
når trygt i ro han ruggar.¹*
Håvamål

These have been four exciting years! I have been able to work with very challenging and interesting problems together with brilliant researchers, travel around Europe and get friends and acquaintances from all parts of the world. For this experience, I owe my advisor Professor Arne Brataas my utmost gratitude. His extensive knowledge of physics and understanding of scientific work has been fascinating and instructive.

I would like to thank Wolfgang Belzig for a very good collaboration throughout my PhD studies, from which I have benefited greatly. By email and also during two visits in Basel and Konstanz, he has taught me a lot about mesoscopic superconductivity and full counting statistics, and it has been a pleasure to co-author with him.

The enthusiasm and innovative approach of Daniel Huertas-Hernando has been very stimulating, and I would like to thank him for all the good times we have had working together during the last three years. Additionally, we have communicated very well on the personal level.

I am grateful to Professors Christoph Bruder, Yuri Galperin, and Jon Andreas Støvneng who have agreed to constitute the evaluating committee for the present thesis and the defense to be held on March 28, 2008.

Thanks to Daniel Huertas-Hernando and Mathieu Taillefumier for careful proofreading of the thesis introduction, and thoughtful comments.

¹English translation: Many believe the man, who is not questioned to know much, and so he escapes their scorn.

My friends in the department have provided a unique working atmosphere, not only as an arena to discuss science, but also the even more important things in life. Thanks a lot to all of you! Particularly, I would like to thank Martin Grønsleth (takk for all moro vi har hatt sammen gjennom 13 år med parallelle studier!), Jan Øystein Haavig Bakke, Christian Andresen, Daniel Huertas-Hernando, Jo Smiseth, Stein Olav Skrøvseth, Anh Kiet Nguyen, Eskil Dahl, Steinar Kragseth, Frantz Stabo-Eeg, Jørn Foros, Hans Joakim Skadsem, Håvard Haugen, Jan Manschot, Mathieu Taillefumier, Edrun Schnell, Dionne Klein, Thomas Ramstad, Lars Erik Walle, Terje Røsten, Øyvind Borck, Eivind Smørgrav and Bjarte Solheim for a great time at the department.

Thanks to my beloved sister and parents, as well as my extended family for all your care and inspiration.

Kjære Janne Helene og Kjersti, takk for at dere gir mening og formål med livet.

A Notation

Operators

For operators/matrices A and B ,

- the (anti)commutator is denoted $[A, B]_{(+)-}$.
- the quantum statistical average is denoted $\langle A \rangle$.

Matrix notation

The Pauli matrices are τ_n where $n = 1, 2, 3$ and the vector of Pauli matrices is denoted $\boldsymbol{\tau} = (\tau_1, \tau_2, \tau_3)$. Matrices in $\text{spin} \otimes \text{Nambu} \otimes \text{Keldysh}$ space are constructed by direct products of these where we denote the relevant matrix subspace by accents:

- $\bar{\tau}_n$ is a matrix in spin subspace.
- $\hat{\tau}_n$ is a matrix in Nambu subspace.
- $\check{\tau}_n$ is a matrix in Keldysh subspace.

Unit matrices are usually suppressed, so that i.e. $\bar{\tau}_m \hat{1} \check{1} + \bar{1} \hat{1} \check{\tau}_n$ is written $\bar{\tau}_m + \check{\tau}_n$.

The notation $(A)_{m,n}$ denotes the matrix element in the m -th row and n -th column of A .

Bibliography

- [1] J. P. Morten, A. Brataas, and W. Belzig, Phys. Rev. B **70**, 212508 (2004).
- [2] J. P. Morten, A. Brataas, and W. Belzig, Phys. Rev. B **72**, 014510 (2005).
- [3] N. Poli, J. P. Morten, M. Urech, A. Brataas, D. B. Haviland, and V. Korenivski, to appear in Phys. Rev. Lett. (2008), arXiv:cond-mat/0707.2879.
- [4] J. P. Morten, A. Brataas, G. E. W. Bauer, W. Belzig, and Y. Tserkovnyak, arXiv:0712.2814 (2007).
- [5] J. P. Morten, A. Brataas, and W. Belzig, Phys. Rev. B **74**, 214510 (2006).
- [6] J. P. Morten, A. Brataas, and W. Belzig, Appl. Phys. A **89**, 609 (2007).
- [7] J. P. Morten, Quantum physics and the boundaries of space and time, in *Complexity*, edited by W. Østremg, Centre for Advanced Study, Oslo, 2008.
- [8] J. P. Morten, D. Huertas-Hernando, A. Brataas, and W. Belzig, Europhys. Lett. **81**, 40002 (2008).
- [9] J. P. Morten, D. Huertas-Hernando, A. Brataas, and W. Belzig, Full counting statistics of crossed Andreev reflection, 2008, Unpublished.
- [10] A. Einstein, B. Podolsky, and N. Rosen, Phys. Rev. **47**, 777 (1935).
- [11] P. G. de Gennes, *Superconductivity of Metals and Alloys*, W.A. Benjamin, 1966.
- [12] R. D. Parks, editor, *Superconductivity*, Marcel Dekker, New York, 1969.
- [13] M. Tinkham, *Introduction to Superconductivity*, McGraw-Hill, 1975.
- [14] K. Fossheim and A. Sudbø, *Superconductivity: Physics and Applications*, Wiley, 2004.
- [15] J. Bardeen, L. N. Cooper, and J. R. Schrieffer, Phys. Rev. **108**, 1175 (1957).
- [16] I. Giaever, Phys. Rev. Lett. **5**, 147 (1960).

- [17] W. L. McMillan, Phys. Rev. **175**, 537 (1968); S. M. Freake and C. J. Adkins, Phys. Lett. **7**, 382 (1969); J. Vrba and S. B. Woods, Phys. Rev. B **3**, 2243 (1971); J. R. Toplicar and D. K. Finnemore, Phys. Rev. B **16**, 2072 (1977); A. F. Volkov *et al.*, Physica C **210**, 21 (1993); S. Guéron *et al.*, Phys. Rev. Lett. **77**, 3025 (1996); W. Belzig *et al.*, Phys. Rev. B **54**, 9443 (1996); B. Pannetier and H. Courtois, J. Low Temp. Phys. **118**, 599 (2000); E. Scheer *et al.*, Phys. Rev. Lett. **86** 284 (2001).
- [18] A. F. Andreev, Sov. Phys. JETP **19**, 1228 (1964).
- [19] B. J. van Wees, P. de Vries, P. Magnée, and T. M. Klapwijk, Phys. Rev. Lett. **69**, 510 (1992).
- [20] F. W. J. Hekking and Y. V. Nazarov, Phys. Rev. B **49**, 6847 (1994).
- [21] C. W. J. Beenakker, Rev. Mod. Phys. **69**, 731 (1997).
- [22] J. Y. Gu *et al.*, Phys. Rev. Lett. **89**, 267001 (2002); A. Potenza and C. H. Marrows, Phys. Rev. B **71**, 180503(R) (2005); I. C. Moraru, W. P. Pratt Jr., and N. O. Birge, Phys. Rev. B **74**, 220507 (2006); A. Yu. Rusanov, S. Habraken, and J. Aarts, Phys. Rev. B **73**, 060505(R) (2006).
- [23] B. D. Josephson, Phys. Letters **1**, 251 (1962).
- [24] M. Hämmäläinen, R. Hari, R. J. Ilmoniemi, J. Knuutila, and O. V. Lounasmaa, Rev. Mod. Phys. **65**, 4137 (1993).
- [25] Y. Makhlin, G. Schön, and A. Shnirman, Rev. Mod. Phys. **73**, 357 (2001).
- [26] M. H. Devoret and J. M. Martini, Quant. Inf. Proc. **3**, 163 (2005).
- [27] J. Majer *et al.*, Nature **449**, 443 (2007).
- [28] M. N. Baibich *et al.*, Phys. Rev. Lett. **61**, 2472 (1988).
- [29] G. Binasch, P. Grünberg, F. Saurenbach, and W. Zinn, Phys. Rev. B **39**, 4828 (1989).
- [30] Y. Tserkovnyak, A. Brataas, G. E. W. Bauer, and B. I. Halperin, Rev. Mod. Phys. **77**, 1375 (2005).
- [31] A. Brataas, G. E. W. Bauer, and P. J. Kelly, Phys. Rep. **427**, 157 (2006).
- [32] A. I. Buzdin, Rev. Mod. Phys. **77**, 935 (2005).
- [33] F. S. Bergeret, A. F. Volkov, and K. B. Efetov, Rev. Mod. Phys. **77**, 1321 (2005).
- [34] M. Eschrig *et al.*, J. Low Temp. Phys. **147**, 457 (2007).
- [35] F. S. Bergeret, A. F. Volkov, and K. B. Efetov, Appl. Phys. A **89**, 599 (2007).

-
- [36] A. Schmid, Kinetic equations for dirty superconductors, in *Nonequilibrium Superconductivity, Phonons, and Kapitza boundaries*, edited by K. E. Gray, volume 65 of *NATO Advanced Studies Institute, Series B: Physics*, pages 423–480, Plenum Press, New York, 1981.
- [37] J. Rammer and H. Smith, *Rev. Mod. Phys.* **58**, 323 (1986).
- [38] W. Belzig, F. K. Wilhelm, C. Bruder, G. Schön, and A. D. Zaikin, *Superlatt. Microstruct.* **25**, 1251 (1999).
- [39] V. Chandrasekhar, *The Physics of Superconductors*, chapter An introduction to the quasiclassical theory of superconductivity for diffusive proximity-coupled systems, Springer-Verlag, 2004.
- [40] N. Kopnin, *Theory of Nonequilibrium Superconductivity*, Oxford Science Publications, 2001.
- [41] L. P. Gor'kov, *Zh. Eksp. Theor. Fiz.* **36**, 1918 (1959) [*Sov. Phys. JETP* **9**, 1364 (1959)]; L. P. Gor'kov, *Zh. Eksp. Theor. Fiz.* **37**, 1407 (1959) [*Sov. Phys. JETP* **10**, 998 (1960)].
- [42] G. Eilenberger, *Zeitschrift für Physik A Hadrons and Nuclei* **214**, 195 (1970).
- [43] L. Kadanoff and G. Baym, *Quantum Statistical Mechanics*, Addison-Wesley, Redwood City, 1962.
- [44] A. I. Larkin and Yu. N. Ovchinnikov, *Zh. Eksp. Teor. Fiz.* **68**, 1915 (1976) [*Sov. Phys. JETP* **41**, 960 (1976)].
- [45] K. D. Usadel, *Phys. Rev. Lett.* **25**, 507 (1970).
- [46] A. V. Zaitsev, *Sov. Phys. JETP* **59**, 1015 (1984).
- [47] M. Y. Kupriyanov and V. F. Lukichev, *Sov. Phys. JETP* **67**, 1163 (1988).
- [48] A. Kamenev, Many-body theory of non-equilibrium systems, in *Nanophysics: Coherence and transport*, edited by H. Bouchiat, Y. Gefen, S. Guéron, G. Montambaux, and J. Dalibard, Elsevier B. V., 2005.
- [49] A. M. Zagoskin, *Quantum Theory of Many-Body Systems*, Springer, 1998.
- [50] L. V. Keldysh, *Zh. Eksp. Theor. Phys* **47**, 1515 (1964) [*Sov. Phys. JETP* **20**, 1018 (1965)].
- [51] Yu. V. Nazarov, *Phys. Rev. Lett.* **73**, 1420 (1994).
- [52] Yu. V. Nazarov, *Superlatt. Microstruct.* **25**, 1221 (1999).

- [53] A. Brataas, Y. V. Nazarov, and G. E. W. Bauer, *Phys. Rev. Lett.* **84**, 2481 (2000).
- [54] Yu. V. Nazarov, Quantum transport and circuit theory, in *Handbook of Theoretical and Computational Nanotechnology*, edited by M. Rieth and W. Schommers, chapter 95, pages 1–83, American Scientific Publishers, 2005.
- [55] D. Huertas-Hernando, G. E. W. Bauer, and Yu. V. Nazarov, *Journal of Magnetism and Magnetic Materials* **240**, 174 (2002).
- [56] W. Belzig, A. Brataas, Y. V. Nazarov, and G. E. W. Bauer, *Phys. Rev. B* **62**, 9726 (2000).
- [57] A. D. Stone, P. A. Mello, K. A. Muttalib, and J.-L. Pichard, Random matrix theory and maximum entropy models for disordered conductors, in *Mesoscopic Phenomena in Solids*, edited by B. L. Altshuler, P. A. Lee, and R. A. Webb, North Holland, Amsterdam, 1991.
- [58] D. Huertas-Hernando, *Coherent transport in superconducting and ferromagnetic hybrid structures*, PhD thesis, TU Delft, 2002.
- [59] D. Huertas-Hernando, Y. V. Nazarov, and W. Belzig, (2002), arXiv:cond-mat/0204116.
- [60] A. Cottet and W. Belzig, *Phys. Rev. B* **72**, 180503 (2005).
- [61] A. Cottet, *Phys. Rev. B* **76**, 224505 (2007).
- [62] D. Huertas-Hernando, Y. V. Nazarov, and W. Belzig, *Phys. Rev. Lett.* **88**, 047003 (2002).
- [63] L. S. Levitov and G. B. Lesovik, *JETP Lett.* **58**, 230 (1993).
- [64] W. Belzig and Yu. V. Nazarov, *Phys. Rev. Lett.* **87**, 067006 (2001); W. Belzig and Yu. V. Nazarov, *Phys. Rev. Lett.* **87**, 197006 (2001).
- [65] Yu. V. Nazarov and D. A. Bagrets, *Phys. Rev. Lett.* **88**, 196801 (2002).
- [66] S. Gustavsson et al., *Phys. Rev. Lett.* **96**, 076605 (2006).
- [67] W. Belzig, Full counting statistics of superconductor-normal-metal heterostructures, in *Quantum noise in mesoscopic physics*, edited by Yu. V. Nazarov and Ya. M. Blanter, Kluwer Academic Publishers, Dordrecht, 2003.
- [68] F. J. Jedema, H. B. Heersche, A. T. Filip, J. J. A. Baselmans, and B. J. van Wees, *Nature (London)* **416**, 713 (2002).
- [69] F. J. Jedema, M. S. Nijboer, A. T. Filip, and B. J. van Wees, *Phys. Rev. B* **67**, 085319 (2003).

-
- [70] J. Y. Gu, J. A. Caballero, R. D. Slater, R. Loloee, and W. P. Pratt Jr., Phys. Rev. B **66**, 140507(R) (2002).
- [71] C. Bell, S. Milikisyants, M. Huber, and J. Aarts, Phys. Rev. Lett. **100**, 047002 (2008).
- [72] J. P. Morten, Spin and charge transport in dirty superconductors, Master's thesis, Norwegian University of Science and Technology (NTNU), 2003.
- [73] Y. Yafet, Phys. Lett. A **98**, 287 (1983).
- [74] H. L. Zhao and S. Hershfield, Phys. Rev. B **52**, 3632 (1995).
- [75] F. Aspen and A. M. Goldman, Phys. Rev. Lett. **43**, 307 (1979).
- [76] A. A. Abrikosov and L. P. Gor'kov, Zh. Eksp. Teor. Fiz. **39**, 1781 (1960) [Sov. Phys. JETP **12**, 1243 (1961)].
- [77] A. Schmid and G. Schön, J. Low Temp. Phys. **20**, 207 (1975).
- [78] S. Takahashi, H. Imamura, and S. Maekawa, Phys. Rev. Lett. **82**, 3911 (1999).
- [79] Y. Tserkovnyak and A. Brataas, Phys. Rev. B **65**, 094517 (2002).
- [80] K. Maki, Gapless Superconductivity, in *Superconductivity*, edited by R. D. Parks, volume 2, pages 1035–1106, Marcel Dekker, New York, 1969.
- [81] J. M. Byers and M. E. Flatte, Phys. Rev. Lett. **74**, 306 (1995).
- [82] G. Deutscher and D. Feinberg, Appl. Phys. Lett. **76**, 487 (2000).
- [83] G. Falci, D. Feinberg, and F. W. J. Hekking, Europhys. Lett. **54**, 255 (2001).
- [84] R. Mélin and D. Feinberg, Phys. Rev. B **70**, 174509 (2004).
- [85] S. Russo, M. Kroug, T. M. Klapwijk, and A. F. Morpurgo, Phys. Rev. Lett. **95**, 027002 (2005).
- [86] P. Cadden-Zimansky and V. Chandrasekhar, Phys. Rev. Lett. **97**, 237003 (2006).
- [87] D. Beckmann and H. v. Löhneysen, Appl. Phys. A **89**, 603 (2007).
- [88] D. Beckmann, H. B. Weber, and H. v. Löhneysen, Phys. Rev. Lett. **93**, 197003 (2004).
- [89] D. Beckmann and H. v. Löhneysen, AIP Conference Proceedings **850**, 875 (2006).
- [90] A. L. Yeyati, F. Bergeret, A. Martin-Rodero, and T. Klapwijk, Nature Phys. **3**, 455 (2007).

- [91] J. S. Bell, *Physics* **1**, 195 (1964).
- [92] M. P. Anantram and S. Datta, *Phys. Rev. B* **53**, 16390 (1996).
- [93] T. Martin, *Phys. Lett. A* **220**, 137 (1996).
- [94] V. Rychkov and M. Buttiker, *Phys. Rev. Lett.* **96**, 166806 (2006).
- [95] S. Oberholzer, E. Bieri, C. Schönenberger, M. Giovannini, and J. Faist, *Phys. Rev. Lett.* **96**, 046804 (2006).
- [96] J. Börlin, W. Belzig, and C. Bruder, *Phys. Rev. Lett.* **88**, 197001 (2002).
- [97] G. B. Lesovik, T. Martin, and G. Blatter, *Eur. Phys. J. B* **24**, 287 (2001); P. Samuelsson and M. Büttiker, *Phys. Rev. Lett.* **89**, 046601 (2002); P. Recher and D. Loss, *Phys. Rev. Lett.* **91**, 267003 (2003); P. Samuelsson, E. V. Sukhorukov, and M. Büttiker, *Phys. Rev. Lett.* **91**, 157002 (2003); L. Faoro, F. Taddei, and R. Fazio, *Phys. Rev. B* **69**, 125326 (2004); P. Samuelsson, E. V. Sukhorukov, and M. Büttiker, *Phys. Rev. B* **70**, 115330 (2004).
- [98] P. Recher, E. V. Sukhorukov, and D. Loss, *Phys. Rev. B* **63**, 165314 (2001); N. M. Chtchelkatchev, G. Blatter, G. B. Lesovik, and T. Martin, *Phys. Rev. B* **66**, 161320(R) (2002).
- [99] K. V. Bayandin, G. B. Lesovik, and T. Martin, *Phys. Rev. B* **74**, 085326 (2006).
- [100] D. Sanchez, R. Lopez, P. Samuelsson, and M. Buttiker, *Phys. Rev. B* **68**, 214501 (2003).
- [101] G. Bignon, M. Houzet, F. Pistolesi, and F. W. J. Hekking, *Europhys. Lett.* **67**, 110 (2004).
- [102] G. Burkard, *J. Phys.: Condens. Matter* **19**, 233202 (2007).
- [103] A. Di Lorenzo and Yu. V. Nazarov, *Phys. Rev. Lett.* **94**, 210601 (2005).
- [104] M. A. Nielsen and I. L. Chuang, *Quantum Computation and Quantum Information*, Cambridge, 2000.
- [105] S. S. P. Parkin et al., *Nature Mater.* **3**, 862 (2004).

PAPER 1

Spin transport in diffusive superconductors

Physical Review B **70**, 212508 (2004)

Spin transport in diffusive superconductors

Jan Petter Morten,¹ Arne Brataas,¹ and Wolfgang Belzig²

¹*Department of Physics, Norwegian University of Science and Technology, 7491 Trondheim, Norway*

²*Department of Physics and Astronomy, University of Basel, Klingelbergstrasse 82, 4056 Basel, Switzerland*

(Received 8 September 2004; published 23 December 2004)

We employ the Keldysh formalism in the quasiclassical approximation to study transport in a diffusive superconductor. The resulting 4×4 transport equations describe the flow of charge and energy as well as the corresponding flow of spin and spin energy. Spin-flip scattering due to magnetic impurities is included. We find that the spin-flip length is renormalized in the superconducting case and propose an experimental system to measure the spin accumulation in a superconductor.

DOI: 10.1103/PhysRevB.70.212508

PACS number(s): 74.25.Fy, 72.25.Hg, 72.25.Ba

Manipulation of spin-polarized currents can be used to study fundamental transport processes and might also provide new functionality in electronic devices. In ferromagnets (F), the current is spin-polarized due to the spin-dependent density of states and the spin-dependent scattering potentials. In contrast, in *s*-wave superconductors (S), electrons with spin up and spin down and opposite momentum form Cooper pairs with no net spin. Nanoscale superconductors therefore display strikingly different properties when driven out of equilibrium by spin transport than by charge transport.

Most of the recent activities on the transport properties of F/S junctions have studied effects caused by the physical properties on the F side of the junction. The zero spin Cooper pairs prevent spin-polarized electrons to flow into S. Consequently, a spin-polarized current from F injected into S can result in nonequilibrium spin accumulation near the F/S interface. The competition between electron-hole correlations and spin accumulation on the F side has recently attracted considerable interest.¹ Possible influence of the ferromagnetic order parameter on the superconductor has received less attention. Singlet pairing does not allow a spin accumulation in the superconductor. Consequently, spin accumulation can reduce the superconducting gap and change the transport properties both for transport via quasiparticles and for the supercurrent. Experimentally, spin transport in diffusive S has recently been studied.² Here, the reduced quasiparticle penetration due to spin accumulation results in loss of spin memory which can be measured as a decreased magnetoresistance.

Although the theory of nonequilibrium superconductivity is widely used and developed, it has not been completely generalized to study spin transport. In this paper we thus use the Keldysh formalism and the quasiclassical approximation³⁻⁵ to rigorously obtain a set of equations describing the transport of charge and energy in a diffusive weak coupling S, as well as the transport of spin. This will describe the penetration of spins into S and the associated suppression of the superconducting order parameter. Our description of the transport properties will be based on a 4×4 matrix equation formalism to include spin accumulation as well as electron-hole correlations. Spin-flip scattering from magnetic impurities is included as the dominant spin relaxation process inside the superconductor. We find that the spin-flip length is renormalized in the BCS case, and propose

an experimental system to measure the properties resulting from the superconducting correlations. Many, but not all, experimental systems involving spin transport in superconductors are in the *elastic* transport regime,⁶ which is considered here. Complementary studies based on the Boltzmann equation for spin-transport by quasiparticles in the *inelastic* transport regime have recently been published.⁷ Note that spin injection is qualitatively different in these opposite transport regimes due to the strong energy dependence of quasiparticle flow in superconductors.⁷

Let us now outline the derivation of our main results. We use natural units so that $\hbar = k_B = 1$, and the electron charge is $e = -|e|$. To describe the out-of-equilibrium electron-hole correlations as well as spin accumulation, we define the Keldysh Green's function as

$$\hat{G}_{ij}^K(1,2) = \sum_k (-i)(\hat{\rho}_3)_{ik} \langle [(\psi(1))_k, (\psi^\dagger(2))_j]_- \rangle, \quad (1)$$

where $\psi = [\psi_\uparrow, \psi_\downarrow, \psi_\uparrow^\dagger, \psi_\downarrow^\dagger]^T$ is a four-vector and ψ^\dagger the corresponding adjoint vector. The matrix $\hat{\rho}_3$ is the third Pauli matrix generalized to 4×4 space, $\hat{\rho}_3 = \text{diag}(1, 1, -1, -1)$. The coordinates are $1 = (\mathbf{r}_1, t_1)$ and $2 = (\mathbf{r}_2, t_2)$. Similarly, we define 4×4 retarded and advanced Green's functions (\hat{G}^R, \hat{G}^A) in spin- and particle-hole space. 4×4 matrices are denoted by a "hat" superscript. A compact notation can be obtained by construction of an 8×8 matrix in the Keldysh space (denoted by a "check" superscript).⁵

The quasiclassical Green's function is defined by $\check{g}(\mathbf{R}, T, \mathbf{p}_F, E) = i/\pi \int d\xi_p \check{G}(\mathbf{R}, T, \mathbf{p}, E)$. This function is determined by the Eilenberger equation which in the mixed representation for a stationary state can be written

$$\left[E\hat{\rho}_3 + i\frac{\mathbf{p}}{m} \cdot \hat{\partial} - e\phi\hat{1} - \hat{\Delta} - \check{\sigma}, \check{g} \right]_- = 0, \quad (2)$$

where $\hat{\partial} = \nabla \hat{1} - ie\mathbf{A}\hat{\rho}_3$ is the gauge invariant derivative, $\hat{1}$ is the 4×4 unit matrix, ϕ is the electromagnetic scalar potential, $\hat{\Delta}$ contains the superconducting gap, and $\check{\sigma}$ is the self-energy due to elastic impurity scattering and spin-flip scattering by magnetic impurities in quasiclassical approximation. In the case of strong impurity scattering (dirty limit) transport is diffusive. Expansion of the quasi-

classical Green's function in spherical harmonics then gives the Usadel equations. The symmetries and normalization of the Green's function allows for a parameterization of the quasiclassical, retarded component:⁴

$$\hat{g}_s^R = \begin{pmatrix} \bar{1} \cosh(\theta) & i\bar{\tau}_2 \sinh(\theta)e^{i\chi} \\ i\bar{\tau}_2 \sinh(\theta)e^{-i\chi} & -\bar{1} \cosh(\theta) \end{pmatrix}, \quad (3)$$

where $\bar{1}$ is the 2×2 unit matrix, $\bar{\tau}_2$ is the second Pauli matrix, and θ and χ are position and energy dependent functions. We assume colinear magnetizations along the z axis and s -wave singlet superconducting state. We choose a gauge where the superconducting order parameter Δ is real and positive, and then the supercurrent is contained in the electromagnetic vector potential \mathbf{A} and the chemical potential of the Cooper pairs is included in ϕ . Inspection of the self-consistency relation for Δ reveals that $\chi=0, \pi$ depending on the boundary conditions. This ansatz simplifies the calculations considerably. The advanced Green's function is related to the retarded through $\hat{g}^A = -[\hat{\rho}_3 \hat{g}_s^R \hat{\rho}_3]^\dagger$. Because of normalization, the Keldysh Green's function can be expressed as $\hat{g}^K = \hat{g}^R \hat{h} - \hat{h} \hat{g}^A$ where \hat{h} is a diagonal distribution function matrix.

We will now consider a stationary state. A kinetic equation can be derived from the Usadel equations if we include Keldysh components. The important quantities are the physical particle and energy currents (including particles and holes), which we will denote by \mathbf{j}_T and \mathbf{j}_L , respectively, with the corresponding distribution functions carrying the same indices, h_T and h_L .⁴ The physical spin current is denoted \mathbf{j}_{TS} and the spin energy current \mathbf{j}_{LS} , with distribution functions h_{TS} and h_{LS} . The spin-resolved distribution functions can be expressed by the particle distribution function as $h_{TS(LS)} = -[f_\uparrow(E) - f_\downarrow(E)]/2 - (+)[f_\uparrow(-E) - f_\downarrow(-E)]/2$. The current components \mathbf{j}_T , etc. are spectral quantities, and the total charge current is given as an integral $\mathbf{j}_{\text{charge}}(\mathbf{r}, t) = |e|N_0 \int_{-\infty}^{\infty} dE \mathbf{j}_T(\mathbf{r}, t, E)$, and the spin current is obtained by a similar integral of \mathbf{j}_{TS} . Energy current is given by $\mathbf{j}_{\text{energy}}(\mathbf{r}, t) = |e|N_0 \int_{-\infty}^{\infty} dE E \mathbf{j}_L(\mathbf{r}, t, E)$, and the difference in energy current carried by opposite spins by a similar integral of \mathbf{j}_{LS} .

The equilibrium solutions for the distribution functions are $h_{L,0} = \tanh(\beta E/2)$ and $h_{T,0} = h_{LS,0} = h_{TS,0} = 0$. We derive kinetic equations and find:

$$\nabla \cdot \mathbf{j}_L = 0, \quad (4a)$$

$$\nabla \cdot \mathbf{j}_T = -2|\Delta| \alpha_{TT} h_T, \quad (4b)$$

$$\nabla \cdot \mathbf{j}_{LS} = - \left(2|\Delta| \alpha_{TT} + \frac{1}{\tau_{\text{sf}}} \alpha_{\text{LSLS}} \right) h_{LS}, \quad (4c)$$

$$\nabla \cdot \mathbf{j}_{TS} = - \frac{1}{\tau_{\text{sf}}} \alpha_{\text{TSTS}} h_{TS}. \quad (4d)$$

The right-hand side terms represent renormalized scattering because of superconductivity:

$$\alpha_{TT} = \text{Im}[\sinh(\theta)], \quad (5a)$$

$$\alpha_{\text{LSLS}} = \{\text{Re}[\cosh(\theta)]\}^2 - \{\text{Im}[\sinh(\theta)]\}^2, \quad (5b)$$

$$\alpha_{\text{TSTS}} = \{\text{Re}[\cosh(\theta)]\}^2 + \{\text{Re}[\sinh(\theta)]\}^2. \quad (5c)$$

The $|\Delta| \alpha_{TT}$ terms on the right-hand side in Eq. (4) are due to conversion of quasiparticle current into supercurrent, and the $\alpha_{\text{LSLS}}/\tau_{\text{sf}}$, $\alpha_{\text{TSTS}}/\tau_{\text{sf}}$ terms are due to spin flips. The spin-flip time in the normal state is $\tau_{\text{sf}}^{-1} = 8\pi n_{\text{sf}} N_0 S(S+1) |v_{\text{sf}}|^2/3$, where n_{sf} is the magnetic impurity density, N_0 the density of states at the Fermi level, S the impurity spin quantum number, and v_{sf} is the Fourier transformed spin-flip impurity potential. We assume isotropic scattering. Our definition of τ_{sf} differs from the usual spin-flip lifetime by a renormalization factor $4/3$. This definition reproduces the diffusion equation with a spin-flip length $l_{\text{sf}}^{(N)} = \sqrt{D\tau_{\text{sf}}}$ in the normal state. Thus there is a difference between the spin-flip lifetime measured in, e.g., electron spin resonance and spin-flip transport time.

We introduce generalized energy-dependent diffusion coefficients

$$D_L = D(\{\text{Re}[\cosh(\theta)]\}^2 - \{\text{Re}[\sinh(\theta)]\}^2), \quad (6a)$$

$$D_T = D(\{\text{Re}[\cosh(\theta)]\}^2 + \{\text{Im}[\sinh(\theta)]\}^2), \quad (6b)$$

where $D = \tau v_F^2/3$ is the diffusion constant. The currents can then be expressed as

$$\mathbf{j}_L = -D_L \nabla h_L + \text{Im}\{\mathbf{j}_E\} h_T, \quad (7a)$$

$$\mathbf{j}_T = -D_T \nabla h_T + \text{Im}\{\mathbf{j}_E\} h_L, \quad (7b)$$

$$\mathbf{j}_{LS} = -D_T \nabla h_{LS} + \text{Im}\{\mathbf{j}_E\} h_{TS}, \quad (7c)$$

$$\mathbf{j}_{TS} = -D_L \nabla h_{TS} + \text{Im}\{\mathbf{j}_E\} h_{LS}, \quad (7d)$$

where we have defined the spectral supercurrent as $\mathbf{j}_E = D(\nabla \chi - 2e\mathbf{A}) \sinh^2(\theta)$. The self-consistency relation is

$$\Delta(\mathbf{r}) = -\frac{1}{2} \text{sgn}(\Delta_0) N_0 \lambda \int_{-\infty}^{\infty} dE \sinh(\theta) h_L, \quad (8)$$

where the factor $\text{sgn}(\Delta_0)$ is determined from the boundary condition to give the correct sign and λ is the interaction parameter. The complex part of this equation is neglected as a consequence of charge conservation.⁸

The functions θ and χ are determined by the retarded components of the Usadel equation. We obtain

$$\nabla \cdot \mathbf{j}_E = 0, \quad (9)$$

$$\begin{aligned} D \left(\nabla^2 \theta - \frac{1}{2} (\nabla \chi - 2e\mathbf{A})^2 \sinh(2\theta) \right) \\ = -2iE \sinh(\theta) - 2i \cosh(\theta) |\Delta| + \frac{3}{4} \frac{1}{\tau_{\text{sf}}} \sinh(2\theta), \end{aligned} \quad (10)$$

where Eq. (9) implies that the spectral supercurrent is conserved. In addition we have the following symmetry conditions, $\theta^*(-E) = -\theta(E)$, $\chi^*(-E) = \chi(E)$. Equations (4)–(10) determine all transport properties of S .

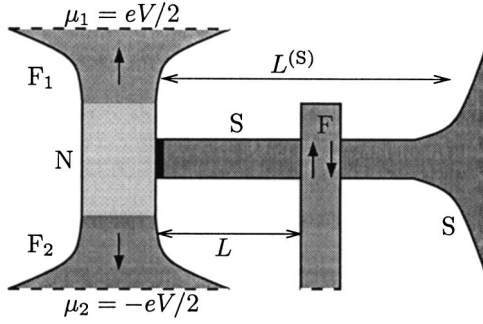


FIG. 1. Spin battery connected to a superconductor. The thick solid line indicates a tunnel barrier.

In general, in a hybrid F/S system, the superconductor cannot be described as in terms of BCS formulas close to the F/S interface due to the proximity effect. Nevertheless, to gain insight into the physics implied by the abovementioned formulas let us now consider the limit of a homogeneous BCS superconductor, and select $\chi=0$. This is relevant for the proposed experiment below. For energies $|E| < |\Delta|$, $\alpha_{\text{TT}} = \Delta/\sqrt{\Delta^2 - E^2}$ and the spin-flip renormalization factors are $\alpha_{\text{TSTS}}=0$, $\alpha_{\text{LSLS}} = -\Delta^2/(\Delta^2 - E^2)$. The generalized diffusion constant $D_L=0$ while $D_T = D\Delta^2/(\Delta^2 - E^2)$. From Eq. (7a) this means that there is no energy current carried by quasiparticles with energy $|E| < |\Delta|$. Gap scattering for quasiparticle energies below the superconducting gap corresponds to a transformation of the charge current (\mathbf{j}_T) into supercurrent. Such scattering is not possible for the physical spin current (\mathbf{j}_{TS}). Consequently, in the absence of spin-flip scattering the quasiparticle spin current into the superconductor vanishes for $|E| < |\Delta|$ since $D_L=0$ in Eq. (7d) and $\alpha_{\text{TSTS}}=0$ in the kinetic Eq. (4d). Note that this result relies on the fact that there are different effective diffusion coefficients for charge current (D_T) and for spin current (D_L). We also observe that the term α_{LSLS} is *negative* below the gap, acting as a source of spin energy.

Above the gap ($|E| > |\Delta|$) the factor α_{TT} vanishes while $\alpha_{\text{LSLS}} = E^2/(E^2 - \Delta^2)$, $\alpha_{\text{TSTS}} = (E^2 + \Delta^2)/(E^2 - \Delta^2)$. For the generalized diffusion coefficients we find that $D_L = D$ and $D_T = DE^2/(E^2 - \Delta^2)$. Now consider the kinetic equations in the BCS case. A charge current carried by quasiparticles with energy $|E| > |\Delta|$ can propagate into S. For quasiparticles at $|E| > |\Delta|$ we see that there is no renormalization for the spin-energy diffusion length in Eq. (4c), whereas the spin diffusion length in Eq. (4d) has an energy dependent renormalization factor which diverges for energies $|E|=|\Delta|$ causing massive spin-flip scattering.

We will now apply this formalism to study spin diffusion, and demonstrate the significance of the renormalization of the spin diffusion length. Experimental studies of spin accumulation and spin injection has recently been performed⁹ in metallic spin valves. The spin accumulation in the physically different *inelastic* regime for a superconductor in this experimental system has also been calculated theoretically.⁷ We will consider the simplified geometry shown in Fig. 1, where there is no charge transport in the superconductor, and calculate the spin-accumulation signal in the *elastic* regime. The F₁/N/F₂ systems act as a spin battery which is connected via

a tunnel junction to the superconductor. A voltage bias between F₁ and F₂ induces a spin accumulation that can flow into S. The superconducting wire is connected to an S reservoir in equilibrium BCS state by a good metallic contact at distance $L^{(S)}$ from the N/S interface. On top of the S wire there is a ferromagnet connected by tunnel barrier which upon switching of the magnetization direction acts as a detector for the spin signal. Measurement of the relative voltage of this electrode between parallel and antiparallel (with respect to the top F reservoir) magnetization gives $\Delta\mu = \mu^{(P)} - \mu^{(AP)}$ which describes the difference between electrochemical potential of spin-up and spin-down quasiparticles located a distance L from the N/S interface. This quantity can be calculated $\Delta\mu = -\int_{-\infty}^{\infty} dE P^{(D)} h_{\text{TS}}(L, E)$, where $P^{(D)}$ is the spin polarization of the tunnel barrier between S and the F detector. We assume a homogeneous order parameter and BCS spectral properties in the S wire since there are tunnel barriers between the N, F, and S elements and perturbation from current and spin-flip is weak.

We can express the difference between the spin-up and spin-down distribution functions in N close to S as $\Delta f^{(N)} \equiv f_{\uparrow}^{(N)} - f_{\downarrow}^{(N)} = P^{(FN)} [f(E - eV/2) - f(E + eV/2)]$, where $P^{(FN)} = (G_{\text{maj}} - G_{\text{min}})/(G_{\text{maj}} + G_{\text{min}})$ is the spin polarization between the F reservoirs and N, $f(E \pm eV/2)$ is the Fermi-Dirac distributions in the F reservoirs and $G_{\text{maj(min)}}$ is the conductance of majority (minority) spin electrons from ferromagnetic reservoir to the middle of N. There is thus no charge current or supercurrent anywhere in S, however there may be a spin current. Equation (7d) states that there is no spin-current for energies below the gap, thus for these energies the N/S interface is effectively insulating. Since the S wire is connected to a reservoir in the other end for $|E| < \Delta$ the spin distribution function equals the equilibrium value $h_{\text{TS}}=0$. We solve the TS kinetic Eq. (4d) for energies $|E| > \Delta$. This equation reduces to a diffusion equation with renormalized spin-flip length $l_{\text{sf}}^{(S)}(E) = l_{\text{sf}} \sqrt{(E^2 - \Delta^2)/(E^2 + \Delta^2)}$, where $l_{\text{sf}} = \sqrt{D\tau_{\text{sf}}}$ is the normal state spin-flip length. The boundary condition at the S reservoir is that the distribution function attains the equilibrium value, and at the S/N interface we match at each energy the tunnel spin current to the spin current inside S, $|e|N_0\mathbf{j}_{\text{TS}}$. We assume that $L^{(S)}/l_{\text{sf}}^{(S)} \gg 1$ which is a relevant physical situation.

The position and energy dependent solution h_{TS} is substituted into the expression for the measured difference in electrochemical potential for parallel and antiparallel configuration, and we obtain

$$\Delta\mu = 2P^{(D)} \int_{\Delta}^{\infty} dE \Delta f^{(N)} e^{-L/l_{\text{sf}}^{(S)}} \frac{R_{\text{sf}}^{(S)}}{R_{\text{sf}}^{(S)} + R^{(I)}}, \quad (11)$$

where $R^{(I)}(E) = 1/[|T|^2 N_{\text{BCS}}(E) N_0]$ is the resistance of the N/S tunnel barrier, $|T|$ is the tunneling matrix element, $N_{\text{BCS}}(E)$ is the BCS density of states, $R_{\text{sf}}^{(S)}(E) = l_{\text{sf}}^{(S)}(E)\rho/A$ is the resistance of the S wire within a spin-flip length and ρ is the resistivity of the material in S when in the normal state ($T > T_c$). This result can be understood as follows. The spin-accumulation close to the tunnel interface is exponentially attenuated by spin-flip scattering in S. The spin signal is also

decreased by the tunnel resistance, and since spin current is strongly suppressed for energies $|E| < \Delta$ only quasiparticles with energies higher than the gap contribute. The effective total resistance is a series of the tunnel interface resistance with the resistance of S within one spin-flip length.

We will now consider some simplified limits for the quantity $\Delta\mu$ defined above. In the normal state where $\Delta \rightarrow 0$ we find that $\Delta\mu/eV = 2P^{(D)}P^{(FN)}R_{sf}^{(S)} \exp(-L/l_{sf}) / (R_{sf}^{(S)} + R^{(I)})$ where $R_{sf}^{(S)}$ and $R^{(I)}$ assume their normal state (energy independent) values. At $k_B T \ll \Delta$ the signal measured by $\Delta\mu$ vanishes when the bias is lower than the energy gap $eV < \Delta$ since spin current is suppressed for quasiparticles below the gap. For higher bias, $eV > \Delta$, and at zero temperature when the bulk resistance dominates, $R_{sf}^{(S)} \gg R^{(I)}$, an approximate solution is $\Delta\mu = 2P^{(D)}P^{(FN)}\Delta e^{-L/l_{sf}} \{ e^{-Lr^2/2l_{sf}} / r - e^{-L/2l_{sf}} + \sqrt{\pi L/2l_{sf}} (\text{erf}[r\sqrt{L/2l_{sf}}] - \text{erf}[\sqrt{L/2l_{sf}}]) \}$, where $r = 2\Delta/eV$. In this case the relation between the energy gap and the bias determines the magnitude of the spin signal, and the exponential decrease of the signal.

The temperature dependence of $\Delta\mu$ in the general case is given by a decrease from a constant value above T_c as the temperature approaches zero. An example of this behavior is shown in Fig. 2. Here we have used the approximate temperature dependence $\Delta = 1.76T_c \tanh(1.74\sqrt{T_c/T - 1})$. Our calculations show that the spin signal decreases due to superconducting correlations. For a large energy gap the spin accumulation vanishes completely at low temperatures. These effects can be explained by suppressed subgap spin current and massive spin-flip at energies close to the gap because of the superconducting correlations.

In conclusion, we have presented a formalism to describe elastic spin transport in superconductors with spin-flip scat-

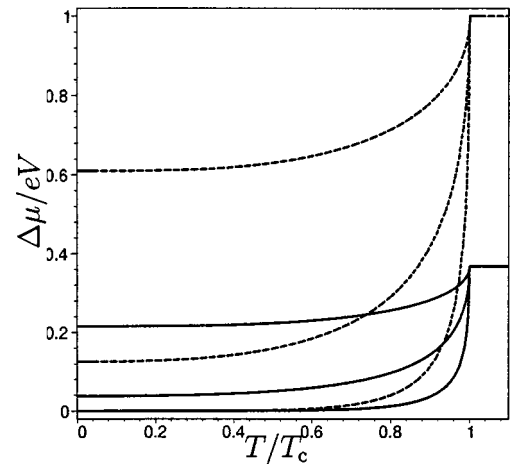


FIG. 2. Temperature dependence of $\Delta\mu/eV$. We use $R_{sf}^{(S)} = R^{(I)}$ in the normal state. For the dotted lines $L/l_{sf} = 6$, and for the solid lines $L/l_{sf} = 7$. The bias eV is $0.1\Delta(T=0)$, $3\Delta(T=0)$, $10\Delta(T=0)$ for the lower curve to the higher curve, respectively.

tering. We find different effective diffusion coefficients for charge- and spin-current. The spin-flip length is renormalized in the superconducting case, and at energies close to the gap there is massive spin-flip. As an illustration we compute the difference in electrochemical potential due to spin-accumulation in an experiment sensitive to the renormalization of spin-flip length.

This work was supported in part by the Research Council of Norway, NANOMAT Grants No. 158518/431 and 158547/431, RTN Spintronics, the Swiss NSF and the NCCR Nanoscience.

- ¹V. T. Petrashov, I. A. Sosnin, I. Cox, A. Parsons, and C. Troadec, Phys. Rev. Lett. **83**, 3281 (1999); M. Giroud, H. Courtois, K. Hasselbach, D. Mailly, and B. Pannetier, Phys. Rev. B **58**, R11872 (1998); V. I. Fal'ko, C. J. Lambert, and A. F. Volkov, Pis'ma Zh. Eksp. Teor. Fiz. **69**, 497 (1999), JETP Lett. **69**, 532 (1999); F. J. Jedema, B. J. van Wees, B. H. Hoving, A. Filip, and T. M. Klapwijk, Phys. Rev. B **60**, 16549 (1999); D. Huertas-Hernando, Yu. V. Nazarov, and W. Belzig, Phys. Rev. Lett. **88**, 047003 (2002).
- ²J. Y. Gu, J. A. Caballero, R. D. Slater, R. Loloee, and W. P. Pratt, Jr., Phys. Rev. B **66**, 140507(R) (2002).
- ³N. Kopnin, *Theory of Nonequilibrium Superconductivity* (Oxford Science, London, 2001).

- ⁴W. Belzig, F. K. Wilhelm, C. Bruder, G. Schön, and A. D. Zaikin, Superlattices Microstruct. **25**, 1251 (1999).
- ⁵J. Rammer and H. Smith, Rev. Mod. Phys. **58**, 323 (1986).
- ⁶Y. Tserkovnyak and A. Brataas, Phys. Rev. B **65**, 094517 (2002).
- ⁷T. Yamashita, S. Takahashi, H. Imamura, and S. Maekawa, Phys. Rev. B **65**, 172509 (2002); S. Takahashi and S. Maekawa, *ibid.* **67**, 052409 (2003).
- ⁸A. Schmid, of NATO Advanced Study Institute Series B, (1981), Vol. 65, pp. 423–480.
- ⁹M. Johnson and R. H. Silsbee, Phys. Rev. Lett. **55**, 1790 (1985); F. J. Jedema, A. Filip, and B. J. van Wees, Nature (London) **410**, 345 (2001).

PAPER 2

*Spin transport and magnetoresistance in
ferromagnet/superconductor/ferromagnet spin valves*

Physical Review B **72**, 014510 (2005)

Spin transport and magnetoresistance in ferromagnet/superconductor/ferromagnet spin valves

Jan Petter Morten,^{1,*} Arne Brataas,¹ and Wolfgang Belzig²

¹*Department of Physics, Norwegian University of Science and Technology, 7491 Trondheim, Norway*

²*Department of Physics and Astronomy, University of Basel, Klingelbergstrasse 82, 4056 Basel, Switzerland*

(Received 25 January 2005; revised manuscript received 7 April 2005; published 6 July 2005)

We consider spin transport and spin relaxation in superconductors using the quasiclassical theory of superconductivity. We include spin relaxation due to spin-orbit interaction as well as magnetic impurities, and show that the energy dependence of the spin-flip rate is different for these two mechanisms. In ferromagnet-superconductor-ferromagnet systems made of Co and Al, interface resistances can be small compared to bulk resistances. This simplifies the description of transport in Co/Al/Co spin valves, for which we numerically calculate the temperature and Al length dependence of the magnetoresistance.

DOI: [10.1103/PhysRevB.72.014510](https://doi.org/10.1103/PhysRevB.72.014510)

PACS number(s): 74.25.Fy, 72.25.Hg, 72.25.Ba

I. INTRODUCTION

Ferromagnetism and superconductivity are two competing phenomena in condensed matter physics. In conventional low temperature superconductors, transport of spins beyond the coherence length is prevented by the formation of spin singlet Cooper pairs. Consequently, due to the competing ordering of ferromagnets (F) and superconductors (S) in hybrid structures, many nontrivial physical effects occur^{1,2} and there are interesting suggested applications such as an absolute spin valve effect³ and solid state memory elements.⁴

Experimental studies of F/S contacts in the diffusive limit showed that the resistance can both decrease and increase relative to the resistance above the critical temperature (T_c) of the superconductor.⁵⁻⁷ Theoretically it was shown that the temperature dependence of this resistance depends sensitively on the contact transparency.⁸⁻¹⁰ The resulting resistance is determined by an interplay between the energy-dependent interface resistance and spin accumulation at the interfaces due to reduced spin transport into the superconductor.

Transport of spins through the bulk of superconductors was recently studied experimentally in an F/S/F heterostructure.¹¹ Here, a decreased magnetoresistance (MR) in the superconducting state was interpreted as a loss of spin memory. Theoretical work on bulk spin transport in superconductors in the inelastic regime¹² and the elastic regime¹³ describes the reduced penetration of spins by spin flipping and reduced penetration of spin-polarized quasiparticles. The F/S/F system of Ref. 11 has been analyzed by assuming a spatially homogeneous superconducting order parameter and neglecting spin flip.¹⁴ However, a thorough understanding of spin transport in F/S systems requires a description of the spatially dependent order parameter in each component as well as the quasiparticles driven out of equilibrium. A theoretical description of the F/S/F system, where the spatial variation of the order parameter, energy-dependent spin flipping in the superconductor, and the effect of the interfaces is taken into account, has to the best of our knowledge not been published.

In order to study the bulk spin-transport properties, it is important to have control over the influence of interfaces.

Typically, in spin valve structures both interface resistances and bulk resistivities contribute to the MR and are affected by superconductivity. In this paper, we study a superconducting spin valve system, where the interface resistances are negligible. In that case, a simplified treatment of the F/S boundaries is possible so that bulk effects can be studied independently of interface effects. As we discuss later, a possible candidate to realize a spin valve with small interface resistance could be a Co/Al/Co system. To describe the transport through a superconducting spin valve, we present a theoretical framework that describes the spin-dependent transport in superconductors in linear response. Spin-flip scattering from magnetic impurities as well as spin-orbit interaction is included in our description, and the full spatial dependence of the pairing potential is calculated self-consistently. We use this formalism for numerical calculations of the magnetization-configuration dependent transport of a Co/Al/Co spin valve. This demonstrates the suppression of spin transport through the superconductor.

The paper is organized in the following way: Section II describes the equations governing elastic transport in a diffusive superconductor. Section III outlines the specific geometry studied and the approximations used. In Sec. IV we discuss the numerical results. Section V summarizes and concludes our work.

II. TRANSPORT THEORY

Using the Keldysh theory in the quasiclassical approximation, we have in Ref. 13 derived kinetic equations for transport of charge, energy, spin, and spin energy in diffusive, *s*-wave superconductors in the presence of spin-flip scattering by magnetic impurities. We will now supplement that treatment with expressions for spin-orbit induced spin relaxation, and derive the resulting transport equations in the linear response limit. For an explanation of the notations used below and more details on the derivations we refer to Ref. 13.

The spin-orbit interaction Hamiltonian is

$$H_{\text{so}} = \frac{\gamma}{2} \sum_{\sigma'\sigma} \int d\mathbf{r} \psi_{\sigma'}^\dagger \{ (\vec{\tau} \times \nabla V_{\text{imp}})_{\sigma'\sigma} \cdot \mathbf{p} + \text{H.c.} \} \psi_{\sigma}, \quad (1)$$

where γ is the interaction strength, ψ_{σ} is the destruction field operator for spin $\sigma = \uparrow, \downarrow$, $\vec{\tau}$ is the vector of Pauli matrices,

V_{imp} is the impurity scattering potential and \mathbf{p} the momentum. The spin-orbit contribution to the self-energy in the Eilenberger equation¹⁵ is

$$\check{\sigma}_{\text{so}} = -\frac{i}{2\tau_{\text{so}}}\frac{1}{4}\hat{\alpha}\hat{\rho}_3\check{g}_s(X,E)\hat{\rho}_3\hat{\alpha}, \quad (2)$$

where we have defined the spin-orbit scattering time $1/\tau_{\text{so}} = 8\gamma^2 p_F^4/9\tau$. Here p_F is the Fermi momentum, τ is the elastic scattering time, $\hat{\alpha}$ is a vector of 4×4 matrices with the Pauli matrix and its transpose on the diagonal block, i.e., $\hat{\alpha} = \text{diag}(\vec{\tau}, \vec{\tau}^T)$, $\hat{\rho}_3 = \text{diag}(1, 1, -1, -1)$, and \check{g}_s is the isotropic part of the Green's function in Keldysh-Nambu-spin-space. Using a convenient representation of the Green's functions, we obtain equations that determine the distribution functions and currents.

Linearized kinetic equations for charge transport in diffusive superconductors were obtained by Schmid and Schön¹⁶ and have been successfully applied to describe various transport phenomena. To study spin-dependent transport it is necessary to include equations that determine the spin current. The relevant equations in the linear response regime are developed below. The approximations are valid when deviations from equilibrium values are small. We also assume that any static supercurrent is small, i.e., that there is no Josephson effect. The transport theory is formulated in terms of the physical particle and energy currents (including particles and holes). These are given by the distribution functions h_{T} and h_{L} (Ref. 17) and the spin-resolved functions h_{TS} and h_{LS} , as well as generalized diffusion coefficients D_{T} , D_{L} and renormalization factors α_{TT} , α_{TSTS} for relaxation processes. The spin-resolved distribution functions can be expressed by the particle distribution functions f_{\uparrow} and f_{\downarrow} as

$$h_{\text{LS}} = -\frac{f_{\uparrow}(E) - f_{\downarrow}(E)}{2} \mp \frac{f_{\uparrow}(-E) - f_{\downarrow}(-E)}{2}. \quad (3)$$

The spectral (retarded) properties depend on the complex function $\theta(E)$ which is determined by the so-called Usadel equation.¹⁷ To describe spin-polarized transport in voltage biased systems in linear response, it is unnecessary to calculate h_{L} and h_{LS} , so the equations that determine these functions have been omitted below.

The charge current and the spin current in S are given by integrals over the spectral quantities. The charge and spin current carried by quasiparticles is²⁹

$$I_{\text{charge}}^{\text{qp}}(x) = \frac{1}{2}eAN_0 \int_{-\infty}^{\infty} dE D_{\text{T}}(E, x) \frac{\partial h_{\text{T}}}{\partial x}, \quad (4)$$

$$I_{\text{spin}}(x) = \frac{1}{2}eAN_0 \int_{-\infty}^{\infty} dE D_{\text{L}}(E, x) \frac{\partial h_{\text{TS}}}{\partial x}, \quad (5)$$

where A is the area of the wire and N_0 is the density of states at the Fermi level for both spins in the normal state. Additionally, charge current is carried by the supercurrent, so that the total charge current is constant. The distribution functions h_{T} and h_{TS} are determined by the diffusion equations

$$\frac{\partial}{\partial x} \left(D_{\text{T}} \frac{\partial h_{\text{T}}}{\partial x} \right) - 2\Delta \alpha_{\text{TT}} h_{\text{T}} = 0, \quad (6)$$

$$\frac{\partial}{\partial x} \left(D_{\text{L}} \frac{\partial h_{\text{TS}}}{\partial x} \right) - \left(\frac{1}{\tau_{\text{m}}} \alpha_{\text{TSTS}}^{\text{m}} + \frac{1}{\tau_{\text{so}}} \alpha_{\text{TSTS}}^{\text{so}} \right) h_{\text{TS}} = 0. \quad (7)$$

Here τ_{m} is the spin-flip scattering time due to magnetic impurities and τ_{so} the spin-flip scattering time due to spin-orbit coupling, both evaluated in the normal state. In the diffusive limit $\tau \ll \tau_{\text{m}}, \tau_{\text{so}}$. The spectral quantities are given in terms of $\theta(E, x)$. We compute that the renormalization of the scattering rates are

$$\alpha_{\text{TT}} = \text{Im}\{\sinh(\theta)\}, \quad (8a)$$

$$\alpha_{\text{TSTS}}^{\text{so}} = (\text{Re}\{\cosh(\theta)\})^2 - (\text{Re}\{\sinh(\theta)\})^2, \quad (8b)$$

$$\alpha_{\text{TSTS}}^{\text{m}} = (\text{Re}\{\cosh(\theta)\})^2 + (\text{Re}\{\sinh(\theta)\})^2, \quad (8c)$$

$$D_{\text{L}} = D[(\text{Re}\{\cosh(\theta)\})^2 - (\text{Re}\{\sinh(\theta)\})^2], \quad (8d)$$

$$D_{\text{T}} = D[(\text{Re}\{\cosh(\theta)\})^2 + (\text{Im}\{\sinh(\theta)\})^2]. \quad (8e)$$

The effect of spin-flip scattering by spin-orbit interaction with renormalization factor $\alpha_{\text{TSTS}}^{\text{so}}$ is a result that did not appear in our previous paper.¹³ Its renormalization is different from the renormalization of the spin-flip scattering by magnetic impurities. The complex function θ is determined by the Usadel equation,

$$\hbar D \frac{\partial^2 \theta}{\partial x^2} = -2i\Delta \cosh(\theta) - 2iE \sinh(\theta) + \frac{3}{4} \frac{\hbar}{\tau_{\text{m}}} \sinh(2\theta). \quad (9)$$

Note that the spin-flip term in (9) arises from magnetic impurities only since spin-orbit scattering does not lead to pair breaking and consequently does not influence the spectral properties of the superconductor. This equation must be solved in conjunction with the self-consistency relation

$$\Delta = \frac{1}{2}N_0\lambda \int_0^{E_{\text{D}}} dE \text{Re}\{\sinh(\theta)\} \tanh\left(\frac{\beta E}{2}\right), \quad (10)$$

where λ is the electron-electron interaction strength, E_{D} the Debye cutoff energy, and β the inverse temperature.

An applied voltage is taken into account as a boundary condition for the distribution functions, h_{T} and h_{TS} . In a reservoir with electrochemical potential μ we have in linear response the equilibrium distributions $h_{\text{T}}^0 = -\beta\mu/[2 \cosh^2(\beta E/2)]$ and $h_{\text{TS}}^0 = 0$.

The different renormalization factors $\alpha_{\text{TSTS}}^{\text{so}}$ and $\alpha_{\text{TSTS}}^{\text{m}}$ arise from spin flipping by spin-orbit interaction or magnetic impurities. In general, $\alpha_{\text{TSTS}}^{\text{so}}$ and $\alpha_{\text{TSTS}}^{\text{m}}$ depend on the spectral properties of the superconductor through θ . In the BCS limit, valid for large bulk superconductors, the energy dependence of these factors is completely different and correspond to the so-called type-I or type-II coherence factors.^{18,19} Using the BCS solution for the Green's functions we find that for energies below the gap (for which there are no quasiparticles in the BCS limit), both $\alpha_{\text{TSTS}}^{\text{so}}$ and $\alpha_{\text{TSTS}}^{\text{m}}$ vanish, and above

the gap $\alpha_{\text{TSTS}}^{\text{so}}=1$ and $\alpha_{\text{TSTS}}^{\text{m}}=(E^2+\Delta^2)/(E^2-\Delta^2)>1$. Furthermore, we see from Eqs. (8b) and (8c) that for any $\theta(E)$, $\alpha_{\text{TSTS}}^{\text{so}}<\alpha_{\text{TSTS}}^{\text{m}}$. This implies that for a given normal state spin-flip length, the rate of spin flipping in the superconducting state is higher when the dominant spin-flip scattering mechanism is caused by magnetic impurities than if it is caused by spin-orbit interaction.

III. MODEL

We consider transport through an F/N/S/N/F hybrid wire (N denotes a normal metal layer). It is assumed that the ferromagnets (Co) are connected via normal metals (Cu) to the superconductor (Al). The distribution functions in the ferromagnet and the normal metal are determined by the Valet-Fert transport theory²⁰ and in the superconductor by the theory described in the preceding section. An applied bias causes spin-polarized quasiparticles to be injected into the S layer. We assume that the magnetizations of the F parts are either parallel (P) or antiparallel (AP). Because of renormalized spin-flip rates and a reduction of the generalized spin-diffusion coefficient (D_{\perp}) in the superconductor, the magnetoresistance $\text{MR}\equiv(R^{\text{AP}}-R^{\text{P}})/R^{\text{P}}$ is reduced for temperatures below T_c compared to the normal metal state.

In order to determine the dominant contributions to the resistance of the system, we examine the magnitude of the resistance of the F/N interface ($R_{\text{F/N}}$) compared to the bulk resistance in F within a spin-flip length (R_{sf}^{F}). The latter quantity is the largest resistance of the ferromagnet within its spin-active part. To this end, consider the ratio

$$\frac{R_{\text{F/N}}}{R_{\text{sf}}^{\text{F}}} = \frac{AR_{\text{F/N}}}{\rho_{\text{F}}^{\text{F}}l_{\text{sf}}^{\text{F}}}. \quad (11)$$

We assume that F layers are made of Co, N layers of Cu, and the S layer of Al. The bulk resistance of Cu as well as the proximity effect is neglected since the Cu layer is very thin, and in addition the typical resistivity of Cu is smaller than that of Co or Al. The interface resistance ($AR_{\text{F/N}}$), resistivity ($\rho_{\text{F}}^{\text{F}}$) and spin-diffusion length (l_{sf}^{F}) for Co is reviewed in Ref. 21. It is found that $AR_{\text{Cu/Co}}\sim 0.5 \text{ f}\Omega\text{m}^2$ at 4.2 K where A is the cross section area. The renormalized resistivity²⁰ is $\rho_{\text{Co}}^*\sim 75 \text{ n}\Omega\text{m}$, and $l_{\text{sf}}^{\text{Co}}=59 \text{ nm}$ at 77 K.²² Thus we can conclude that for Co $R_{\text{F/N}}/R_{\text{sf}}^{\text{F}}\approx 0.1$ as a least estimate since the spin-diffusion length should be longer at 4.2 K. This means that it is a valid approximation to disregard the interface resistances for long enough samples. The N/S interface resistance between Cu and Nb above the critical temperature is found to be larger than the F/N resistance,²³ $AR_{\text{Cu/Nb}}\sim 1.10 \text{ f}\Omega\text{m}^2$, and would give $R_{\text{N/S}}/R_{\text{sf}}^{\text{F}}\approx 0.2$. With Al as the superconducting layer we expect no higher interface resistance. We may also argue that the bulk resistance for dirty Cu/Co layers scales as $AR_{\text{bulk}}^{\text{Co}}\sim 0.1L \text{ (nm) f}\Omega\text{m}^2$,²⁴ where L is the length of the layers expressed in nm. Thus the bulk resistance for a slice of length l_{sf} should be much larger than the interface resistance. Note that the resistance of a direct F/S interface is probably higher than the F/N/S structure in our model ($AR_{\text{Nb/Co}}\sim 3 \text{ f}\Omega\text{m}^2$, Ref. 21), but since we include the Cu layers we can use only well-known parameters for F/S and

N/N interface resistance in the above estimates.

The estimates above show that the interface resistances are much smaller than the relevant bulk resistances with the materials chosen here. The dominant contribution to the resistance and spin polarization of the current then comes from the bulk of F. We will later check that the change in resistance from normal to superconducting state is larger than the interface resistances. A possible approximation is therefore to neglect the interface resistances. This allows us to effectively do calculations for an F/S/F system with the boundary condition that the generalized diffusive current should be continuous which implies that the function θ is continuous at the interface. For strong ferromagnets the superconducting proximity effect into the ferromagnet is negligible and therefore $\theta=0$ in F. Then we have by continuity $\theta\rightarrow 0$ in the superconductor close to the F/S interfaces. This means, e.g., that the gap vanishes at the interface. In this case, it is the bulk transport properties that dominate the system, and there are no free parameters so that it is possible to give an unambiguous description of the transport properties. This is our aim in the rest of the paper.

The F/S/F system was motivated by the experiments of Gu *et al.* However, in those experiments Py was used for the ferromagnet, and because of the very short spin-diffusion length in this alloy ($l_{\text{sf}}^{\text{Py}}=5.5 \text{ nm}$) the interface resistances are of the same order as R_{sf}^{F} . Consequently, in these experiments both the interface resistances and the bulk resistance of Al are governed by superconductivity. Thus the model discussed above is not applicable, and the resistance of the spin-polarizing interface must be taken into account. To be specific, we no longer have that $\theta\rightarrow 0$ at the interfaces, and superconductivity is not completely suppressed at the interface as in the Co/Al/Co system. Using the approximations discussed above in calculations for the Py/Nb/Py system of Ref. 11 would therefore give a too low T_c . Numerical simulations and comparison with Ref. 11 show that this is indeed the case (not shown). A complete description of this experiment requires boundary conditions for the spin-polarizing interfaces given by scattering theory. This would describe the proximity effect in N as well as a reduction of the superconducting pairing amplitude close to the interface. However, as noted by Huertas-Hernando *et al.*,²⁵ this approach would require full knowledge about the interface scattering matrix, which is generally not available except for in simplified models at this moment.

IV. CALCULATIONS

We have performed numerical calculations for a Co/Cu/Al/Cu/Co spin valve. Parameters for the superconductor are mostly taken from Ref. 26. The bulk value of the pairing potential at zero temperature is $\Delta_0=192 \mu\text{eV}$ and the critical temperature $T_c=1.26 \text{ K}$ with interaction parameter $N_0\lambda/2=0.18$.²⁷ The normal state diffusion coefficient of Al is $D=160 \text{ cm}^2/\text{s}$, and the density of states at Fermi level $N_0=2.2\times 10^{47} \text{ J}^{-1} \text{ m}^{-3}$ corresponding to a resistivity $\rho_{\text{Al}}^{\text{N}}=11 \text{ n}\Omega\text{m}$. The normal state spin-flip relaxation length by spin-orbit interaction is given by the sample independent parameter $\varepsilon=l_{\text{sf}}/l\approx 30$,²⁸ and we assume that the elastic mean

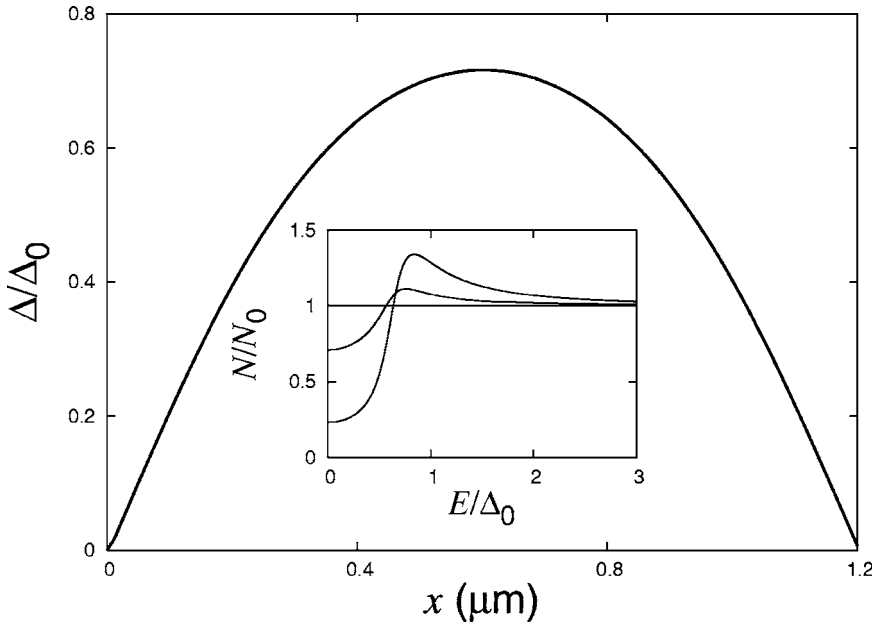


FIG. 1. Spatial variation of the pairing potential at $T/T_c=0.40$ scaled by Δ_0 . Inset, density of states at positions 0.0, 0.2, and 0.6 μm into the S wire. The curve evaluated at $x=0.0 \mu\text{m}$ is identical to the normal state DOS (flat curve).

free path is $l=37 \text{ nm}$. This gives $l_{\text{sf}}=1.11 \mu\text{m}$ for spin-orbit induced spin-flip. In calculations for magnetic impurity induced spin-flip we take the normal state value of the spin-flip length identical to the spin-orbit induced l_{sf} , but in general this length is determined by the impurity concentration which is sample specific. We take the length of the (identical) ferromagnetic elements to be 100 nm with a bulk spin asymmetry $\beta=0.4$.²¹ Figure 1 shows the spatial variation of the pairing potential resulting from complete suppression of superconductivity at the F/S interfaces at reduced temperature $T/T_c=0.40$ for a 1.2 μm Al wire with magnetic impurities. The density of states at various locations in the superconductor is shown in the inset, and resembles the bulk BCS shape close to the center of the wire where the gap is largest.

A calculation of the resistance of the F/S/F system for parallel magnetizations is shown in Fig. 2. The AR^{P} values above the critical temperature agrees with analytical results

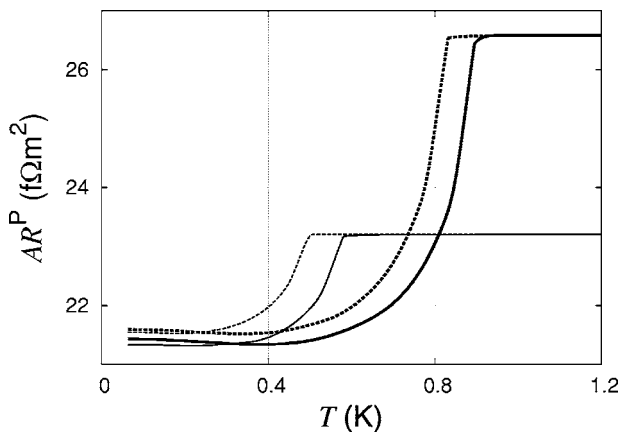


FIG. 2. Temperature dependence of resistance in parallel geometry for spin-orbit (solid lines) and magnetic impurity induced spin flip. The thick curves are with Al length 1200 nm, and the thin curves with Al length 900 nm. T_c is lowered by the presence of the magnetic impurities.

based on the Valet-Fert theory. Below T_c the resistance drops rapidly, but remains finite in the limit $T \rightarrow 0$. The change in resistance from normal to superconducting state is of the order of 2–6 $\text{f}\Omega\text{m}^2$ depending on the length of the superconductor, and this change is larger than the typical interface resistance, which should be checked as noted in Sec. III. The resistance of the system below T_c is due to the F elements as well as the regions in the S wire next to the F/S interface where there is conversion of current into supercurrent.²⁶ The systems with magnetic impurities have the higher resistance as $T \rightarrow 0$, since the length of the resistive region near the interfaces is longer. This is because the conversion of current into supercurrent happens over a length scale determined by the coherence length $\xi = \sqrt{\hbar D / 2\pi\Delta}$ which for a superconductor with magnetic impurities is longer since Δ is suppressed due to a term in the Usadel equation (9).

The dependence of the resistance on the magnetization configuration is shown in Fig. 3 where the excess resistance $\Delta R = A(R^{\text{AP}} - R^{\text{P}})$ is plotted as a function of temperature. We show curves for systems with only spin-flip scattering from magnetic impurities or spin-orbit interaction. The systems with magnetic impurities provide a weaker suppression of the spin signal than systems with spin-orbit interaction. The opposite could be expected since as noted above $\alpha_{\text{TSTS}}^{\text{m}} > \alpha_{\text{TSTS}}^{\text{so}}$. However, the pairing potential is lower in a superconductor with magnetic impurities due to the detrimental effect of the impurities on superconductivity, and this is the dominant effect. This is confirmed by simulations of systems with equal strengths of the pairing potential, in which magnetic impurities is the strongest spin relaxation mechanism. From Fig. 3 we see that the difference in suppression of spin signal between spin-orbit and magnetic impurity induced spin-flip is smaller for the longer wires, since in this case the difference in Δ is also smaller. For long wires the excess resistance tends to zero at low temperatures as expected, because in this case the transport of spins through the superconductor is completely suppressed.

In Fig. 4 we show the spatial variation of the quasiparticle charge and spin current and supercurrent for the F/N/S/N/F

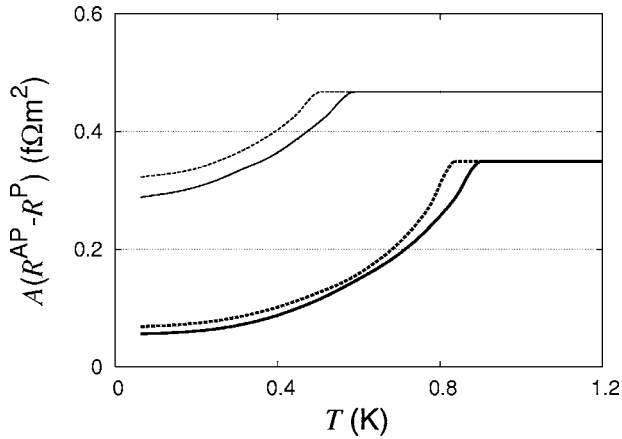


FIG. 3. Temperature dependence of the magnetoresistance for spin-orbit (solid lines) and magnetic impurity (dashed lines) induced spin flip. The top set of curves is a system with Al length 900 nm, and the lower curves with Al length 1200 nm.

spin valve with parallel magnetizations. The charge current is constant in the F parts of the wire, and is gradually converted into supercurrent in S. Spin current injection into S is suppressed, as a comparison with the magnitude of spin current in the normal state shows. This leads to spin accumulation in F at the interfaces. We see that the spin current is reduced below T_c inside the superconductor due to Cooper pairing. On the other hand, the total charge current increases below T_c due to the reduced resistance of the superconductor. In Fig. 5 we show the spin accumulation $\mu_{\uparrow} - \mu_{\downarrow}$ for the same system. Comparison with the normal state shows that the spin accumulation is larger in the S case, due to the reduced penetration of spins into S and since the net spin current out of the reservoirs is larger in the S case because the total resistance is lower. The spin accumulations that build up at the interfaces are relaxed through spin-flip in S. These spin

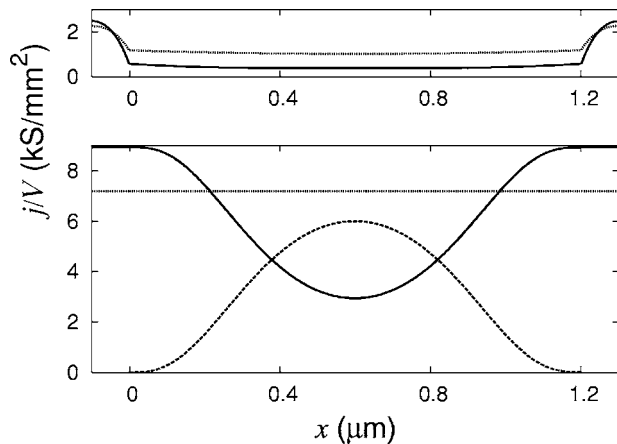


FIG. 4. Top panel, spatial dependence of the spin current for the F/S/F structure with Al length $1.2 \mu\text{m}$ at $T/T_c=0.40$ (spin-orbit induced spin-flip). The normal state ($T > T_c$) spin current is shown with the dotted line. The F-S interfaces are at $x=0 \mu\text{m}$ and $x=1.2 \mu\text{m}$. Bottom panel, spatial dependence of the quasiparticle charge current (solid line) and supercurrent (dashed line) for the same system as in the top panel. Normal state current is shown with dotted line.

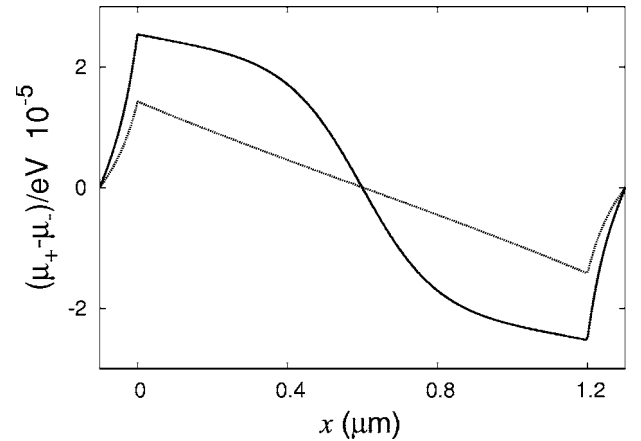


FIG. 5. The spatial dependence of the spin potential for the F/S/F structure with Al length $1.2 \mu\text{m}$ at $T/T_c=0.40$ (solid line) and $T > T_c$ (dotted line) (spin-orbit induced spin flip). The F/S interfaces are at $x=0 \mu\text{m}$ and $x=1.2 \mu\text{m}$.

accumulations can be measured, e.g., by tunnel coupling between the superconductor and a third probe ferromagnet.

Qualitatively, our results for the MR are in agreement with the experiment by Gu *et al.*¹¹ A contribution from the interfaces which is most probably important in the experiment, will not qualitatively change the properties of the system except for a higher T_c as noted above. Therefore, quantitative differences between the experiment and our calculations using material parameters corresponding to the system in Ref. 11 are not surprising. A more detailed theoretical analysis, which accounts for interface resistance, should be made to enable a quantitative comparison with the experiments of Ref. 11, but this is beyond the scope of our present work. We emphasize again, that our predictions are, however, experimentally testable in Co/Al/Co spin valves, which can be fabricated using state-of-the-art technology.

V. SUMMARY AND CONCLUSIONS

In conclusion we have studied spin-transport properties of an F/S/F trilayer. We have developed transport equations using the quasiclassical theory of superconductivity and included the effects of spin-flip relaxation. An experimental system is proposed where interface resistance can be neglected and a simple description of the physics is possible. For this system we have performed numerical calculations of the magnetization-configuration dependent resistance. This demonstrates the dependence of the spin-transport suppression on different spin-flip mechanisms, i.e., magnetic impurities and spin-orbit interaction.

ACKNOWLEDGMENTS

This work was supported in part by The Research Council of Norway, NANOMAT Grants Nos. 158518/431 and 158547/431, RTN Spintronics, the Swiss NSF, the NCCR Nanoscience, and EU via Project No. NMP2-CT-2003-505587 "SFINx."

*Electronic address: jan.morten@phys.ntnu.no

- ¹D. Beckmann, H. B. Weber, and H. v. Löhneysen, Phys. Rev. Lett. **93**, 197003 (2004).
- ²B. Leridon, J. Lesueur, and M. Aprili, cond-mat/0411500 (unpublished).
- ³D. Huertas-Hernando, Y. V. Nazarov, and W. Belzig, Phys. Rev. Lett. **88**, 047003 (2002).
- ⁴S. Oh and D. Youm, Appl. Phys. Lett. **71**, 2376 (1997); L. R. Tagirov, Phys. Rev. Lett. **83**, 2058 (1998); A. I. Buzdin, A. V. Vedyayev, and N. V. Ryzhanova, Europhys. Lett. **48**, 686 (1999).
- ⁵V. T. Petrashov, I. A. Sosnin, I. Cox, A. Parsons, and C. Troadec, Phys. Rev. Lett. **83**, 3281 (1999).
- ⁶M. Giroud, H. Courtois, K. Hasselbach, D. Mailly, and B. Panetier, Phys. Rev. B **58**, R11872 (1998).
- ⁷J. Aumentado and V. Chandrasekhar, Phys. Rev. B **64**, 054505 (2001).
- ⁸F. J. Jedema, B. J. van Wees, B. H. Hoving, A. T. Filip, and T. M. Klapwijk, Phys. Rev. B **60**, 16549 (1999).
- ⁹V. I. Fal'ko, C. J. Lambert, and A. F. Volkov, JETP Lett. **69**, 532 (1999).
- ¹⁰W. Belzig, A. Brataas, Y. V. Nazarov, and G. E. W. Bauer, Phys. Rev. B **62**, 9726 (2000).
- ¹¹J. Y. Gu, J. A. Caballero, R. D. Slater, R. Loloee, and W. P. Pratt, Jr., Phys. Rev. B **66**, 140507(R) (2002).
- ¹²T. Yamashita, S. Takahashi, H. Imamura, and S. Maekawa, Phys. Rev. B **65**, 172509 (2002).
- ¹³J. P. Morten, A. Brataas, and W. Belzig, Phys. Rev. B **70**, 212508 (2004).
- ¹⁴T. Yamashita, H. Imamura, S. Takahashi, and S. Maekawa, Phys. Rev. B **67**, 094515 (2003).
- ¹⁵A. Schmid, NATO ASI Ser., Ser. B **65**, 423 (1981).
- ¹⁶A. Schmid and G. Schön, J. Low Temp. Phys. **20**, 207 (1975).
- ¹⁷W. Belzig, F. K. Wilhelm, C. Bruder, G. Schön, and A. D. Zaikin, Superlattices Microstruct. **25**, 1251 (1999).
- ¹⁸M. Tinkham, *Introduction to Superconductivity* (McGraw-Hill, New York, 1975).
- ¹⁹Y. Yafet, Phys. Lett. **98A**, 287 (1983).
- ²⁰T. Valet and A. Fert, Phys. Rev. B **48**, 7099 (1993).
- ²¹J. Bass and W. P. Pratt, Jr., J. Magn. Magn. Mater. **200**, 274 (1999).
- ²²L. Piraux, S. Dubois, A. Fert, and L. Belliard, Eur. Phys. J. B **4**, 413 (1998).
- ²³W. Park, D. V. Baxter, S. Steenwyk, I. Moraru, W. P. Pratt, Jr., and J. Bass, Phys. Rev. B **62**, 1178 (2000).
- ²⁴A. A. Kovalev, A. Brataas, and G. E. W. Bauer, Phys. Rev. B **66**, 224424 (2002).
- ²⁵D. Huertas-Hernando, Y. V. Nazarov, and W. Belzig, cond-mat/0204116 (unpublished).
- ²⁶G. R. Boogaard, A. H. Verbruggen, W. Belzig, and T. M. Klapwijk, Phys. Rev. B **69**, 220503(R) (2004).
- ²⁷H. Ibach and H. Lüth, *Solid State Physics* (Springer-Verlag, GmbH, 1995), p. 245, Table 10.1.
- ²⁸F. J. Jedema, M. S. Nijboer, A. T. Filip, and B. J. van Wees, Phys. Rev. B **67**, 085319 (2003).
- ²⁹The quasiparticle charge current depends on the coordinate x , but conservation of charge is satisfied when including the supercurrent contribution so that the total charge current does not depend on x .

PAPER 3

Spin injection and relaxation in a mesoscopic superconductor

Physical Review Letters (2008)

Spin injection and relaxation in a mesoscopic superconductor

Ninos Poli,¹ Jan Petter Morten,² Mattias Urech,¹ Arne Brataas,² David B. Haviland,¹ and Vladislav Korenivski¹

¹*Nanostructure Physics, Royal Institute of Technology, S-10691 Stockholm, Sweden*

²*Department of Physics, Norwegian University of Science and Technology, N-7491 Trondheim, Norway*

We study spin transport in a superconducting nanowire using a set of closely spaced magnetic tunnel contacts. We observe a giant enhancement of the spin accumulation of up to five orders of magnitude on transition into the superconducting state, consistent with the expected changes in the density of states. The spin relaxation length decreases by an order of magnitude from its value in the normal state. These measurements, combined with our theoretical model, allow us to distinguish the individual spin flip mechanisms present in the transport channel. Our conclusion is that magnetic impurities rather than spin-orbit coupling dominate spin-flip scattering in the superconducting state.

PACS numbers: 72.25.-b 74.25.Fy 74.78.Na 85.75.-d

Non-local measurement technique [1] is a powerful way to directly probe non-equilibrium spin populations. The technique has been used to uncover a number of spin-dependent phenomena in nanostructures, such as electron spin precession [2], spin Hall effect [3], and spin injection and propagation in Si [4] and graphene [5]. Experiments reported to date, have focused on normal metals and semiconductors. In this work, we present direct measurements of the spin transport parameters in a superconductor, performed using a multi-electrode nanodevice with tunnel junction injection and simultaneous spin-sensitive detection at different mesoscopic distances from the injection point. We observe dramatic changes in the properties of the injected non-equilibrium spins on transition of the nanowire into the superconducting state. An interpretation of the observed effects is given by extending recently developed theories [6–10].

Non-equilibrium superconductivity has been studied since the pioneering experiments on tunnel injection of quasi-particles (QP's) into superconductors (S) from normal (N) and ferromagnetic (F) metals [11, 12]. It was found that the injected electrons remain unpaired QP's for about 10 μ s before they combine to form Cooper pairs and condense in the superconducting ground state [13, 14]. The first experimental study on *spin-dependent* injection and detection in S (Nb) using a non-local measurement configuration indicated a strong reduction in the spin-flip length (λ_{sf}) at $T < T_c$ [16]. On the other hand, local measurements on metal stacks containing Nb were used to infer only a small reduction in λ_{sf} on transition into the S state [17]. A two-fold decrease in λ_{sf} of Al below T_c was estimated by studying injection from F into S and using *spin-independent* detection [18]. All of these experiments on spin injection and relaxation in S used metallic contacts between the ferromagnetic electrodes and the superconductor, which is known to lead to proximity effects suppressing the gap in S and strong processes [19]. Furthermore, λ_{sf} was not measured directly as the magnitude of spin splitting in S versus the distance from the spin injection point, but rather inferred from the charge transport characteristics. Our device al-

lows us to simultaneously measure the spin splitting at several points along the superconducting nanowire, and thereby directly determine λ_{sf} in S, without the complications due to the proximity effects or Andreev processes.

Fig. 1(a) shows a scanning electron microscopy (SEM) image of our device, together with a schematic of the measurement arrangement, which is an extension of the configuration first used by Johnson and Silsbee [1]. The

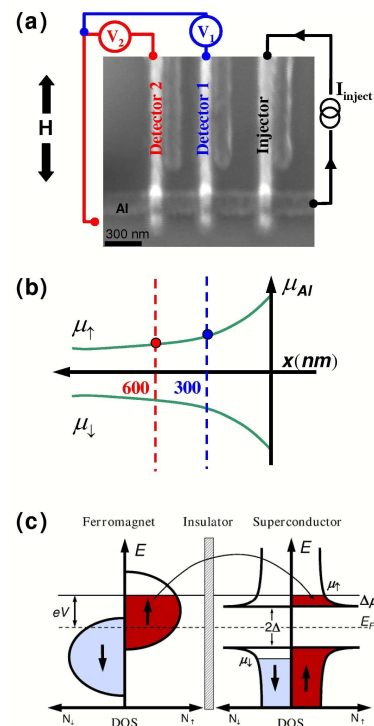


Figure 1: (a) SEM image of the sample together with the non-local measurement configuration. The electrical circuit schematic illustrates the measurement arrangement used for directly measuring λ_{sf} . (b) λ_{sf} is the exponential decay length of the spin accumulation away from the injection point. (c) Schematic density of states, illustrating spin accumulation ($\Delta\mu = \mu_{\uparrow} - \mu_{\downarrow}$) due to tunneling between a ferromagnet and a superconductor.

samples were fabricated using *e*-beam lithography and a two-angle deposition technique. For the details of the fabrication process and magnetic characterization see [21–23]. A set of Co/Al-O/Al tunnel junctions closely spaced along the nanowire of Al were formed. Not only does the use of tunnel junctions increase the effective spin polarization and thereby the spin signal to be detected [20], it is also important in providing true QP injection and suppressing Andreev reflection effects.

Due to the difference in the density of states at the Fermi level in the spin up and spin down sub bands in F, the spin-polarized charge current injected from the ferromagnetic electrodes into the Al nano-wire induces a spin accumulation near the injection point. This accumulation decays away from the injection point due to spin relaxation, as shown in Fig. 1(b), with the spatial profile governed by the diffusion equation:

$$\nabla^2(\mu_{\uparrow} - \mu_{\downarrow}) = \frac{1}{\lambda_{sf}^2}(\mu_{\uparrow} - \mu_{\downarrow}), \quad (1)$$

where $\mu_{\uparrow(\downarrow)}$ is the electro chemical potentials for the spin-up and spin-down carrier populations, $\lambda_{sf} = \sqrt{D\tau_{sf}}$ the spin flip length, D the diffusion constant, and τ_{sf} the spin flip time. The voltage difference taken between the parallel (P) and anti-parallel (AP) magnetic states of the injector/detector, normalized by the current, defines the non-local spin signal, which in the N-state is given by [1, 2, 8]:

$$R_S(x) = \frac{V_P - V_{AP}}{I_{inj}} = P^2 R_N \exp(-x/\lambda_{sf}), \quad (2)$$

where P is the spin polarization, $R_N = \rho\lambda_{sf}/A$ the characteristic resistance of N, ρ the resistivity of Al, and A the cross sectional area of the Al strip.

A number of novel effects connected with spin injection and relaxation in superconductors (S) have been predicted recently [6–10]. Cooper pairs have zero spin and carry only charge. It is therefore spin-polarized electrons tunneling into the QP branches that transport spin in S. Fig. 1(c) illustrates the spin accumulation ($\mu_{\uparrow} - \mu_{\downarrow}$) in S due to spin polarized tunneling from F. Observe that the minimum injection energy is the gap energy in the superconductor $\Delta \approx 200\mu\text{eV}$ for Al. If the injection energy is close to the gap energy (Δ), then spin-polarized QP's can be created and charge imbalance avoided [15]. A dramatic increase in the spin accumulation compared to that in the normal state for the same injection current and near-gap bias is then expected [8]. This is understood as originating from the reduction in the density of states of the QP's due to the opening of the gap in the energy spectrum. Considering spin relaxation due to spin-orbit interaction, the proper spin signal in S is obtained by scaling R_N in Eq. 2 with the density factor $(2f_0(\Delta))^{-1}$, [8]:

$$R_S(x) = P^2 \frac{R_N}{2f_0(\Delta)} \exp(-x/\lambda_{sf}), \quad (3)$$

where $f_0(E) = 1/(\exp(E/kT) + 1)$ is the Fermi distribution function for a given temperature T . Thus, a diverging spin signal is expected in S as $T \rightarrow 0$.

More generally, relaxation of the above non-equilibrium spin accumulation in S is governed by two main mechanisms: scattering by spin-orbit interaction and magnetic impurities. In the elastic limit, these two mechanisms have been studied theoretically and are expected to result in a different energy and temperature dependence of the spin flip processes [9, 10]. Hence, λ_{sf} becomes an energy and temperature dependent quantity in the S-state and can not be quantified by a number, but rather by a function. Seemingly a complication, this $\lambda_{sf}(T)$ dependence can be used to distinguish between the different spin relaxation mechanisms in our device, thus leading to a novel spin flip spectroscopy. The specific prediction is that spin flip by magnetic impurities is enhanced for QP energies close to Δ , whereas spin flip due to spin-orbit interaction is the same in S and N states. We assume that the spectral properties of the aluminum are given by the spatially homogeneous BCS solutions with the temperature dependence of the gap $\Delta \approx 1.76 T_C \tanh(1.74 \sqrt{T/T_C - 1})$, where $t = T/T_C$ is the normalized temperature. This assumption is valid when the contacts to the superconductor are of low transparency and of spatial dimensions smaller than the coherence length in S - the geometry chosen in this experiment with ~ 50 nm scale tunnel contacts. In the linear response limit, the non-local spin signal at the detector contact at a distance x away from the injection point becomes

$$R_S(x) = P^2 R_N \frac{g(x/\lambda_{sf}, t)}{\chi(t) h(t)}, \quad (4)$$

where $\chi(t) = -2 \int_{\Delta}^{\infty} \frac{E}{\sqrt{E^2 - \Delta^2}} \frac{\partial f_0(E)}{\partial E} dE$ is the Yosida function, and $g(x/\lambda_{sf}, t)$ and $h(t)$ are rather complex energy integrals that can be approximated in S as $h(t) \approx (1 - P^2) \chi(t)$ and

$$g(x/\lambda_{sf}) \approx \int \frac{\partial f_0(E)}{\partial E} \frac{-4N^2(E) e^{-x/(\lambda_{sf}\alpha)}}{2\alpha + N(E)R_N/R_I} dE. \quad (5)$$

Here R_I is the injector tunnel resistance, $N(E)$ the density of states of the superconductor and $\alpha = \sqrt{(E^2 - \Delta^2)/(E^2 + \beta\Delta^2)}$ gives the renormalization of λ_{sf} . The parameter $\beta = (\tau_{so} - \tau_m)/(\tau_{so} + \tau_m)$, with τ_{so} and τ_m being the normal state spin-orbit and magnetic impurity spin relaxation times, respectively, is a measure of the relative contributions from the two scattering mechanisms. β is expected to approach 1 if magnetic impurities dominate spin flip processes, i.e $\tau_m \ll \tau_{so}$, which results in a substantial decrease in λ_{sf} . For dominating spin-orbit induced spin flip, i.e $\tau_m \gg \tau_{so}$, $\beta = -1$ which gives $\alpha = 1$, so that there is no renormalization of λ_{sf} in Eq. 4. The effective λ_{sf} can be extracted by fitting the theoretical R_S of Eq. 4 to the R_S measured by the two detectors placed at 300 and 600 nm.

The multi-electrode nano-device discussed above and illustrated in Fig. 1(a) is capable of direct measurements of the spin accumulation and the spin flip length, and is therefore ideal for exploring the fundamental properties of spin transported in S. Measuring the spin signal versus the distance, x , from the injection point, as shown in Fig. 1(b), allows a direct determination of the spin flip length, λ_{sf} . In our case of multiple spin detectors, this direct measurement of λ_{sf} is done in-situ in the same device, in a single field sweep. The measurements were performed using the lock-in technique, with a 7 Hz bias signal applied to the injector and the right end of the Al wire. Typical values of the bias current used were $I_{inject} = 5 \mu\text{A}$ rms in the N state and 1 – 10 nA in the S state of the nano-wire. The non-local voltages V_1 and V_2 were measured using pre-amplifiers with very high input impedance ($\sim 10^{15} \Omega$) and low input bias currents (~ 10 fA) in order to minimize spurious contributions to the detected signals. At 4 K the typical junction resistance is 50-200 k Ω with a resistance area product of $\sim 1\text{k}\Omega\mu\text{m}^2$. The resistivity of the thin Al is 5-10 $\mu\Omega\text{cm}$. Using the Einstein relation $\sigma = e^2 N_{Al} D_N$, with $N_{Al} = 2.4 \times 10^{28} \text{eV}^{-1}\text{m}^3$ [2] being the density of states at the Fermi level, gives the diffusion constant $D_N = (3 - 9) \times 10^{-3} \text{m}^2\text{s}^{-1}$. Fitting the data from typical R_S vs. H (applied magnetic field) curves [22, 23] to Eq. 2 yields $\lambda_{sf} = 800 - 1100$ nm, $\tau_{sf} \approx 100$ ps and the effective spin polarization of $P = 12\%$. These spin transport parameters in the N state are in good agreement with the recent results for similar structures [2, 3, 24, 25].

It is important that the spin channel is maintained superconducting throughout the magneto-transport measurements. The typical bias current used for the transport measurements in the S state is ~ 1 nA, which is low enough not to suppress superconductivity due to QP injection. Moreover, from critical current measurements, similar to those reported previously [23], we conclude that possible changes in the fringing fields have no effect on the superconducting parameters relevant for the spin transport properties discussed below.

Figure 2 shows the normalized R_S for sample 1 for $x = 300$ nm as a function of temperature. The bias current was kept at 1 nA in order not to affect the superconducting gap by the QP injection [23], and to obtain near gap injection energies. R_S is enhanced in the S state by 4 to 5 orders of magnitude. This is by far the largest R_S measured in a metal/oxide nano-structure. The theoretical fit using Eq. 4-5 approximates well the experimental data for temperatures down to $T \sim 0.2T_C$, at which point the measured R_S starts leveling off. We believe this to be due to an effective QP temperature higher than that given by the thermometer in the 10-100 mK range [27]. The QP's are relatively decoupled from the phonon bath at the lowest temperatures. The noise due to the electromagnetic environment in the measurement system, affects the injected QP's and raises their

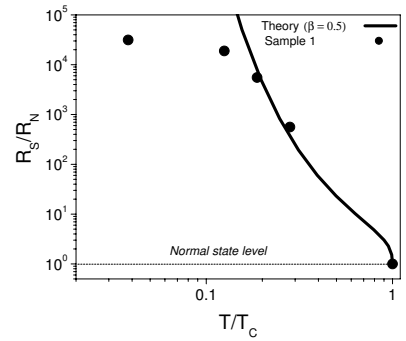


Figure 2: Normalized spin signal (R_S) for sample 1, as a function of normalized temperature. $T_C \approx 1.6$ K and $R_S(4 \text{ K}) \approx 50 \text{ m}\Omega$.

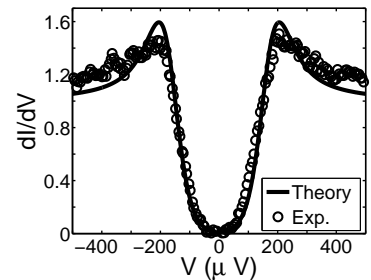


Figure 3: Normalized differential conductance of the injection junction measured at 22 mK, together with a theoretical fit [26]. The best fit was obtained for $T_{eff} \approx 0.2T_C$.

temperature. This heat is not fully dissipated by the phonon bath, since the phonon population vanishes as T approaches zero. In order to determine the effective QP temperature, we model the normalized differential conductance of the injection junction, measured at 22 mK. Using the model of [26], Figure 3 shows the best fit, which was obtained for $T_{eff} \approx 0.2T_C$. This value is consistent with the saturation behavior of R_S , further supporting our interpretation. Thus, the measured R_S saturates as $T \rightarrow 0$, but its dramatic enhancement of 4-5 orders of magnitude is a strong confirmation of the recent theoretical predictions on spin injection in superconductors [8, 10].

Another key quantity determining spin transport in S is the spin relaxation length, which can be used to differentiate the different spin relaxation mechanisms present in the device. Figure 4 shows the normalized λ_{sf} for two samples as a function of temperature. The critical temperature for both samples is $T_C \approx 1.6$ K and $\lambda_{sf}(T \gtrsim T_C) \approx 1 \mu\text{m}$. The measured λ_{sf} decreases substantially at low temperature, by a factor of ten at 20 mK compared to its value in the N state. This temperature dependence of λ_{sf} is inconsistent with the behavior predicted for pure spin-orbit scattering [6, 8] but is in good agreement with the predictions for magnetic im-

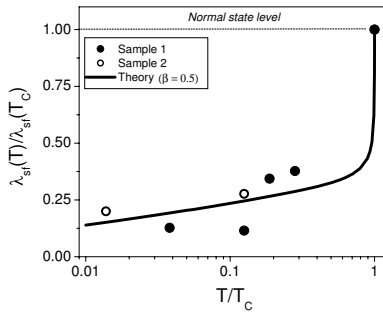


Figure 4: Normalized spin diffusion length (λ_{sf}) for two samples, 20-25 nm in thickness, as a function of normalized temperature (T/T_C). $T_C \approx 1.6$ K and $\lambda_{sf}(4$ K) ≈ 1 μ m. The error bars (not shown) are approximately of the size of the symbols representing the data points.

purity mediated spin flip [9, 10]. The $\lambda_{sf}(T)$ data are well described by the theoretical dependence of Eq.4, as shown in Fig. 4 by the solid line. The best fit was obtained for $\beta = 0.5$, which is equivalent to $1/\tau_m = 3/\tau_{so}$. This means that spin flip scattering due to magnetic impurities is three times more likely than spin-flip by spin-orbit interaction. With $\beta = 0.5$ the renormalization of the scattering rates described by α yields a diverging spin flip rate as T approaches zero, since the spins are injected close to the gap edge, where $\alpha \approx 0$.

A magnetic impurity concentration of $\sim 1\%$ is known to suppress superconductivity [28–30], which would manifest in a reduced T_C . Our measured T_C is greater than that of pure Al due to non-magnetic impurity scattering, typical for thin films (grain boundary and surface scattering). From this we estimate an upper limit on the concentration of magnetic impurities at 0.1%. Previous results show that even a magnetic impurity concentration of 0.005% can lead to a significant renormalization of λ_{sf} in the superconducting state [29]. Thus, the spin flip rate can be significantly enhanced even for low concentrations of magnetic impurities.

In conclusion, we report direct measurements of the main parameters of spin transport in a superconductor. The mesoscopic multi-terminal device used allows an in-situ determination of the spin accumulation and the spin relaxation length of quasi-particles, which carry the spin current in the superconducting state. We observe a record high enhancement of the spin injection efficiency for near-gap bias, up to 4 to 5 orders in magnitude compared to the normal state, and an order of magnitude reduction in the spin relaxation length at $T \ll T_C$. These effects are explained theoretically as being due to changes in the quasi-particle density of states caused by opening of the superconducting gap, and strong enhancement in spin flip scattering from magnetic impurities at energies close to the gap energy.

Financial support from the Swedish SSF, Wallenberg and Gustafsson Foundations are gratefully acknowledged.

-
- [1] M. Johnson, R. H. Silsbee, Phys. Rev. Lett., **55**, 1790, 1985.
 - [2] F. J. Jedema H. B. Heersche, A. T. Filip, J. J. S. Baselmans, B. J. van Wees, Nature, **416**, 713 (2002).
 - [3] S. O. Valenzuela, M. Tinkham, Nature, **442**, 176, 2006.
 - [4] I. Appelbaum, B. Q. Huang, and D. J. Monsma, Nature, **447**, 295, 2007.
 - [5] N. Tombros, C. Jozsa, M. Popinciuc, H. T. Jonkman, B. J. van Wees, Nature, **448**, 571, 2007.
 - [6] H. L. Zhao, S. Hershfield, Phys. Rev. B, **52**, 3632 (1995).
 - [7] T. Yamashita, S. Takahashi, H. Imamura, S. Maekawa, Phys. Rev. B, **65**, 172509 (2002).
 - [8] S. Takahashi, S. Maekawa, Phys. Rev. B, **67**, 052409 (2003).
 - [9] J.P. Morten, A. Brataas, W. Belzig, Phys. Rev. B, **70**, 212508 (2004).
 - [10] J.P. Morten, A. Brataas, W. Belzig, Phys. Rev. B, **72**, 014510 (2005).
 - [11] J. Clarke, Phys. Rev. Lett., **28**, 1363 (1972).
 - [12] P. M. Tedrow, R. Meservey, Phys. Rev. B, **7**, 318 (1973).
 - [13] J. L. Levine, S. Y. Hsieh, Phys. Rev. Lett., **20**, 994 (1968).
 - [14] S. Y. Hsieh, J. L. Levine, Phys. Rev. Lett., **20**, 1502 (1968).
 - [15] M. Tinkham, J. Clarke, Phys. Rev. Lett. **28**, 1366 (1972).
 - [16] M. Johnson, Appl. Phys. Lett., **65**, 1460 (1994).
 - [17] J. Y. Gu, J. A. Caballero, R. D. Slater, R. Loloee, W. P. Pratt, Jr., Phys. Rev. B, **66**, 140507(R) (2002).
 - [18] Y.S. Shin, H. J. Lee, H. W. Lee, Phys. Rev. B, **71**, 144513 (2005).
 - [19] A. F. Andreev, Sov. Phys. JETP, **19**, 1228 (1964).
 - [20] E. I. Rashba, Phys. Rev. B, **62**, R16267 (2000).
 - [21] M. Urech, V. Korenivski, N. Poli, and D. B. Haviland, Nano Lett., **6**, 871, 2006.
 - [22] N. Poli, M. Urech, V. Korenivski, D.B. Haviland J. Appl. Phys., **99**, 08H701 (2006).
 - [23] M. Urech, J. Johansson, N. Poli, V. Korenivski, D. B. Haviland, J. Appl. Phys., **99**, 08M513, (2006).
 - [24] S. Garzon, I. Zutic, and R. A. Webb, Phys. Rev. Lett., **94**, 176601, 2005.
 - [25] S. O. Valenzuela, D. J. Monsma, C. M. Marcus, V. Narayanamurti, and M. Tinkham, Phys. Rev. Lett, **94**, 196601, 2005.
 - [26] I. Giaever, K. Megerle, Phys. Rev. **122**, 1101 (1961)
 - [27] S. Corlevi, W. Guichard, F.W. J. Hekking, and D. B. Haviland, Phys. Rev. Lett., **97**, 096802 (2006). In related experiments using the same measurement system, the effective QP temperature due to the electromagnetic environment in the system was estimated to be $\approx 0.2T_C$:
 - [28] R. C. Bruno and B. B. Schwartz, Phys. Rev. B, **8**, 3161 (1973)
 - [29] F. Aspen and A. M. Goldman, Phys. Rev. Lett., **43**, 307 (1979)
 - [30] P. Jalkanen, V. Tubolstev, A. Virtanen, K. Arutyunov, J. Räisänen, O. Lebedev and G. V. Tendeloo, Solid state comm., **142**, 407 (2007)

PAPER 4

*Proximity effect-assisted absorption of spin currents in
superconductors*

Preprint (2007)

Proximity effect-assisted absorption of spin currents in superconductors

Jan Petter Morten,^{1,2} Arne Brataas,^{1,2} Gerrit E. W. Bauer,^{3,2} Wolfgang Belzig,^{4,2} and Yaroslav Tserkovnyak^{5,2}

¹*Department of Physics, Norwegian University of Science and Technology, NO-7491 Trondheim, Norway*

²*Centre for Advanced Study at the Norwegian Academy of Science and Letters, Drammensveien 78, NO-0271 Oslo, Norway*

³*Kavli Institute of NanoScience, Delft University of Technology, 2628 CJ Delft, The Netherlands*

⁴*University of Konstanz, Department of Physics, D-78457 Konstanz, Germany*

⁵*Department of Physics and Astronomy, University of California, Los Angeles, California 90095, USA*

(Dated: December 17, 2007)

The injection of pure spin current into superconductors by the dynamics of a ferromagnetic contact is studied theoretically. Taking into account suppression of the order parameter at the interfaces (inverse proximity effect) and the energy-dependence of spin-flip scattering, we determine the temperature-dependent ferromagnetic resonance linewidth broadening. Our results agree with recent experiments in Nb|permalloy bilayers [C. Bell *et al.*, arXiv:cond-mat/0702461, accepted for publication by Phys. Rev. Lett.].

PACS numbers: 74.25.Fy, 74.78.Na, 85.75.-d, 72.25.-b

Cooper pairs in conventional superconductors are spin-singlet states and therefore cannot carry a spin current. Some aspects of the resilience of the superconducting state against spin-current injection have been experimentally demonstrated in hybrid ferromagnet-superconductor spin valves [1], switches [2], and π -junctions [3]. In these experiments, the spin current flow in the superconducting state can only be inferred via charge current measurements. This complicates the understanding of the spin current flow in superconductors.

Injection of a pure spin current into a superconductor has recently been demonstrated by Bell *et al.* [4] in ferromagnet|superconductor structures under ferromagnetic resonance (FMR) conditions, in which the precessing magnetization acts as a “spin pump” [5]. The spin angular momentum lost by the ferromagnet can be observed directly in terms of an increased broadening of the FMR spectrum. In this Letter we demonstrate theoretically that the spin transport thus measured as a function of temperature and device/material parameters offers direct insight into spin-flip relaxation and the inverse proximity effect in superconductors. Our theory agrees well with the recent experimental results [4], and we provide suggestions and predictions for future experiments.

The theoretical challenge of spin-pumping into superconductors as compared to normal conductors is the strong energy dependence of quasiparticle transport properties around the superconducting energy gap [6]. Also, the energy dependent spin-flip scattering rates caused by spin-orbit coupling or magnetic impurities differ. Experiments that directly probe spin transport, such as Ref. 4, therefore provide unique information about the spin-flip scattering mechanism. A complicating factor is the inverse proximity effect [7] that suppresses the superconducting order parameter close to a metallic interface with ferromagnets like Ni, Co, and Fe. The resulting spatial dependence of the superconducting gap requires

solution of the full transport equations in the entire superconducting layer. The spin currents measured at such interfaces therefore serve as probes of superconducting correlations in magnetic heterostructures, and the temperature dependence of the FMR linewidth near and below the critical temperature can provide a wealth of information about spin-flip processes and superconducting proximity physics, with potential implications for different areas of mesoscopic physics.

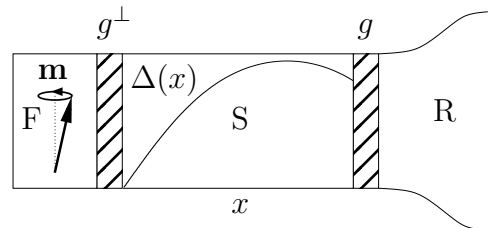


FIG. 1: The ferromagnet|superconductor|spin reservoir (F|S|R) structure. Precession of magnetization $\mathbf{m}(t)$ pumps spins into S, which can diffuse and dissipate in R. The F|S interface spin-mixing conductance for spins polarized transverse to the magnetization direction is g^\perp and the S|R interface conductance is g . The superimposed superconducting gap $\Delta(x)$ is suppressed close to the interfaces (inverse proximity effect).

In the following we develop a theory of energy-dependent spin pumping at a ferromagnet|superconductor interface and the resulting spectral spin current flow in the superconductor. We consider a diffusive metallic heterostructure consisting of a superconducting layer (S) of thickness L that is sandwiched by a ferromagnet (F) of thickness d and a spin reservoir (“spin sink”) (R), see Fig. 1. The slowly precessing magnetization $\mathbf{m}(t)$ emits a spin current that is transversely polarized with respect to the instantaneous magnetization direction [5]. The spin current that flows through S is immediately dissipated upon reaching R. R thus increases the sensitivity of the

experiments to the spin transport properties of S. R represents either a cap of an efficient spin-flip scattering material such as Pt or a large reservoir of a high mobility metal [5]. We assume sufficient thermal anchoring so that heating from absorbed FMR microwave radiation can be disregarded.

The magnetization dynamics is determined by the generalized Landau-Lifshitz-Gilbert equation,

$$\frac{d\mathbf{m}}{dt} = -\gamma\mathbf{m} \times \mathbf{H}_{\text{eff}} + \frac{G_0}{\gamma M_S} \mathbf{m} \times \frac{d\mathbf{m}}{dt} + \frac{\gamma}{M_S V} \mathbf{I}_s. \quad (1)$$

Here γ is the gyromagnetic ratio, \mathbf{H}_{eff} is the effective magnetic field, M_S is the saturation magnetization, and V is the volume of the ferromagnet. The intrinsic dissipation in the bulk ferromagnet is parameterized by the Gilbert damping constant G_0 . \mathbf{I}_s is the total spin (i.e. angular momentum) current generated by the precessing ferromagnet. This loss of angular momentum is equivalent to an interface contribution to the magnetization damping and is observable in terms of the enhanced FMR linewidth broadening. Our task is to evaluate the effect of superconducting correlations on \mathbf{I}_s . The results can be summarized in terms of an effective resistor model for the spin transport. We find an energy-dependent spin transport resistance of S in series with the spin-mixing resistance $r^\perp = 1/g^\perp$ of the F|S interface in the normal state and the conventional resistance $r = 1/g$ of the S|R interface.

To illustrate the physics we first sketch the results for $\mathbf{m}(t)$ rotating in the xy -plane and in the absence of spin-flip scattering (the derivation for the general situation will be outlined subsequently). The magnetization then emits a time-independent spin current that is polarized along the z -axis [5]. The superconducting condensate consists of spin-singlet Cooper pairs. A spin current can therefore only be carried in S by excited quasiparticles. Since the low-energy density of quasiparticle states is suppressed by superconducting correlations, the spin transport resistivity is enhanced when S is in the superconducting state, resulting in reduced spin injection from the ferromagnet. The energy-dependent spin resistance is governed by a spectral Ohm's law,

$$R_{\text{eff}}^\perp(E) = \frac{r^\perp}{N(0, E)} + \int_0^L dx' \frac{\rho_L(x', E)}{A} + \frac{r}{N(L, E)}, \quad (2)$$

where $\rho_L = 1/(hN_0D_L)$ is the effective resistivity of the superconductor for spin transport in units of e^2/h , N_0 is the density of states at the Fermi level in the normal state, $D_L(x, E)$ and $N(x, E)$ are the effective spin diffusion coefficient and the normalized density of state at position x and energy E , respectively [6]. At zero temperature, the relevant quasiparticle energy E is determined by the FMR frequency which is typically $f_{\text{FMR}} \sim 10$ GHz. For BCS superconductors $hf_{\text{FMR}}/\Delta_0 \approx 0.3 K/T_c$ where Δ_0 is the bulk zero-temperature energy gap and T_c the

critical temperature of the superconductor. For small-angle precession, the effective ‘‘rotation’’ frequency can be introduced as $f \sim \phi f_{\text{FMR}}$, where ϕ is the angle of precession. Thus the relevant energy scale for FMR-generated excitations is in practice expected to be much smaller than hf_{FMR} , and the characteristic energy of pumped electrons is set by the temperature, see Eq. (3) below. At the F|S interface $N(x=0, E) \approx 1$ due to the inverse proximity effect (see below). R_{eff}^\perp depends on temperature through the local gap $\Delta(x, T)$ which determines $N(x, E)$ and $\rho_L(x, E)$. The spin current loss of the ferromagnet is consistent with the Gilbert phenomenology in terms of an increased damping parameter G . It is determined by the spin angular momentum escape rate through S and reads

$$G = G_0 + \frac{(g_L \mu_B)^2}{2\pi\hbar} \frac{1}{d} \int dE \frac{-df_{\text{FD}}(E)/dE}{AR_{\text{eff}}^\perp(E)}, \quad (3)$$

where g_L is the g -factor, μ_B is the Bohr magneton, A is the sample cross section area, and f_{FD} is the Fermi-Dirac distribution function.

At temperatures $T \ll T_c$, $\Delta(x)$ as a function of the distance from the F|S interface approaches the bulk value on the scale of the bulk superconducting coherence length $\xi_0 = \sqrt{\hbar D/2\pi k_B T_c}$. Since the relevant spin resistivity $\rho_L(x, E)$ and thus R_{eff}^\perp are very large for $E < \Delta$, ξ_0 sets the penetration length scale for spin current into the superconductor. At low temperatures and $L > \xi_0$ the Gilbert damping (3) will therefore be weakly enhanced. On the other hand, at $T \lesssim T_c$ the gap is suppressed throughout S and transport channels at energies $E \gtrsim \Delta$ become accessible. R_{eff}^\perp and the Gilbert damping then approach the normal state values.

Spin-flip scattering in S dissipates spin current emitted from F, and enhances G by suppressing the back-flow of spins into the ferromagnet. The spin-flip length in the normal state is given by $l_{\text{sf}} = \sqrt{D\tau_{\text{sf}}}$, where D is the normal state diffusion coefficient. We take spin-flips into account that are caused by magnetic impurities as well as spin-orbit coupling at impurities in terms of the spin-flip rate $1/\tau_{\text{sf}} = 1/\tau_{\text{m}} + 1/\tau_{\text{so}}$ [6]. The spin-orbit coupling respects the symmetry of singlet Cooper pairs, whereas the pair-breaking scattering by magnetic impurities suppresses superconductivity and reduces T_c . Below T_c , the spin-flip rates in S depend on energy. For $E < \Delta$ spin-flip rates both due to spin-orbit coupling and magnetic impurities are suppressed. For $T \ll T_c$ and $L > \xi_0$, the Gilbert damping will therefore be weakly enhanced. On the other hand, for $E > \Delta$ the spin-flip rate due to magnetic impurities is enhanced whereas the spin-flip rate due to spin-orbit coupling is similar to that in the normal state. We therefore predict a non-monotonic temperature dependence of the Gilbert damping close to the critical temperature when spin-flip is dominated by magnetic impurities. Experimental data indicate that $l_{\text{sf}} > \xi_0$ for typical S. $l_{\text{sf}} = 48$ nm and $\xi_0 = 13$ nm has been reported

for Nb [1] (which is used in Ref. 4) whereas $l_{\text{sf}} = 1.1 \mu\text{m}$ and $\xi_0 = 124 \text{ nm}$ for Al [8, 9]. When $L \leq \xi_0$ spin-flip in S is therefore inefficient since $L \leq \xi_0 < l_{\text{sf}}$ in these materials. We are then allowed to disregard spin-flip scattering [5]. On the other hand, when $L \gg l_{\text{sf}}$ the spin current never reaches R so that G is governed exclusively by spin-flip in S for all temperatures. In the interesting regime where $l_{\text{sf}} \approx L$, the full theoretical treatment sketched in the following has to be invoked in order to compute the competing effects that determine G .

The total spin current leaving the ferromagnet in the F|S|R heterostructure can be expressed as an energy integral over the balance of the spectral pumping and back-flow currents $\mathbf{I}_s = \int dE (\mathbf{i}_s^{\text{inj}} - \mathbf{i}_s^{\text{back}})$. The spin current injected into S by the precessing magnetization is [5, 10]:

$$\mathbf{i}_s^{\text{inj}}(E) = \frac{\hbar N(0, E)}{4\pi} \frac{f_{\text{FD}}(E - hf/2) - f_{\text{FD}}(E + hf/2)}{hf} \times \left(g_r^\perp \mathbf{m} \times \frac{d\mathbf{m}}{dt} + g_i^\perp \frac{d\mathbf{m}}{dt} \right), \quad (4)$$

where f is the instantaneous rotation frequency. Here, g_r^\perp and g_i^\perp are the real and imaginary parts of spin-mixing conductance. For metallic interfaces, $g_r^\perp \gg g_i^\perp$ [11]. We therefore disregard the ‘‘effective field’’ g_i^\perp in (4), although it contributes to the interface boundary conditions discussed below. The magnetization damping that follows from (4) is frequency dependent beyond the Gilbert phenomenology. We have checked numerically that the f -dependent terms contribute weakly to the damping even when $hf \lesssim \Delta_0$ for the parameters studied. We therefore restrict attention to the linear response regime in which the Fermi-Dirac functions in (4) can be expanded to first order in hf . This leads to frequency-independent enhanced Gilbert damping damping in (1). The spectral back-flow of spin current into F induced by the spin accumulation on the S side is

$$\mathbf{i}_s^{\text{back}}(E) = - \frac{N(0, E)}{4\pi} g_r^\perp \mathbf{h}_{\text{TS}}(0, E). \quad (5)$$

The nonequilibrium spin distribution function $\mathbf{h}_{\text{TS}}(x, E)$ can be computed by Keldysh transport theory [6]. In the S bulk, the total spin current $\mathbf{I}_s(x) = \hbar AN_0 \int_{-\infty}^{\infty} dE D_L(E, x) \partial_x \mathbf{h}_{\text{TS}}(x, E)/2$ follows from the diffusion equation

$$\left(N \partial_t + \partial_x D_L \partial_x - \frac{\alpha_{\text{TSTS}}^{\text{m}}}{\tau_{\text{m}}} - \frac{\alpha_{\text{TSTS}}^{\text{so}}}{\tau_{\text{so}}} \right) \mathbf{h}_{\text{TS}} = 0. \quad (6)$$

Diffusion through S is taken to be instantaneous on the scale of the FMR frequency as long as $f < D/L^2$ and/or $f \ll 1/\tau_{\text{sf}}$ so that \mathbf{h}_{TS} in (6) becomes time-independent. $\alpha_{\text{TSTS}}^{\text{m}} = [\text{Re} \cosh \theta]^2 + (-)[\text{Re} \sinh \theta]^2$ are energy-dependent renormalization factors for the spin-flip rates due to magnetic impurities (spin-orbit coupling), and the energy dependent spin diffusion coefficient $D_L/D = \alpha_{\text{TSTS}}^{\text{so}}$. The spectral properties of the superconductor parameterized by $\theta(x, E)$ are determined

by the Usadel equation for the retarded Green function $\hat{G}^{\text{R}} = \hat{\tau}_3 \cosh \theta + i \hat{\tau}_2 \sinh \theta$,

$$\frac{\hbar D}{2} \frac{\partial^2 \theta}{\partial x^2} = i \Delta \cosh(\theta) - i E \sinh(\theta) + \frac{3}{8} \frac{\hbar}{\tau_{\text{m}}} \sinh(2\theta), \quad (7)$$

to be solved with the BCS gap equation $\Delta = (N_0 \lambda / 2) \int_0^{E_{\text{D}}} dE \tanh(E/2k_{\text{B}}T) \text{Re} \sinh(\theta)$ [6]. Here, E_{D} is the Debye cut-off energy and λ the interaction parameter.

The boundary condition for the diffusion equation (6) is conservation of spin current at the interfaces. At $x = 0$, $\hbar AN_0 D_L \partial_x \mathbf{h}_{\text{TS}}/2 = \mathbf{i}_s^{\text{inj}} - \mathbf{i}_s^{\text{back}}$. We use boundary conditions derived in Ref. 12 for (7) at the S|R interface. At the F|S interface we impose complete suppression of superconducting correlations, $\theta(x = 0, E) = 0$ for the following reasons. The large exchange energy in transition metal ferromagnets completely suppress superconducting correlations, so that the F adjacent to S is a source of incoherent particles. Additionally, spin dependent interface scattering at the S side [13] induces an effective pair-breaking exchange field, which we estimate as $B_{\text{eff}} = \hbar g_i^\perp / e^2 g_{\text{L}} \mu_{\text{B}} N_0 A \xi_0$ [14]. Here, $N_0 A \xi_0$ is the number of states at the Fermi energy within ξ_0 from the interface. With $g_i^\perp \approx 0.05 g_{\text{Sh}}$, where g_{Sh} is the Sharvin conductance [11], and approximating N_0 by the free-electron value, $\mu_{\text{B}} B_{\text{eff}}$ is comparable to Δ_0 , e.g. $\mu_{\text{B}} B_{\text{eff}}(\text{Nb}) \sim 0.56 \text{ meV}$, $\mu_{\text{B}} B_{\text{eff}}(\text{Al}) \sim 69 \mu\text{eV}$. The bulk F exchange splitting and the induced B_{eff} by spin-dependent interface scattering leads to a vanishing gap (and θ) at the F|S interface [15, 16].

The spin diffusion equation (6) can be solved analytically in the absence of spin-flip, proving (2). We now use the full machinery sketched above to make contact with experimental results for a F|S device (without R) similar to sample C in Ref. 4. Numerically computing \mathbf{I}_s including spin-flip caused by magnetic impurities [17], we obtain the enhanced Gilbert damping G from (1). In the experiment, F is a permalloy layer with $d = 2 \text{ nm}$, and $g_{\text{L}} = 2.1$. S is Nb with $L = 70 \text{ nm}$, bulk critical temperature $T_{\text{c}0} = 8.91 \text{ K}$, $l_{\text{sf}} = 48 \text{ nm}$, and $D = 5.41 \text{ cm}^2 \text{ s}^{-1}$ [1, 18]. For the interface conductances we use $Ar = 3 \text{ f}\Omega\text{m}^2$ [19]. We find $G - G_0 = 0.777 \times 10^8 \text{ s}^{-1}$ at $T_{\text{c}}/2 = 3.6 \text{ K}$ and $1.19 \times 10^8 \text{ s}^{-1}$ in the normal state. When the inhomogeneous linewidth broadening is small, the width of the FMR spectra are proportional to G and the experimental data gives $[G(T > T_{\text{c}}) - G(T = T_{\text{c}}/2)]/G(T > T_{\text{c}}) \approx 21 \%$. Using $G_0 = 0.7 \times 10^8 \text{ s}^{-1}$ [5] we obtain 22 %. The measured reduction of the Gilbert damping upon cooling the sample from above T_{c} to $T_{\text{c}}/2$ agrees *quantitatively* with our calculation.

We can make additional predictions for the Gilbert damping in F|S|R systems, focusing on Al as S since its spin-flip length is much larger than that of Nb, and as a weak coupling superconductor is better described by BCS theory. The Al material parameters are $T_{\text{c}0} = 1.26 \text{ K}$, $l_{\text{sf}} = 1.1 \mu\text{m}$, and $D = 160 \text{ cm}^2 \text{ s}^{-1}$. In the left panel

of Fig. 2 we show the temperature dependence of $G - G_0$ for three different thicknesses L when spin-flip is induced exclusively by either magnetic disorder or spin-orbit coupling to impurities. In contrast to spin-orbit scatterers, magnetic impurities reduce T_c due to the pair-breaking term in (7). For $L > l_{sf}$ and $T \ll T_c$, as well as for $T > T_c$, the results do not depend on the nature of the spin-flip scattering. In general, we observe that T_c strongly depends on L due to the inverse proximity effect. We also note that the difference in damping between the normal state and the superconducting state is small when $L \sim \xi_0$ since only a small gap develops.

The experiments of Ref. 4 probed the regimes $L \ll \xi_0$ as well as $L \gg \xi_0$. We also present results for arbitrary L/ξ_0 . In the normal state, G decreases with increasing L due to increasing bulk spin transport resistance, which limits relaxation in R, until L reaches the value of l_{sf} where R becomes irrelevant (inset Fig. 2). When $T \ll T_c$, on the other hand, the relevant length scale for spin penetration into S is ξ_0 . This explains the more rapid decay of $G - G_0$ as a function of L in the superconducting state. When $L > \xi_0$, the spin-current absorption is completely determined by the inverse proximity effect: Spin dissipation in R by transport through S is suppressed by the superconducting gap, and, furthermore, spin relaxation deep in S is suppressed by the superconductivity. However, the inverse proximity effect enhances the density of states at low energy as well as spin-flip scattering rates close to the F|S interface.

When $L < l_{sf}$, the results depend strongly on the S|R contact described by g . In the right panel of Fig. 2, we show the temperature dependence of $G - G_0$ for $L = 900$ nm in an F|S system (no R or $g = 0$). At $T > T_c$, the damping is much smaller in the F|S system (the right panel) than in the F|S|R system with the same L (the middle pair of curves in the left panel). T_c is also higher since there is no inverse proximity effect at $x = L$. At very low temperatures, $T \ll T_c$, $G - G_0$ saturates at the same value for the F|S system as the F|S|R system with the larger thickness, $L = 1300$ nm. For such thick S, T_c is unaffected by R and spins cannot diffuse through S and dissipate in R, so that the resulting damping is the same as in the F|S system. We also see from the right panel of Fig. 2 that when $T \lesssim T_c$ the enhanced Gilbert damping can be somewhat larger than above T_c when spin-flip is induced by magnetic impurities, because the induced spin accumulation of quasiparticles with energy $k_B T \gtrsim \Delta$ experiences an enhanced spin-flip rate through α_{TSTS}^m . In the F|S-R system, this effect is overwhelmed by the spin accumulation drain in R.

In conclusion, our theory quantitatively reproduces the measured FMR linewidth broadening in ferromagnet|superconductor structures. We make additional predictions for varying system sizes and temperatures, and the nature and strength of spin-flip scattering. We hope to stimulate more experiments that should

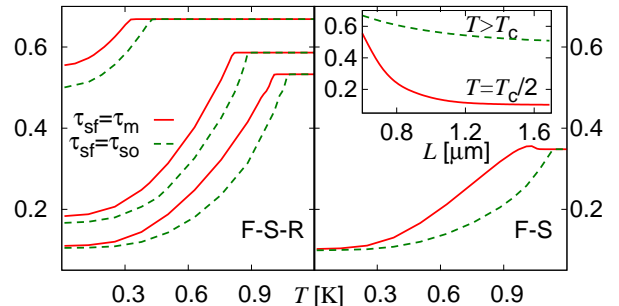


FIG. 2: Calculated $G - G_0$ [10^8 s^{-1}] (same ordinate in all plots). Red solid (green dashed) lines for system where $\tau_{sf} = \tau_m$ ($\tau_{sf} = \tau_{so}$). Left panel: F|S|R system with L [nm] from top to bottom: 600, 900, 1300. Right panel: F|S system (no R) with $L = 900$ nm. Inset: L dependence [μm] of $G - G_0$ for $T > T_c$ (green dashed line) and $T \ll T_c$ (red solid line).

reveal information about the strong inverse proximity effect and energy dependence of spin flip scattering in these systems.

We would like to thank C. Bell and J. Aarts for discussions. This work has been supported by NanoNed, the EC Contracts NMP-505587-1 "SFINX" and IST-033749 "DynaMax", the DFG through SFB 513 and the Landesstiftung Baden-Württemberg.

-
- [1] J. Y. Gu *et al.*, Phys. Rev. B **66**, 140507(R) (2002).
 - [2] J. Y. Gu *et al.*, Phys. Rev. Lett. **89**, 267001 (2002); A. Potenza and C. H. Marrows, Phys. Rev. B **71**, 180503(R) (2005); I. C. Moraru, W. P. Pratt Jr., and N. O. Birge, Phys. Rev. B **74**, 220507 (2006); A. Yu. Rusanov, S. Habraken, and J. Aarts, Phys. Rev. B **73**, 060505(R) (2006).
 - [3] V. V. Ryazanov *et al.*, Phys. Rev. Lett. **86**, 2427 (2001); V. V. Ryazanov, V. A. Oboznov, A. V. Veretennikov, and A. Yu. Rusanov, Phys. Rev. B **65**, 020501(R) (2001); T. Kontos *et al.*, Phys. Rev. Lett. **89**, 137007 (2002); H. Sellier, C. Baraduc, F. Lefloch, and R. Calemczuk, Phys. Rev. B **68**, 054531 (2003); A. Bauer *et al.*, Phys. Rev. Lett. **92**, 217001 (2004); V. A. Oboznov *et al.*, Phys. Rev. Lett. **96**, 197003 (2006). M. Weides *et al.*, Phys. Rev. Lett. **97**, 247001 (2006).
 - [4] C. Bell, S. Milikisyants, M. Huber, and J. Aarts (2007), cond-mat/0702461, accepted for publication by Phys. Rev. Lett.
 - [5] Y. Tserkovnyak, A. Brataas, G. E. W. Bauer, and B. I. Halperin, Rev. Mod. Phys. **77**, 1375 (2005); Y. Tserkovnyak, A. Brataas, and G. E. W. Bauer, Phys. Rev. Lett. **88**, 117601 (2002); Y. Tserkovnyak, A. Brataas, and G. E. W. Bauer, Phys. Rev. B **66**, 224403 (2002).
 - [6] J. P. Morten, A. Brataas, and W. Belzig, Phys. Rev. B **70**, 212508 (2004); J. P. Morten, A. Brataas, and W. Belzig, Phys. Rev. B **72**, 014510 (2005).

- [7] M. A. Sillanpaa, T. T. Heikkila, R. K. Lindell, and P. J. Hakonen, *Europhys. Lett.* **56**, 590 (2001).
- [8] F. J. Jedema, M. S. Nijboer, A. T. Filip, and B. J. van Wees, *Phys. Rev. B* **67**, 085319 (2003).
- [9] G. R. Boogaard, A. H. Verbruggen, W. Belzig, and T. M. Klapwijk, *Phys. Rev. B* **69**, 220503(R) (2004).
- [10] M. Büttiker, H. Thomas, and A. Prêtre, *Z. Phys. B* **94**, 133 (1994).
- [11] A. Brataas, G. E. W. Bauer, and P. J. Kelly, *Phys. Rep.* **427**, 157 (2006).
- [12] M. Y. Kupriyanov and V. F. Lukichev, *Sov. Phys. JETP* **67**, 1163 (1988).
- [13] D. Huertas-Hernando and Y. Nazarov, *Eur. Phys. J. B* **44** (2005).
- [14] G. E. W. Bauer *et al.*, *Phys. Rev. Lett.* **92**, 126601 (2004).
- [15] G. Sarma, *J. Phys. Chem. Solids* **24**, 1029 (1963).
- [16] W. Belzig, A. Brataas, Y. V. Nazarov, and G. E. W. Bauer, *Phys. Rev. B* **62**, 9726 (2000).
- [17] N. Poli *et al.* (2007), arXiv:cond-mat/0707.2879.
- [18] R. T. W. Koperdraad and A. Lodder, *Phys. Rev. B* **51**, 9026 (1995).
- [19] J. Bass and W. P. Pratt Jr., *J. Magn. Magn. Mater.* **200**, 274 (1999).

PAPER 5

Circuit theory of crossed Andreev reflection

Physical Review B **74**, 214510 (2006)

Circuit theory of crossed Andreev reflectionJan Petter Morten,^{1,*} Arne Brataas,^{1,2} and Wolfgang Belzig³¹*Department of Physics, Norwegian University of Science and Technology, N-7491 Trondheim, Norway*²*Centre for Advanced Study, Drammensveien 78, Oslo, N-0271 Norway*³*Department of Physics, University of Konstanz, D-78457 Konstanz, Germany*

(Received 21 June 2006; revised manuscript received 11 September 2006; published 18 December 2006)

We consider transport in a three-terminal device attached to one superconducting and two normal-metal terminals, using the circuit theory of mesoscopic superconductivity. We compute the nonlocal conductance of the current out of the first normal-metal terminal in response to a bias voltage between the second normal-metal terminal and the superconducting terminal. The nonlocal conductance is given by competing contributions from crossed Andreev reflection and electron cotunneling, and we determine the contribution from each process. The nonlocal conductance vanishes when there is no resistance between the superconducting terminal and the device, in agreement with previous theoretical work. Electron cotunneling dominates when there is a finite resistance between the device and the superconducting reservoir. Dephasing is taken into account, and the characteristic time scale is the particle dwell time. This gives rise to an effective Thouless energy. Both the conductance due to crossed Andreev reflection and electron cotunneling depend strongly on the Thouless energy. We suggest experimental determination of the conductance due to crossed Andreev reflection and electron cotunneling in measurement of both energy and charge flow into one normal-metal terminal in response to a bias voltage between the other normal-metal terminal and the superconductor.

DOI: [10.1103/PhysRevB.74.214510](https://doi.org/10.1103/PhysRevB.74.214510)

PACS number(s): 74.45.+c, 74.25.Fy, 73.23.-b

I. INTRODUCTION

Crossed Andreev reflection^{1,2} transforms an incident electron from one conductor, attached to a superconductor, into a hole in a geometrically separated second attached conductor. In an alternative, equivalent picture, two quasiparticles from two separate conductors are transferred into a superconductor as a Cooper pair. Electrons can also be transferred between the conductors by electron cotunneling, where an incident electron tunnels via a virtual state in the superconductor. The nonlocal conductance, defined in a three-terminal device as the current response in one normal-metal terminal to a voltage bias between the other normal metal and the superconductor, is determined by contributions from both crossed Andreev reflection and electron cotunneling. Crossed Andreev reflection and electron cotunneling give opposite contributions to the nonlocal conductance. In this way, crossed Andreev reflection competes with electron cotunneling. The realization of a system where crossed Andreev reflection can be observed, has been the aim of both experimental^{3,4} and theoretical⁵⁻⁹ work lately. This interest is due to the fact that crossed Andreev reflection is an inherently mesoscopic phenomenon, with the prospect of creating entangled electrons.¹⁰⁻¹²

The nonlocal conductance of a device where two normal conductors are tunnel coupled to a bulk superconductor was calculated in second order perturbation theory for quantum tunneling¹³ in Ref. 5. The conductance originating from crossed Andreev reflection was predicted to exactly cancel the conductance due to electron cotunneling. Subsequently, disorder¹⁴ and higher order quantum interference effects^{15,16} have been incorporated into this approach, and the noise and cross correlations have been considered.¹⁷ Ferromagnetic contacts were also considered in Ref. 5. Crossed Andreev reflection is favored in an antiparallel configuration of the

magnetizations, since Cooper pairs in singlet superconductors consist of two electrons with opposite spins. Electron cotunneling is favored in a parallel configuration.

The predicted dependence of the nonlocal conductance on the magnetization configuration was observed experimentally in a hybrid superconducting-ferromagnetic device.³ Subsequently, a bias dependent nonlocal conductance was observed in a more complicated geometry with only *normal-metal* contacts to the superconductor.⁴ For bias voltages corresponding to energies below the Thouless energy associated with the distance between the two normal terminals, a nonlocal signal with sign corresponding to electron cotunneling was seen. Thus, in contrast to the results of Refs. 5 and 14, experiments showed a finite nonlocal conductance at low bias. Additionally, the sign of the nonlocal signal in Ref. 4 changes when the bias voltage exceeds the Thouless energy, and this was interpreted as a consequence of crossed Andreev reflection dominating the nonlocal signal. These experimental findings are currently not understood.

In previous theoretical works, it is assumed that superconducting properties, e.g., the magnitude of the gap, are not modified by the presence of the contacts. This assumption is valid as long as the coupling between the normal or ferromagnetic conductor and the superconductor is weak or has a small cross section compared to the superconducting coherence length. None of the mentioned theoretical works describe a dependence in the conductances on the Thouless energy.

The circuit theory of mesoscopic transport^{18,19} is a suitable framework to understand transport properties of mesoscopic small normal-metal–superconducting systems. Circuit theory is a discretization of the quasiclassical theory of superconductivity,²⁰ and can treat nonequilibrium effects and dephasing. A circuit is modeled as a network of cavities, connectors, and terminals—similar to the way we understand classical electric circuits. Terminals are voltage probes in lo-

cal thermodynamic equilibrium, whereas cavities can be driven out of equilibrium. Cavities and terminals may be normal metals or superconductors. The connectors can represent physical interfaces between cavities and terminals or model diffusion. Connectors representing interfaces are described by their sets of transmission probabilities. “Kirchhoff’s rules” determine the matrix Green’s functions (potentials) of the cavities and the matrix currents through the connectors. The matrix currents describe not only the flow of charge and energy, but, e.g., also the flow of quasiparticle correlation. Circuit theory has been applied successfully to explain various phenomena in superconductor and normal-metal–ferromagnet hybrid structures, like the proximity effect,¹⁸ multiple Andreev reflections,²¹ spin transport,^{22,23} and unconventional superconductivity.²⁴ Circuit theory has also proved to be a successful approach to calculate the full counting statistics of hybrid structures.^{25–28} A circuit theory of magnetoelectronics has been developed for hybrid systems of ferromagnets and normal metals; see Ref. 29 and references therein.

We apply circuit theory to calculate the nonlocal conductance of a three-terminal device with contacts to one superconducting and two normal-metal terminals. We substantially generalize previous theoretical approaches by computing analytically the nonlocal conductance with general connectors ranging from, e.g., ballistic point contacts via diffusive contacts to tunnel junctions. We take the proximity effect into account, in which superconducting correlations affect the spectral properties of a normal metal. We also take dephasing into account, where the dwell time gives rise to an effective Thouless energy. We consider low bias transport so that the relevant energies are much smaller than the superconducting gap. The model we consider has a simple and generic geometrical structure. We do not consider Josephson effects. We recover several aspects seen in experiments.⁴ Crossed Andreev reflection and electron cotunneling do not cancel each other. However, in the limiting case of strong coupling between the device and the superconducting terminal, our results agree with previous theoretical work, and the nonlocal conductance vanishes. The differential conductances depend on the effective Thouless energy. A dependence on the Thouless energy has been observed experimentally.⁴ However, we do not find an agreement with the sign of the measured nonlocal conductance above the Thouless energy for the simple model we study.

The paper is organized in the following way. In Sec. II we give an overview of our model and the circuit components. In Sec. III we present the mathematical description and calculation that determine the conductances associated with the various transport processes in the system. We show numerical results for some experimentally relevant systems in Sec. IV. Finally, we give our conclusions in Sec. V.

II. MODEL

We consider a three-terminal system where one superconducting terminal and two normal-metal terminals are connected to a small normal-metal cavity. We assume that the cavity is large enough that charging effects can be neglected,

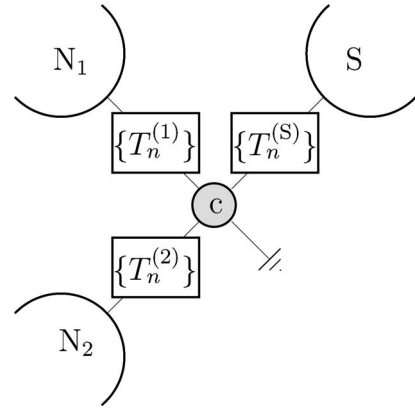


FIG. 1. Our circuit theory model. A normal-metal chaotic cavity (c) is connected to one superconducting (S) and two normal-metal terminals (N_1 and N_2). The three connectors are described by their sets of transmission probabilities. A coupling to ground represents the “leakage of coherence” (see text).

and that the Green’s functions are isotropic due to chaotic scattering. A physical realization of the chaotic cavity could be a small piece of diffusive metal, embedded in a circuit by, e.g., tunneling contacts to the terminals. The assumptions on the chaotic cavity are quite general and can also be satisfied for, e.g., a quantum dot with ballistic point contacts, if the conductance of the contacts is much less than the Sharvin estimation of the cavity conductance.¹⁹ The circuit theory representation of our model is shown in Fig. 1. The normal terminals N_1 and N_2 , and the superconducting terminal S are connected to the chaotic cavity c through general connectors represented by their sets of transmission probabilities $\{T_n^{(i)}\}$ where $i=1,2,S$, and the index n numbers the conductance channels. These connectors can represent anything from ballistic point contacts to tunnel junctions.²² For a ballistic connector all transmission eigenvalues are equal to 1 for the propagating channels and 0 otherwise. For a tunnel junction, all transmission probabilities are small. Dephasing is represented in the circuit diagram by a coupling to ground, although no energy or charge current can flow to this terminal. The dephasing will be discussed in more detail in Sec. III. Our model has a generic geometrical structure and will capture the physics of crossed Andreev reflection and electron cotunneling for a wide range of systems.

Let us now identify the various transport processes in the system. We expect the following contributions to the current: Electron cotunneling (EC) between terminals N_1 and N_2 , direct Andreev (DA) reflection between the superconductor and either normal terminal N_1 or N_2 , and crossed Andreev (CA) reflection between the superconductor and both normal metal terminals N_1 and N_2 . In direct Andreev reflection, an injected particle from one terminal gives rise to a reflected hole in the same terminal, whereas in crossed Andreev reflection an injected particle from terminal N_2 (N_1) gives rise to a reflected hole in terminal N_1 (N_2). These processes are illustrated in Fig. 2.

Semiclassical probability arguments show that the spectral charge current in the connector between N_1 and c at energy E has the following structure:²²

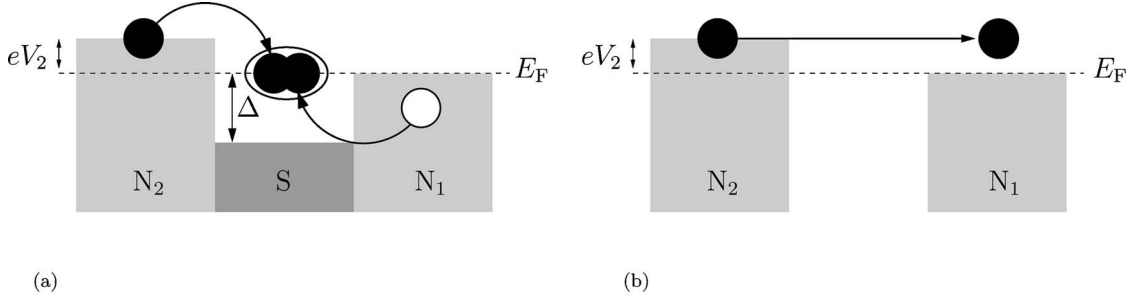


FIG. 2. Transport processes in the three-terminal device. (a) Crossed Andreev reflection: A particle from N_2 with energy eV_2 and a particle from N_1 with energy $-eV_2$ form a Cooper pair in S. (b) Electron cotunneling: A particle from N_2 at energy eV_2 tunnels through the cavity c into N_1 . The density of states in the cavity c is suppressed due to the proximity effect from the superconducting terminal.

$$I_1(E) = \frac{G_{EC}(E)}{e} [f_2(E) - f_1(E)] + 2 \frac{G_{DA}(E)}{e} [1 - f_1(E) - f_1(-E)] + \frac{G_{CA}(E)}{e} [1 - f_1(E) - f_2(-E)], \quad (1)$$

where $f_i(\pm E)$ denote the Fermi-Dirac distribution functions in normal terminal i at energy $\pm E$. The energy dependent conductances $G(E)$ are even functions of energy. Andreev reflection couples an electron with energy E in terminal N_1 to an electron with energy $-E$ in either terminal N_1 (DA) or N_2 (CA). The factor 2 for direct Andreev reflection takes into account that two charges are transmitted in this process. We divide currents and distribution functions into even and odd parts with respect to energy. The even part contributes to spectral charge current, and the odd part contributes to spectral energy current. We therefore construct $I_{T,1}(E) \equiv [I_1(E) + I_1(-E)]/2$:

$$I_{T,1}(E) = \frac{1}{e} \left(\frac{1}{2} G_{EC} + \frac{1}{2} G_{CA} + 2G_{DA} \right) h_{T,1} - \frac{1}{2e} (G_{EC} - G_{CA}) h_{T,2}, \quad (2)$$

where $h_{T,i}$ are the reservoir distribution functions determined by Fermi-Dirac functions.⁴⁰ The total charge current is found by integrating over all energies $I_{\text{charge},1} = \int dE I_{T,1}$. We define the nonlocal differential conductance as the current response in one normal terminal to a voltage between the other normal terminal and the superconductor. Using Eq. (2), this quantity becomes

$$\frac{\partial I_{\text{charge},1}}{\partial V_2} = - \int dE [G_{EC}(E) - G_{CA}(E)] \frac{\partial f(E - eV_2)}{\partial E}, \quad (3)$$

where V_2 is the voltage in terminal N_2 . At low temperature, the derivative of the Fermi function gives a δ -function at energy eV_2 . The integral then gives $\partial I_{\text{charge},1} / \partial V_2 = G_{EC}(eV_2) - G_{CA}(eV_2)$, thus the nonlocal differential conductance is determined by the difference of the cotunneling conductance and the crossed Andreev reflection conductance for quasiparticles at energy eV_2 . Consequently, a measurement

of the nonlocal conductance does not uniquely determine the conductance for both processes.

In Sec. III we show that according to the circuit theory, $G_{EC} - G_{CA}$ is positive at all energies for the generic network considered. This means that the conductance resulting from electron cotunneling is larger than the conductance resulting from crossed Andreev reflection, and thus the nonlocal differential conductance is always positive.

The odd part of the current in Eq. (1) with respect to energy contributes to energy transport. Direct Andreev reflection does not contribute since two particles of energies E and $-E$ are transmitted. The spectral energy current in the connector between N_1 and c has the following structure:⁴⁰

$$I_{L,1}(E) \equiv \frac{I_1(E) - I_1(-E)}{2} = \frac{1}{2e} (G_{EC} + G_{CA}) (h_{L,1} - h_{L,2}). \quad (4)$$

The total energy current is obtained from the spectral energy current $I_{L,1}$ by $I_{\text{energy},1} = \int dE E I_{L,1} / e$. The energy current into the terminal is related by the heat capacity to the rate of change of the temperature. Thus a nonlocal differential conductance for energy transport could in principle be measured by considering the heat flow into terminal N_1 . We define the nonlocal differential conductance for energy transport as the energy current response in one terminal to a voltage between the other normal terminal and the superconductor. From Eq. (4) this quantity becomes

$$\frac{\partial I_{\text{energy},1}}{\partial V_2} = - \int dE \frac{E}{e} [G_{EC}(E) + G_{CA}(E)] \frac{\partial f(E - eV_2)}{\partial E}. \quad (5)$$

At low temperatures, this gives $\partial I_{\text{energy},1} / \partial V_2 = V_2 [G_{EC}(eV_2) + G_{CA}(eV_2)]$; thus the nonlocal differential conductance for energy transport is determined by the sum of the cotunneling conductance and the crossed Andreev reflection conductance for quasiparticles at energy eV_2 .

The discussion above shows that the conductance of electron cotunneling and crossed Andreev reflection can be determined independently from two experimental quantities. Measurements of the nonlocal differential conductance for both charge and energy transport determine the difference and sum of G_{EC} and G_{CA} , respectively. Thus the conductances of electron cotunneling and crossed Andreev reflection

tion are experimentally accessible and can be compared to results from theoretical models.

III. CIRCUIT THEORY

The rules of circuit theory allows calculation of the cavity Green's functions in a network when the terminal Green's functions and structure of the connectors are determined. The terminals are characterized by known quasiclassical equilibrium matrix Green's functions \check{G}_i in Nambu-Keldysh space.³⁰ The Green's functions depend on quasiparticle energy, and terminal temperature and chemical potential. The cavity Green's function in our model is denoted \check{G}_c . The Green's functions are 4×4 matrices including 2×2 Keldysh space and 2×2 Nambu space. For an explanation of our standard matrix notation, see the Appendix. The general expression for the matrix current through the connector between terminal i and the cavity is¹⁹

$$\check{I}_i = -2 \frac{e^2}{\pi \hbar} \sum_n T_n^{(i)} [\check{P}_n^{(i)} \check{G}_i, \check{G}_c], \quad (6)$$

where

$$\check{P}_n^{(i)} = \frac{1}{4 + T_n^{(i)} (\{\check{G}_i, \check{G}_c\} - 2)}. \quad (7)$$

$\check{P}_n^{(i)}$ commutes with the Green's functions in Eq. (6) since it can be expanded in anticommutators of \check{G}_i and \check{G}_c .²⁷ The matrix inversion in Eq. (7) can be performed analytically in Keldysh space due to the symmetries of these matrices. The spectral charge current can be obtained from the expression for the matrix current as $I_{T,i} = \text{Tr} \{ \hat{\sigma}_3 \check{I}_i^{(K)} \} / 8e$, and the spectral energy current as $I_{L,i} = \text{Tr} \{ \hat{I}_i^{(K)} \} / 8e$. The K superscript denotes the Keldysh matrix block of the current.

Correlation between quasiparticles with opposite excitation energy from the Fermi surface is induced in the cavity due to Andreev scattering at the superconducting terminal. Cooper pairs transferred from the superconductor into the cavity give rise to an electron with excitation energy E and a hole with excitation energy $-E$. The electron and hole quantum wave functions are initially in phase, but a relative phase will arise due to a small mismatch of the wave vectors.¹⁹ Their wave vectors are $k = k_F \sqrt{1 \pm E/E_F}$ where k_F is the Fermi momentum and E_F the Fermi energy. The relevant transport energy scale is the maximum of the temperature $k_B T$ and bias voltage eV . The phase difference between the electron and the hole becomes $\Delta\phi \sim 2E\tau/\hbar \approx 2 \max(eV, k_B T)\tau/\hbar$, where the dwell time in the cavity is τ . The dwell time will be discussed in the next paragraph. We denote by $E_{\text{Th}} = \hbar/(2\tau)$ the effective Thouless energy of the cavity. Let us consider the regime of negligible dephasing, characterized by $\max(eV, k_B T) \ll E_{\text{Th}}$. The presence of a superconducting terminal leads to prevailing electron-hole correlations since $\Delta\phi \sim \max(eV, k_B T)/E_{\text{Th}} \ll 1$. In the regime of complete dephasing, on the other hand, $\max(eV, k_B T) \gg E_{\text{Th}}$, and initial many-particle phase correlation is lost since $\Delta\phi$ is finite and can only be described statistically. Thus the induced su-

perconducting correlations due to Andreev scattering are lost, and the wave functions of the quasiparticles in the cavity are not in phase. This dephasing effect is described in circuit theory by an additional terminal for "leakage of coherence."¹⁹ Note that no charge or energy flows into this terminal. Circuit theory emerges from a discretization of the Usadel equation, and the dephasing term stems from the energy term in this differential equation. The expression for the matrix current due to dephasing is¹⁹

$$\check{I}_D = ie^2 \nu_0 V_c E [\hat{\sigma}_3 \bar{1}, \check{G}_c] / \hbar, \quad (8)$$

where ν_0 is the density of states in the normal state and V_c is the volume of the cavity.

Let us now discuss the dwell time τ defined above. The dwell time can be expressed as $\tau = e^2 \nu_0 V_c R_{\text{total}}$. R_{total} is the total resistance to escape from the system, and it includes contributions from the contacts and diffusion. Diffusion is modeled by representing the diffusive region as a network of cavities connected by tunnel-like conductors with resistance times area $\tilde{r} = \rho d$. Here ρ is the resistivity and d the lattice size in the discretized network.¹⁹ These connectors contribute to R_{total} . When diffusion is the dominating contribution to R_{total} , the definition of the effective Thouless energy gives $E_{\text{Th}} = \hbar D / (2L^2)$ in agreement with the continuum theory from which the circuit theory is derived. D is the diffusion constant and L the typical length between contacts. E_{Th} is the relevant energy scale for the proximity effect in diffusive systems with negligible contact resistances.³¹ In this paper, however, we will consider the opposite limit that R_{total} is dominated by the contact resistances. Spatial variation of the Green's function inside the system is neglected, and we may discretize with only one cavity. The effective Thouless energy is in this case $E_{\text{Th}} = \hbar / (2e^2 \nu_0 \tilde{R}L)$, where \tilde{R} is the sum of the interface resistances in parallel times area. The contact resistances induce an energy scale for dephasing similar to systems where diffusion is the dominant contribution to R_{total} . In Sec. IV we show in numerical calculations that the effective Thouless energy is the relevant energy scale for the proximity effect in the cavity.

We assume that inelastic processes in the cavity can be neglected since the characteristic time for inelastic interaction is assumed to be much larger than the dwell time. The cavity Green's function is determined by demanding matrix current conservation at each energy. The sum of all matrix currents flowing into the cavity should vanish,

$$\left[-\frac{2e^2}{\pi \hbar} \sum_{i=1,2,S} T_n^{(i)} \check{P}_n^{(i)} \check{G}_i + i \frac{e^2}{\hbar} \nu_0 V_c E \hat{\sigma}_3 \bar{1}, \check{G}_c \right] = 0. \quad (9)$$

This equation determines the Green's function on the cavity, \check{G}_c . The retarded and advanced components of \check{G}_c can be parametrized in terms of one complex function $\theta(E)$ as $\hat{G}_c^R = \hat{\sigma}_3 \cos(\theta) + \hat{\sigma}_1 \sin(\theta)$ and $\hat{G}_c^A = -\hat{\sigma}_3 \cos(\theta^*) + \hat{\sigma}_1 \sin(\theta^*)$.³² The definition of the Green's function implies that $\text{Re}\{\cos(\theta)\}$ is the normalized, energy-dependent density of states in the cavity, $\nu(E)/\nu_0$.

The Keldysh part of the Green's function is parametrized as $\hat{G}_c^K = \hat{G}_c^R \hat{h}_c - \hat{h}_c \hat{G}_c^A$, where $\hat{h}_c = \hat{1} h_{L,c} + \hat{\sigma}_3 h_{T,c}$. The normal terminals have Green's functions $\check{G}_{1(2)} = \hat{\sigma}_3 \bar{\tau}_3 + (\hat{\sigma}_3 h_{L,1(2)} + \hat{1} h_{T,1(2)}) (\bar{\tau}_1 + i \bar{\tau}_2)$, and the Green's function of the superconducting terminal is $\check{G}_S = \hat{\sigma}_1 \bar{1}$. We have assumed that any bias voltage $eV \ll \Delta$, where Δ is the gap of the superconducting terminal. Therefore, the only transport process into S is Andreev reflection since there are no accessible quasiparticle states in this terminal.

The retarded part of matrix current conservation, Eq. (9), gives an equation that determines the pairing angle θ , the retarded "Usadel equation" of the cavity:

$$\left(i \frac{e^2}{\hbar} \nu_0 V_c E - \frac{e^2}{\pi \hbar} \sum_{i=1,2,n} \frac{T_n^{(i)}}{2 + T_n^{(i)} [\cos(\theta) - 1]} \right) \sin(\theta) + \frac{e^2}{\pi \hbar} \sum_n \frac{T_n^{(S)}}{2 + T_n^{(S)} [\sin(\theta) - 1]} \cos(\theta) = 0. \quad (10)$$

The physical effect on the spectral properties from the various terms can be understood by comparing this equation to the corresponding diffusion equation for a bulk superconductor.³³⁻³⁵ This is given in Eq. (II.29b) of Ref. 33 and becomes in our notation⁴¹

$$\frac{\hbar D}{2} \frac{\partial^2 \theta}{\partial x^2} + \left(iE - \frac{\hbar}{2\tau_E} \right) \sin \theta + \Delta \cos \theta - \frac{\hbar}{\tau_{sf}} \sin \theta \cos \theta = 0,$$

where D is the diffusion constant, Δ the gap to be determined self-consistently, $1/\tau_E$ the inelastic scattering rate, and $1/\tau_{sf}$ the spin-flip scattering rate. Comparing this to Eq. (10), we see that the coupling to the superconductor induces superconducting correlations, and that the coupling to the normal terminals gives quasiparticles a finite lifetime. Spin-flip scattering could be included by taking into account magnetic impurities in the cavity. We consider a normal-metal cavity. To describe a superconducting cavity, we would have to include a pairing term in the Hamiltonian. This would result in a term in Eq. (9) with the same structure as the term corresponding to coupling to the superconducting terminal. As long as we do not consider Josephson effects, the effect of superconductivity in the cavity could therefore be included by a quantitative renormalization of the coupling strength to S, which is straightforward.

In the regime of complete dephasing, the term proportional to $\sin(\theta)$ dominates in Eq. (10) because of the large factor E/E_{Th} . The solution in this limit is $\theta=0$, which means that there are no electron-hole correlations in the cavity.

Let us now consider the Keldysh part of Eq. (9). We take the trace of this matrix block after first multiplying it by $\hat{\sigma}_3$. The resulting equation determines the distribution function $h_{T,c}$ in the cavity,

$$G_{T,1}(h_{T,1} - h_{T,c}) + G_{T,2}(h_{T,2} - h_{T,c}) + G_{T,S}(0 - h_{T,c}) = 0. \quad (11)$$

This implies charge conservation at each energy, with effective energy-dependent conductances $G_{T,i}$ between the cavity and terminals N_1 , N_2 , and S. The zero in the term $G_{T,S}(0$

$-h_{T,c})$ represents the charge distribution function in the superconductor, $h_{T,S}$, which vanishes since the superconductor is grounded. The conductance $G_{T,S}$ controls the Andreev reflection rate in the cavity since it is the conductance between the cavity and the superconducting terminal. The effective conductances are given in terms of the pairing angle and the transmission probabilities as

$$G_{T,i} = 2 \frac{e^2}{\pi \hbar} \sum_n T_n^{(i)} \frac{(2 - T_n^{(i)}) \text{Re}\{\cos(\theta)\} + T_n^{(i)} D_T}{|2 + T_n^{(i)} [\cos(\theta) - 1]|^2}, \quad (12a)$$

$$G_{T,S} = 2 \frac{e^2}{\pi \hbar} \sum_n T_n^{(S)} \frac{(2 - T_n^{(S)}) \text{Re}\{\sin(\theta)\} + T_n^{(S)} D_T}{|2 + T_n^{(S)} [\sin(\theta) - 1]|^2}. \quad (12b)$$

Here $D_T = [\text{Re}\{\cos(\theta)\}]^2 + [\text{Re}\{\sin(\theta)\}]^2$ and $i=1,2$. The term proportional to $G_{T,S}$ in Eq. (11) describes conversion of quasiparticles in the cavity into condensate in the superconducting terminal. There is an analogous term in the Boltzmann equation for a continuum superconductor,^{35,36} which describes conversion between quasiparticles and superconducting condensate over the coherence length. This analogous term has a similar dependence on θ . The rate of this conversion is controlled by Δ in the continuum case, and by $G_{T,S}$ in the cavity of our discretized theory.

In the regime of complete dephasing $\theta=0$, the conductances to the normal terminals $G_{T,i}$ coincide with the Landauer-Büttiker formula. $G_{T,S} = 2e^2 \sum_n (T_n^{(S)})^2 / [\pi \hbar (2 - T_n^{(S)})^2]$ corresponds to the Andreev conductance of an N-S interface in a diffusive system, calculated by Beenakker.³⁷ Thus the distribution function $h_{T,c}$ can be determined in the regime of complete dephasing from well-known results by demanding charge current conservation.

In the tunnel barrier limit, all transmission probabilities are small, and we can expand to first order in $T_n^{(i)}$ in Eqs. (12). We define $g_i = e^2 \sum_n T_n^{(i)} / (\pi \hbar)$ for $i=1,2,S$. For the normal terminals ($i=1,2$) we find $G_{T,i} = g_i \text{Re}\{\cos(\theta)\}$. $\text{Re}\{\cos(\theta)\}$ gives the normalized density of states in the cavity which is under the influence of the proximity effect. The tunnel conductance to the superconductor becomes $G_{T,S} = g_S \text{Re}\{\sin(\theta)\}$, which vanishes when there is complete dephasing, $\theta=0$. This is expected since the Andreev conductance of a tunnel barrier between incoherent normal and superconducting terminals vanishes.³⁸

The trace of the Keldysh block of Eq. (9) gives an equation that determines the distribution function $h_{L,c}$ in the cavity,

$$G_{L,1}(h_{L,1} - h_{L,c}) + G_{L,2}(h_{L,2} - h_{L,c}) = 0. \quad (13)$$

This is energy conservation at each energy, with effective energy-dependent conductances for energy transport $G_{L,i}$. No energy current can flow through the contact between the cavity and the superconducting terminal since no net energy is transferred into S by Andreev reflection. Our calculation is restricted to $E \ll \Delta$, but in the general case a quasiparticle current which carries energy can flow into the superconducting terminal for $E > \Delta$. The effective conductances for en-

ergy transport are given in terms of the pairing angle and the transmission probabilities as

$$G_{L,i} = 2 \frac{e^2}{\pi \hbar} \sum_n T_n^{(i)} \frac{(2 - T_n^{(i)}) \text{Re}\{\cos(\theta)\} + T_n^{(i)} D_L}{|2 + T_n^{(i)}[\cos(\theta) - 1]|^2}. \quad (14)$$

Here $D_L = [\text{Re}\{\cos(\theta)\}]^2 - [\text{Im}\{\sin(\theta)\}]^2$ and $i=1,2$.

In the tunnel barrier limit we find that $G_{L,i} = G_{T,i} = g_i \text{Re}\{\cos(\theta)\}$ for $i=1,2$, which means that the effective conductances for energy transport and charge transport into the normal terminals are equal. The conductances correspond to the usual quasiparticle tunnel conductance in this case.

Equations (10), (11), and (13) determine the Green's function in the cavity. The charge and energy currents $I_{T,i}$ and $I_{L,i}$ between terminal i and the cavity can be calculated once \check{G}_c is known. Comparison of Eqs. (2) and (4) with the expressions for $I_{T,1}$ and $I_{L,1}$ obtained from circuit theory, allows us to determine the conductances associated with the various transport processes:

$$G_{\text{DA}}(E) = \frac{1}{4} \left(\frac{G_{T,1}(G_{T,2} + G_{T,S})}{G_{T,1} + G_{T,2} + G_{T,S}} - \frac{G_{L,1}G_{L,2}}{G_{L,1} + G_{L,2}} \right), \quad (15a)$$

$$G_{\text{CA}}^{\text{EC}}(E) = \frac{1}{2} \left(\frac{G_{L,1}G_{L,2}}{G_{L,1} + G_{L,2}} \pm \frac{G_{T,1}G_{T,2}}{G_{T,1} + G_{T,2} + G_{T,S}} \right). \quad (15b)$$

These formulas are the main result of our calculation. Equation (15b) shows that $G_{\text{EC}} - G_{\text{CA}}$ is positive. Thus the nonlocal conductance $\partial I_1 / \partial V_2$ is positive. In the limit where the coupling to the superconducting terminal vanishes, i.e., all $T_n^{(S)} \rightarrow 0$, only G_{EC} remains nonzero and the conductance agrees with the result for a normal double-barrier system. If the conductance to one of the normal terminals vanishes, i.e., all $T_n^{(i)} \rightarrow 0$ for, e.g., $i=2$, only G_{DA} is nonzero. When the coupling between the superconducting terminal and the cavity is very strong $G_{T,S} \gg G_{T,1}, G_{T,2}$, we recover the result of Ref. 5 that $G_{\text{EC}} = G_{\text{CA}}$, which means that the nonlocal conductance vanishes since transport by electron cotunneling is exactly canceled by crossed Andreev reflection.

To describe a device where spatial variation in a bulk region is important, a model with several cavities connected in a network is required. The connectors between cavities represent the intrinsic resistance due to diffusion, and contribute to R_{total} and thus to the effective Thouless energy $E_{\text{Th}} = \hbar / (2e^2 \nu_0 V_c R_{\text{total}})$. However, as long as there are no Josephson currents in the network, the symmetry $G_{\text{EC(CA)}} = \alpha + (-)\beta$ of Eq. (15b) persists. Here α and β are positive numbers. This follows since the currents flowing out of the normal terminals given by circuit theory can be written $I_{L,i}(E) = C_L^{(i)}(h_{L,1} - h_{L,2})$ and $I_{T,i}(E) = C_{T1}^{(i)} h_{T,1} - C_{T2}^{(i)} h_{T,2}$ where $C_L^{(i)}$, $C_{T1}^{(i)}$, and $C_{T2}^{(i)}$ are coefficients. Comparing these expressions to Eqs. (2) and (4), we see, e.g., that $G_{\text{EC}} - G_{\text{CA}} = 2e C_{T2}^{(i)} > 0$ for contact i , regardless of the internal structure of the network of cavities. Thus the sign of the nonlocal conductance is not affected by diffusion or network geometry. We interpret this result as the consequence of a symmetry between

the crossed Andreev reflection and electron cotunneling. Both processes involve the transfer of quasiparticles through the contacts to the normal metals and the network between them, but the crossed Andreev reflection also involves Andreev reflection at the interface to the superconducting terminal. Thus the resistance limiting crossed Andreev reflection can at minimum be as small as the resistance for electron cotunneling unless other physical processes affect these quantities. We believe that an explanation of the measurements in Ref. 4 requires additional physical effects not considered here.

A. Analytically solvable limits

In this section, we give results for two limits where it is possible to solve Eq. (10) analytically and obtain simple expressions for the conductances in Eqs. (15).

1. The regime of complete dephasing

When $E \gg E_{\text{Th}}$ there is complete dephasing. In this case the conductances $G_{T,i} = G_{L,i} = g_i$ for $i=1,2$ agree with the Landauer-Büttiker formula and $G_{T,S}$ is Beenakker's result for the conductance of an N-S interface in a diffusive system, as noted above. In this limit, the conductances in Eq. (15) become

$$G_{\text{DA}} = \frac{g_1^2}{4} \frac{G_{T,S}}{(g_1 + g_2)(g_1 + g_2 + G_{T,S})}, \quad (16a)$$

$$G_{\text{CA}}^{\text{EC}}(E) = \frac{g_1 g_2}{2} \frac{1}{(g_1 + g_2)(g_1 + g_2 + G_{T,S})} \times \begin{cases} 2(g_1 + g_2) + G_{T,S} & \text{for EC,} \\ G_{T,S} & \text{for CA.} \end{cases} \quad (16b)$$

The currents resulting from these expressions using Eq. (1) can also be calculated from a semiclassical approach by demanding charge conservation in the cavity using the well-known theory for incoherent N-S transport. The result for $G_{\text{EC}} - G_{\text{CA}}$ was shown in Ref. 7, where also spin polarizing contacts are employed to give a negative nonlocal conductance. Again, in the limit of strong coupling to the superconductor, $g_i / G_{T,S} \ll 1$, we see that $G_{\text{EC}} = G_{\text{CA}}$ and thus the nonlocal conductance vanishes.

2. Tunnel barrier limit

In the tunnel barrier limit, all transmission probabilities are small. We expand to first order in $T_n^{(i)}$ in the expressions for the matrix currents. This corresponds to putting $\check{p}_n^{(i)} \rightarrow 1/4$ in Eq. (6). The resulting Eq. (9) can be solved analytically without resorting to a parametrization of \check{G}_c .¹⁹ The solution is of course equivalent to what we obtain from Eqs. (10), (11), and (13) in the same limit. Let us consider the resulting expressions for the conductances of nonlocal transport in some limits. At zero energy, we obtain

$$G_{\text{DA}} = \frac{g_1^2}{4} \frac{g_S^2}{[(g_1 + g_2)^2 + g_S^2]^{3/2}}, \quad (17a)$$

$$G_{EC} = \frac{g_1 g_2}{2} \frac{2(g_1 + g_2)^2 + g_S^2}{[(g_1 + g_2)^2 + g_S^2]^{3/2}}, \quad (17b)$$

$$G_{CA} = \frac{g_1 g_2}{2} \frac{g_S^2}{[(g_1 + g_2)^2 + g_S^2]^{3/2}}. \quad (17c)$$

These results correspond to completely phase-coherent transport. The full counting statistics for the same system in this regime has been calculated in Ref. 28. In that paper, it is found that the cross-correlation noise can have both signs in the three-terminal device.

If there is complete dephasing, the cavity spectral properties are like those of a normal metal. This gives $G_{T,S}=0$ since the Andreev conductance of a tunnel barrier vanishes for incoherent N-S transport.³⁸ Therefore, there are no transport channels into the superconducting terminal and it is effectively isolated from the circuit. Only the conductance for electron cotunneling is nonzero, and we obtain from (17b)

$$G_{EC} = \frac{1}{1/g_1 + 1/g_2}, \quad (18)$$

i.e., addition of the conductances between the cavity and both normal-metal terminals in series. This result corresponds to normal-state tunneling between N_1 and N_2 .

IV. RESULTS

In an experimental situation, nonlocal transport can be probed in measurements of the voltage or current in terminal N_1 resulting from the injection of current through terminal N_2 .^{3,4} At zero temperature, the nonlocal differential conductance $\partial I_{\text{charge},1}/\partial V_2$ as a function of eV_2/E_{Th} corresponds to $G_{EC}-G_{CA}$ [see Eq. (3)]. This quantity is given by Eqs. (15b) and is always positive within our model. The detailed behavior as a function of eV_2 depends on the pairing angle of the cavity, θ , which is determined by Eq. (10). This equation can be solved numerically, and determines the spectral properties and thus the nonlocal conductances when the parameters of the model are fixed. We will show results for three systems with different combinations of contacts which can be fabricated with state of the art nanotechnology. The contacts we study are tunnel barriers or metallic contacts. The systems represent various realizations where our circuit theory model applies. We show that the nonlocal conductances are very sensitive to the type of contacts in the system, and have a strong dependence on the Thouless energy. We have also investigated effect of inelastic scattering inside the cavity, and have found no notable qualitative differences on the conductances as compared to the elastic case; thus these results are not shown here.

A. Tunnel barriers

When all the three contacts are tunnel barriers, the equation for matrix current conservation can be solved analytically as mentioned in Sec. III A 2. The resulting expressions are quite complicated. We expand to first order in the transmission probabilities since $T_n^{(i)} \ll 1$ for $i=1,2,S$, and let g_i

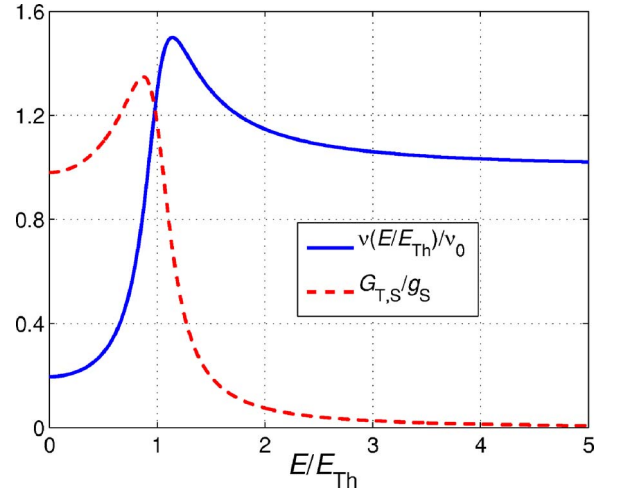


FIG. 3. (Color online) Spectral properties of the cavity when all contacts are of tunnel type with $g_1/g_S=g_2/g_S=0.1$. Solid line (blue) shows normalized density of states $\nu(E)/\nu_0$. Dashed line (red) shows $G_{T,S}/g_S$ which is the parameter that determines the Andreev reflection rate of quasiparticles.

denote tunnel barrier conductance in the normal-metal state. Let us first consider a symmetric system, $g_1/g_S=g_2/g_S=0.1$. We define the Thouless energy in this case as $E_{\text{Th}} = \hbar g_S / (2e^2 \nu_0 V_c)$. The spectral properties of the cavity are shown in Fig. 3. In this plot we show the normalized density of states in the cavity and the conductance $G_{T,S}$ which controls the Andreev reflection rate. From Fig. 3 we see that below the Thouless energy of the cavity, the quasiparticle density of states is suppressed due to electron-hole correlations. This affects all transport processes since they rely on quasiparticles propagating through the cavity. Above the Thouless energy, the density of states approaches the value in the normal state. This is the typical behavior for proximity coupled systems.³⁴ The conductance between the cavity and the superconducting terminal, $G_{T,S}$, approaches the normal-state value at low energies. At high energies, $G_{T,S}$ vanishes, as expected for tunnel barriers in the regime $E < \Delta$ when the proximity effect can be neglected.³⁸ This affects the crossed and direct Andreev reflections, which vanish when $G_{T,S}$ goes to zero.

A plot of the conductances for electron cotunneling, and crossed and direct Andreev reflections is shown in Fig. 4. The conductances have a rapid increase near $E=E_{\text{Th}}$ related to the energy dependence of the density of states. At high energies G_{EC} approaches the value for normal double-barrier tunneling, Eq. (18). G_{CA} and G_{DA} vanish at high energy. These conductances are determined by an interplay of the density of states and the Andreev reflection rate, and is small when either of these quantities is small. The measurable nonlocal differential conductance $G_{EC}-G_{CA}$ is a monotonically increasing function with increasing energy, which starts at a small value and approaches G_{EC} above the Thouless energy.

Let us now consider the effect of asymmetry between the tunnel barriers to the normal metals. The expressions for the conductances at zero energy, Eqs. (17), show that the direct Andreev conductance of one contact, $G_{DA}^{(1)}$ for example, is proportional to g_1^2 since two electrons have to tunnel through

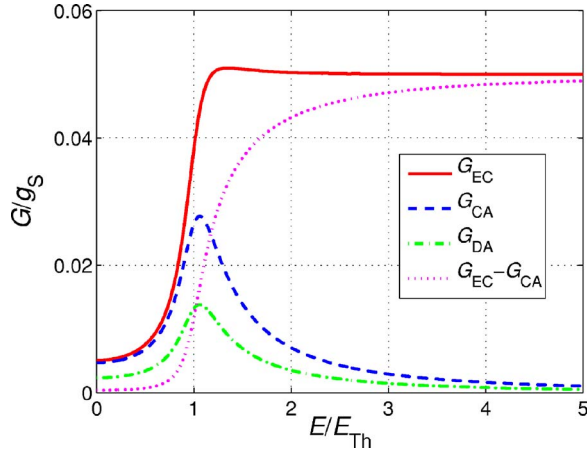


FIG. 4. (Color online) Conductance for the various transport processes through the cavity when all contacts are of tunnel type. The two normal contacts have the same conductance in this plot, $g_1/g_S = g_2/g_S = 0.1$. Solid line (red), G_{EC}/g_S ; dashed line (blue), G_{CA}/g_S ; dash-dotted line (green), G_{DA}/g_S ; and dotted line (purple), $(G_{EC} - G_{CA})/g_S$.

the connector with conductance g_1 . $G_{DA}^{(1)}$ is, however, only weakly dependent on g_2 . The same is true for the direct Andreev conductance of connector 2 with $g_1 \leftrightarrow g_2$. The direct Andreev conductances are therefore relatively independent of the asymmetry. On the other hand, nonlocal conductances are proportional to $g_1 g_2$ because a quasiparticle has to tunnel through both connectors. These conductances are sensitive to the asymmetry which we define as $a = g_1/g_2$. For the conductance measured at terminal N_1 we see that $G_{EC(CA)}^{(1)}/G_{DA}^{(1)} \propto 1/a$. Conversely, the conductance measured at terminal N_2 gives $G_{EC(CA)}^{(2)}/G_{DA}^{(2)} \propto a$. Thus asymmetry suppresses the nonlocal conductance of one contact, and enhances the nonlocal conductance of the other contact. In Fig. 5 we show the conductances for a system where $g_1/g_S = 0.1$ and $g_2/g_S = 0.3$.

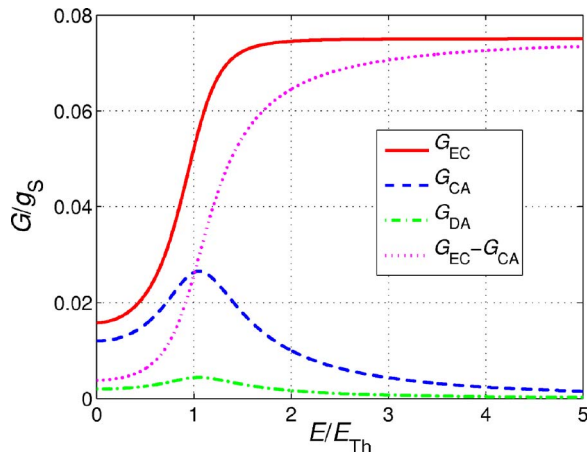


FIG. 5. (Color online) Conductance for the various transport processes through the cavity when all contacts are of tunnel type. Conductances are normalized by g_S , and parameter values are $g_1/g_S = 0.1$, $g_2/g_S = 0.3$. Solid line (red), G_{EC}/g_S ; dashed line (blue), G_{CA}/g_S ; dash-dotted line (green), G_{DA}/g_S ; and dotted line (purple), $(G_{EC} - G_{CA})/g_S$.

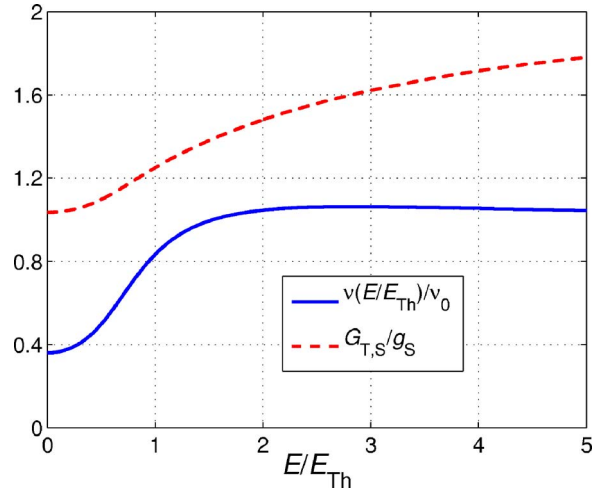


FIG. 6. (Color online) Spectral properties of the cavity when the contact to the superconducting reservoir is metallic with $T_n^{(S)} = 1$ for all propagating channels and zero otherwise, and the contacts to the normal reservoirs are of tunnel type with $g_1/g_S = 0.1$ and $g_2/g_S = 0.3$. Solid line (blue) shows normalized density of states in the cavity, $\nu(E)/\nu_0$, and dashed line (red) shows $G_{T,S}/g_S$, which is the parameter that determines the Andreev reflection rate of quasiparticles in the cavity.

The asymmetry is now $a = 1/3$, thus the effect of nonlocal processes is enhanced when we consider the conductances measured at terminal N_1 . The spectral properties in this case are similar to those of the symmetric system shown in Fig. 3, and are not shown here. Comparing Figs. 4 and 5, we see that the conductances for the crossed and direct Andreev reflections are not as peaked in the asymmetric system as in the symmetric system. We also see that the relative magnitude of the nonlocal conductances to the direct Andreev conductance has increased. In the remainder of the paper, we consider the conductances of contact 1 in asymmetric structures $a = 1/3$ since we are mostly interested in the conductance resulting from nonlocal processes.

B. Tunnel contacts to N_1 and N_2 ; metallic contact to S

Systems where two normal-metal terminals are connected to a cavity, in which the cavity may itself be part of a larger superconducting structure, can be studied in our model. The contact to the superconductor could in this case be, e.g., diffusive or metallic. In this section, we assume tunnel contacts to the two normal metals, and metallic contact to the superconductor. The metallic contact is described by the transmission probabilities $T_n^{(S)} = 1$ for all propagating channels and zero otherwise. We choose parameters $g_1/g_S = 0.1$ and $g_2/g_S = 0.3$. The Thouless energy is $E_{Th} = \hbar g_S / (2e^2 \nu_0 V_C)$. In Fig. 6 we show the spectral properties of the cavity. Below the Thouless energy, the quasiparticle density of states is suppressed. At low energy, $G_{T,S}$ approaches the value in the normal state. This is similar to the reentrant behavior in diffusive systems.^{31,39} With increasing energy, the rate of Andreev reflection at the superconducting terminal increases. The value of $G_{T,S}/g_S$ reaches its maximum value 2 for

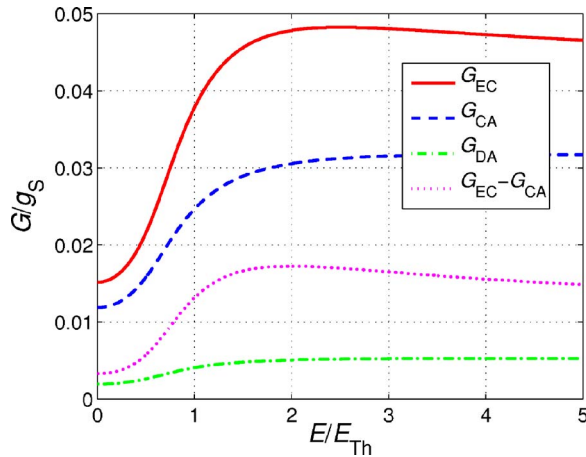


FIG. 7. (Color online) Conductances for the various transport processes when the contact to the superconducting reservoir is metallic with $T_n^{(S)}=1$ for all propagating channels and zero otherwise, and the contacts to the normal reservoirs are of tunnel type with $g_1/g_S=0.1$ and $g_2/g_S=0.3$. Solid line (red), G_{EC}/g_S ; dashed line (blue), G_{CA}/g_S ; dash-dotted line (green), G_{DA}/g_S ; and dotted line (purple), $(G_{EC}-G_{CA})/g_S$.

$E/E_{Th} \approx 20$. This result agrees with the Blonder-Tinkham-Klapwijk formula for high transmission probabilities, valid when proximity effect is negligible.³⁸

The conductances for this system are shown in Fig. 7. All conductances are suppressed below the Thouless energy by the low density of states. Above the Thouless energy, the increasing Andreev reflection rate leads to a suppression of G_{EC} and an enhancement of G_{CA} . The overall behavior of the nonlocal conductances is determined by the interplay of the dependence on the density of states and the Andreev reflection rate. The two conductances associated with Andreev reflection, G_{CA} and G_{DA} , reach their maximum at approximately $E/E_{Th}=4$ and then decrease slowly, reaching their final value at $E/E_{Th} \approx 20$.

C. Metallic contacts to N_1 and N_2 ; tunnel contact to S

Let us now consider a system where the normal terminals N_1 and N_2 are connected to the cavity through metallic contacts described by $T_n^{(i)}=1$ for all propagating channels and zero otherwise. The superconducting terminal is connected by a tunnel barrier of conductance g_S , and the Thouless energy is $E_{Th}=\hbar g_S/(2e^2\nu_0V_c)$. The spectral properties of this system are very similar to the tunneling case in Sec. IV A, and we do not show them here. However, the conductances between the normal terminals and the cavity are qualitatively different in the present case. In Fig. 8 we show $G_{T,1}$ for both the tunneling case in Sec. IV A, and where the normal terminals are connected by metallic contacts. At energies below the Thouless energy, $G_{T,1}$ is in the tunneling case qualitatively similar to the density of states. However, with metallic contacts to the normal reservoirs, $G_{T,1}$ is large at zero energy and decreases as the energy increases beyond E_{Th} . At high energy, $G_{T,1}$ is equal for the two cases and corresponds to the result in the normal state since g_1/g_S is the same for the two curves. $G_{T,1}$ for a metallic contact is qualitatively similar to

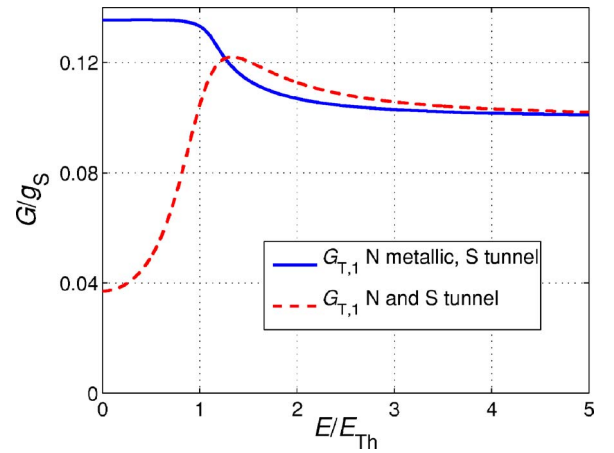


FIG. 8. (Color online) Energy dependence of conductance $G_{T,1}$ for the present case of metallic contacts to normal reservoirs and tunnel contact to the superconducting reservoir in solid line (blue), and for the case with only tunnel barriers studied in Sec. IV A in dashed line (red). In both cases we have put the parameters $g_1/g_S=0.1$ and $g_2/g_S=0.3$.

the conductance of a metallic normal-metal–superconductor interface, except that in this case the “superconductor” is the cavity which is under the influence of the proximity effect from S and the relevant energy scale is E_{Th} instead of Δ .

The conductances for the present system are shown in Fig. 9. A new feature here is a small dip in G_{EC} at $E=E_{Th}$ before the rapid increase above E_{Th} . G_{EC} is proportional to $G_{T,1}$ and inversely proportional to $G_{T,S}$. The dip in G_{EC} can therefore be understood by the decreasing charge current conductance ($G_{T,1}$) and the peak in $G_{T,S}$ around $E=E_{Th}$. At higher energy G_{EC} increases as $G_{T,S}$ vanishes. The dip in G_{EC} leads to a larger dip in $G_{EC}-G_{CA}$ since G_{CA} increases with increasing energy at $E < E_{Th}$. In the tunneling case of Sec.

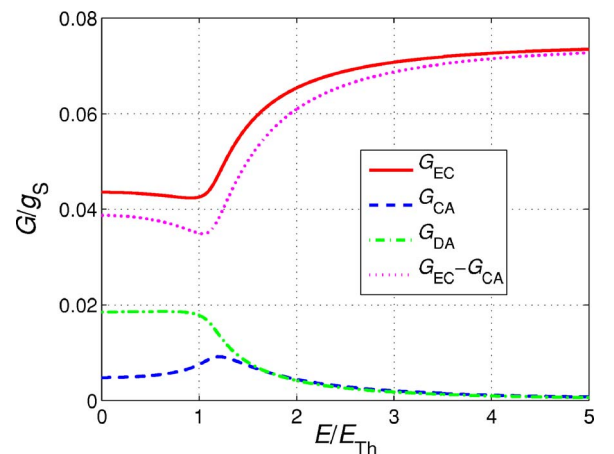


FIG. 9. (Color online) Conductances for the various transport processes when the contacts to the normal reservoirs are of metallic type with $T_n^{(i)}=1$ where $i=1,2$ for all propagating channels and zero otherwise, and the contact to the superconducting reservoir is of tunnel type with conductance g_S . In this plot $g_1/g_S=0.1$ and $g_2/g_S=0.3$. Solid line (red), G_{EC}/g_S ; dashed line (blue), G_{CA}/g_S ; dash-dotted line (green), G_{DA}/g_S ; and dotted line (purple), $(G_{EC}-G_{CA})/g_S$.

IV A, the increase of the Andreev conductance is compensated by an increasing charge current conductance in $G_{EC} - G_{CA}$, and there is no dip in the nonlocal differential conductance. At high energy, G_{CA} and G_{DA} vanish since the Andreev reflection rate vanishes.

V. CONCLUSION

In conclusion, we have studied nonlocal transport in a three-terminal device with two normal-metal terminals and one superconducting terminal. To this end we have applied the circuit theory of mesoscopic transport. The connectors between the circuit elements are represented by general expressions, relevant for a wide range of contacts. Dephasing is taken into account, and is governed by the inverse dwell time. This gives rise to an effective Thouless energy. For this model we have calculated the conductance associated with crossed Andreev reflection and electron cotunneling, as well as direct Andreev reflection. We find that for any contacts, electron cotunneling is the dominant nonlocal transport process. Results for various combinations of contacts of tunnel and metallic type are shown, and this demonstrates the strong dependence on the nature of the contacts. The conductance of nonlocal transport has a strong dependence on the Thouless energy. This is because, at these energies, dephasing leads to a loss of induced superconducting correlations. Several of the characteristics of our model have been observed in experiments, although we do not make complete qualitative contact to experimental data since electron cotunneling always dominates crossed Andreev reflection. We sug-

gest determining the conductance due to these processes independently by carrying out additional energy transport measurements.

ACKNOWLEDGMENTS

This work was supported in part by The Research Council of Norway through Grants No. 167498/V30, No. 162742/V00, No. 1534581/432, No. 1585181/143, and No. 1585471/431, RTN Spintronics, the Swiss NSF, the NCCR Nanoscience, the Deutsche Forschungsgemeinschaft through SFB 513, the Landesstiftung Baden-Württemberg through the Research Network "Functional Nanostructures," the National Science Foundation under Grant No. PHY99-07949, and the EU via Project No. NMP2-CT-2003-505587 "SFINx."

APPENDIX: NOTATION

Matrices in Nambu and Keldysh matrix space are denoted by a caret (\hat{M}) and an overbar (\bar{M}), respectively. The symbol used for a unit matrix is $\mathbb{1}$, and the Pauli matrices are denoted $\hat{\sigma}_n$ and $\bar{\tau}_n$ in Nambu and Keldysh space where $n=1,2,3$. Compositions of matrices in Nambu and Keldysh space are formed by a direct product to make up 4×4 matrices in Nambu-Keldysh matrix space, so that, e.g.,

$$\hat{\sigma}_3 \bar{\tau}_1 = \begin{pmatrix} 0 & 0 & 1 & 0 \\ 0 & 0 & 0 & -1 \\ 1 & 0 & 0 & 0 \\ 0 & -1 & 0 & 0 \end{pmatrix}. \quad (\text{A1})$$

*Electronic address: jan.morten@phys.ntnu.no

¹J. M. Byers and M. E. Flatte, Phys. Rev. Lett. **74**, 306 (1995).

²G. Deutsher and D. Feinberg, Appl. Phys. Lett. **76**, 487 (2000).

³D. Beckmann, H. B. Weber, and H. v. Lohneysen, Phys. Rev. Lett. **93**, 197003 (2004).

⁴S. Russo, M. Kroug, T. M. Klapwijk, and A. F. Morpurgo, Phys. Rev. Lett. **95**, 027002 (2005).

⁵G. Falci, D. Feinberg, and F. W. J. Hekking, Europhys. Lett. **54**, 255 (2001).

⁶T. Yamashita, S. Takahashi, and S. Maekawa, Phys. Rev. B **68**, 174504 (2003).

⁷D. Sanchez, R. Lopez, P. Samuelsson, and M. Buttiker, Phys. Rev. B **68**, 214501 (2003).

⁸N. M. Chtchelkatchev, JETP Lett. **78**, 230 (2003).

⁹F. Giazotto, F. Taddei, R. Fazio, and F. Beltram, Phys. Rev. Lett. **97**, 087001 (2006).

¹⁰P. Recher, E. V. Sukhorukov, and D. Loss, Phys. Rev. B **63**, 165314 (2001).

¹¹N. M. Chtchelkatchev, G. Blatter, G. B. Lesovik, and T. Martin, Phys. Rev. B **66**, 161320(R) (2002).

¹²P. Recher and D. Loss, Phys. Rev. Lett. **91**, 267003 (2003).

¹³F. W. J. Hekking and Y. V. Nazarov, Phys. Rev. B **49**, 6847 (1994).

¹⁴D. Feinberg, Eur. Phys. J. B **36**, 419 (2003).

¹⁵R. Mélin and D. Feinberg, Phys. Rev. B **70**, 174509 (2004).

¹⁶R. Mélin, Phys. Rev. B **73**, 174512 (2006).

¹⁷G. Bignon, M. Houzet, F. Pistolesi, and F. W. J. Hekking, Europhys. Lett. **67**, 110 (2004).

¹⁸Y. V. Nazarov, Phys. Rev. Lett. **73**, 1420 (1994).

¹⁹Y. V. Nazarov, Superlattices Microstruct. **25**, 1221 (1999).

²⁰A. Schmid and G. Schön, J. Low Temp. Phys. **20**, 207 (1975).

²¹E. V. Bezuglyi, E. N. Bratus', V. S. Shumeiko, G. Wendin, and H. Takayanagi, Phys. Rev. B **62**, 14439 (2000).

²²W. Belzig, A. Brataas, Y. V. Nazarov, and G. E. W. Bauer, Phys. Rev. B **62**, 9726 (2000).

²³D. Huertas-Hernando, Y. V. Nazarov, and W. Belzig, Phys. Rev. Lett. **88**, 047003 (2002).

²⁴Y. Tanaka, Y. V. Nazarov, and S. Kashiwaya, Phys. Rev. Lett. **90**, 167003 (2003).

²⁵W. Belzig and Y. V. Nazarov, Phys. Rev. Lett. **87**, 197006 (2001).

²⁶W. Belzig and Y. V. Nazarov, Phys. Rev. Lett. **87**, 067006 (2001).

²⁷M. Vanevic and W. Belzig, Phys. Rev. B **72**, 134522 (2005).

²⁸J. Börlin, W. Belzig, and C. Bruder, Phys. Rev. Lett. **88**, 197001 (2002).

²⁹A. Brataas, G. E. W. Bauer, and P. J. Kelly, Phys. Rep. **427**, 157 (2006).

³⁰J. Rammer and H. Smith, Rev. Mod. Phys. **58**, 323 (1986).

³¹T. H. Stoof and Y. V. Nazarov, Phys. Rev. B **53**, 14496 (1996).

³²W. Belzig, F. K. Wilhelm, C. Bruder, G. Schön, and A. D. Zaikin, Superlattices Microstruct. **25**, 1251 (1999).

- ³³A. Schmid, in *Nonequilibrium Superconductivity, Phonons, and Kapitza Boundaries*, edited by Kenneth E. Gray, NATO Advanced Studies Institute, Series B: Physics (Plenum, New York, 1981), Vol. 65, pp. 423–480.
- ³⁴D. Estève, H. Pothier, S. Guéron, and N. O. Birge, in *Mesoscopic Electron Transport*, edited by Lydia L. Sohn, Leo P. Kouwenhoven, and Gerd Schön, NATO Advanced Study Institute, Series E: Applied Science (Kluwer Academic, Dordrecht, 1997), Vol. 345, pp. 375–406.
- ³⁵J. P. Morten, A. Brataas, and W. Belzig, Phys. Rev. B **70**, 212508 (2004).
- ³⁶J. P. Morten, A. Brataas, and W. Belzig, Phys. Rev. B **72**, 014510 (2005).
- ³⁷C. W. J. Beenakker, Phys. Rev. B **46**, 12841 (1992).
- ³⁸G. E. Blonder, M. Tinkham, and T. M. Klapwijk, Phys. Rev. B **25**, 4515 (1982).
- ³⁹C.-J. Chien and V. Chandrasekhar, Phys. Rev. B **60**, 15356 (1999).
- ⁴⁰The distribution functions $h_T(E)$, $h_L(E)$ can be written in terms of the particle distribution function $f(E)$ as $h_T=1-f(E)-f(-E)$ and $h_L=-f(E)+f(-E)$ (see Ref. 32).
- ⁴¹To make contact with our notation we must identify $\alpha=\cos \theta$ and $\beta=\sin \theta$ in Eq. (II.29b) of Ref. 33. In addition to this, we put $\gamma=0$ since there is no such component in the retarded Green's function of the cavity, $\dot{\Phi}=0$ since we are considering stationary phenomena, and $\mathbf{v}_S=\mathbf{0}$ since there is no supercurrent in the cavity.

PAPER 6

*Circuit theory for crossed Andreev reflection
and nonlocal conductance*

Applied Physics A **89**, 609 (2007)

Paper VI is not included due to copyright.

PAPER 7

Quantum physics and the boundaries of space and time

In *Complexity*, edited by W. Østrem,
Centre for Advanced Study, Oslo, (2008)

Paper VII is not included due to copyright.

PAPER 8

*Elementary charge transfer processes in a
superconductor-ferromagnet entangler*

Europhysics Letters **81**, 40002 (2008)

Elementary charge transfer processes in a superconductor-ferromagnet entangler

J. P. MORTEN^{1,2(a)}, D. HUERTAS-HERNANDO^{1,2}, W. BELZIG^{3,2} and A. BRATAAS^{1,2}

¹ Department of Physics, Norwegian University of Science and Technology - N-7491 Trondheim, Norway

² Centre for Advanced Study - Drammensveien 78, N-0271 Oslo, Norway

³ University of Konstanz, Department of Physics - D-78457 Konstanz, Germany

received 23 October 2007; accepted in final form 8 December 2007
published online 15 January 2008

PACS 03.67.Mn – Entanglement production, characterization, and manipulation
PACS 74.40.+k – Fluctuations (noise, chaos, nonequilibrium superconductivity, localization, etc.)
PACS 72.25.Mk – Spin transport through interfaces

Abstract – We study the production of spatially separated entangled electrons in ferromagnetic leads from Cooper pairs in a superconducting lead. We give a complete description of the elementary charge transfer processes, i) transfer of Cooper pairs out of the superconductor by Andreev reflection and ii) distribution of the entangled quasiparticles among the ferromagnetic leads, in terms of their statistics. The probabilities that entangled electrons flow into spatially separated leads are completely determined by experimentally measurable tunnel conductances and polarizations. Finally, we investigate how currents, noise and cross-correlations are affected by transport of entangled electrons.

Copyright © EPLA, 2008

A solid-state entangler is an electronic analog of the optical setups used for experimental Bell inequality tests, quantum cryptography and quantum teleportation [1]. Ideally, such a device should produce separated currents of entangled electrons. Superconductors are suitable candidates as sources in solid-state entanglers since Cooper pairs constitute entangled states. This prospect has motivated several papers addressing the properties of hybrid superconductor and normal metal entanglers [2–6]. One of the challenges is to prevent processes where pairs of entangled particles reach the same lead, *i.e.* are not spatially separated. Electrons from Cooper pairs are entangled in spin and energy space, and separation of pairs into different leads using ferromagnets or quantum dots has been suggested [3]. Upon filtering, only the spin or energy part of the two-particle wave function collapses, depending on whether ferromagnets or quantum dots are used. Respectively, energy or spin entanglement remains [4]. Here we consider separation by ferromagnets.

Solid-state entanglers have been analyzed in refs. [2–6] in terms of currents, noise and cross-correlations. A more direct approach, describing the elementary charge transfer processes in terms of experimentally controllable parameters is certainly desirable. We demonstrate how

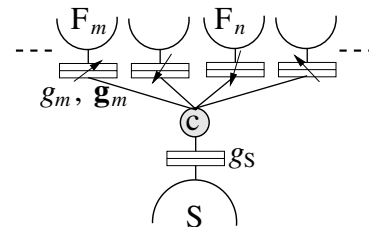


Fig. 1: Circuit theory representation of a generic F-S entangler. Entangled electrons from the singlet superconductor S enter the cavity c through a tunnel barrier with conductance g_s and escape through ferromagnetic tunnel barriers with conductance g_n and spin polarization $|\mathbf{g}_n|/g_n$ into drains F_n . Arrows indicate magnetization directions $\mathbf{g}_m/|\mathbf{g}_m|$.

this is possible through the full distribution of current fluctuations, the full counting statistics (FCS), of the solid-state entangler [7–10]. The FCS provides complete information about currents, noise, cross-correlations and higher cumulants, and even more importantly, allows direct access to the probability for transfer of charge between different parts of the device.

We consider the singlet superconductor-ferromagnet (S-F) device shown in fig. 1. A normal metal cavity (c) is connected to one superconducting terminal at ground

^(a)E-mail: jan.morten@ntnu.no

and several equally biased ferromagnetic terminals at voltage V via tunnel junctions. The cavity is under the influence of the proximity effect. In this device, charge transport occurs via two processes: i) transfer of Cooper pairs out of the superconductor by Andreev reflection and ii) distribution of the entangled quasiparticles among the ferromagnetic leads. The distribution can occur via direct Andreev (DA) reflection, where an entangled pair is transferred into lead F_n or crossed Andreev (CA) reflection, where each particle of the entangled pair is transferred into spatially separated leads F_m and F_n ($m \neq n$). CA reflection produces spatially separated entangled electrons. Since the ferromagnetic terminals are at the same voltage and we consider zero temperature, there is no direct electron transport between the ferromagnetic terminals [11].

Our general results for the counting statistics show that the processes i) and ii) are independent and therefore the statistics can be factorized. This novel factorization and the probability distribution for process ii) reveals the precise dependence of the probabilities for CA and DA processes on the experimentally measurable conductances and polarizations of the ferromagnetic leads. We find the probability to detect in terminals m and n the electrons of a Cooper pair which has been transferred out of S,

$$p_{mn} = (g_m g_n - \mathbf{g}_m \mathbf{g}_n) / (g^2 - \mathbf{g}^2), \quad (1)$$

where $g = \sum_n g_n$ and $\mathbf{g} = \sum_n \mathbf{g}_n$. The probabilities p_{mn} depend solely on the conductances g_n and spin polarization conductances \mathbf{g}_n of the ferromagnetic leads which can be determined by magnetoresistance measurement in the normal state. Equation (1) shows that the detected two-particle processes originate from a *pure spin singlet* density matrix subspace [12]. We emphasize that (1) in combination with the Cooper pair transfer probability, to be discussed below, allows for an unambiguous identification of all statistical properties of the charge transfer.

Using the magnetization dependence of the probabilities (1) one can violate the Bell-Clauser-Horne-Shimony-Holt inequality [13,14] and demonstrate entanglement. Consider a device with four F_n ($n=1-4$) terminals. Drains 1, 2 and 3, 4 have pairwise equal conductances and antiparallel magnetizations, $g_1 = g_2$ and $\mathbf{g}_1 = -\mathbf{g}_2$ etc. The terminal pairs are spin detectors with respect to magnetizations $\mathbf{g}_{1(3)}$ so that spins up in drains 1, 2 (3, 4) are measured by the current in $F_{1(3)}$ and so on. Experiments are performed with each spin detector in two different magnetization directions $\mathbf{g}_{1(3)}$ and $\mathbf{g}'_{1(3)}$. We find for the Bell parameter $\mathcal{E} = |\mathbf{g}_1 \mathbf{g}_3 + \mathbf{g}'_1 \mathbf{g}_3 + \mathbf{g}_1 \mathbf{g}'_3 - \mathbf{g}'_1 \mathbf{g}'_3| / (g_1 g_3)$. The largest possible value of \mathcal{E} in a local theory is 2. Violation of Bell's inequality $\mathcal{E} \leq 2$ can be observed provided the detectors are efficient enough. The condition on the spin polarizations is $|\mathbf{g}_{1(3)}| / g_{1(3)} \geq 2^{-1/4}$ which can be experimentally realized in the devices we consider [15].

Our results for the S-F entangler determine the spectral properties of the cavity, currents, cross-correlations

and higher-order cumulants in terms of the transport conductances measured in the *normal state*. This is possible for the spin-active tunnel barriers we consider because the parameters that determine not only the average transport, but all statistical properties, are the sums of spin-dependent transmission eigenvalues $\sum_k T_{k,\sigma}^n$ (conductances) [16] and not the individual values of $T_{k,\sigma}^n$ [10]. Specifically, our result does not depend on individual scattering matrix elements for the nanostructure [17] or phenomenological dephasing that removes the complication of coherence effects [5]. The experimental control parameters are the relative orientations of the magnetizations, which from our calculation determine the fraction of the CA current, and thus the spatially separated entangled pair currents for a given set of conductances and spin polarizations.

Ferromagnet detection of entangled spin singlets from a ballistic normal conductor was considered in ref. [12]. In that device, there are also one-particle transfers, which can contribute substantially to the current and the noise. Another important qualitative difference between our device and the system in ref. [12] is the latter's strong coupling to the detectors which can distort the spin singlets emitted from the source and induce triplet correlations upon detection. Also, in the limit of a weak coupling to the detectors, there are no two-particle processes in the system of ref. [12]. In contrast, the electrons in our S-F device are always detected from a pure spin singlet state.

The charge transfer probabilities are obtained by identifying the elementary processes in the many-body charge counting statistics. The statistics is determined by the cumulant generating function (CGF) $S(\chi_1, \chi_2, \dots) = S(\{\chi_n\})$ of the probability $P(\{N_n\})$ to transfer in a time interval t_0 , N_1 electrons to F_1 , N_2 electrons to F_2 , and so on. Our main finding is the statistics

$$P(\{N_n\}) \equiv \int \frac{d^M \chi}{(2\pi)^M} e^{S(\{\chi_n\}) - i \sum_n \chi_n N_n} \quad (2a)$$

$$= P_S \left(\sum_n N_n \right) P \left(\{N_n\} \middle| \sum_n N_n \right) \quad (2b)$$

for $\sum_n N_n$ even and positive and M the total number of terminals in the circuit. The interpretation of this result is that the charge transfer is given by two independent processes. The first factor $P_S(2N)$ is the probability that $N = \sum_n N_n / 2$ Cooper pairs are emitted from the superconducting source terminal into any of the detectors. The second factor $P(\{N_n\} | 2N)$ in (2b) is the conditional probability that N_n out of the $2N$ electrons have been transferred into the ferromagnetic terminal F_n . Below we will explain in detail how our calculation yields concrete expressions for the elementary processes described by $P(\{N_n\} | 2N)$. These results facilitates a unique interpretation of the transfer of spin singlet electron pairs.

We now supply the microscopic expressions for the two probabilities in (2b). The Cooper pair transfer probability

is obtained from $P_S(2N) = \int d\chi_S / (2\pi) \exp(S_S(\chi_S) - iN_S\chi_S)$ with a CGF $S_S(\chi_S)$ given by

$$\frac{t_0 V}{\sqrt{2e}} \sqrt{g_S^2 + \sqrt{(g_S^2 - g^2 + \mathbf{g}^2)^2 + 4g_S^2(g^2 - \mathbf{g}^2)} e^{2i\chi_S}}, \quad (3)$$

where $g_S^2 = g_S^2 + g^2 + \mathbf{g}^2$. The contact to the superconducting terminal is characterized by a spin-independent conductance g_S . The π -periodicity of $S_S(\chi_S)$ on χ_S ensures that an even number of charges is transferred. The $2N$ electrons are distributed among the F_n terminals according to the multinomial distribution $P(\{N_n\}|2N) = \int d^{M-1}\chi / (2\pi)^{M-1} \exp(S_N(\{\chi_n\}) - i\sum_n \chi_n N_n)$ with a CGF

$$S_N(\{\chi_n\}) = N \ln \left(\sum_{mn} p_{mn} e^{-i\chi_m - i\chi_n} \right). \quad (4)$$

The concrete form of the two-particle probabilities p_{mn} to detect one charge in terminal m and one in terminal n is given in (1).

We will explain below how our calculation determines (1), (3), and (4). The interpretation in terms of two independent processes of charge transfer is based on a general result for the calculated counting statistics. We have not made any *a priori* assumptions on the initial state of the superconducting source or the ferromagnetic terminals, except that they are reservoirs at zero temperature with a voltage bias eV applied between the source and the terminals. The experimental condition for this approximation is that the energy scale set by temperature $k_B T$ is smaller than the Thouless energy of the cavity and the superconducting gap. The *direct result* of our calculation is the CGF $S(\{\chi_n\})$ of the S-F entangler of fig. 1 which leads to the factorization (2b) in terms of the CGFs given by (3) and (4). $S(\{\chi_n\})$ is recovered from (3) by replacing the factor $e^{2i\chi_S}$ with $\exp\{S_N(\{\chi_n\})/N\}$ given in (4). The factorization in (2) can be proven straightforwardly from $S(\{\chi_n\})$. Actually, such a factorization is valid for any CGF where the χ -dependence is $\exp\{S_N(\{\chi_n\})/N\}$, irrespectively of its form or the probabilities p_{mn} .

We now discuss some consequences of the charge counting statistics. FCS enables us to express the current and noise correlations in a compact and meaningful form. The currents $I_n = (ie/t_0) \partial S(\{\chi_n\}) / \partial \chi_n |_{\chi_n=0}$ are

$$I = GV, \quad G = \frac{g_S^2(g^2 - \mathbf{g}^2)}{\sqrt{g_S^2 + g^2(g^2 - \mathbf{g}^2)}}, \quad I_n = I p_n, \quad (5)$$

where $p_n = \sum_m p_{mn}$ is the probability to detect one of the electrons in terminal n , irrespectively of where the second electron goes. The combined probabilities can be directly accessed in the noise correlators between current fluctuations in terminals m and n , $C_{mn} = (-2e^2/t_0) \partial^2 S(\{\chi_n\}) / \partial \chi_m \partial \chi_n |_{\chi_{n,m}=0}$:

$$C_{mn} = 2eI [p_{mn} + p_n \delta_{mn} - 2(1 - F_2) p_m p_n]. \quad (6)$$

The Fano factor for Cooper pair transport is defined as the ratio of the full current noise $C = \sum_{mn} C_{mn}$ to the Poissonian noise of doubled charges, $F_2 = C/4eI$, and is explicitly found to be $2(1 - F_2) = [5 - \mathbf{g}^2/(g_S^2 + g^2)]x/(1+x)^2$, where $x = g_S^2/(g^2 - \mathbf{g}^2)$. These expressions for the current and the noise provide a transparent interpretation of the transport processes. The current in (5) is proportional to $g_S^2(g^2 - \mathbf{g}^2)$, since two particles have to tunnel through the double junction to transfer a Cooper pair from S. The denominator is due to the proximity effect [18–20] and enhances the current drastically in comparison to calculations based on the tunneling Hamiltonian [11]. The current into each terminal I_n is then weighted according to the probability p_n . We might also distinguish the contributions to the current originating from crossed and direct Andreev reflection. The probability to detect a DA reflection in terminal n is given by p_{nn} , and the probability for CA detection in different terminals $m \neq n$ is given by p_{mn} . We find the ratio of the crossed current to the total current as

$$\frac{I_n^{\text{CA}}}{I_n} = \frac{p_n - p_{nn}}{p_n} = \frac{g_n(g - g_n) - \mathbf{g}_n(\mathbf{g} - \mathbf{g}_n)}{g_n g - \mathbf{g}_n \mathbf{g}}. \quad (7)$$

This ratio is independent of the coupling to the superconducting terminal. We further observe that the crossed current is enhanced by increasing the polarization of the contact n and is additionally favored by aligning the magnetization \mathbf{g}_n opposite to the average magnetization \mathbf{g} . These results are a direct consequence of the spin singlet nature of the Cooper pairs. Enhancing the magnitude of the polarization $|\mathbf{g}_n|/g_n$ of one terminal reduces the total current, but enhances the crossed part of the Andreev current, since the tunneling of one spin singlet electron-hole pair through the same contact is strongly suppressed.

The sign of cross-correlations in three-terminal beam splitters has been considered for various devices both experimentally [21] and theoretically [5,6,22,23]. Studies of noise [24] and FCS [25] for a beam splitter with entangled electrons show that entanglement gives qualitatively different noise characteristics compared to transport of non-entangled electrons. The physical origin of positive and negative contributions to the cross-correlators can in our case be understood from the dependence on the two-particle probabilities in (6). CA reflection leads to positive cross-correlations since two particles are transferred simultaneously into F_m and F_n (bunching behavior) [24]. A negative contribution (anti-bunching) that does not depend on entanglement, is induced by the fermion exclusion principle: The transfer of one electron-hole pair into F_m by DA reflection, prevents the simultaneous transfer of another pair into F_n . However, if the electron-hole pair transfers are not temporally correlated (Poissonian statistics), the exclusion principle does not affect the cross-correlations. This is the case when there is strong asymmetry in the junction conductances g and g_S ($g \gg g_S$ or $g \ll g_S$) so that the Fano factor $F_2 = 1$. In this limit the negative contribution $-2(1 - F_2)p_m p_n$ in (6) vanishes.

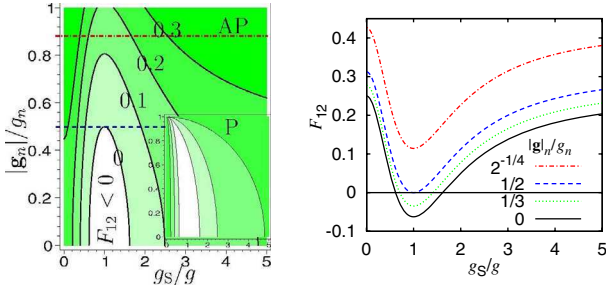


Fig. 2: (Color online) Left: contour plots of F_{12} for antiparallel and parallel (inset) configuration ($|\mathbf{g}_1| = |\mathbf{g}_2|$). Positive regions in green. Right: plots of F_{12} in antiparallel configuration as a function of the conductance asymmetry g_S/g ; the legend denotes the value of the polarization $|\mathbf{g}_n|/g_n$. Red and blue horizontal lines in the left panel correspond to red and blue curves in the right panel. Polarization $|\mathbf{g}_n|/g_n \geq 2^{-1/4}$ (above the red line) is needed to violate the Bell inequality.

Scattering matrix calculations give similar results for C_{mn} [17].

The strongly asymmetric case is particularly interesting since the cross-correlations ($m \neq n$) $C_{mn} = 2eI p_{mn}$, are a *direct* measure of the probability that electrons from a Cooper pair are transferred into different terminals.

To illustrate our theory, let us now consider the three-terminal version of fig. 1 with the superconducting source terminal S and two ferromagnetic drains F_1 and F_2 . The ferromagnetic magnetizations can in this device be utilized as filters to produce currents of entangled electrons in separated leads. Let us consider $|\mathbf{g}_1| = |\mathbf{g}_2|$ in the following and define Fano factors $F_{mn} = C_{mn}/(2eI)$. The autocorrelation noise $F_{11(22)}$ will be reduced in antiparallel alignment $\mathbf{g}_1 = -\mathbf{g}_2$ as compared to a S-N system ($\mathbf{g}_n = 0$) due to enhancement of CA reflection. The cross-correlation F_{12} , shown in fig. 2 can have both positive and negative sign depending on the conductance asymmetry g_S/g and the spin polarization. The positive contribution to F_{12} is proportional to $g_1 g_2 + (-)|\mathbf{g}_1||\mathbf{g}_2|$ in the antiparallel (parallel) alignment demonstrating how spin filtering of entangled pairs enhances (reduces) the correlation between currents in F_1 and F_2 with respect to an S-N system [5,6]. Note that for sufficiently large spin polarization, F_{12} can be positive for the entire range of g_S/g in the antiparallel alignment (region above the blue online line in the left panel of fig. 2), whereas it remains always negative in the parallel alignment for $g_S/g \simeq 1$ (inset of fig. 2). The change of sign in F_{12} by switching from antiparallel to parallel alignment is due to the enhanced probability of CA events, see (7).

We will finally outline the calculation that yields the FCS of the considered devices. We utilize the circuit theory of mesoscopic superconductivity [8,26] and represent the circuit in terms of terminals, cavities and connectors. Terminals are described by equilibrium quasiclassical Green's function matrices \check{G}_n determined by electrochemical potential and temperature. Our notation for matrix

subspace is: $\hat{}$ for spin, $\hat{}$ for Nambu, and $\check{}$ for Keldysh. Pauli matrices are denoted τ_j . At zero temperature we consider $0 < E \leq eV$ where the Green's functions for all ferromagnetic terminals F_n are $\check{G} = \hat{\tau}_3 \check{\tau}_3 + (\check{\tau}_1 + i\check{\tau}_2)$, V is the voltage of the ferromagnetic terminals and E the quasiparticle energy. We consider that eV is much smaller than the Thouless energy of the cavity. The superconductor S is at zero voltage and has Green's function $\check{G}_S = \hat{\tau}_1$, where we assume $E \ll \Delta$, Δ being the gap of S. The terminals are connected to a cavity c which is under the influence of the proximity effect from S. The cavity is described by an unknown Green's function \check{G}_c , assumed isotropic due to chaotic or diffusive scattering. We assume that c is large enough so that charging effects can be disregarded, and small enough so that \check{G}_c is spatially homogeneous. The circuit theory is formulated in terms of generalized matrix currents \check{I}_j in spin \otimes Nambu \otimes Keldysh matrix space and from the matrix current conservation $\sum_j \check{I}_j = 0$. This determines the Green's function on the node together with the normalization condition $\check{G}_c^2 = 1$. The matrix currents can have arbitrary structure, and allow to derive the FCS by introducing the counting fields χ_n for each terminal according to [8] $\check{G}_n(\chi) = e^{i\chi_n \hat{\tau}_3 \check{\tau}_1/2} \check{G}_n e^{-i\chi_n \hat{\tau}_3 \check{\tau}_1/2}$. Spin-active connectors are taken into account by spin-dependent transmission and reflection amplitudes $t_{k,\sigma}^n$ and $r_{k,\sigma}^n$ for particles incident on the interface n from the cavity side in channel k with spin σ . The matrix current through a spin-active tunnel barrier between c and F_n evaluated at the cavity side is [16,27] $\check{I}_n = [g_n \check{G}_n/2 + \{\mathbf{g}_n \hat{\tau} \check{\tau}_3, \check{G}_n\}/4, \check{G}_c]$. Here, $g_n = g_Q \sum_{k,\sigma} |t_{k,\sigma}^n|^2$ is the tunnel conductance and $g_Q = e^2/h$ the conductance quantum. The magnetization direction is encoded in the direction of \mathbf{g}_n , and the conductance polarization in that quantization axis is $|\mathbf{g}_n| = g_Q \sum_k (|t_{k,\uparrow}^n|^2 - |t_{k,\downarrow}^n|^2)$. We have neglected here an additional term related to spin-dependent phase shifts upon reflection at the interface [16,27], as these are small in some material combinations or can be suppressed by a thin, non-magnetic oxide layer [28]. The matrix current between c and S is $\check{I}_S = g_S [\check{G}_S, \check{G}_c]/2$ [26]. We take into account the spin structure of matrix currents \check{I}_n and Green's functions in S-F systems, and derive the CGF in the linear response regime and for $eV \ll \Delta$, generalizing ref. [23]: $S = t_0/(4e^2) \int dE \sum_p \sqrt{\lambda_p^2}$, where $\{\lambda_p\}$ is the set of eigenvalues of the matrix \check{M} defined by writing matrix current conservation in the cavity $\sum_j \check{I}_j \equiv [\check{M}, \check{G}_c] = 0$. The non-trivial spin matrix structure of \check{I}_n determines the magnetization dependence of transport processes in the system. Carrying out this procedure yields the FCS for the setup in fig. 1.

In conclusion, we have investigated the elementary charge transfer processes of a S-F entangler. Charge transfers occur via two statistically independent processes, i) Cooper pairs are transferred out of the superconductor by Andreev reflection and ii) entangled quasiparticles are distributed among the different ferromagnetic leads. The

probabilities for entangled electrons to flow into spatially separated leads are completely determined by experimentally measurable conductances and polarizations. This allows complete knowledge of the statistics of charge transfer in the S-F entangler.

We would like to thank YU. V. NAZAROV, A. DI LORENZO, A. A. GOLUBOV, A. BRINKMAN, P. SAMUELSSON, D. SANCHEZ, and M. BÜTTIKER for discussions. This work was supported in part by The Research Council of Norway through Grants Nos. 167498/V30, 162742/V00, 1534581/432, 1585181/143, 1585471/431, the DFG through SFB 513, the Landestiftung Baden-Württemberg, the NSF Grant No. PHY99-07949, and EU via project NMP2-CT-2003-505587 “SFINx”.

REFERENCES

- [1] TITTEL W. and WEIHS G., *Quantum Inf. Comput.*, **1** (2001) 3 and references therein.
- [2] LESOVIK G. B., MARTIN T. and BLATTER G., *Eur. Phys. J. B*, **24** (2001) 287; SAMUELSSON P. and BÜTTIKER M., *Phys. Rev. Lett.*, **89** (2002) 046601; RECHER P. and LOSS D., *Phys. Rev. Lett.*, **91** (2003) 267003; SAMUELSSON P., SUKHORUKOV E. V. and BÜTTIKER M., *Phys. Rev. Lett.*, **91** (2003) 157002; FAORO L., TADDEI F. and FAZIO R., *Phys. Rev. B*, **69** (2004) 125326; SAMUELSSON P., SUKHORUKOV E. V. and BÜTTIKER M., *Phys. Rev. B*, **70** (2004) 115330.
- [3] RECHER P., SUKHORUKOV E. V. and LOSS D., *Phys. Rev. B*, **63** (2001) 165314; CHTCHELKATCHEV N. M., BLATTER G., LESOVIK G. B. and MARTIN T., *Phys. Rev. B*, **66** (2002) 161320(R).
- [4] BAYANDIN K. V., LESOVIK G. B. and MARTIN T., *Phys. Rev. B*, **74** (2006) 085326; ZENG Z. Y., ZHOU L., HONG J. and LI B., *Phys. Rev. B*, **74** (2006) 085312.
- [5] SANCHEZ D., LOPEZ R., SAMUELSSON P. and BUTTIKER M., *Phys. Rev. B*, **68** (2003) 214501.
- [6] BIGNON G., HOUZET M., PISTOLESI F. and HEKING F. W. J., *Europhys. Lett.*, **67** (2004) 110.
- [7] LEVITOV L. S. and LESOVIK G. B., *JETP Lett.*, **58** (1993) 230.
- [8] BELZIG W. and NAZAROV YU. V., *Phys. Rev. Lett.*, **87** (2001) 067006; 197006.
- [9] NAZAROV YU. V. (Editor), *Quantum Noise in Mesoscopic Physics* (Kluwer Academic Publishers, Dordrecht) 2003.
- [10] NAZAROV YU. V., *Quantum transport and circuit theory in Handbook of Theoretical and Computational Nanotechnology*, edited by RIETH M. and SCHOMMERS W. (American Scientific Publishers) 2005, Chapt. 95, pp. 1–83.
- [11] FALCI G., FEINBERG D. and HEKING F. W. J., *Europhys. Lett.*, **54** (2001) 255.
- [12] DI LORENZO A. and NAZAROV YU. V., *Phys. Rev. Lett.*, **94** (2005) 210601.
- [13] CLAUSER J. F., HORNE M. A., SHIMONY A. and HOLT R. A., *Phys. Rev. Lett.*, **23** (1969) 880.
- [14] ASPECT A., GRANGIER P. and ROGER G., *Phys. Rev. Lett.*, **49** (1982) 91.
- [15] PARKIN S. S. P., KAISER C., PANCHULA A., RICE P. M., HUGHES B., SAMANT M. and YANG S., *Nat. Mater.*, **3** (2004) 862.
- [16] HUERTAS-HERNANDO D., NAZAROV YU. V. and BELZIG W., *Phys. Rev. Lett.*, **88** (2002) 047003 and cond-mat/0204116; HUERTAS-HERNANDO D., PhD Thesis, TU Delft (2002).
- [17] TORRÈS J. and MARTIN T., *Eur. Phys. J. B*, **12** (1999) 319.
- [18] VOLKOV A. F., ZAITSEV A. V. and KLAPWIJK T. M., *Physica C*, **210** (1993) 21.
- [19] NAZAROV YU. V., *Phys. Rev. Lett.*, **73** (1994) 1420.
- [20] MORTEN J. P., BRATAAS A. and BELZIG W., *Phys. Rev. B*, **74** (2006) 214510.
- [21] OBERHOLZER S., BIERI E., SCHONENBERGER C., GIOVANNINI M. and FAIST J., *Phys. Rev. Lett.*, **96** (2006) 046804.
- [22] TADDEI F. and FAZIO R., *Phys. Rev. B*, **65** (2002) 134522.
- [23] BÖRLIN J., BELZIG W. and BRUDER C., *Phys. Rev. Lett.*, **88** (2002) 197001.
- [24] BURKARD G., LOSS D. and SUKHORUKOV E. V., *Phys. Rev. B*, **61** (2000) R16303.
- [25] TADDEI F. and FAZIO R., *Phys. Rev. B*, **65** (2002) 075317.
- [26] NAZAROV YU. V., *Superlattices Microstruct.*, **25** (1999) 1221.
- [27] HUERTAS-HERNANDO D. and NAZAROV YU. V., *Eur. Phys. J. B*, **44** (2005) 373; COTTET A. and BELZIG W., *Phys. Rev. B*, **72** (2005) 180503(R); BRAUDE V. and NAZAROV YU. V., *Phys. Rev. Lett.*, **98** (2007) 077003.
- [28] TEDROW P. M., TKACZYK J. E. and KUMAR A., *Phys. Rev. Lett.*, **56** (1986) 1746.

PAPER 9

Full counting statistics of crossed Andreev reflection

Preprint (2008)

Full counting statistics of crossed Andreev reflection

Jan Petter Morten,^{1,*} Daniel Huertas-Hernando,¹ Wolfgang Belzig,² and Arne Brataas¹

¹*Department of Physics, Norwegian University of Science and Technology, N-7491 Trondheim, Norway*

²*University of Konstanz, Department of Physics, D-78457 Konstanz, Germany*

(Dated: February 22, 2008)

We calculate the full counting statistics of transport in three-terminal hybrid structures with a superconducting source and normal-metal or ferromagnet drains. We obtain the probability distribution for the transport resulting from crossed Andreev reflection and electron transfer between the normal-metal terminals, which demonstrates how the microscopic probability for each process is determined by the conductance parameters of the system. The cross-correlation noise has competing contributions from crossed Andreev reflection and electron transfer, in addition to a contribution due to the antibunching effect of the Pauli exclusion principle. In the case of spin-active connectors that filter the electronic spins, we show how the contributions to nonlocal transport from crossed Andreev reflection and electron transfer depends differently on the magnetization configuration, and can be controlled by magnetizations and voltage bias.

PACS numbers: 74.40.+k 72.25.Mk 73.23.-b 74.50.+r

I. INTRODUCTION

In crossed Andreev reflection (CA), a Cooper pair in a superconductor (S) is converted into an electron-hole quasiparticle pair in normal-metal terminals (N_n) or vice versa.^{1,2} This process has potential applications in quantum information experiments since the created electron-hole pairs in spatially separated terminals are in entangled quantum states. The performance of entanglers utilizing this effect is diminished by the parasitic contribution from electron transfers between the N_n terminals. This process will be referred to as electron transfer (ET) (also denoted electron cotunneling or elastic cotunneling).

It has been suggested that the noise properties of crossed Andreev reflection can be used to investigate the competition with electron transfer between the normal-metal terminals.³ The noise properties of a mesoscopic transport can also reveal information about the charge carriers which would otherwise not be accessible through current measurements. In a system with several drain terminals, i.e. current beam splitters, noise measurements can reveal correlations between the current flow in separated terminals. The cross-correlation noise has attained interest recently since it can be utilized to study entanglement⁴ and correlated transport.

Crossed Andreev reflection in superconductor-normal-metal systems has been experimentally studied in Refs. 5–7. In Ref. 5 the nonlocal voltage was measured in a multilayer Al/Nb structure with tunnel contacts between the superconducting Nb and the normal-metal Al layers. Current was injected through one of the normal-metal-superconductor contacts, and a nonlocal voltage measured between the superconductor and the other normal-metal. At injection voltage below the Thouless energy $E_{Th} = \hbar D/d^2$ associated with the separation d between the normal-metals, positive nonlocal voltage was measured and this was interpreted as the result of dominating ET. For voltage eV above E_{Th} the nonlocal voltage

changed sign, which was interpreted as a consequence of dominating CA. Subsequently, measurements reported in Ref. 6 on nonlocal voltages in Au probes connected to a wire of superconducting Al by transparent interfaces indicated that the ET contribution is larger than the contribution from CA.

The competition between CA and ET and the resulting sign of the nonlocal voltage has been studied theoretically using various approaches^{8–16} including the circuit theory of mesoscopic superconductivity utilized in this paper.^{17,18} We will consider the linear response nonlocal conductance G_{nl} . In superconductor-normal-metal hybrid devices where transport in one normal-metal terminal N_1 is measured in response to an applied voltage in another normal metal-terminal N_2 , this quantity is defined by

$$\partial_{V_2} I_1 = -G_{nl} = -(G_{ET} - G_{CA}), \quad (1)$$

where we have introduced conductances associated with the charge transfer processes introduced above, G_{CA} for crossed Andreev reflection, and G_{ET} for electron transfer.⁸ The sign of the nonlocal conductance determines the dominating contribution due to the competition between ET and CA. Theoretical calculations based on second order perturbation theory in the tunneling Hamiltonian formalism predicted that the nonlocal conductance resulting from CA reflection is equivalent in magnitude to the contribution from ET.⁸ Thus the induced voltage in N_1 in response to the bias on N_2 should vanish since CA and ET give currents with opposite sign, in contrast to the measurements reported in Refs. 5–7. The tunneling limit was also considered in Refs. 14,17,19, and it has been found that the nonlocal conductance is in fact of fourth order in the tunneling and favours ET.

Experimental investigations of crossed Andreev reflection in superconductor-ferromagnet (S-F) structures have been reported in Refs. 20,21. The measurements in Ref. 20 were modeled using the theory of Ref. 8.

Experimental studies of the CA and ET noise prop-

erties can be used to determine the relative contributions of these processes to the nonlocal conductance. It was shown theoretically in studies of noise correlations that CA contributes positively to the cross correlations, whereas ET gives a negative contribution.³ Calculations of higher order noise correlators or the noise dependence on spin-polarizing interfaces can reveal further information about the CA and ET processes.

We will consider the full counting statistics (FCS) which encompasses all statistical moments of the current flow.^{22–24} The noise properties of ET and CA reflection thus obtained can be used to study the competition between these processes and reveal information that is not accessible in the mean currents. Our calculation also determines the contribution to the noise coming from the fermion statistics (Pauli exclusion principle). Moreover, the charge transfer probability distribution provided by FCS reveals information about the probability of elementary processes in the circuit.²⁵

In this paper we calculate the FCS of multiterminal superconductor-normal metal and superconductor-ferromagnet proximity structures, and study the currents, noise and cross correlations associated with the various transport processes. We obtain the probability distribution for transport at one normal-metal drain, and show that the probability associated with ET is larger than the probability associated with CA. For spin-active interfaces we show how spin filtering can be utilized to control the relative magnitude of the CA and ET contributions to the transport. Finally, we consider crossed Andreev reflection for spin triplet superconductors.

The paper is organized in the following way: In Sec. II we outline the formalism utilized to calculate the cumulant generating function of the probability distributions. In Sec. III we discuss the results in the case of normal metals, and in Sec. IV we consider the spin-active connectors. Finally, our conclusions are given in Sec. V.

II. MODEL

The systems we have in mind can be represented by the circuit theory diagram (see Sec. II A) shown in Fig. 1. A superconducting source terminal (S) and normal metal drain terminals (N_n) are connected by tunnel barriers with conductance g_n to a common scattering region which is modeled as a chaotic cavity (c). The assumptions on the cavity is that the Green function is isotropic due to diffusion or chaotic scattering at the interfaces, and that charging effects and dephasing can be disregarded. We consider that the tunnel barrier interfaces can be spin-active with spin polarization g_{MRn}/g_n . We consider elastic transport at zero temperature. The superconducting terminal is grounded, and biases V_n are applied to the normal terminals. We assume that $V_n \ll \Delta_0$, where Δ_0 is the gap of the superconducting terminal. In addition to the ET and CA processes described above, there can also be direct Andreev (DA)

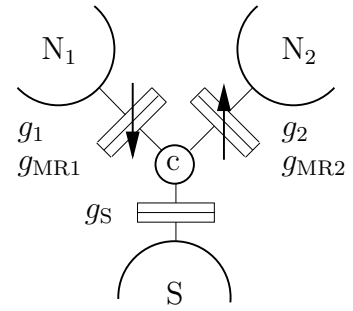


FIG. 1: Circuit theory representation of the considered beam-splitter where supercurrent flows from a superconducting reservoir (S) into normal metal drains (N_n). Tunnel barriers between cavity (c) and the drains can be spin-active, and are characterized by the conductances g_n and spin polarizations g_{MRn}/g_n .

reflection between the superconductor and one normal-metal terminal, where both particles of the Andreev reflected pair are transferred into N_n . Semiclassical probability arguments show that the subgap charge current in the connector between N_1 and c in the three terminal network in Fig. 1 has the following structure,^{8,17}

$$I_1(E) = G_{CA}(V_1 + V_2) - G_{ET}(V_2 - V_1) + 2G_{DA1}V_1, \quad (2)$$

where we have introduced the conductance G_{DA1} associated with direct Andreev reflection between terminal N_1 and S. Eq. (2) leads to the definition of the nonlocal conductance in (1) which shows that when $V_2 > V_1$, ET and CA give competing negative and positive contributions respectively to the current. The conductances in (2) will be determined in the calculation below.

A. Circuit theory

The circuit theory of mesoscopic transport is reviewed in Ref. 26 and is a suitable formalism to study proximity effects in superconducting nanostructures. The theory is developed from a discretization of the quasiclassical theory of superconductivity,²⁷ in combination with a theory of boundary conditions based on scattering theory.

The circuit theory is formulated in terms of the quasiclassical Green functions of the terminals and nodes in the system. Nodes can represent small islands or lattice points of diffusive parts of the system. Under the assumptions described above, the Green function of the spin-singlet S terminal in Fig. 1 is $\check{G}_S = \hat{\tau}_1$ where $\hat{\tau}_k$ is a Pauli matrix in Nambu space. The Green functions \check{G}_n of normal-metal terminals N_n are given by

$$\check{G}_c(E) = \begin{cases} \hat{\tau}_3 \check{\tau}_3 + (\check{\tau}_1 + i\check{\tau}_2) & |E| < eV_n, \\ \hat{\tau}_3 \check{\tau}_3 + \text{sgn}(E) \hat{\tau}_3 (\check{\tau}_1 + i\check{\tau}_2) & |E| \geq eV_n, \end{cases} \quad (3)$$

where $\check{\tau}_k$ are Pauli matrices in Keldysh space.

Matrix currents \check{I} describe the flow of charge, energy and coherence between terminals and nodes through connectors, and conservation of these currents are imposed at each node. This generalized Kirchhoff law determines the Green function of the cavity \check{G}_c . The balance of matrix currents \check{I}_n flowing between each terminal $n = 1, 2, S$ and the cavity, including the effect of superconducting pairing in c , can be written

$$\sum_n \check{I}_n - \left[\frac{e^2 \nu_0 \mathcal{V}_c}{\hbar} \Delta_c \hat{\tau}_1, \check{G}_c \right] = 0. \quad (4)$$

Here, Δ_c is the superconducting order parameter on the cavity, ν_0 is the density of states and \mathcal{V}_c the volume of the cavity.^{18,27} Since the pairing term has the same structure as the coupling to the superconducting terminal (see (5)), it gives quantitative effects that are captured by renormalizing $e^2 \nu_0 \mathcal{V}_c \Delta_c / \hbar + g_S \rightarrow g_S$ and will be omitted in the following. Here, g_S is the superconductor tunnel conductance.

Spin dependent transmission and reflection is described by tunneling amplitudes $t_{k,\sigma}^n$ and $r_{k,\sigma}^n$ for electrons with spin σ incident from the cavity side on the interface between the cavity and terminal n in channel k . The matrix current \check{I}_n through such spin-active interfaces is²⁸

$$\check{I}_n = \frac{g_n}{2} [\check{G}_n, \check{G}_c] + \frac{g_{MRn}}{4} [\{\mathbf{m}_n \cdot \bar{\boldsymbol{\sigma}} \bar{\tau}_3, \check{G}_n\}, \check{G}_c]. \quad (5)$$

Here, $g_n = g_Q \sum_{k,\sigma} |t_{k,\sigma}^n|^2$ is the tunnel conductance where $g_Q = e^2/h$ is the conductance quantum, $g_{MRn} = g_Q \sum_k (|t_{k,\uparrow}^n|^2 - |t_{k,\downarrow}^n|^2)$ is the conductance polarization, $\bar{\boldsymbol{\sigma}}$ is the vector of Pauli matrices in spin space, and the unit vector \mathbf{m}_n points in the direction of the magnetization of the spin polarizing contact. In (5) we have neglected an additional term related to spin dependent phase shifts from reflection at the interface which can be suppressed by a thin, non-magnetic oxide layer.^{29,30} The effects of spin filtering by g_{MRn} , which can be obtained experimentally using ferromagnetic terminals, will be studied in Sec. IV.

In systems where all the connectors are tunnel barriers described by the matrix current (5), it is possible to solve (4) analytically and obtain the cavity Green function in terms of the terminal Green functions and the tunneling parameters. To this end, we note that it is possible to write (4) as $[\check{M}, \check{G}_c] = 0$. Employing the normalization condition $\check{G}_c^2 = 1$, the solution can be expressed in terms of the matrix \check{M} as³¹

$$\check{G}_c = \check{M} / \sqrt{\check{M}^2}. \quad (6)$$

This result facilitates calculation of the cumulant generating function of the charge transfer probability distribution in tunnel barrier multiterminal circuits.

B. Full counting statistics

Full counting statistics is a useful tool to compute currents and noise in a multiterminal structure,³² and also provides the higher statistical moments that may become experimentally accessible in these systems. Additionally, one can obtain information about the elementary charge transport processes by studying the probability distributions.²⁵ The cumulant generating function (CGF) $\mathcal{S}(\{\chi_n\})$ of the probability distribution is directly accessible by the Green function method, and is defined by

$$e^{-\mathcal{S}(\{\chi_n\})} = \sum_{N_n} P(\{N_n\}; t_0) e^{-i \sum_n \chi_n N_n}$$

$$P(\{N_n\}; t_0) = \frac{1}{(2\pi)^M} \int_{-\pi}^{\pi} d^M \chi e^{-\mathcal{S}(\{\chi_n\}) + i \sum_n N_n \chi_n}. \quad (7)$$

Here, $P(\{N_n\}; t_0)$ is the probability to transfer N_1, N_2, \dots, N_n electrons into terminal N_1, N_2, \dots, N_n in time t_0 , and M is the total number of terminals in the circuit. The CGF is a function of the set of counting fields $\{\chi_n\}$ which are embedded in the Green function at each terminal by the transformation $\check{G}_n \rightarrow e^{i\chi_n \bar{\tau}_K / 2} \check{G}_n e^{-i\chi_n \bar{\tau}_K / 2}$ where $\bar{\tau}_K = \hat{\tau}_3 \bar{\tau}_1$. The CGF will be determined by the following relation,³²

$$\frac{ie}{t_0} \frac{\partial \mathcal{S}(\{\chi_n\})}{\partial \chi_n} = \int dE I_n(\{\chi_n\}), \quad (8)$$

where $I_n(\{\chi_n\})$ is the particle (counting) current through connector n in presence of the counting fields. Our task is now to integrate this equation and obtain the CGF $\mathcal{S}(\{\chi_n\})$. Using the general solution to the matrix current conservation (6), it was found in Ref. 31, that this is possible by rewriting the counting current in terms of a derivative of \check{M} with respect to the counting fields. Explicit derivation shows that

$$I_n(\{\chi_n\}) = \frac{1}{8e} \text{Tr} \{ \bar{\tau}_K \check{I}_n(\{\chi_n\}) \} = \frac{1}{4ei} \partial_{\chi_n} \text{Tr} \{ \sqrt{\check{M}^2} \}. \quad (9)$$

This result is valid also in the presence of spin-active contacts (5). Combining (9) with (8) yields $\mathcal{S}(\{\chi_n\})$ straightforwardly.

Practical calculations of CGFs are performed by diagonalizing the matrix \check{M} , which allows us to express the CGF in terms of the eigenvalues of \check{M} ,

$$\mathcal{S} = -\frac{t_0}{4e^2} \int dE \sum_k \sqrt{\lambda_k^2}. \quad (10)$$

In this equation, $\{\lambda_k\}$ is the set of eigenvalues of \check{M} .

We can obtain the cumulants of the transport probability distribution by successive derivatives of the CGF.²⁴ Specifically, we obtain the mean current from

$$I_n = -\frac{ie}{t_0} \left. \frac{\partial \mathcal{S}(\{\chi\})}{\partial \chi_n} \right|_{\{\chi=0\}}. \quad (11)$$

The current noise power is given by

$$C_{m,n} = 2 \frac{e^2}{t_0} \left. \frac{\partial^2 \mathcal{S}(\{\chi\})}{\partial \chi_m \partial \chi_n} \right|_{\{\chi=0\}}, \quad (12)$$

where in the multiterminal structure, the autocorrelation noise at terminal n is given by $C_{n,n}$. When $m \neq n$, (12) gives the noise cross-correlations.

III. NORMAL METAL DRAINS

In this section, we will consider the FCS of the superconducting beamsplitter in Fig. 1 when the connectors are not spin polarizing, and generalize previous works by taking into account a difference in drain terminal voltages $V_1 \neq V_2$.

In the regime $E < eV_1, eV_2$ the only contribution to the nonlocal conductance comes from CA since we consider zero temperature. The resulting CGF was studied in Ref. 31 where it was assumed that $V_1 = V_2$. In the general

case $V_1 \neq V_2$, the total CGF \mathcal{S} following from (10) has one contribution from the energy range $E < eV_1, eV_2$, and if the voltages are different, another contribution in the energy range $eV_1 \leq E < eV_2$ (we assume $V_2 > V_1$),

$$\begin{aligned} \mathcal{S} &= -\frac{t_0}{4e^2} \sum_k \left(\int_{-eV_2}^{-eV_1} + \int_{-eV_1}^{eV_1} + \int_{eV_1}^{eV_2} \right) dE \sqrt{\lambda_k^2(E)} \\ &= \mathcal{S}_a(V_1) + \mathcal{S}_b(V_2 - V_1). \end{aligned} \quad (13)$$

There is no contribution to transport at $|E| > eV_2$. Here, we have defined two separate contributions to the CGF that govern transport in the regime $E < eV_1, eV_2$ (\mathcal{S}_a) where only Andreev reflections (CA and DA) can occur, and the regime $eV_1 \leq E < eV_2$ (\mathcal{S}_b) where in addition to Andreev reflections, ET can take place. The contribution \mathcal{S}_a was calculated in Ref. 31, see (14a), where we have defined $g_\Sigma = [g_S^2 + g^2]^{1/2}$ and $g = g_1 + g_2$. The counting factors $e^{2i\chi_S - i\chi_m - i\chi_n}$ describe processes where two particles are transferred from S, and one particle is counted at terminal N_m and at terminal N_n ($m, n = 1, 2$).

$$\mathcal{S}_a = -\frac{t_0 V_1}{\sqrt{2}e} \sqrt{g_\Sigma^2 + \sqrt{g_\Sigma^4 + 4g_S^2 \sum_{m,n} g_m g_n (e^{2i\chi_S - i\chi_m - i\chi_n} - 1)}}, \quad (14a)$$

$$\begin{aligned} \mathcal{S}_b &= -\frac{t_0(V_2 - V_1)}{\sqrt{2}e} \\ &\times \sqrt{g_\Sigma^2 + 2g_1 g_2 (e^{i\chi_1 - i\chi_2} - 1) + \sqrt{g_\Sigma^4 + 4g_S^2 \sum_n g_n g_2 (e^{2i\chi_S - i\chi_n - i\chi_2} - 1) + 4g_1 g_2 g^2 (e^{i\chi_1 - i\chi_2} - 1)}} \end{aligned} \quad (14b)$$

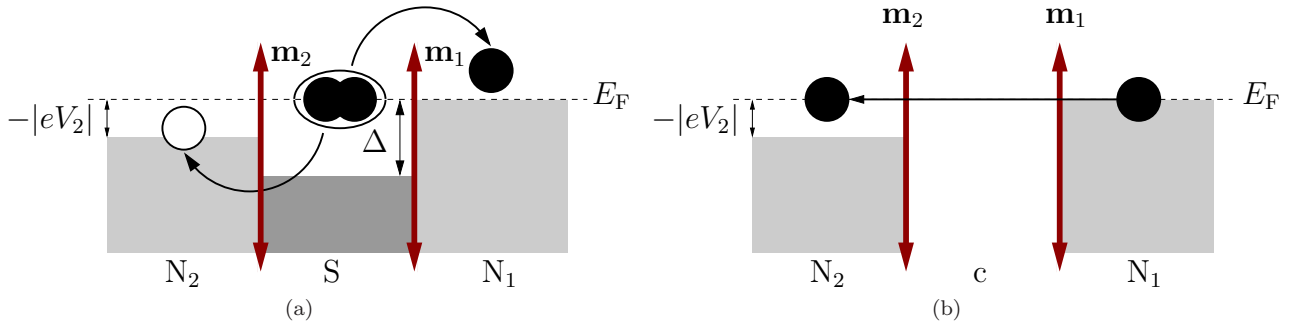


FIG. 2: Transport processes in the three terminal device when $eV_1 = 0$: (a) Crossed Andreev reflection: A Cooper pair from S is converted into an electron-hole pair in c by Andreev reflection, and the electron with energy $+E$ is transferred into N_1 , and the hole with energy $-E$ is transferred into N_2 . Tunnel barriers between the reservoirs may be spin-active and are described by magnetization vectors \mathbf{m} that in this paper are considered collinear. (b) Electron transfer: A particle from N_1 tunnels through the cavity c into N_2 . The density of states in the cavity c is suppressed due to the proximity effect from the superconducting terminal.

In (14b) we show the calculated \mathcal{S}_b which has con-

tributions from electron transfer. The counting factor

$e^{i\chi_1 - i\chi_2}$ describes events where an electron is transferred from N_1 to N_2 . Compared to \mathcal{S}_a , we see that DA events between S and N_1 that would be described by counting factors $e^{2i\chi_S - 2i\chi_1}$ no longer occur. This can be understood from the electron-hole nature of Cooper pairs, see Fig. 2. Two quasiparticles, with energy $+E$ for the electron and $-E$ for the hole constitute the Andreev reflected quasiparticle pairs in c . In the energy range considered here, $eV_1 \leq E < eV_2$, the states in N_1 are occupied, precluding DA reflection into N_1 . A similar argument shows that in CA processes, the electron must be transferred into N_1 and the hole into N_2 .

The nonlocal conductance $G_{nl} = G_{ET} - G_{CA}$ following from (14b) is in agreement with Ref. 17 where

$$G_{ET} = \frac{g_1 g_2}{2} \frac{2g^2 + g_S^2}{[g^2 + g_S^2]^{3/2}}, \quad G_{CA} = \frac{g_1 g_2}{2} \frac{g_S^2}{[g^2 + g_S^2]^{3/2}}. \quad (15)$$

The nonlocal conductance is dominated by ET and is of order $\mathcal{O}(g_n^4)$.^{14,17} When $g_S/g \gg 1$, the nonlocal conductance vanishes due to equal probability for ET and CA as we will explicitly show by inspection of the probability distribution below.

Let us now consider cross-correlations. In general, CA leads to a positive contribution and ET leads to a negative contribution to the cross-correlation. An additional, negative contribution is induced by the Pauli exclusion principle. The cross-correlation between N_1 and N_2 following from (13) is

$$C_{1,2} = 2e(V_1 + V_2)G_{CA} - 2e(V_2 - V_1)G_{ET} \quad (16a)$$

$$- \frac{10eV_1}{g_\Sigma} (G_1 - G_{nl})(G_2 - G_{nl}) \quad (16b)$$

$$+ \frac{4e(V_2 - V_1)}{g_\Sigma} [G_{CA}(G_2 + 2G_{DA2}) - G_{DA2}G_{nl}], \quad (16c)$$

where we have defined the local differential conductances $G_n = \partial_n I_n$ and the conductance for direct Andreev reflection into terminal n is $G_{DA n} = g_S^2 g_n^2 / 2g_\Sigma$.¹⁷ We now focus on the competition between CA and ET. When the two normal-metal terminals are at equal voltage $V_1 = V_2$ the contribution from ET and also the term in (16c) vanishes and we are left with a positive contribution to the cross-correlations from CA due to the correlated particle transfer into N_1 and N_2 . An additional, negative contribution due to the Pauli principle in (16b) vanishes in the limit of asymmetric conductances $g_S \gg g$ or $g_{1(2)} \gg g_{2(1)}, g_S$ due to the noisy (Poissonian) statistics of the incoming supercurrent. A negative contribution from ET in (16a) is induced when there is a voltage difference between the normal-metal terminals due to the currents with opposite signs in N_1 and N_2 resulting from this process. This demonstrates that it is possible to tune the sign of cross-correlations by the voltages V_1 and V_2 .³ The contribution in (16c) that appears when there is a voltage difference vanishes in the limit of asymmetric conductances.

It is interesting to compare \mathcal{S}_b with the corresponding CGF when S is in the normal state,

$$\mathcal{S}_b = - \frac{t_0(V_2 - V_1)}{2e} \times \sqrt{(g_1 + g_S + g_2)^2 + 4g_2 g_1 e^{i\chi_1 - i\chi_2} + 4g_2 g_S e^{i\chi_S - i\chi_2}}. \quad (17)$$

Here we see a contribution due to transport between N_1 and N_2 that is similar to the one outside the double square root in (14b). Superconductivity leads to the double square root in (14b) that takes into account the correlation of transport through c by Andreev reflections and ET. The complicated dependence on the counting fields in (14b) precludes a simple interpretation of \mathcal{S}_b in terms of the probabilities of elementary charge transfer processes. However, when $g_S \gg g$ or $g_{1(2)} \gg g_{2(1)}, g_S$ we can expand the square roots in \mathcal{S}_b and obtain the CGF

$$\mathcal{S}_b = - \frac{t_0(V_2 - V_1)}{2g_S^3 e} \left[g_1 g_2 (g_S^2 + 2g^2) e^{i\chi_1 - i\chi_2} + g_S^2 g_1 g_2 e^{2i\chi_S - i\chi_1 - i\chi_2} + g_S^2 g_2^2 e^{2i\chi_S - 2i\chi_2} \right]. \quad (18)$$

In this limit the CGF describes independent CA, ET, and DA Poisson processes. The prefactors determine the average number of charges transferred by each process in time t_0 .

To illustrate the physics described by \mathcal{S}_b in the limit introduced above, let us examine the probability distribution obtained by the definition in (7). If we consider the current response in N_1 to a voltage in N_2 , we can consider that $V_1 = 0$ and the only contribution to the total CGF \mathcal{S} comes from \mathcal{S}_b . The normalized probability distribution for the transport at terminal N_1 following from (18) then becomes

$$P(N_1; t_0) = e^{-\bar{N}_1 g_S^2 / g^2} \sum_{\substack{k \geq |N_1| \\ k + \bar{N}_1 \text{ even}}} \times \left(\bar{N}_1 \frac{g_S^2}{2g^2} \right)^{\frac{k + \bar{N}_1}{2}} \left[\bar{N}_1 \left(\frac{g_S^2}{2g^2} + 1 \right) \right]^{\frac{k - \bar{N}_1}{2}} \times \left[\left(\frac{k + \bar{N}_1}{2} \right)! \left(\frac{k - \bar{N}_1}{2} \right)! \right]^{-1}. \quad (19)$$

Here we have defined the mean number of particles transferred in time t_0 ,

$$\bar{N}_1 = \frac{|I_1| t_0}{e} = \frac{V_2 t_0}{e} \frac{g_1 g_2}{g(1 + g_S^2 / g^2)^{3/2}}. \quad (20)$$

Eq. (19) describes a joint probability distribution for CA and ET processes with Poissonian statistics, and is constrained such that the number of CA events described by the weight $g_S^2 / 2g^2$ subtracted by the number of ET events described by the weight $g_S^2 / 2g^2 + 1$, is N_1 as required. When $g_S/g \gg 1$, the mean number of particles

transferred vanishes according to (20) and the probability distribution (19) is symmetric around $N_1 = 0$. This means that the average current vanishes, since the probabilities for ET and CA are equal. In general, the probability distribution has its maximum for negative N_1 , i.e. ET is more probable than CA reflection. In Fig. 3 we have plotted the probability distribution (19) for different values of g_S/g . For small values of g_S/g parameter, ET dominates and the probability distribution is centered at a negative value for N_1 . As expected, we see that the center of the probability distribution (mean number of particles transferred) is shifted from a negative value towards zero with increasing g_S/g . The width of the distribution, described by the autocorrelation noise $C_{1,1}$ (see (12)), decreases with increasing g_S/g .

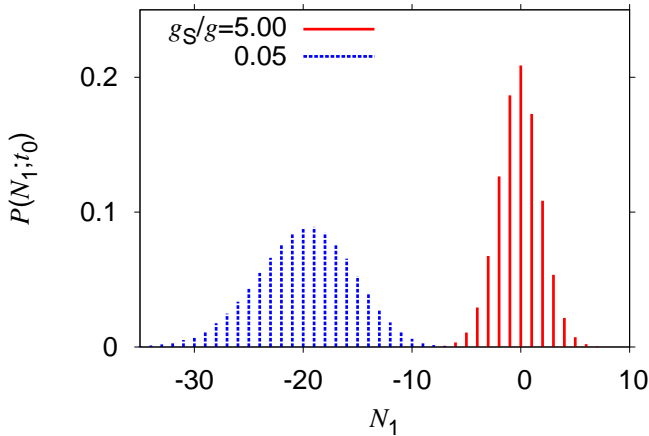


FIG. 3: Probability distribution for transport of N_1 electrons into terminal N_1 , $P(N_1; t_0)$ (19). We show distributions for two different values of the parameter $g_S/g = 5.00$ (red solid impulses), and 0.05 (blue dotted impulses). We have chosen the parameter $\alpha = g_1 g_2 V_2 t_0 / e g = 20$, which gives the mean value \bar{N}_1 for small g_S/g , see (20).

IV. SPIN-ACTIVE CONNECTORS

Qualitatively, the effect of spin polarizing interfaces on the competition between CA and ET processes in S-F systems can be understood as follows. The ET process is favoured when magnetizations of ferromagnetic leads are parallel since the same spin must traverse both the interfaces between c and the ferromagnets. On the other hand, CA reflection is favoured in an antiparallel configuration since two particles with opposite spins must traverse the interfaces. This behaviour was experimentally observed in Refs. 20,21 where ferromagnetic Fe probes were contacted to a superconducting Al wire.

The FCS of a beam splitter with spin-active contacts and $V_1 = V_2$ was considered in our previous paper Ref. 25 and constitutes \mathcal{S}_a , see (21a). In this case the only transport processes are DA and CA reflection, and we found that CA is enhanced in an antiparallel alignment of the magnetizations as expected.

When $V_2 > V_1$, there can also be ET, and an additional effect is spin accumulation at the node. With collinear magnetizations (sign of g_{MRn} describes magnetization directions up (positive) or down (negative) along the z quantization axis), we find that in the regime $eV_1 < E < eV_2$, $\mathcal{S}_b = \mathcal{S}_{b+} + \mathcal{S}_{b-}$ where $\mathcal{S}_{b\sigma}$ is given below (21b).

$$\mathcal{S}_a = -\frac{t_0 V}{\sqrt{2} e} \sqrt{1 + \sqrt{1 - \frac{4g_{MR}^2}{g_\Sigma^4} (g_S^2 + g^2) + \frac{4g_S^2}{g_\Sigma^4} \sum_{m,n} (g_m g_n - g_{MRm} g_{MRn}) (e^{2i\chi} - i\chi_m - i\chi_n - 1)}}, \quad (21a)$$

$$\mathcal{S}_{b\sigma} = -\frac{t_0 g_\Sigma (V_2 - V_1)}{2\sqrt{2} e} \left\{ 1 + \frac{2}{g_\Sigma^2} (g_1 + \sigma g_{MR1})(g_2 + \sigma g_{MR2}) (e^{i\chi_1} - i\chi_2 - 1) \right. \\ \left. + \left[1 - \frac{4g_{MR}^2}{g_\Sigma^4} (g_S^2 + g^2) + \frac{4g_S^2}{g_\Sigma^4} \sum_n (g_n - \sigma g_{MRn})(g_2 + \sigma g_{MR2}) (e^{2i\chi_S} - i\chi_n - i\chi_2 - 1) \right. \right. \\ \left. \left. + \frac{4(g - g_{MR})^2}{g_\Sigma^4} (g_1 + \sigma g_{MR1})(g_2 + \sigma g_{MR2}) (e^{i\chi_1} - i\chi_2 - 1) \right]^{1/2} \right\}^{1/2}. \quad (21b)$$

Here we have redefined $g_\Sigma = (g_S^2 + g^2 + g_{MR}^2)^{1/2}$ and intro-

duced $g_{MR} = g_{MR1} + g_{MR2}$. The expression for \mathcal{S}_b reduces

to the result for nonpolarizing contacts, Eq. (14b), in the limit that $g_{\text{MR}n} \rightarrow 0$. The two terms $\mathcal{S}_{b\sigma}$ correspond to the two possible directions of the spin(s) involved in the charge transfer processes. The spin-dependent conductance for a spin up (down) is $g_n + (-)g_{\text{MR}n}$. In ET, one spin must traverse the two spin-active interfaces, thus the counting factor for spin σ is proportional to the weight $(g_1 + \sigma g_{\text{MR}1})(g_2 + \sigma g_{\text{MR}2})$. The two spin channels are independent. The two opposite spins of an Andreev reflected quasiparticle pair can be CA reflected into terminals with different polarizations $g_{\text{MR}1}$ and $g_{\text{MR}2}$ according to the prefactor $(g_1 - \sigma g_{\text{MR}1})(g_2 + \sigma g_{\text{MR}2})$, and each possibility for the directions of the two spins gives an independent contribution to the CGF \mathcal{S}_b .

In the limit that $g_S \gg g$ or $g_{1(2)} \gg g_{2(1)}$, g_S ($g_{\text{MR}n} \leq g_n$ by definition) we can expand the double square roots and perform the summation over $\mathcal{S}_{b\sigma}$ which yields

$$\begin{aligned} \mathcal{S}_b = & -\frac{t_0(V_2 - V_1)}{2eg_S^3} \\ & \times \left\{ [g_S^2 + (g - g_{\text{MR}})^2] (g_1 g_2 + g_{\text{MR}1} g_{\text{MR}2}) e^{i\chi_1 - i\chi_2} \right. \\ & + g_S^2 (g_1 g_2 - g_{\text{MR}1} g_{\text{MR}2}) e^{2i\chi_S - i\chi_1 - i\chi_2} \\ & \left. + g_S^2 (g_2^2 - g_{\text{MR}2}^2) e^{2i\chi_S - 2i\chi_2} \right\}. \end{aligned} \quad (22)$$

The nonlocal conductance following from (22) is given by

$$G_{\text{ET}} = (g_1 g_2 + g_{\text{MR}1} g_{\text{MR}2}) \frac{[g_S^2 + (g - g_{\text{MR}})^2]}{2g_S^3}, \quad (23a)$$

$$G_{\text{CA}} = (g_1 g_2 - g_{\text{MR}1} g_{\text{MR}2}) \frac{g_S^2}{2g_S^3}. \quad (23b)$$

This immediately demonstrates that ET is favoured in a parallel configuration of the magnetizations ($g_{\text{MR}1} g_{\text{MR}2} > 0$) as the same spin in this case tunnels through both interfaces. On the other hand, CA reflection is favoured by antiparallel magnetizations ($g_{\text{MR}1} g_{\text{MR}2} < 0$) since the opposite spins of a singlet tunnel through different interfaces. These qualitative features are in agreement with Ref. 8.

The cross-correlation following from (22) is

$$C_{1,2} = 2e(V_2 + V_1)G_{\text{CA}} - 2e(V_2 - V_1)G_{\text{ET}}. \quad (24)$$

The sign of $C_{1,2}$ can now be tuned by two experimental control parameters: The bias voltages through the prefactors in (24), and the relative magnetization direction that determines the magnitudes of G_{ET} and G_{CA} .

In the energy range $V_1 < E < V_2$ we are in this setup measuring the energy of the quasiparticles involved in crossed Andreev reflection, see Fig. 2. Since the electron-like quasiparticle with energy $+E$ must flow into N_1 , and the $-E$ hole-like quasiparticle must flow into N_2 , this means that the entanglement in the energy degree of freedom of Andreev reflected quasiparticle pairs has collapsed.

A. Triplet superconductivity

Superconducting correlations with triplet pairing symmetry in the spin space can be induced by magnetic exchange fields in singlet superconductor heterostructures. This effect has attained considerable interest, and has recently been experimentally demonstrated (see Refs. 33–35 and references within). We have studied the FCS when S is a source of spin triplet quasiparticle pairs, and in this subsection we summarize our results for collinear magnetizations when $V_1 = V_2$.

The CGF for the spin triplet Cooper pairs with $S_z |\Psi\rangle = 0$, where S_z is the spin operator along the z -axis and $|\Psi\rangle$ is the spin part of the Cooper pair wave function, is identical to the CGF for conventional spin singlet superconductors. We showed in Ref. 25 that the CGF (21a) reveals the entangled nature of the quasiparticle pairs. The $S_z |\Psi\rangle = 0$ spin triplet states are also one of the maximally entangled Bell states which implies that the magnetization dependence for CA is the same for singlet and triplet in the collinear case. This result can be shown also straightforwardly by computing the two-electron tunneling probability $p_{1,2}$ which is proportional to $\langle \Psi | (g_1 + g_{\text{MR}1} \bar{\sigma}_3) \otimes (g_2 + g_{\text{MR}2} \bar{\sigma}_3) | \Psi \rangle + 1 \leftrightarrow 2$.

The triplet states where $S_z |\Psi\rangle = \pm \hbar$ give rise to a different dependence on the magnetization configurations in the CGF since the quasiparticle pairs are not in spin entangled states, but rather in product states. Compared to the singlet case (21a), we obtain a CA counting prefactor in the CGF that factorizes into $(g_1 + \sigma g_{\text{MR}1})(g_2 + \sigma g_{\text{MR}2})$ for equal-spin σ triplet Cooper pairs. This is consistent with the magnetization dependence obtained by calculating the two-particle tunneling probability $p_{1,2}$ as discussed above.

V. CONCLUSION

We have calculated the full counting statistics of multiterminal superconductor–normal-metal and superconductor–ferromagnet beam splitter devices, and studied the resulting currents and cross-correlation. The probability distribution for transport at a normal-metal drain contact demonstrates that the probability for electron transport between two normal-metal terminals is larger than the probability for crossed Andreev reflection. A finite voltage difference between the normal-metal contacts introduces competing contributions to the cross-correlations from electron transport between normal terminals and crossed Andreev reflection. Finally, we have shown how spin-active contacts act as filters for spin, and calculated the cumulant generating function. The sign of the cross-correlation due to the competing contributions from electron transport between drain terminals and crossed Andreev reflection can in this case be determined by two external control parameters, i.e. bias voltages and the relative magnetization orientation. Finally, we make some remarks about the counting statis-

tics in the case of spin triplet superconductors.

162742/V00, DFG through SFB 513 and the Landestiftung Baden-Württemberg.

Acknowledgments

This work has been supported by the the Research Council of Norway through Grants No. 167498/V30,

-
- * Electronic address: jan.morten@ntnu.no
- ¹ J. M. Byers and M. E. Flatte, Phys. Rev. Lett. **74**, 306 (1995).
 - ² G. Deutscher and D. Feinberg, Appl. Phys. Lett. **76**, 487 (2000).
 - ³ G. Bignon, M. Houzet, F. Pistolesi, and F. W. J. Hekking, Europhys. Lett. **67**, 110 (2004).
 - ⁴ G. Burkard, J. Phys.: Condens. Matter **19**, 233202 (2007).
 - ⁵ S. Russo, M. Kroug, T. M. Klapwijk, and A. F. Morpurgo, Phys. Rev. Lett. **95**, 027002 (2005).
 - ⁶ P. Cadden-Zimansky and V. Chandrasekhar, Phys. Rev. Lett. **97**, 237003 (2006).
 - ⁷ D. Beckmann and H. v. Löhneysen, Appl. Phys. A **89**, 603 (2007).
 - ⁸ G. Falci, D. Feinberg, and F. W. J. Hekking, Europhys. Lett. **54**, 255 (2001).
 - ⁹ T. Yamashita, S. Takahashi, and S. Maekawa, Phys. Rev. B **68**, 174504 (2003).
 - ¹⁰ N. M. Chtchelkatchev, JETP Lett. **78**, 230 (2003).
 - ¹¹ D. Sanchez, R. Lopez, P. Samuelsson, and M. Buttiker, Phys. Rev. B **68**, 214501 (2003).
 - ¹² A. Brinkman and A. A. Golubov, Phys. Rev. B **74**, 214512 (2006).
 - ¹³ M. S. Kalenkov and A. D. Zaikin, Phys. Rev. B **75**, 172503 (2007).
 - ¹⁴ D. S. Golubev and A. D. Zaikin, Phys. Rev. B **76**, 184510 (2007).
 - ¹⁵ M. S. Kalenkov and A. D. Zaikin, Phys. Rev. B **76**, 224506 (2007).
 - ¹⁶ A. L. Yeyati, F. Bergeret, A. Martin-Rodero, and T. Klapwijk, Nature Phys. **3**, 455 (2007).
 - ¹⁷ J. P. Morten, A. Brataas, and W. Belzig, Phys. Rev. B **74**, 214510 (2006).
 - ¹⁸ J. P. Morten, A. Brataas, and W. Belzig, Appl. Phys. A **89**, 609 (2007).
 - ¹⁹ R. Mélin and D. Feinberg, Phys. Rev. B **70**, 174509 (2004).
 - ²⁰ D. Beckmann, H. B. Weber, and H. v. Löhneysen, Phys. Rev. Lett. **93**, 197003 (2004).
 - ²¹ D. Beckmann and H. v. Löhneysen, AIP Conference Proceedings **850**, 875 (2006).
 - ²² L. S. Levitov and G. B. Lesovik, JETP Lett. **58**, 230 (1993).
 - ²³ W. Belzig and Yu. V. Nazarov, Phys. Rev. Lett. **87**, 067006 (2001); W. Belzig and Yu. V. Nazarov, Phys. Rev. Lett. **87**, 197006 (2001).
 - ²⁴ W. Belzig, in *Quantum noise in mesoscopic physics*, edited by Yu. V. Nazarov and Ya. M. Blanter (Kluwer Academic Publishers, Dordrecht, 2003).
 - ²⁵ J. P. Morten, D. Huertas-Hernando, A. Brataas, and W. Belzig, Europhys. Lett. **81**, 40002 (2008).
 - ²⁶ Yu. V. Nazarov, in *Handbook of Theoretical and Computational Nanotechnology*, edited by M. Rieth and W. Schommers (American Scientific Publishers, 2005), chap. 95, pp. 1–83.
 - ²⁷ Yu. V. Nazarov, Superlatt. Microstruct. **25**, 1221 (1999).
 - ²⁸ D. Huertas-Hernando, Y. V. Nazarov, and W. Belzig, Phys. Rev. Lett. **88**, 047003 (2002).
 - ²⁹ A. Cottet and W. Belzig, Phys. Rev. B **72**, 180503 (2005).
 - ³⁰ P. M. Tedrow, J. E. Tkaczyk, and A. Kumar, Phys. Rev. Lett. **56**, 1746 (1986).
 - ³¹ J. Börlin, W. Belzig, and C. Bruder, Phys. Rev. Lett. **88**, 197001 (2002).
 - ³² Yu. V. Nazarov and D. A. Bagrets, Phys. Rev. Lett. **88**, 196801 (2002).
 - ³³ A. I. Buzdin, Rev. Mod. Phys. **77**, 935 (2005).
 - ³⁴ F. S. Bergeret, A. F. Volkov, and K. B. Efetov, Rev. Mod. Phys. **77**, 1321 (2005).
 - ³⁵ M. Eschrig, T. Löfwander, T. Champel, J. C. Cuevas, J. Kopu, and G. Schön, J. Low Temp. Phys. **147**, 457 (2007).